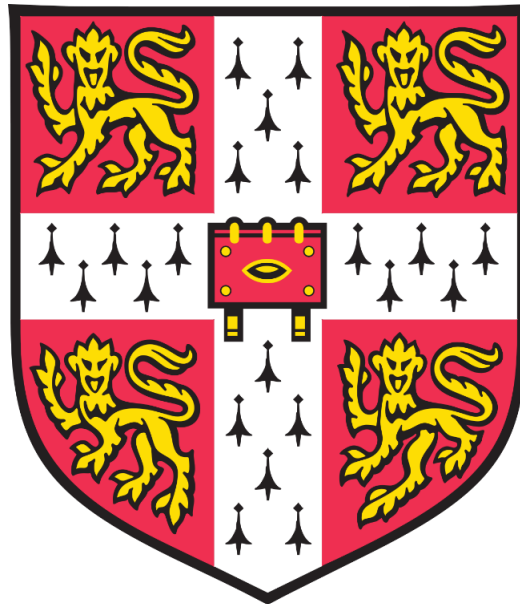


Understanding the biochemical properties
and physiological function of the protein
syncollin



Submitted for the Degree of Doctor of
Philosophy

Rosie Ann Waters

July 2021

Department of Pharmacology

University of Cambridge

St Catherine's College

DECLARATION

This thesis is the result of my own work and includes nothing which is the outcome of work done in collaboration except as declared in the preface and specified in the acknowledgement text.

Part of this work has been published in:

Waters RA, Robinson J, Edwardson JM. Syncollin is an antibacterial polypeptide. *Cell Microbiol.* 2021 Jun 21:e13372. doi: 10.1111/cmi.13372. Epub ahead of print. PMID: 34152077.

This thesis is not substantially the same as any work that has already been submitted before for any degree or other qualification except as declared in the preface and specified in the text.

This thesis does not exceed the prescribed word limit of 60,000 words, excluding references, for the Biology Degree Committee.

Rosie Waters

July 2021

ABSTRACT

Understanding the biochemical properties and physiological function of the protein syncollin

Rosie Ann Waters

Syncollin is a 16-kDa protein that was originally isolated from the pancreatic zymogen granule. It is now known also to be expressed in the gut, the spleen and in neutrophils. The protein contains intramolecular disulphide bonds and is present both free within the ZG lumen and tightly associated with the luminal leaflet of the ZG membrane; it is also secreted into the pancreatic juice. Syncollin is able to oligomerize, and assemble into doughnut-shaped structures, which might explain its known pore-forming activity. Syncollin appears to be involved in a number of gut-based disease states. For instance, syncollin expression was found to be down-regulated in the colon when a bacterial suspension was administered to germ-free mice, and in mice with chemically-induced colitis-associated cancer. The available evidence suggests that syncollin plays an important role in the gut, and possibly elsewhere. This dissertation describes my attempts to understand this role and its structural basis.

I first assessed various methods for purification of recombinant syncollin. Syncollin was expressed with various epitope tags (including His, GST and Strep) in bacteria, insect cells and mammalian cells. The best results were obtained by expressing syncollin bearing a double-Strep tag at its C terminus (syncollin-Strep) in mammalian (tsA-201) cells and purifying the protein from the cell supernatant using the Strep-Tactin XT™ system. Syncollin-Strep purified in this way contained intra-molecular disulphide bonds and recapitulated the ability of the native protein to bind to syntaxin 2 and permeabilize membranes.

In the pancreatic juice, syncollin will encounter an environment rich in proteolytic activity. One might expect, therefore, that its structure would be highly stable. To test this hypothesis, I assessed the thermal stability of the protein using circular dichroism (CD) spectroscopy. The CD spectrum of syncollin-Strep indicated a predominantly beta-sheet structure. When the protein was subjected to a temperature ramp up to 90°C, the spectrum became flattened, although complete unfolding did not occur, indicating that the protein does indeed have a very high thermal stability. A model for syncollin, based on its primary sequence, predicts a predominantly beta-sheet structure, consistent with my CD data, and suggests the presence of intramolecular disulphide bonds. When I disrupted potential bonds by mutation of appropriate cysteine residues, syncollin-Strep retained its antibacterial efficacy, but its thermal stability was reduced, suggesting the involvement of disulphide bonding in stabilizing the structure of the protein.

With regard to its potential role in the gut, I found that syncollin-Strep binds to bacterial peptidoglycan, and restricts the growth of representative Gram-positive (*Lactococcus lactis*) and Gram-negative (*Escherichia coli*) bacteria. Syncollin induces propidium iodide uptake into *E. coli* (but not *L. lactis*), indicating permeabilization of the bacterial membrane. In support of this idea, I confirmed that syncollin-Strep, like native syncollin, has pore-forming properties. Syncollin-Strep causes surface structural damage in both *L. lactis* and *E. coli*, as visualized by scanning electron microscopy. In addition, syncollin-Strep had additive effects on *L. lactis* when combined with either ampicillin (bactericidal) or tetracycline (bacteriostatic) in *L. lactis*. In light of these results, I propose that syncollin is a previously unidentified member of a large group of antimicrobial polypeptides that control the gut microbiome.

I found that expression of syncollin in neutrophils is punctate and granular. Upon activation of the neutrophils, syncollin became mobilized at the plasma membrane, and was also secreted from the cells. Secreted syncollin bound to decondensed chromatin structures characteristic of neutrophil extracellular traps (NETs). Further, when neutrophils were activated in the presence of bacteria, the bacteria became coated with secreted syncollin, consistent with the anti-bacterial role proposed above.

In conclusion, the results presented in this dissertation indicate that, through its antibacterial effects, syncollin plays a role in host defence in both the gut and the bloodstream.

ACKNOWLEDGEMENTS

First and foremost, I would like to express my gratitude to my supervisor Prof Mike Edwardson. It has been a privilege to be supervised by Mike and I would like to express my thanks for his encouragement, patience and vast knowledge. Throughout the last four years he has given me freedom and independence with experiment design and ideas, encouraged collaboration and increased my confidence as a scientist, which has been invaluable. I would also like to thank my AZ supervisor, Dr James Robinson, for his support throughout my project, including his frequent contributions to project direction, and for providing valuable guidance and collaborations within AstraZeneca. I would like to thank Dr Jon Read from AstraZeneca for X-Ray crystallography with syncollin. His positive attitude and enthusiasm was not only very much appreciated by myself, but was also refreshing to learn from his vast knowledge and expertise in the field.

I feel very lucky to have carried out my PhD in the supportive and friendly environment of the Department of Pharmacology. As my project required collaboration, I am grateful for the vast expertise I have learned from the various different labs in the department. In particular I would like to thank Dr Pam Rowling, Dr Marie Synakewicz., Dr Rohan Eapen, Dr Janet Kumita and all members of Prof Laura Itzhaki's lab for assistance and guidance with protein purification, circular dichroism and biophysical techniques. However also, I would like to thank them for incorporating me into their lab, including inviting me to their lab meetings and social events, I am highly grateful for this. I would also like to thank Rebecca Riddle, Dr Sarah Millington-Burgess and all other members of Dr Matthew Harper's lab for providing neutrophils, guidance on immunofluorescence, allowing me to join them in their group's office and again incorporating me into their lab. It has been a privilege to work closely with both the Itzhaki and Harper labs. I would like to thank Dr Paul Miller for guidance on protein purification and DIBMA, to Dr Sagar Raturi and Charlotte Guffick for *L.lactis* bacteria and fluorimeter guidance, and to Dr Ioanna Mela and Eduardo Santander for AFM imaging. I would also like to thank Karin Mueller from CAIC for assistance with SEM imaging.

For funding my studies, I would like to thank the Department of Pharmacology and AstraZeneca.

Last but not least, I am of course very grateful for the constant motivation, support and priceless encouragement I have had from my partner, family and friends, not just throughout this PhD but always - this is truly invaluable.

TABLE OF CONTENTS

DECLARATION	i
ABSTRACT	ii
ACKNOWLEDGEMENTS	iv
LIST OF FIGURES & TABLES	x
LIST OF ABBREVIATIONS.....	xiii
1. INTRODUCTION	1
1.1 THE PANCREAS AND ACINAR CELLS	2
1.2 THE ER-TO-GOLGI PATHWAY	3
1.3 ZYMOGEN GRANULE FORMATION.....	4
1.4 EXOCYTOSIS AND ENDOCYTOSIS	6
1.5 THE SNARE PROTEIN FAMILY.....	8
1.6 EXOCYTOSIS IN THE PANCREATIC ACINAR CELL	10
1.7 SYNCOLLIN AND EXOCYTOSIS	11
1.8 THE LIPID BILAYER	13
1.8.1 PROTEINS IN THE LIPID BILAYER	14
1.8.2 ZYMOGEN GRANULE MEMBRANES AND SYNCOLLIN	15
1.9 MEMBRANE INTERACTING OLIGOMERIC PROTEINS	15
1.9.1 BAX/BAK	17
1.9.2 α -SYNUCLEIN	17
1.9.3 PERFRINGOLYSIN O.....	18
1.10 SYNCOLLIN BIOCHEMISTRY AND MEMBRANE INTERACTIONS.....	19
1.11 SYNCOLLIN AND DISEASE	21
1.12 THE IMMUNE SYSTEM.....	22
1.12.1 THE INNATE AND ADAPTIVE IMMUNE SYSTEMS	22
1.12.2 NEUTROPHILS.....	23
1.13 ANTI-MICROBIAL PROTEINS	26
1.13.1 ZG16P	26
1.13.1.1 GREEK KEY MOTIF AND CRYSTALLINS	28
1.13.2 REGENERATING-ISLET DERIVED PROTEINS	31
1.13.3 DEFENSINS.....	34

1.14 AIMS AND OBJECTIVES	37
2. SYNCOLLIN PURIFICATION AND BIOCHEMICAL CHARACTERIZATION.....	39
2.1 INTRODUCTION	39
2.2 METHODS.....	40
2.2.1 BACTERIAL EXPRESSION	40
2.2.1.1 CLONING	40
2.2.1.2 BACTERIAL TRANSFORMATION AND PROTEIN EXTRACTION.....	40
2.2.1.3 AFFINITY CHROMATOGRAPHY	42
2.2.2 INSECT CELL EXPRESSION.....	42
2.2.2.1 CLONING	42
2.2.2.2 CELL CULTURE	44
2.2.2.3 CELL TRANSFECTION	44
2.2.2.4 PROTEIN PURIFICATION.....	45
2.2.3 MAMMALIAN CELL EXPRESSION.....	46
2.2.3.1 CLONING	46
2.2.3.2 CELL CULTURE	46
2.2.3.3 CELL TRANSFECTION	47
2.2.3.4 PROTEIN PURIFICATION.....	47
2.2.4 PROTEIN ANALYSIS	47
2.2.4.1 SODIUM DODECYL SULPHATE-POLYACRYLAMIDE GEL ELECTROPHORESIS (SDS-PAGE)	47
2.2.4.2 COOMASSIE BLUE STAINING	48
2.2.4.3 SILVER STAINING.....	48
2.2.4.4 PROTEIN QUALITY CONTROL	49
2.2.4.5 PROTEOLIPOSOME FORMATION FOR AFM IMAGING.....	49
2.2.4.6 AFM IMAGING	50
2.2.4.7 LIPOSOME BINDING ASSAY	50
2.2.4.8 SYNCOLLIN OLIGOMERIZATION	50
2.2.4.9 ERYTHROCYTE PERMEABILIZATION	51
2.2.4.10 QUANTITATION OF LIPOSOME PERMEABILIZATION USING BCECF RELEASE	51
2.3 RESULTS	52
2.3.1 BACTERIAL EXPRESSION	52
2.3.1.1 BL21 CELLS	52
2.3.1.2 T7 SHUFFLE CELLS.....	55

2.3.1.3 ROSETTA CELLS.....	58
2.3.2 INSECT CELL EXPRESSION OF SYNCOLLIN.....	60
2.3.3 MAMMALIAN CELL EXPRESSION	63
2.3.3.1 AFM IMAGING OF SYNCOLLIN ON LIPID BILAYERS.....	69
2.3.3.3 SYNCOLLIN OLIGOMERIZATION	72
2.3.3.4 ERYTHROCYTE PERMEABILIZATION	72
2.3.3.5 LIPOSOME PERMEABILIZATION	73
2.4 DISCUSSION	76
3. SYNCOLLIN STRUCTURAL CHARACTERISTICS.....	78
3.1 INTRODUCTION	78
3.1.1 PROTEIN STRUCTURE.....	78
3.1.2 STRUCTURE DETERMINATION	81
3.1.2.1 SECONDARY STRUCTURE AND CIRCULAR DICHROISM.....	81
3.1.2.2 X-RAY CRYSTALLOGRAPHY	83
3.1.2.3 CRYO-ELECTRON MICROSCOPY	85
3.1.3 PROBLEMATIC PROTEINS.....	86
3.1.4 MUTATIONAL ANALYSIS.....	86
3.1.5 PROTEIN-PROTEIN INTERACTION SURFACES AND HYDROPHOBIC RESIDUES.....	87
3.1.6 ELECTROSTATIC AND POLAR RESIDUES.....	87
3.1.7 CYSTEINE RESIDUES AND DISULPHIDE BRIDGES	88
3.1.8 CYSTEINE MUTANTS	88
3.1.8.1 ABCG2.....	88
3.1.8.2 HUMAN α GALACTOSIDASE A.....	89
3.1.8.3 PANCREATITIS ASSOCIATED PROTEIN 2 (PAP2)	89
3.2 METHODS	90
3.2.1 STRUCTURE PREDICTIONS	90
3.2.2 CIRCULAR DICHROISM SPECTROSCOPY.....	90
3.2.3 X-RAY CRYSTALLOGRAPHY	91
3.2.4 SYNCOLLIN SEQUENCE HOMOLOGY	91
3.2.5 SYNCOLLIN MUTANT GENERATION	91
3.2.6 SUSCEPTIBILITY TO DENATURATION.....	92
3.2.7 DYNAMIC LIGHT SCATTERING	92
3.2.8 MEASUREMENT OF HYDRODYNAMIC RADIUS	93

3.3 RESULTS	93
3.3.1 PREDICTED STRUCTURE OF SYNCOLLIN	93
3.3.2 CD SPECTROSCOPY	97
3.3.3 X-RAY CRYSTALLOGRAPHY	99
3.3.4 SYNCOLLIN SEQUENCE HOMOLOGY	100
3.3.5 DESIGN OF SYNCOLLIN MUTANTS	100
3.3.6 DISULPHIDE BOND SHIFT OF SYNCOLLIN CYSTEINE MUTANTS	101
3.3.7 LIPOSOME PERMEABILIZATION BY SYNCOLLIN CYSTEINE MUTANTS	102
3.3.8 CD SPECTROSCOPY OF SYNCOLLIN CYSTEINE MUTANTS	103
3.3.9 LIPOSOME PERMEABILIZATION BY SYNCOLLIN POSITIVE CHARGE MUTANTS	106
3.3.10 SUSCEPTIBILITY TO DENATURATION	106
3.3.11 DIBMA PURIFICATION AND DLS	107
3.3.12 MEASUREMENT OF HYDRODYNAMIC RADIUS	109
3.4 DISCUSSION	110
4. ANTI-BACTERIAL ACTIONS OF SYNCOLLIN	113
4.1 INTRODUCTION	113
4.1.1 BACTERIAL MEMBRANE LANDSCAPE	113
4.1.2 MICROBES AND DISEASE	116
4.1.2.1 ULCERATIVE COLITIS AND INFLAMMATORY BOWEL DISORDERS	116
4.1.2.2 COLITIS-ASSOCIATED CANCER	117
4.1.3 ANTI-BACTERIAL DRUG ACTION	117
4.1.3.1 BACTERIAL GROWTH	118
4.1.3.2 ANTIBIOTIC CLASSES	119
4.1.3.3 ANTIBIOTIC RESISTANCE AND COMBINATION	121
4.1.4 ANTI-BACTERIAL PROTEINS	121
4.2 METHODS	122
4.2.1 PEPTIDOGLYCAN BINDING ASSAY	122
4.2.2 BACTERIAL GROWTH CURVES	122
4.2.3 STATISTICAL ANALYSIS OF BACTERIAL GROWTH CURVES	123
4.2.4 CHECKERBOARD ASSAY	123
4.2.5 DETERMINATION OF BACTERIAL VIABILITY BY PROPRIDIUM IODIDE STAINING	125
4.2.6 ATOMIC FORCE MICROSCOPY IMAGING OF BACTERIA FOLLOWING SYNCOLLIN TREATMENT	125
4.2.7 SCANNING ELECTRON MICROSCOPY (SEM) IMAGING OF BACTERIA FOLLOWING SYNCOLLIN TREATMENT	125

4.3 RESULTS	126
4.3.1 BINDING OF SYNCOLLIN TO PEPTIDOGLYCAN	126
4.3.2 EFFECT OF SYNCOLLIN ON BACTERIAL GROWTH	128
4.3.3 EFFECT OF SYNCOLLIN ON BACTERIAL GROWTH IN COMBINATION WITH ANTIBIOTICS.....	132
4.3.4 CHECKERBOARD ASSAY OF SYNCOLLIN/ANTIBIOTIC INTERACTIONS	134
4.3.5 DETERMINATION OF BACTERIAL VIABILITY BY PROPIDIUM IODIDE STAINING	135
4.3.6 ATOMIC FORCE MICROSCOPY IMAGING OF BACTERIAL SURFACES	138
4.3.7 DETERMINATION OF BACTERIAL VIABILITY USING SCANNING ELECTRON MICROSCOPY (SEM)	139
4.4 DISCUSSION	141
5. SYNCOLLIN NEUTROPHIL EXPRESSION AND BACTERIAL INTERACTION	143
5.1 INTRODUCTION	143
5.1.1 NEUTROPHIL GRANULES AND EXOCYTOSIS.....	143
5.2 METHODS.....	144
5.2.1 NEUTROPHIL ISOLATION.....	144
5.2.2 IMMUNOFLUORESCENCE	145
5.2.3 NEUTROPHIL ACTIVATION	146
5.2.4 ANALYSIS OF NEUTROPHIL ACTIVATION BY IMMUNOBLOTTING.....	147
5.2.5 IMAGING OF NEUTROPHILS AFTER ACTIVATION BY BACTERIAL INFECTION.....	147
5.3 RESULTS	147
5.3.1 SYNCOLLIN LOCALIZATION	147
5.3.2 SYNCOLLIN GRANULAR LOCALIZATION	149
5.3.3 SYNCOLLIN MOBILITY UPON NEUTROPHIL ACTIVATION	151
5.3.4 NEUTROPHIL NET STRUCTURES.....	153
5.3.5 BINDING OF SYNCOLLIN-STREP TO BACTERIA.....	155
5.3.6 BACTERIA AND NEUTROPHIL CO-STAINING.....	156
5.4 DISCUSSION	158
6. FINAL COMMENTS	159
7. REFERENCES	162
8. APPENDIX	178

LIST OF FIGURES & TABLES

Figure 1.1	Schematic diagram of a pancreatic acinar cell
Figure 1.2	Overview of intracellular protein traffic
Figure 1.3	SNARE protein involvement in exocytosis
Figure 1.4	Evidence for the involvement of syncollin in exocytosis
Figure 1.5	Mechanism of oligomerization of Bax/Bak, α -synuclein and perfringolysin O on membranes
Figure 1.6	Syncollin-membrane interactions
Figure 1.7	Three modes of operation of neutrophils
Figure 1.8	ZG16p structure and function
Figure 1.9	$\beta\gamma$ -crystallins
Figure 1.10	Bactericidal activity of RegIII
Figure 1.11	Anti-microbial actions of defensins
Table 1.1	Summary of anti-microbial proteins
Figure 2.1	SnapGene schematic of Strep-tagged syncollin sequence
Figure 2.2	Strep-Tactin XT™ affinity chromatography
Figure 2.3	Purification of syncollin-His ₆ from BL21 <i>E. coli</i>
Figure 2.4	Purification of syncollin-His ₆ purified from BL21 cells from inclusion bodies followed by refolding
Figure 2.5	Refolding of syncollin-His ₆ purified from BL21 inclusion bodies
Figure 2.6	Optimization of syncollin-His ₆ expression in T7 shuffle express cells.
Figure 2.7	Gel filtration analysis of syncollin-His ₆ isolated from T7 shuffle cells
Figure 2.8	Periplasmic expression of syncollin-His ₆ in Rosetta 2 cells
Figure 2.9	Binding of syncollin-His ₆ to syntaxin 2
Figure 2.10	Schematic diagram of the bac-to-bac baculovirus purification system
Figure 2.11	Insect cell expression of syncollin-Strep
Figure 2.12	Elution of syncollin-Strep from Strep-Tactin XT™ beads
Figure 2.13	Behaviour of syncollin-Strep on gel filtration columns
Figure 2.14	Immunoblot showing syncollin-Strep purified in the presence and absence of detergent (DDM)

Figure 2.15	Immunoblots of syncollin-Strep purified from mammalian cells and run in the presence and absence of β -mercaptoethanol (β ME).
Figure 2.16	Binding of syncollin-Strep to syntaxin 2
Figure 2.17	Purification of syncollin-Strep from HEK-293F cells in suspension HEK-293F
Figure 2.18	AFM imaging of syncollin-Strep in association with lipid bilayers.
Figure 2.19	Syncollin binding to liposomes
Figure 2.20	Time-course of oligomerization of syncollin-Strep
Figure 2.21	Permeabilization of erythrocytes by syncollin-Strep
Figure 2.22	Permeabilization of liposomes by syncollin-Strep
Table 2.1	Optimization of detergent conditions for purification of syncollin-His ₆ from T7 shuffle express cells
Table 2.2	Conditions trialed to facilitate the solubility of purified syncollin-Strep
Table 2.3	Table summarizing syncollin purification in mammalian, bacterial and insect cells.
Figure 3.1	Protein structure
Figure 3.1	Circular dichroism
Figure 2.3	Origins of the phase problem in X-ray crystallography
Figure 3.3	Predicted structure of syncollin based on sequence
Figure 3.4	Predicted characteristics of the syncollin molecule
Figure 3.6	Syncollin structure predicted using the public database for DeepMind's AlphaFold software
Figure 3.7	CD spectroscopy of syncollin
Figure 3.8	Crystallization of syncollin-Strep
Figure 3.9	Syncollin homology logo
Figure 3.10	Design of syncollin mutants based on the predicted structure
Figure 3.11	Biochemical properties of syncollin-Strep cysteine mutants Cys23Gly (1), Cys38Gly (2), Cys52Gly (3) and Cys86Gly (4)
Figure 3.12	Brain liposome permeabilization and BCECF release
Figure 3.13	CD temperature ramps of syncollin-Strep and the cysteine mutants by syncollin-Strep and cysteine mutants
Figure 3.14	Changes in CD spectra with temperature
Figure 3.15	Liposome permeabilization by positive charge mutants
Figure 3.16	Denaturation of syncollin
Figure 3.17	Syncollin solubilization with DIBMA

Figure 3.18	Hydrodynamic radius of syncollin-GFP
Figure 4.1	Schematic diagram illustrating the differences between Gram-positive and Gram-negative bacterial cell walls
Figure 4.2	Schematic diagram of bacterial growth
Figure 4.3	Diagram illustrating the various antibiotic targets
Figure 4.4	Checkerboard assay
Figure 4.5	Syncollin binds to PGN (1)
Figure 4.6	Syncollin binds to PGN (2)
Figure 4.7	Effect of syncollin-Strep on the growth of <i>L. lactis</i>
Figure 4.8	Effect of syncollin-Strep on the growth of <i>E. coli</i>
Figure 4.9	Control for the presence of protein in the bacterial growth assay
Figure 4.10	Effect of syncollin-Strep on the growth of <i>L. lactis</i> in combination with antibiotics
Figure 4.11	Effect of syncollin-Strep on the growth of <i>E. coli</i> in combination with antibiotics
Figure 4.12	Checkerboard assay to investigate the interaction between syncollin-Strep and antibiotics on <i>L. lactis</i>
Figure 4.13	Effect of syncollin-Strep addition on bacterial viability
Figure 4.14	AFM analysis of the effects of syncollin-Strep on the structure of <i>E. coli</i> (A) and <i>L. lactis</i> (B)
Figure 4.15	SEM analysis of the effects of syncollin-Strep on bacterial structure
Figure 5.1.	Syncollin expression in isolated human neutrophils
Figure 5.2.	Granular localization of syncollin
Figure 5.3.	Effect of activation on syncollin staining in neutrophils
Figure 5.4.	Quantitation of syncollin secretion from activated neutrophils
Figure 5.5.	Immunoblot analysis of syncollin release from activated neutrophils
Figure 5.6.	<i>E. coli</i> -activated neutrophil immunofluorescence
Figure 5.7	Syncollin-Strep binds the bacterial surface
Figure 5.8	Decoration of bacteria by syncollin secreted by activated neutrophils
Table 5.1	Summary of antibodies (primary and secondary) used for neutrophil immunofluorescent studies

LIST OF ABBREVIATIONS

ABCG	ATP Binding Cassette Superfamily G
AFM	Atomic force microscopy
AMP	Anti-microbial protein/peptide
APBS	Adaptive Poisson-Boltzmann Solver
APC	allophycocyanin
AZ	AstraZeneca
β -ME	β -mercaptoethanol
β -OG	n-octyl-beta-D-glucopyranoside
β -PFP	Beta-pore forming protein
BCECF	(2',7'-Bis-(2-Carboxethyl)-5-(and-6)-carboxyfluorescein, acetoxymethyl ester)
BCL2	B-cell lymphocyte 2
BSA	Bovine serum albumin
CAC	Colitis-associated cancer
cAMP	Adenosine 3', 5'-cyclic monophosphate
CCD	Charge-coupled device
CD	Circular dichroism
CHAPS	(3-((3-cholamidopropyl)dimethylammonio)-1-propanesulfonate)
Cryo-EM	Cryo-electron microscopy
CSP	Cysteine string protein
CTLTD	C-type lectin type domain
DAPI	4',6'-diamidino-2-phenylindole dihydrochloride
DCG	Dense core granule
DDM	Dodecylmaltoside
DIBMA	Diisobutylene maleic acid
DIC	Differential interference contrast
DMEM	Dulbecco's modified Eagle medium
DNA	Deoxyribonucleic acid
DSS	Dextran sodium sulfate
DSS	Disuccinimidyl suberate

DTE	Dithioerythritol
<i>E. coli</i>	<i>Escherichia coli</i>
ECL	Enhanced chemiluminescence
ECM	Extracellular matrix
EDTA	Ethylenediaminetetraacetic acid
ER	Endoplasmic reticulum
FBS	Fetal bovine serum
FIC	Fractional inhibitory concentrations
FITC	Fluorescein isothiocyanate
GFP	Green fluorescent protein
GnHCL	Guanidine hydrochloride
GP2	Glycoprotein 2
GPI	Glycosyl-phosphatidyl inositol
GST	Glutathione S- transferase
HABA	4'-hydroxyazobenzene-2-carboxylic acid
HBS	HEPES-buffered saline
HEK	Human embryonic kidney
HEPES	4-(2-hydroxyethyl)-1-piperazineethanesulfonic acid
HRP	Horseradish peroxidase
HSC70	Heat shock cognate protein 70
HT	High tension
IBD	inflammatory bowel disease
IP3	Inositol trisphosphate
IPTG	Isopropyl- β -D-thiogalactoside
kDa	KiloDalton
KO	Knock out
<i>L. lactis</i>	<i>Lactococcus lactis</i>
LB	Luria Bertoni
LPS	Lipopolysaccharide
MIC	Minimum inhibitory concentrations
MPO	Myeloperoxidase
mRNA	Messenger RNA

NADPH	Nicotinamide adenine dinucleotide phosphate
NDSB	Non-detergent sulfolbetaine
NET	Neutrophil extracellular trap
NG	Nonylglucoside
NSF	N-ethylmaleimide-sensitive factor
OD	Optical density
PAMP	Pathogen-associated molecular pattern
PAP2	Pancreatitis-associated protein 2
PBP	Penicillin binding protein
PBS	Phosphate-buffered saline
PC	Phosphatidylcholine
PCR	Polymerase chain reaction
PDB	Protein data bank
PE	Phosphatidylethanolamine
PEI	Polyethyleneimine
PES	Polyethersuphone
PFA	Paraformaldehyde
PFO	Perfringolysin O
PG	Phosphatidylglycerol
PGN	Peptidoglycan
PI	Propidium iodide
PI-PLC	Phosphoinositide-phospholipase C
PMSF	Phenylmethylsulphonyl fluoride
PS	Phosphatidylserine
REG	Regenerating islet derived
RIPA	Radioimmunoprecipitation assay buffer
RNA	Ribonucleic acid
RNAse A	Ribonuclease
ROS	Reactive oxygen species
RPMI	Roswell Park Memorial Institute
SAD/MAD	Single/multiple- wavelength anomalous dispersion
SDS-PAGE	Sodium dodecyl sulphate polyacrylamide gel electrophoresis

SEM	Scanning electron microscopy
SIR/MIR	Single/multiple isomorphous replacement
SM	Sphingomyelin
SNARE	Soluble N-ethylmaleimide-sensitive factor attachment protein receptor
SOC	Super optimal broth with catabolite repression
TBS	Tris-buffered saline
TBST	TBS containing 0.1% (v/v)Tween-20
TCEP	Tris (2-carboxyethyl)phosphine
TEM	Transmission electron microscopy
TEV	Tobacco etch virus
TGN	Trans-Golgi network
TMD	Transmembrane domain
tRNA	Transfer ribonucleic acid
t-SNARE	Target SNARE
UC	Ulcerative colitis
VIP	Vasoactive intestinal peptide
v-SNARE	Vesicular SNARE
WT	Wild type
X-GAL	5-bromo-4-chloro-3-indolyl- β -D-galactopyranoside
ZG	Zymogen granule

1. INTRODUCTION

Syncollin is a 16-kilodalton (kDa) protein that was originally identified in a search for a vesicular soluble N-ethylmaleimide-sensitive factor (NSF) attachment protein receptor (v-SNARE) on the membrane of the pancreatic zymogen granule (ZG). Syncollin was found to bind to the target SNARE (t-SNARE) syntaxin in a Ca^{2+} -sensitive manner, suggesting that it might play a role in ZG exocytosis (Edwardson *et al.*, 1997). It was soon realized, however, that syncollin was located on the luminal side of the ZG membrane, where it existed both tightly bound to the ZG membrane and also free in the ZG lumen (An *et al.*, 2000). This finding cast serious doubt on the physiological significance of its interaction with syntaxin. Syncollin is in fact a secretory protein, albeit one with unusual properties. This dissertation deals with the structure and function of syncollin; however, before considering in detail what was known about the protein at the outset of my investigations, I will first discuss the pathway taken by syncollin in the pancreatic acinar cell, from its synthesis on the endoplasmic reticulum (ER) membrane to its packaging in the ZG.

1.1 THE PANCREAS AND ACINAR CELLS

The pancreas is an essential organ consisting of two components: the endocrine pancreas, required for the control of blood sugar via the release of hormones, and the exocrine pancreas, required for digestion of foods via the release of digestive enzymes.

The endocrine pancreas consists of diffusely distributed islets of Langerhans, which are responsible for the release of hormones into the bloodstream. Two main hormones are required for the control of blood sugar levels: insulin, released from pancreatic beta cells, which lowers blood sugar levels, and glucagon, released from pancreatic alpha cells, which raises them. If blood sugar levels deviate significantly from the norm, this is detected by glucose sensing cells in the brain, which control the release of the two hormones. When blood sugar is too high, insulin stimulates glucose uptake into adipose cells; when blood sugar is too low, glucagon triggers glucose release by hepatocytes (Röder *et al.*, 2016).

The exocrine pancreas accounts for the majority of the pancreatic tissue, and consists of acinar cells arranged in spherical structures (acini). These cells are responsible for the synthesis of digestive enzymes and their release via ZG exocytosis, as illustrated in Figure 1.1. The digestive enzymes include trypsin and chymotrypsin, which digest polypeptides; amylase, which digests carbohydrates; and lipases, which digest fatty acids. Many of these enzymes are stored in the ZGs as inactive zymogens, which are activated by proteolysis after their release from the acinar cells (Pandol, 2010).

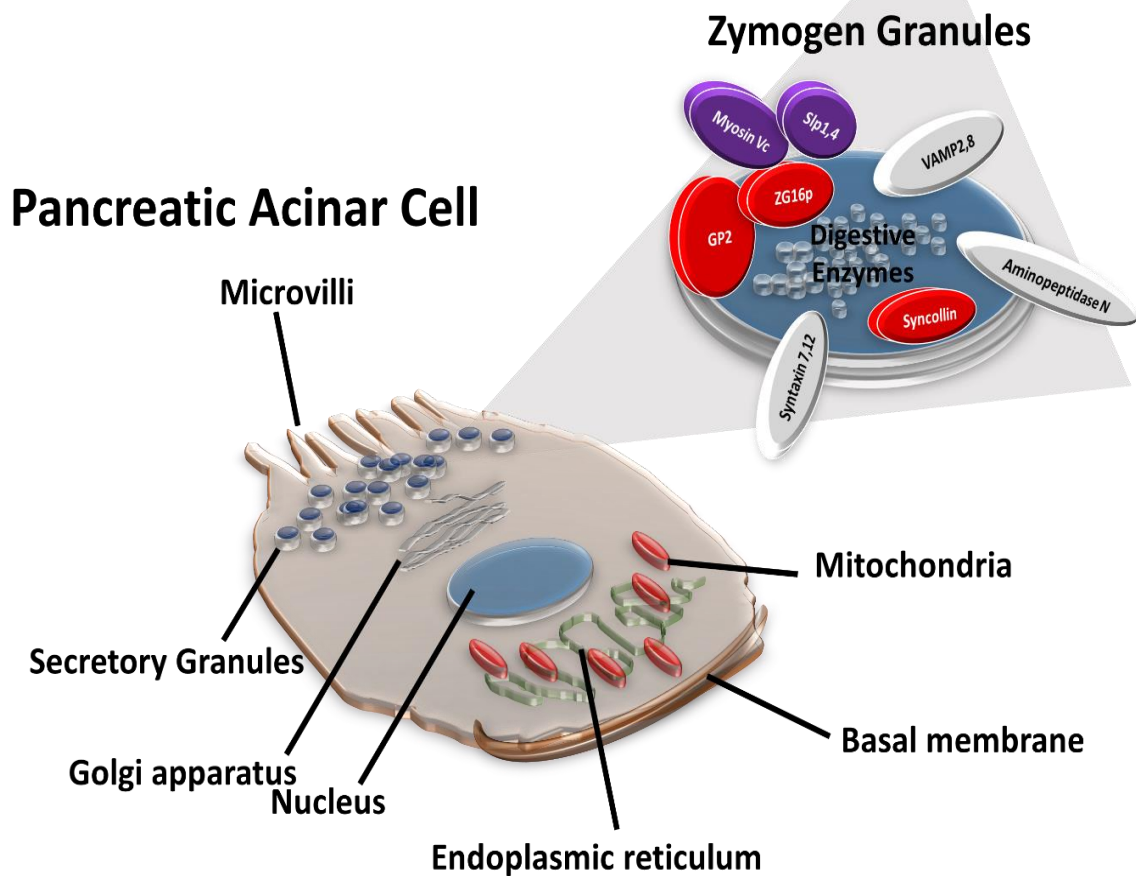


Figure 1.1. Schematic diagram of a pancreatic acinar cell. The cell is polarized, with apical and basolateral plasma membrane domains. Secretory (zymogen) granules (ZGs) are located in the apical region of the cell in preparation for exocytosis. The ZGs contain digestive enzymes, some as inactive precursors, which will be secreted upon exocytosis. The ZG membranes contain many proteins that serve various purposes. Examples include proteins exposed on the luminal side of the ZG membrane (red) such as GP2 and syncollin, and transmembrane proteins such as vesicle-associated membrane proteins (VAMPs) 2 and 8 and syntaxins 7 and 11. Proteins present on the basolateral membrane include myosin Vc and Slp 1 and 4. Adapted from Chen (2018); Logsdon and Ji (2013).

1.2 THE ER-TO-GOLGI PATHWAY

Proteins destined for packaging into ZGs for exocytosis are synthesized on ribosomes bound to the rough ER. As mRNA encoding a secretory protein is translated into an amino acid chain in the cytosol, the signal peptide becomes bound by a signal recognition particle and the whole complex then docks onto a signal recognition particle receptor in the ER membrane (Cooper, 2000). Protein translocation sites (translocons) then mediate the passage of the nascent polypeptide into the ER lumen, where the

signal sequence is cleaved by a signal peptidase (Lodish *et al.*, 2000). Once the protein has entered the lumen of the ER, various modifications can occur, including N-linked glycosylation, disulphide bond formation and oligomerization, all of which may be involved in enhancing protein stability, correct folding, and efficient intracellular transport. Once processed, the protein is then packaged into COPII-coated transport vesicles which pinch off the ER at exit sites that lack ribosomes. Providing the proteins are correctly folded, the secretory proteins can now enter the secretory pathway and be directed to the Golgi apparatus. If there is incorrect folding or oligomerization, the proteins are retained in the ER and bound by chaperones which prevent their exit (Benham, 2012; Schwarz and Blower, 2016).

Following exit from the ER, the transport vesicles enter an ER-Golgi intermediate compartment. This structure is poorly understood but is thought to consist of mobile transport complexes that can shuttle the proteins from the ER to the Golgi apparatus. The Golgi apparatus consists of a stack of cisternae (flattened membrane sacs), and is polarized, with two faces - *cis* and *trans*. Incoming vesicles enter the Golgi at its *cis* face. Secretory proteins then pass then through the *medial* Golgi en route to the *trans* face. There is still dispute about whether protein progression through the Golgi occurs via sequential budding and fusion of vesicles, or whether the cisternae themselves undergo a process of maturation (according to the 'cisternal progression' model). Whatever the mechanism of transport, the proteins usually undergo various further modifications, for example changes in their glycosylation state, during intra-Golgi transport. Following their exit from the *trans*-Golgi, the proteins enter a structure known as the *trans*-Golgi network (TGN), where sorting occurs for delivery to various intracellular destinations. In this compartment, secretory proteins are directed towards the plasma membrane for eventual release via exocytosis (Cooper, 2000).

The mechanism by which vesicles traffic within the cell cytoplasm is widely debated. There is much evidence for the involvement of the cytoskeleton, and in particular for a role for microtubules in the delivery of vesicles to the plasma membrane (Noordstra and Akhmanova, 2017).

1.3 ZYMOGEN GRANULE FORMATION

In order for digestive enzymes to be packaged into ZGs for regulated exocytosis, they need to be sorted and packaged away from constitutively secreted proteins (see below). There are two models for granule sorting: sorting-for-entry and sorting-by-retention. Sorting-for-entry involves the selection of regulated secretory proteins at the TGN, via interactions with 'receptors', before packaging of the proteins into granules. Sorting-by-retention on the other hand, occurs by default and is much less specific, involving aggregation of granule proteins in the environment within the TGN lumen (acidic,

oxidizing, high-Ca²⁺), leading to the formation of dense-core granules (DCGs). In the DCGs, further maturation and sorting occurs to exclude constitutively secreted proteins. The DCGs then bind to specific regions of the TGN membrane to initiate exocytosis of immature secretory vesicles (condensed vacuoles), which pinch off and undergo further maturation into ZGs (Wäsle and Edwardson, 2002; Chen, 2018; Hummer *et al.*, 2020).

Sorting of regulated and constitutively secreted proteins in the TGN is facilitated by additional proteins, including glycoprotein-2 (GP2). GP2 is the most abundant ZG protein and is attached to the luminal surface of the ZG membrane via a glycosyl-phosphatidyl inositol (GPI) anchor. It is believed that the sorting activity of GP2 is promoted by its ability to form pH-dependent complexes, a process that occurs upon release of the protein from the ZG membrane during exocytosis, through the activity of phosphoinositide-phospholipase C (PI-PLC). GP2, in combination with sulphated proteoglycans and other glycoproteins in the ZG, forms the sub-membranous matrix which contributes to protein sorting. In particular, sulphated proteoglycans promote sorting and aggregation of secretory proteins via electrostatic interactions: negatively-charged sulphated proteoglycans bind positively-charged protein groups, such as amines and peptidases, which facilitate sorting by specifically binding the carbohydrate domains of secretory proteins. The sub-membranous matrix is thought to facilitate the binding of DCGs to the ZG membrane in a process mediated by the protein ZG16p. ZG16p forms stable dimers; it is protease-resistant and binds to DCG and ZG membranes under acidic conditions, thereby acting as a linker between the two. The key role of ZG16p and proteoglycans in ZG formation is illustrated by the fact that in their absence, the sub-membranous matrix breaks down and the sorting of proteins into the ZG becomes less efficient (Kleene *et al.*, 1999; Aroso *et al.*, 2015).

As for GP2, the sub-membranous matrix is released from the ZG during exocytosis in response to exposure to a basic environment and through the action of PI-PLC. Significantly, GP2 is not indispensable for protein sorting in the pancreatic acinar cell, because ZGs form in its absence (Kleene *et al.*, 1998; Chen, 2018). Other proteins must therefore be involved. These so-called 'helper proteins' include ZG16p, chymase, cyclophilin B, RNase A and carboxyl ester lipase (Aroso *et al.*, 2015).

Although this dissertation focuses on exocytotic membrane fusion, it is important to note that exocytosis is not the only type of membrane fusion. Mitochondria and the endoplasmic reticulum, for example, undergo fusion events mediated by GTPase proteins, mitofusin and atlastin, respectively (Moon and Jun, 2020).

1.4 EXOCYTOSIS AND ENDOCYTOSIS

As mentioned above, there are two broad categories of exocytosis: constitutive and regulated. In constitutive exocytosis, budded vesicles fuse continuously with the plasma membrane without the requirement for additional signals. This process occurs in all cell types and is important when continuous delivery of proteins (e.g. integral proteins) to the plasma membrane is required. Regulated exocytosis is less common and occurs in specialized secretory cells, such as epithelial cells, which may release large quantities of secretory products, such as hormones, in response to a specific stimulus, such as an intracellular signal initiated by the binding of a ligand at a cell-surface receptor (Alberts *et al.*, 2002). Three types of regulated exocytosis are recognised. In 'kiss-and-run' exocytosis, the secretory vesicle fuses with the plasma membrane only temporarily and a fusion pore opens to permit content release. The fusion pore then closes and the vesicle remains intact. In the more 'conventional' type of regulated exocytosis, the secretory vesicle collapses fully into the plasma membrane in order to release its contents. Finally, in compound exocytosis, one vesicle fuses with the plasma membrane, releasing its contents, and then further vesicles lying deeper within the cytoplasm fuse with the first vesicle in order to amplify content release. Compound exocytosis occurs in cell types in which large amounts of secretory material need to be released over a short time in response to a stimulation; in this case the membrane surface area over which release occurs is greatly increased by the fusion between vesicles (Wu *et al.*, 2014). The three types of exocytosis discussed above are illustrated in Figure 1.2.

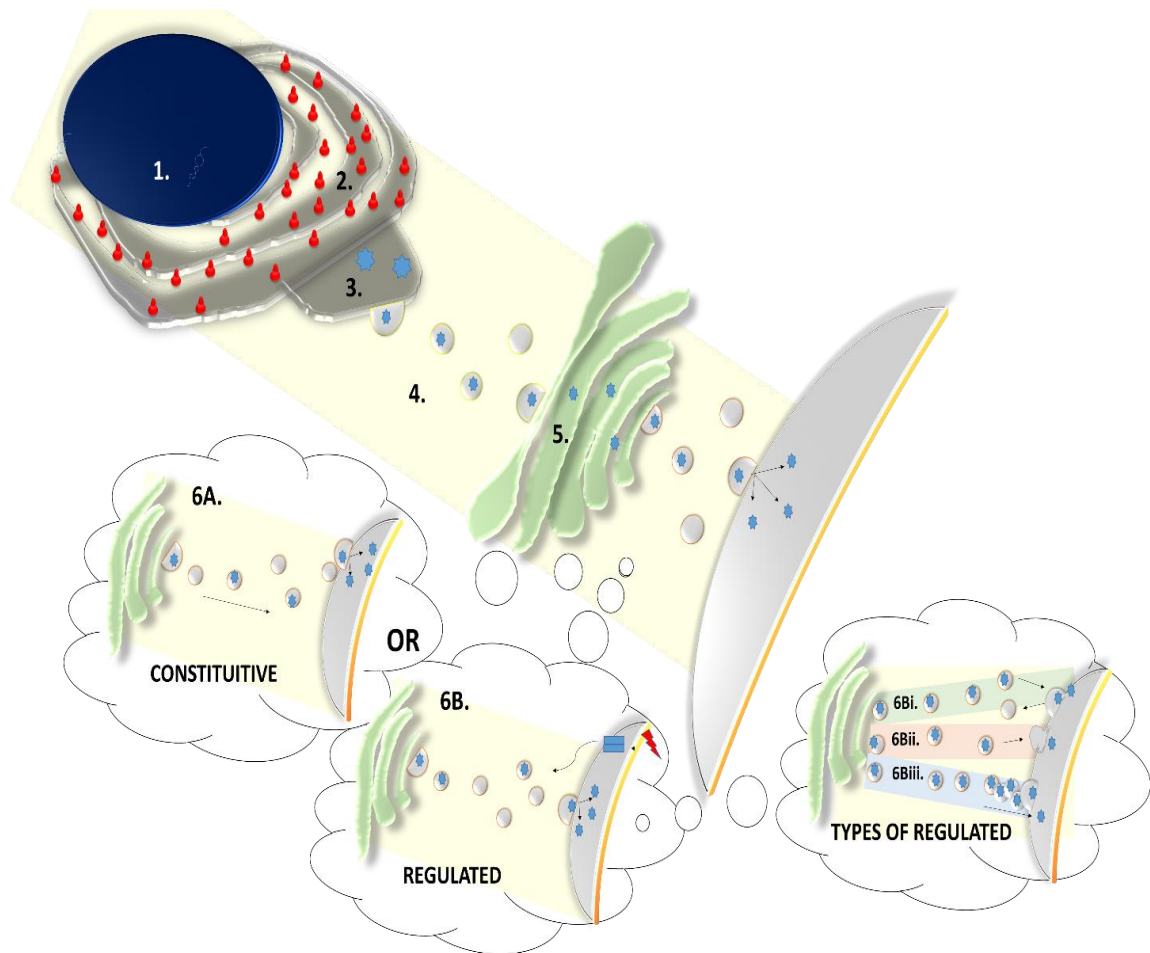


Figure 1.2. Overview of intracellular protein traffic. 1. Deoxyribonucleic acid (DNA) in the nucleus is transcribed into messenger ribonucleic acid (mRNA). 2. In the cytoplasm, mRNA binds to ribosomes attached to the rough ER. mRNA is translated and newly-synthesized proteins are passed into the ER via translocon protein transporters. 3. In the ER, proteins may undergo particular modifications, including signal sequence cleavage, oligomerization and disulphide bond formation. Proteins exit the ER via a ribosome-free region in COPII-coated budding vesicles. 4. COP II-coated vesicles are transported to the Golgi apparatus either by diffusion or transport on microtubules. 5. Proteins pass through the Golgi apparatus, receiving further modifications such as modification of glycosylation before leaving the Golgi via its *trans* face in their mature form. Exocytosis can be either constitutive (6A) or regulated (6B). Constitutive exocytosis occurs in all cell types and does not require a stimulus; rather, secretory vesicles are constantly delivered from the Golgi to the plasma membrane. This route is used when rapid, pulsatile delivery is not required (e.g. for proteins destined for delivery to the plasma membrane). Regulated exocytosis occurs where release is required in response to a stimulus (e.g. in secretion of enzymes or hormone release). Exocytosis is often triggered through the action of a ligand at a cell-surface receptor. Regulated exocytosis can occur through a kiss-and-run mechanism (6Bi), which involves the opening and closing of a fusion pore, membrane collapse (6Bii), where the secretory vesicle fuses completely with the plasma membrane, and finally compound exocytosis (6Biii), where content release involves granule-granule fusion. Adapted from Bonifacino and Glick (2004); Revelo *et al.* (2019); Wu *et al.* (2014).

Following exocytosis of the vesicle and the release of vesicle contents, membrane and associated proteins are recaptured by endocytosis. Membrane collapse into the plasma membrane is followed by the classical type of endocytosis involving clathrin-mediated invagination of the plasma membrane and dynamin-driven budding off of a nascent vesicle. Endocytosis following compound exocytosis results in more extensive membrane invaginations, in order to recapture the additional membrane delivered to the cell surface. In kiss-and-run exocytosis, the opening and closing of the fusion pore does not result in the delivery of new membrane to the cell surface, and hence endocytosis is not required (Wu *et al.*, 2014; Liang *et al.*, 2017).

1.5 THE SNARE PROTEIN FAMILY

The fusion of the secretory granules with the plasma membrane in exocytosis, is mediated by the SNARE family of proteins. Within this protein family are the v-SNAREs, present on the vesicle, and the t-SNAREs, present on the target membrane. The v- and t-SNAREs 'zipper up' through the formation of a four-helix bundle between the two membranes, bringing them into close proximity. In neurons, where the mechanism underlying exocytosis is best understood, the bundle is composed of one helix from the v-SNARE synaptobrevin, one helix from the t-SNARE syntaxin and two helices from the t-SNARE SNAP-25 (Figure 1.3).

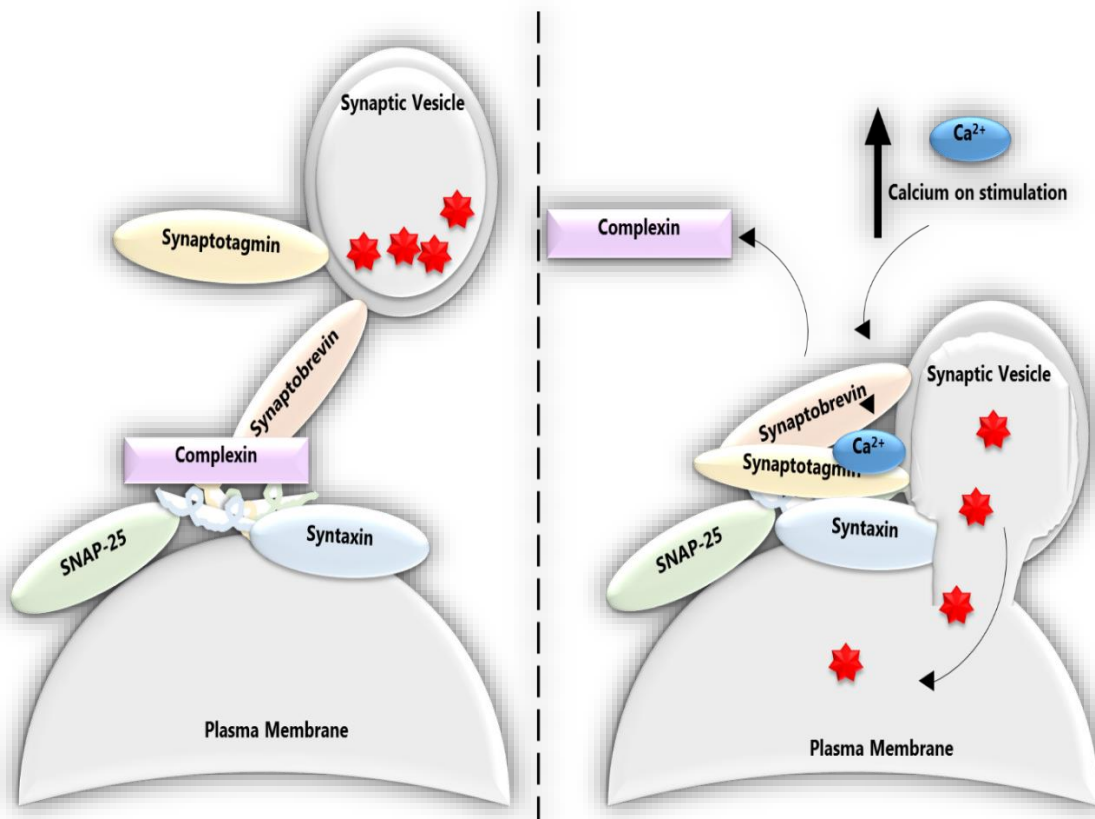


Figure 1.3. SNARE protein involvement in exocytosis. Left; before fusion is triggered. Synaptotagmin is present on the synaptic vesicle and the SNARE four-helix bundle, composed of synaptobrevin, syntaxin and SNAP-25 spans the gap between the vesicle and the plasma membrane. Complexin may act as a physical barrier, preventing completion of fusion. Right; after triggering of fusion. Ca^{2+} binds to the two C2 domains on synaptotagmin, which facilitates the removal of complexin and the association of synaptotagmin with the primed SNARE complex. Membrane fusion can now occur, leading to the release of the secretory granule contents. Adapted from Carr and Munson (2007).

Initiation of exocytosis in neurons begins with an action potential depolarizing the pre-synaptic membrane, resulting in the opening of voltage-sensitive Ca^{2+} channels. The incoming Ca^{2+} binds to synaptotagmin, a Ca^{2+} -sensing protein in the vesicle membrane. Ca^{2+} -loaded synaptotagmin displaces complexin from the primed SNARE complex, allowing completion of the zippering up of the SNARE complex and subsequent fusion between the docked vesicle and the plasma membrane. The vesicle contents are then released from the nerve terminal (Figure 1.3; Palfreyman and Jorgensen, 2008). In neurons and neuroendocrine cells, additional proteins have been found to be essential for priming of the SNARE complex on the membrane, including Munc-13 and CAPS, amongst others (James and Martin, 2013).

1.6 EXOCYTOSIS IN THE PANCREATIC ACINAR CELL

The mechanism of exocytosis in pancreatic acinar cells shows some similarities with, but also important differences from, exocytosis in neurons. For instance, in the acinar cell SNAREs account for only 0.1% of total cellular proteins, compared with 1% in neuro-endocrine cells. On the ZG membrane, the principal SNAREs are synaptobrevins 8 and 2, and syntaxin 3 (Williams and Yule, 2012). Syntaxin 3 is involved in ZG-ZG fusion during compound exocytosis, and cleavage of syntaxin 3 results in a 50% reduction in granule fusion (Hansen *et al.*, 1999). Two other syntaxin isoforms are present in acinar cells: syntaxin 2 on the apical membrane and syntaxin 4 on the basolateral membrane (Hansen *et al.*, 1999; Messenger *et al.*, 2014). SNAP-23 (a homologue of the neuronal and neuroendocrine SNAP-25) is found on the basolateral membrane, and SNAP-29 is present on both the ZG membrane and the apical plasma membrane. Synaptobrevin 8 is the predominant v-SNARE involved in regulated fusion between ZGs and the plasma membrane (Weng *et al.*, 2007) and also in compound exocytosis, whereas synaptobrevin 3 is involved in constitutive exocytosis. Under pathological conditions, for example in pancreatitis, ZGs can fuse with the basolateral plasma membrane in a process mediated by syntaxin 4, SNAP 23 and synaptobrevin 8 (Messenger *et al.*, 2014). Note that during exocytosis the ZG membrane does not collapse into the plasma membrane, unlike the situation in neurons (Hansen *et al.*, 1999; Dolai *et al.*, 2012).

During membrane fusion SNARE proteins require assistance from the so-called SM proteins. These are hydrophilic proteins containing ~600 amino acids in size with no known recognizable motifs. They form SM/*trans*-SNARE complexes with v-SNAREs and t-SNAREs (Carr and Rizo, 2010). The SM proteins act as chaperones for syntaxin, allowing it to enter the SNARE complex. In the acinar cell, the main SM proteins are Munc18b and Munc18c. Cab45b is a Ca²⁺-binding protein in the Golgi apparatus, which binds to Munc18b with a higher affinity in the presence of Ca²⁺ and contributes to the Munc18b-syntaxin interactions described above. Mutations in Cab45 that interfere with Munc-18b binding, result in inhibited Ca²⁺-stimulated exocytosis; hence, Cab45b is classed as an essential Ca²⁺ sensor for exocytosis in the acinar cell (Dolai *et al.*, 2012; Messenger *et al.*, 2014).

As in neuro-endocrine cells, complexin 2, present on the apical membrane, must be displaced during stimulation of the acinar cell to allow the formation of a 'primed' state. Other proteins involved include synaptotagmin 1, on ZG and apical plasma membranes and synaptotagmins 3, 6 and 7 in acini, which act as the Ca²⁺ sensors to initiate the final fusion event. In addition to the synaptotagmins, cysteine-string protein (CSP)- α on the ZG membrane interacts with the chaperone heat shock cognate protein 70 (HSC70) to modulate SNARE behaviour (Dolai *et al.*, 2012).

As in neurons, Ca^{2+} is a key trigger for exocytosis in acinar cells. However, acinar cells do not express voltage-gated Ca^{2+} channels in their plasma membranes; rather, Ca^{2+} is released into the cytosol from ER stores. G protein-coupled receptors are located on the basolateral membrane of the acinar cell, and control exocytosis at the apical membrane. For example, activation of G_q -coupled muscarinic receptors (both M_1 and M_3) by acetylcholine causes an increase in cytosolic levels of inositol trisphosphate (IP_3), which acts on IP_3 receptors in the ER membrane to cause Ca^{2+} release. Ryanodine receptors are also involved in sustaining Ca^{2+} -induced Ca^{2+} release. Activation of the muscarinic receptor also causes increased levels of diacylglycerol, which can activate protein kinase C. Cholecystokinin acting via its own G_q -coupled receptor initiates a similar signalling pathway. Separately, vasoactive intestinal peptide (VIP) can activate its receptor which is G_{α_s} -coupled, causing an increase in cyclic adenosine monophosphate (cAMP) levels, which in turn results in activation of protein kinase A (Pandol, 2010). Protein kinases are thought to trigger exocytosis by phosphorylating effector proteins such as protein kinase C, which is thought to result in site-specific phosphorylation of SNAP-25 and Munc18, thereby facilitating exocytosis (Morgan *et al.*, 2005). During exocytosis, the contents of the ZGs are released into the pancreatic duct, where some of the digestive enzymes are proteolytically cleaved and activated (Li *et al.*, 2014). The pancreatic duct then takes the pancreatic juice into the common bile duct and from there into the duodenum where digestion occurs.

1.7 SYNCOLLIN AND EXOCYTOSIS

Although it is very unlikely that its interaction with syntaxin (the means by which it was discovered) is physiologically relevant (Figure 1.4A-C), there is evidence that syncollin does play a role in exocytosis in the pancreatic acinar cell, although it is also expressed in other tissues (Figure 1.4D), based on the phenotype of a syncollin knockout (KO) mouse (Wäsle *et al.*, 2005). The mice were viable and fertile; however, the pancreas was specifically hypertrophied and had a paler appearance than a wild type (WT) pancreas, suggesting that the acinar cells might contain more ZGs (which are white when isolated; Figure 1.4E). When exocytotic events were monitored at the single-acinus level via the uptake of the dye calcium green dextran through opening fusion pores, there was no significant reduction in the overall number of exocytotic events; however, compound exocytosis was significantly compromised, consistent with a role for syncollin in ZG-ZG fusion (Figure 1.4F-I). Note however that an alternative explanation of this result is that the absence of syncollin from the luminal surface of the ZG membrane, where it is normally present in high quantities, might simply destabilize the membrane in some way that indirectly affects membrane fusion. The observation that syncollin expression in the rat duodenum falls when animals are fasted and rises above control levels upon feeding, (Tan and Hooi, 2000) could also suggest a role in the secretion of digestive enzymes.

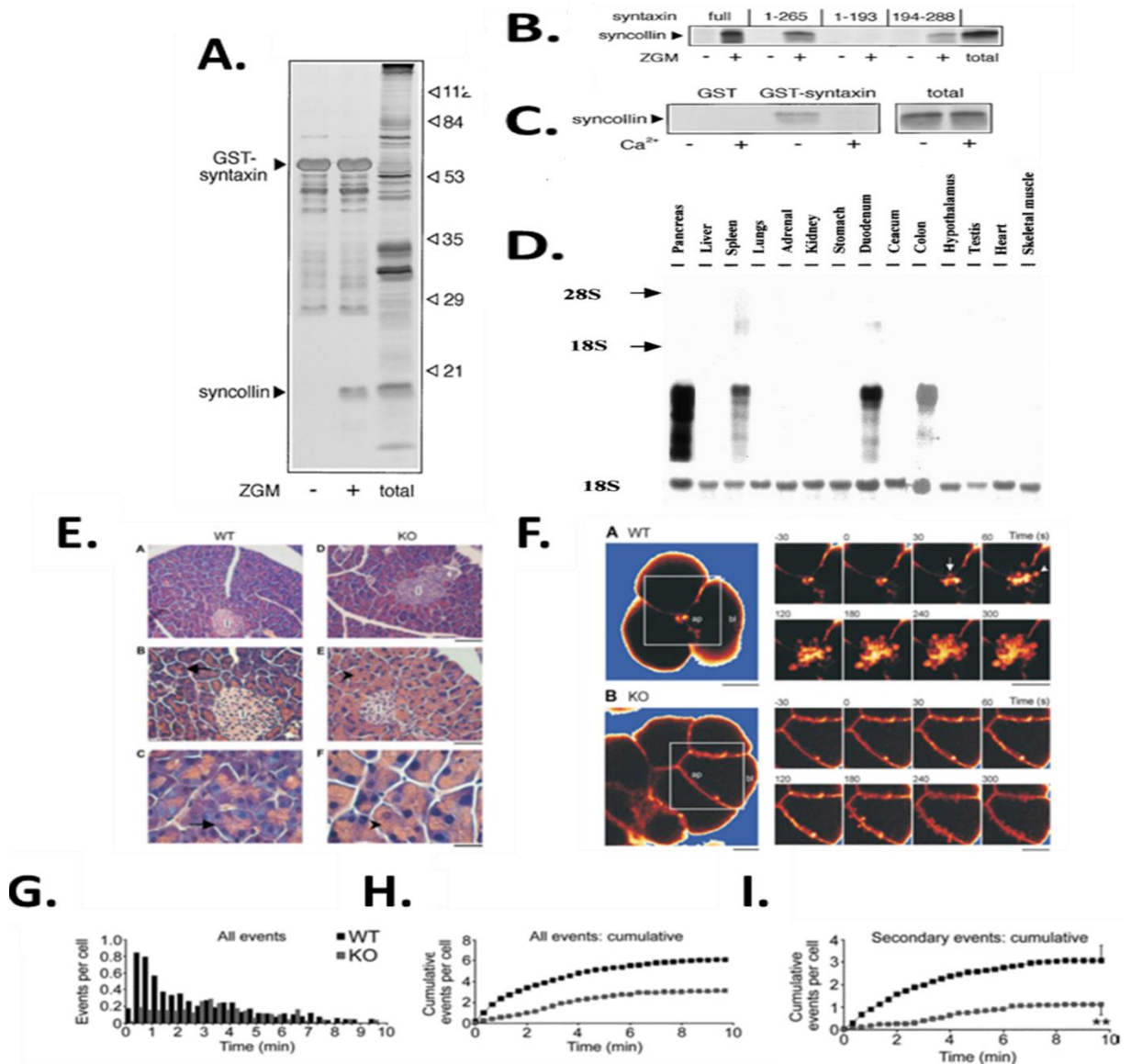


Figure 1.4. Evidence for the involvement of syncollin in exocytosis. A. Syncollin (16 kDa) from a detergent extract of ZG membranes binds to GST-syntaxin 1A immobilized on glutathione agarose, as shown on a silver-stained gel (Edwardson *et al.*, 1997). B. Syncollin binds to the SNARE motif, located towards the C-terminal end of syntaxin 1A (Edwardson *et al.*, 1997). C. Syncollin binds to GST-syntaxin in the absence but not in the presence of Ca^{2+} (Edwardson *et al.*, 1997). D. Syncollin expression profile, as shown by northern blotting. Syncollin is expressed at differing levels in the pancreas, spleen, duodenum and colon (Tan and Hooi, 2000). E. Appearance of the pancreas in syncollin KO mouse. Haematoxylin and eosin staining of a pancreas section shows more extensive pink areas (ZGs) in the syncollin KO mouse (Wäsle *et al.*, 2005). F. Visualization of exocytosis in pancreatic acinar cells. The membrane-impermeant dye calcium green was added to acinar cells before stimulation with acetylcholine. Upon fusion of granule and membrane, dye entered the granule and could be visualized (Wäsle *et al.*, 2005). G-I. Analysis of exocytotic events in F. The total number of exocytotic events in acini from KO and WT mice was not significantly different (G, H); however compound exocytotic events were significantly reduced in the KO mouse (I; Wäsle *et al.*, 2005).

Interestingly, the form of digestion in herbivores has been found to affect syncollin gene expression, in particular whether the herbivores are hindgut or foregut fermenters. The gene SYCN has been lost in herbivores including the naked mole rat, the domestic guinea pig, the horse, the rhinoceros and African and Asian elephant; however, it is present in other herbivores, including the rabbit, the alpaca, the cow, the bison and the goat (Hecker *et al.*, 2019). The species which have lost the syncollin gene are generally hindgut fermenters whereas those which have retained it are foregut fermenters. A fundamental difference between hindgut and foregut fermenters is the location of digestion and microbial action. Foregut fermenters contain a forestomach, which is a pre-gastric fermentation chamber, where the microbes are housed and where digestion occurs. The main method for digestion in foregut fermenters is regurgitation, where large particles which are not broken down in the rumen of the forestomach (non-cellulose) are able to float into and collect in the reticulum before regurgitation and travel back to the mouth in order to repeat this cycle. This cycle of breakdowns ensures that eventually particles get passed onto the intestine. In contrast, hindgut fermenters have enlarged compartments in the caecum and colon, permitting initial digestion in the stomach before further digestion in the enlarged caecum and finally fermentation and absorption in the large intestine (Mackie, 2002).

Although syncollin appears to have links to exocytosis and in particular to digestion, other possibilities can be envisaged, such as a role in host defence (see below). As syncollin is known to bind to membranes, the lipid bilayer and other membrane binding proteins will be discussed next.

1.8 THE LIPID BILAYER

According to the 'fluid mosaic model', biological membranes consist of a mobile 2D array of lipids in which embedded and peripheral proteins are free to diffuse. The particular composition of the membrane varies depending on the cell type and location, but in all cases the plasma membrane acts as a barrier between intracellular and extracellular compartments, and also plays additional roles, for example in protein scaffolding and cell signalling (Nicolson, 2014).

Lipids constitute 50% of a typical membrane by weight. Phospholipids are amphipathic, with hydrophilic head-groups and hydrophobic hydrocarbon tails. Because of this amphipathic property, phospholipids in an aqueous solution will spontaneously form bilayers, in which the head-groups are exposed to the solution and the hydrocarbon tails are shielded in the centre of the bilayer. The central hydrophobic barrier renders the membrane almost impermeable to water and ions, so that passage of water and ions across the membrane requires specialized channel and carrier proteins. The long

hydrocarbon chains of the phospholipids often contain unsaturated carbon-carbon bonds, which have a kinked structure. This in turn reduces the tightness of the lipid packing, thus conferring membrane fluidity (Opekarová and Tanner, 2003).

The four major phospholipids in the membranes of mammalian cells are phosphatidylcholine (PC), phosphatidylethanolamine (PE), phosphatidylserine (PS) and sphingomyelin (SM; Pichot *et al.*, 2013). It should be borne in mind, however, that even relatively minor phospholipids, such as phosphatidylinositol-4,5-bisphosphate, can play key roles in cell signalling. Lipids possess different charges at physiological pH. Most are neutral (e.g. cholesterol) or zwitterionic (e.g. PC), where the functional group has both a positive and a negative charge. However, some lipids are either cationic (e.g. sphingosine), or (more commonly) anionic (e.g. PS). Lipids are distributed unevenly between the two leaflets of the plasma membrane: the outer leaflet contains mainly neutral and zwitterionic lipids, including cholesterol, PC and SM, whereas the inner leaflet contains neutral, zwitterionic and anionic lipids, including cholesterol, phosphatidylinositol, PE and PS (Slochower *et al.*, 2014). Significantly, PS is restricted to the cytoplasmic leaflet in healthy cells but is flipped to the extracellular leaflet during apoptosis (Bever and Williamson, 2016).

Cholesterol is an essential component of bilayers and is present in roughly the same quantity as the phospholipids. A high concentration of cholesterol in the membrane results in rigidity, through its ability to intercalate between the phospholipids, with its polar hydroxyl group associating with the phospholipid head groups (Subczynski *et al.*, 2017). The ability of cholesterol to confer rigidity on the membrane is highly temperature-dependent; for example at high temperatures, cholesterol reduces the fluidity of the outer leaflet, thereby reducing its permeability, whereas at low temperatures cholesterol intercalates between fatty acid tails, preventing freezing of the bilayer (Cooper, 2000).

Glycolipids contain exposed sugar moieties and are found on the outer leaflet of the lipid bilayer. Although only comprising less than 10% of the total membrane composition, glycolipids are thought to be important for the recognition of glycoproteins (carbohydrate-containing proteins) and for cell-cell recognition and adhesion (Study.com, 2016; Cooper, 2000).

1.8.1 PROTEINS IN THE LIPID BILAYER

Proteins constitute ~50% of most biological membranes by weight, and fall predominantly into two groups: integral and peripheral membrane proteins. Integral membrane proteins are inserted into the lipid bilayer, thereby disrupting the hydrophobic interior. These proteins contain at least one transmembrane domain (TMD), often either a hydrophobic alpha-helix or beta-barrel. In order to

remove an integral membrane protein from the lipid bilayer, conditions are required that disturb the bilayer but shield the protein's hydrophobic TMD. Most commonly, detergents are used; these are amphipathic molecules that bind to the hydrophobic regions of proteins while exposing a hydrophilic surface to the exterior, resulting in removal of the protein from the membrane and its solubilization (Lodish *et al.*, 2000; Alberts, 2002).

Peripheral membrane proteins are attached to the lipid bilayer via either protein-protein or protein-lipid interactions. These proteins do not interrupt the hydrophobic interior of the bilayer and can easily be dissociated by pH changes or salt addition; once dissociated, they often exist as soluble globular proteins in solution (Cooper, 2000).

In contradiction of the fluid mosaic model, lipids and proteins are not uniformly distributed in many biological membranes; rather, some membrane domains are enriched in cholesterol and sphingolipids, and specific proteins become clustered in these domains, which are known as lipid rafts. By enabling quick and efficient interactions, this localization is crucial for many cell signalling events (Alonso and Millan, 2001; Silvius, 2003).

1.8.2 ZYMOGEN GRANULE MEMBRANES AND SYNCOLLIN

The ZG membrane is adapted for its roles in the transport, storage and secretion of digestive enzymes in response to stimulation, and different proteins are expressed on its cytoplasmic and luminal faces. Syncollin is present in the luminal side of the ZG membranes, apparently within lipid raft-based microsignalling domains in association with other proteins such as ZG16p (a lectin), GP2 (a GPI-anchored membrane protein), and sulphated proteoglycans, in addition to the SNAREs synaptobrevin 2 and syntaxin 3 (Chen, 2018). Syncollin is known to be a peripheral membrane protein, likely associating with the ZG membrane as an oligomer and susceptible to removal from the membrane at high pH (>10.0). It has also been shown that the binding of syncollin to artificially generated lipid bilayers is enhanced upon the addition of cholesterol (Hodel *et al.*, 2001).

1.9 MEMBRANE INTERACTING OLIGOMERIC PROTEINS

Many proteins, likely including syncollin, exist on biological membranes as oligomers. In some cases, monomers associate on the membrane to form oligomers, whereas in others the monomers oligomerize in solution and then subsequently bind to membranes. In the latter case, the exposure of hydrophobic residues upon oligomerization may facilitate insertion into the membrane. Here, three

examples of membrane-associated oligomers are discussed: Bax/Bak, α -synuclein and perfringolysin O (PFO; Figure 1.5).

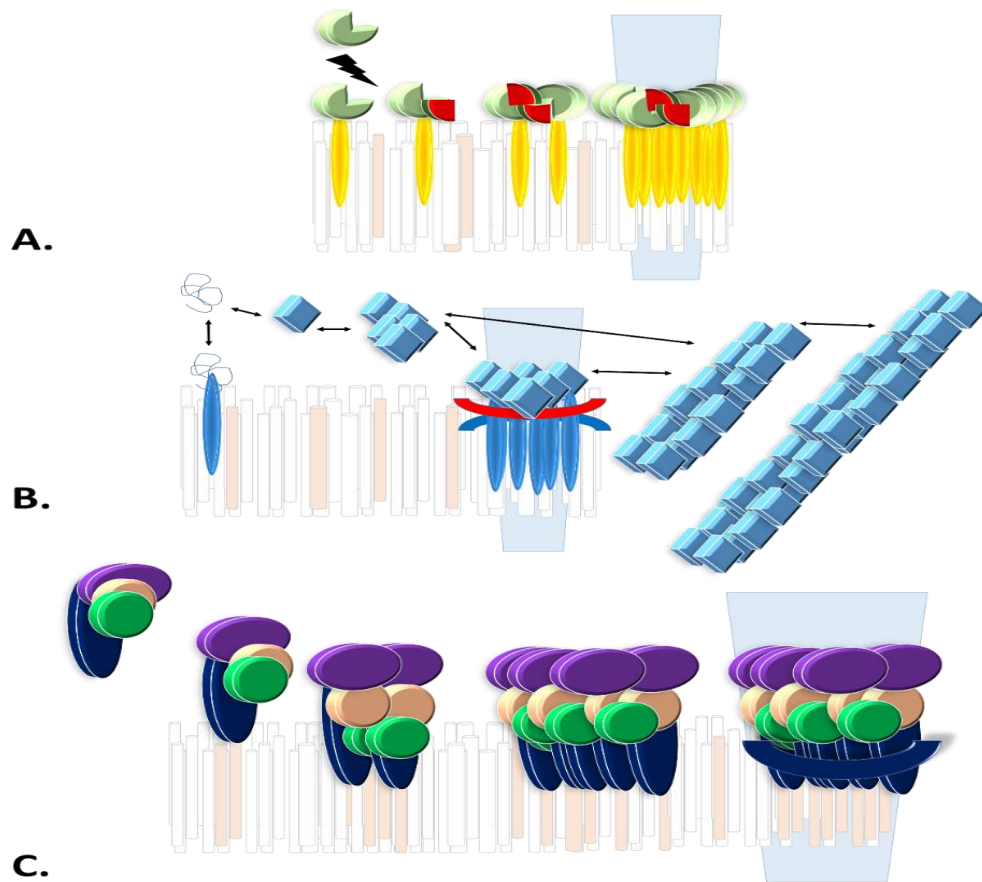


Figure 1.5. Mechanism of oligomerization of Bax/Bak, α -synuclein and perfringolysin O on membranes. A. Bax and Bak typically exist in healthy cells as inactive monomers or dimers and require activation. This occurs through binding BH3 proteins (Bim/Bid). Binding of the BH3 proteins (red) to the hydrophobic BH3 domains initiates exposure of the TM domain (yellow). As hydrophobic BH3 domains are exposed, the initiation of oligomerization can occur to shield these hydrophobic domains. Now the oligomer is formed, aromatic hydrophobic residues allow interruption of the lipid bilayer and permeabilization. B. α -synuclein is considered disordered as it is able to transition easily between oligomeric states. Oligomers (of up to 30 monomers) are capable of interacting with and permeabilizing the membrane through shielding of their hydrophobic surfaces and binding to anionic lipids. Alternatively, α -synuclein can form fibrils which ultimately can become deposited in Lewy bodies and result in neurodegeneration. C. Perfringolysin O recognises and binds cholesterol (red) in the mammalian bilayer, a process that is also facilitated through electrostatic interactions. Binding induces a conformational change in the monomer which allows for beta-sheet interactions to occur and subsequently the formation of oligomers. The pre-pore complex is formed by diffusion of monomers in the plane of the membrane, which allows for the formation of a ring structure. Finally, the transition from the pre-pore complex to the pore complex (up to 50 monomers) can occur once exposed hydrophobic beta-hairpins are inserted into the lipid bilayer to form a beta-barrel, resulting in membrane permeabilization.

1.9.1 BAX/BAK

Bax and Bak are pro-apoptotic members of the B-cell lymphocyte 2 (BCL2) family, which upon oligomerization form pores in mitochondrial membranes that drive cells into apoptosis. Bax is predominantly cytosolic and kept at low concentrations in mitochondria in healthy cells because of its active retro-translocation into the cytosol. Bax exists as two forms which are both inactive: a monomer and an auto-inhibited dimer, in which the N-terminal domain of one monomer binds the C-terminal domain of another to prevent unwanted activation. Bak, on the other hand, is constitutively inserted into the mitochondrial outer membrane as a monomer through its transmembrane alpha-helix 9 (Peña-Blanco and García-Sáez, 2018).

In normal healthy cells, Bax and Bak exist as inactive monomers or dimers, which require activation for their oligomeric assembly onto the membrane. Activation is achieved through the binding of members of a class of proteins known as BH3-only proteins, which include Bid and Bim. As inactive monomers, Bax and Bak are predominantly alpha-helical in structure, with characteristic features: a hydrophobic helix 5 that forms the 'core', alpha-helix 9, which contains the TM domain, a hydrophobic BH3 domain that is sheltered in the inactive form, and various hydrophobic grooves. The BH3-only proteins bind to these grooves, initiating activation via conformational changes in the proteins. Upon binding of a BH3-only protein in the grooves, alpha-helices 1 and 2 become displaced, resulting in the exposure of the TM domain through dissociation of latch alpha-helices (6-8) away from the core helices (2-5). Both Bax and Bak contain hydrophobic BH3-only binding domains, which can be hidden by assembly of the oligomer. Once the oligomer is assembled, a number of aromatic residues become exposed on one face of the oligomer. Because these residues are hydrophobic, the lipophilic face of the oligomer can interrupt the lipid bilayer through displacement of phospholipid head-groups, enhancing membrane curvature, and causing rupture, pore formation and permeabilization. In the case of Bax/Bak, permeabilization results in release from mitochondria of components such as cytochrome c, which through various signalling pathways results in the cell becoming destined for apoptosis (Westphal *et al.*, 2011; Westphal *et al.*, 2014; Peña-Blanco and García-Sáez, 2018).

1.9.2 α -SYNUCLEIN

α -synuclein exists in three predominant forms: monomer, oligomer and fibril. The protein is considered to be structurally disordered because of its ability to exist in many conformations in all three states, and its ability to interchange between these states. The important structural regions in α -synuclein include a basic N-terminal region, a hydrophobic non-amyloid beta-component in the

centre and an acidic and disordered C-terminal region. Physiologically, α -synuclein interchanges between a soluble unfolded monomeric form and an alpha-helical membrane-bound form. α -synuclein monomers are able to associate with membranes avidly because of their hydrophobic and 'sticky' nature. The N-terminal region forms an amphipathic alpha-helix which permits insertion of the protein into the membrane (Andreasen *et al.*, 2015).

Pathologically, α -synuclein can form oligomers and fibrils, and it is not known whether these are derived from the unfolded monomeric form or from the alpha-helical membrane-associated form (Pineda and Burré, 2017). The interaction of α -synuclein with the membrane occurs because the oligomers have an increased hydrophobic surface area and selectively bind to anionic lipids. The α -synuclein monomer assembles into oligomers, which can contain up to 30 monomers. As with Bax/Bak, the highly stable oligomer is much more toxic than the monomer, and is able under some circumstances to permeabilize membranes. The α -synuclein oligomers preferentially bind to liquid disordered domains of membranes, as opposed to liquid ordered domains, because here the phospholipids are less tightly packed and therefore more susceptible to disruption and manipulation by the prevailing anti-parallel beta-sheet secondary structure of α -synuclein. It is widely known that many pre-fibrillar oligomers of different protein origins, including α -synuclein, are able to interact with the bilayer, capturing lipids and assembling with them into aggregates. Pore formation by α -synuclein can have various deleterious effects on cells, including mitochondrial dysfunction and ER stress (Bernal-Conde *et al.*, 2020; Falke *et al.*, 2019).

There are two known types of oligomers: off-pathway oligomers, which do not assemble into amyloid fibrils, and on-pathway oligomers, derived from monomers, which nucleate, elongate and ultimately form amyloid fibrils. These fibrils are toxic because of their ability to recruit additional α -synuclein and eventually to trigger synucleinopathies (Alam *et al.*, 2019). Fibrils have a beta-sheet secondary structure, consisting of hydrogen-bonded beta-strands in the form of straight, unbranched structures. These straight fibrils are also able to interact with membranes, via their 'sticky' ends, and to cause membrane perturbation. The fibrils can become deposited into so-called Lewy bodies, which result in neurodegeneration, as occurs in Parkinson's disease (Andreasen *et al.*, 2015).

1.9.3 PERFRINGOLYSIN O

Perfringolysin O is a β -pore forming protein (β -PFP), which inserts a beta-sheet into the lipid bilayer to initiate pore formation. As with, Bax (above), conformational changes in the protein are necessary to transform it from an inactive water-soluble form into an active oligomer. In the case of PFO, this

transformation is facilitated by cholesterol recognition and binding. Hence, PFO is an important member of the cholesterol-dependent cytolysin family. PFO is secreted by Gram-positive bacteria and has four domains with distinct characteristics: domain 1 (an elongated portion not involved in pore formation), domain 2 (beta-strand in structure, which facilitates insertion of hairpins), domain 3 (beta-sheet in structure with some alpha-helices, which co-operates with domain 2 in beta-barrel formation), and domain 4 (a beta-sheet sandwich, which contains tryptophan-rich loops thought to be essential for cholesterol recognition and membrane binding). PFO has a signal sequence that directs its secretion. Significantly, it only becomes active upon cholesterol recognition in the membranes of mammalian cells; hence, it has no adverse effect on its bacterial host (Johnson and Heuck, 2014).

The action of PFO on a membrane is initiated by electrostatic interactions that bring the protein into close proximity with its target. The protein is then able to bind cholesterol via a tyrosine and a lysine residue, which allows binding to the membrane and causes a conformational change in the monomer. Specifically, a core beta-sheet is exposed via a glycine hinge, which enables interactions between beta-sheets; this in turn leads to the formation of dimers and oligomers. Additional monomers then diffuse in the plane of the membrane to support the assembly of the pre-pore complex, in which multiple dimers are aligned in a ring structure. This process is thought to be facilitated by the tryptophan-rich loops in domain 4 (Rossjohn *et al.*, 2007; Johnson and Heuck, 2014).

The transition from pre-pore complex to pore complex involves the insertion of exposed hydrophobic beta-hairpins (two per monomer) into the lipid bilayer. Given that there are 30-50 monomers in the pre-pore complex, this process leads to the formation of a beta-barrel, which permeabilizes the membrane. The extent of membrane binding and permeabilization by PFO depends on the cholesterol concentration within the membrane. Specifically, the concentration of cholesterol has to be at least 40 mol% in order for it to be exposed and thereby rendered accessible to PFO (Heuck *et al.*, 2007; Maekawa *et al.*, 2016).

1.10 SYNCOLLIN BIOCHEMISTRY AND MEMBRANE INTERACTIONS

The biochemistry of syncollin has been extensively investigated and it displays many similarities with the membrane binding proteins detailed above. The protein can be detached from ZG membranes by incubation at high pH (>10.0), and subsequent restoration of the pH to 7.0 by dialysis causes precipitation of the protein in almost pure form. Amino acid sequencing of the purified protein revealed the absence of the predicted hydrophobic (signal) sequence at the amino terminus. It has also been shown that syncollin exists in many oligomeric states - with bands at approximately 16, 30,

50, 100 kDa observed in unheated ZG membrane samples (Figure 1.6A). Even after heating of samples, a likely dimer at approximately 30 kDa is still visible on gels, suggesting that the oligomers have a high thermal stability. It was observed on immunoblots that syncollin migrated more slowly in the presence than in the absence of the reducing agent β -mercaptoethanol (Figure 1.6B; An *et al.*, 2000). Rat syncollin has 7 cysteine residues and it is therefore expected that it may contain disulphide bonds. There is also evidence that syncollin can interact with cholesterol; for example, it can precipitate [3 H]cholesterol, and it shows improved binding to liposomes when cholesterol is present (Figure 1.6C; Hodel *et al.*, 2001).

When purified syncollin in association with lipid bilayers was visualized using atomic force microscopy (AFM), doughnut-shaped structures, apparently composed of multiple subunits were seen, but only at pH 7.0 and not at pH 11.0, consistent with the behaviour described above (Figure 1.6D; Geisse *et al.*, 2002). This striking doughnut shape suggests that syncollin might have pore-forming properties, and indeed, syncollin was able to permeabilize membranes, causing the release of haemoglobin from erythrocytes (Figure 1.6E; Wäsle *et al.*, 2004) and of carboxyfluorescein dye from liposomes (Geisse *et al.*, 2002).

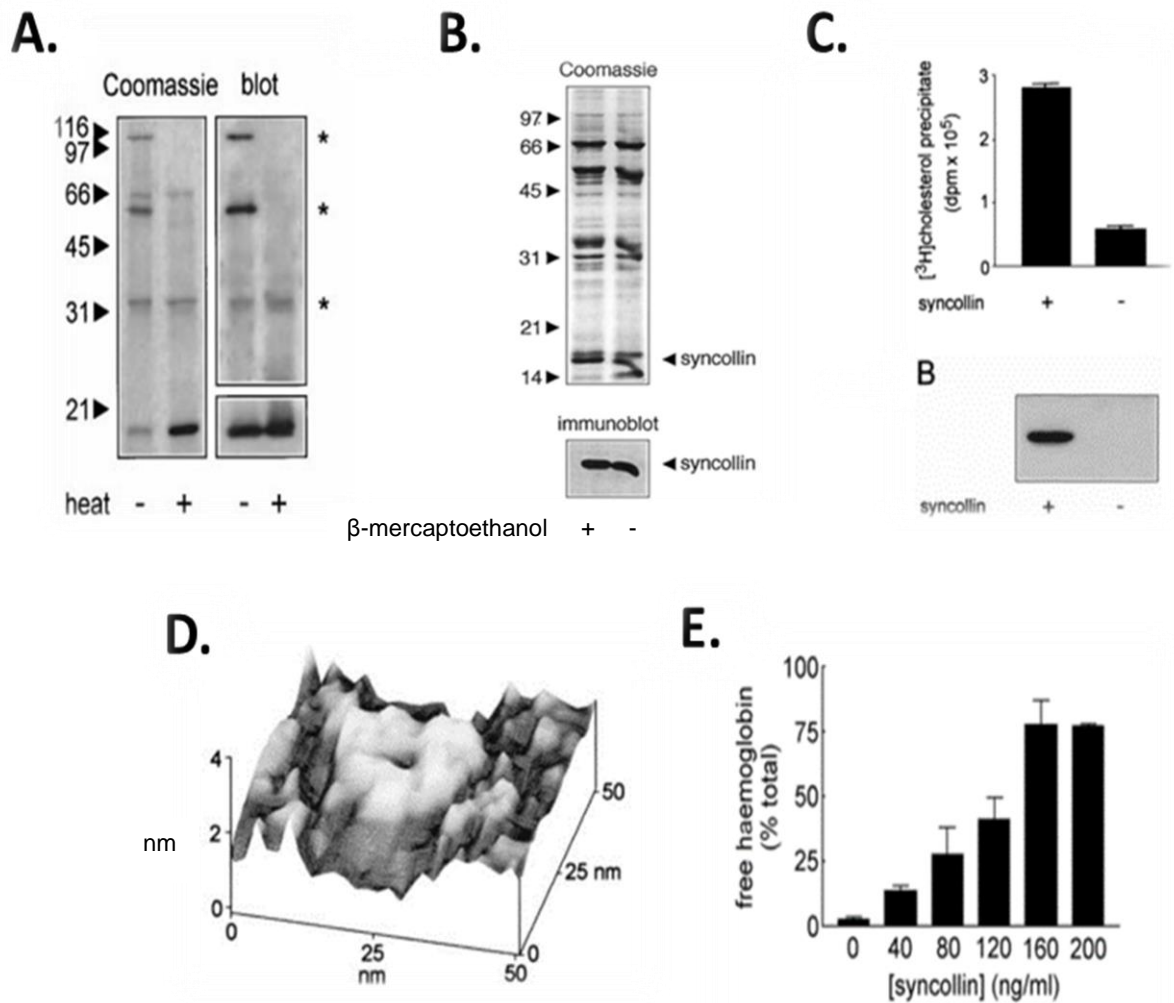


Figure 1.6. Syncollin-membrane interactions. A. Syncollin forms oligomers. In unheated samples of purified protein, syncollin oligomers of up to 110 kDa in size can be seen on Coomassie-stained gels and immunoblots (Geisse *et al.*, 2002). B. Syncollin contains disulphide bonds. β -mercaptoethanol causes syncollin to run more slowly on Coomassie-stained gels and immunoblots (An *et al.*, 2000). C. Syncollin binds cholesterol, as seen in its ability to pull down $[^3\text{H}]$ cholesterol. (Hodel *et al.*, 2001). D. Syncollin forms doughnut-shaped structures of approximate diameter 25 nm. Purified syncollin was incubated with brain lipids and supported lipid bilayers imaged by AFM (Geisse *et al.*, 2002). E. Syncollin can permeabilize membranes. Syncollin was added at various concentrations to erythrocytes, and haemoglobin release measured (via absorbance at 414 nm) as a percentage of total release (in 1% Triton X-100; Geisse *et al.*, 2002).

1.11 SYNCOLLIN AND DISEASE

At present, a potential role for a pore, composed of a syncollin oligomer, in ZG-ZG fusion during compound exocytosis in the pancreatic acinar cell cannot be ruled out; however, it is clear that fusion

pore formation in other cell types (e.g. neurons) does not require the involvement of syncollin. Furthermore, the viability of the syncollin KO mouse indicates that the protein is not essential for survival. There are other clues, too, that point to a role for syncollin external to the acinar cell. For instance, syncollin is secreted from the cells along with the digestive enzymes, and is present in the pancreatic juice. In addition, syncollin levels are elevated in the serum of patients with pancreatic cancer (Makawita *et al.*, 2013), which might result from a general breakdown of the acinar structure in this condition rather than a direct role of syncollin in cancer. Finally, there is a significant reduction in levels of syncollin in mice with colitis-associated colorectal cancer (Li *et al.*, 2014).

With respect to a potential role in inflammation, syncollin appears to exist within lipid raft domains on the luminal surface of the ZG membrane. Two other ZG proteins have also been found in these domains: GP2, which is known to bind to syncollin (Kalus *et al.*, 2002), and ZG16p (see below). Significantly, both of these proteins are known to have antimicrobial effects in the gut. Another potential link with inflammation relates to the expression of syncollin in neutrophils and its release upon neutrophil activation (Bach *et al.*, 2006).

ZG16p and other anti-microbial proteins are discussed in more detail below; however, I will first outline how the body responds to inflammation, focusing on the role of neutrophils.

1.12 THE IMMUNE SYSTEM

1.12.1 THE INNATE AND ADAPTIVE IMMUNE SYSTEMS

The immune system provides both innate and adaptive immunity. Innate immunity involves an immediate and non-specific response to infection, whereas adaptive immunity represents a second line of defence, which is slower in onset but much more specific. This specificity is conferred through the recognition of an antigen presented on the surface of the pathogen, which triggers the clonal expansion of the lymphocytes (B and T) involved in the adaptive immune system. This process results in each cell expressing the same antibody to target the antigen. The T cells also provide a sustained response, because of their 'long-term memory' (Janeway *et al.*, 2001).

Innate immunity, which is the focus of the discussion below, includes many different cellular responses. Initially there are physical barriers such as skin and hair which prevent pathogens accessing further tissues and organs. Then there are the members of the family of white blood cells, which are able to respond to small-scale inflammation and contain it. This response is facilitated by humoral

defence, where enzymes from bodily fluids and blood prevent bacterial spread and the complement system, which is able to mark and dissolve bacterial cell walls (InformedHealth, 2010).

White blood cells are the main cells involved in innate immunity. All blood cells originate in bone marrow from a universal cell type known as the haematopoietic stem cell. Through a process known as haematopoiesis, the stem cells differentiate into three blood cell types – erythrocytes, white blood cells and platelets. The white blood cells can then differentiate to become either lymphoid (e.g. B and T lymphocytes) or myeloid (e.g. neutrophils, basophils, eosinophils and monocytes; Kondo, 2010). Members of the myeloid class can be further categorized into monocytes, which emerge from marrow cells and are destined to form macrophages and dendritic cells in the tissues, and granulocytes, which include neutrophils, basophils and eosinophils. Granulocytes have some common features, including cytoplasmic granules, a multi-lobed (typically 2-6 lobes) nucleus, and the ability to migrate and release their granule contents in response to infection (Monie, 2017).

1.12.2 NEUTROPHILS

The most abundant white blood cell, accounting for 40-70% of the total population, and also the first responder to infection, is the neutrophil. As mentioned above, the nuclei of granulocytes have multiple lobes and neutrophils are termed polymorphonuclear to reflect this property. Neutrophils are attracted to microbes through various mechanisms, including recognition of pathogen-associated molecular patterns (PAMPs) on the pathogen surface, and recognition of antigens indirectly through their surface Fc receptors. In addition, neutrophils can migrate in response to various secreted or released chemokines (e.g. from bacteria or leukocytes), in a process known as chemotaxis (Mayadas *et al.*, 2014). Neutrophils normally have a very short lifetime of approximately 8 hours. However, in response to inflammation the presence of inflammatory cytokines, among other similar signalling molecules, prolongs their lifetime, allowing them to carry out various roles, including phagocytosis and/or NETosis in response to infection (Summers *et al.*, 2010).

Phagocytosis is the main antimicrobial mechanism used by neutrophils. In some cases, the bacteria can be 'opsonized' which involves marking of the pathogens with antibodies. The main opsonin receptor expressed by neutrophils, the Fc receptor, can then bind to the immunoglobulins present on the bacteria to initiate phagocytosis. After phagocytosis has occurred, neutrophils initiate various signalling cascades, such as increased reactive oxygen species (ROS) production and degranulation, in order to bring about microbial death (van Kessel *et al.*, 2014).

During large-scale infections, phagocytosis alone may not be sufficient to eliminate the bacteria. In this case, neutrophils may undergo programmed suicide or NETosis, during which cell lysis occurs and neutrophil extracellular traps (NETs) are generated. Here, the backbones of the NETs are formed by decondensation of nuclear chromatin. Granular proteins including myeloperoxidase (MPO) and elastase are also released. The initiation of NET formation begins with increased ROS production from oxidants, including those generated by the enzyme nicotinamide adenine dinucleotide phosphate (NADPH) oxidase in the phagocyte, and also through the action of MPO released during granular lysis (Branzk and Panayannopoulos, 2013; Yipp and Kubes, 2013). These different modes of operation of neutrophils are illustrated in Figure 1.7.

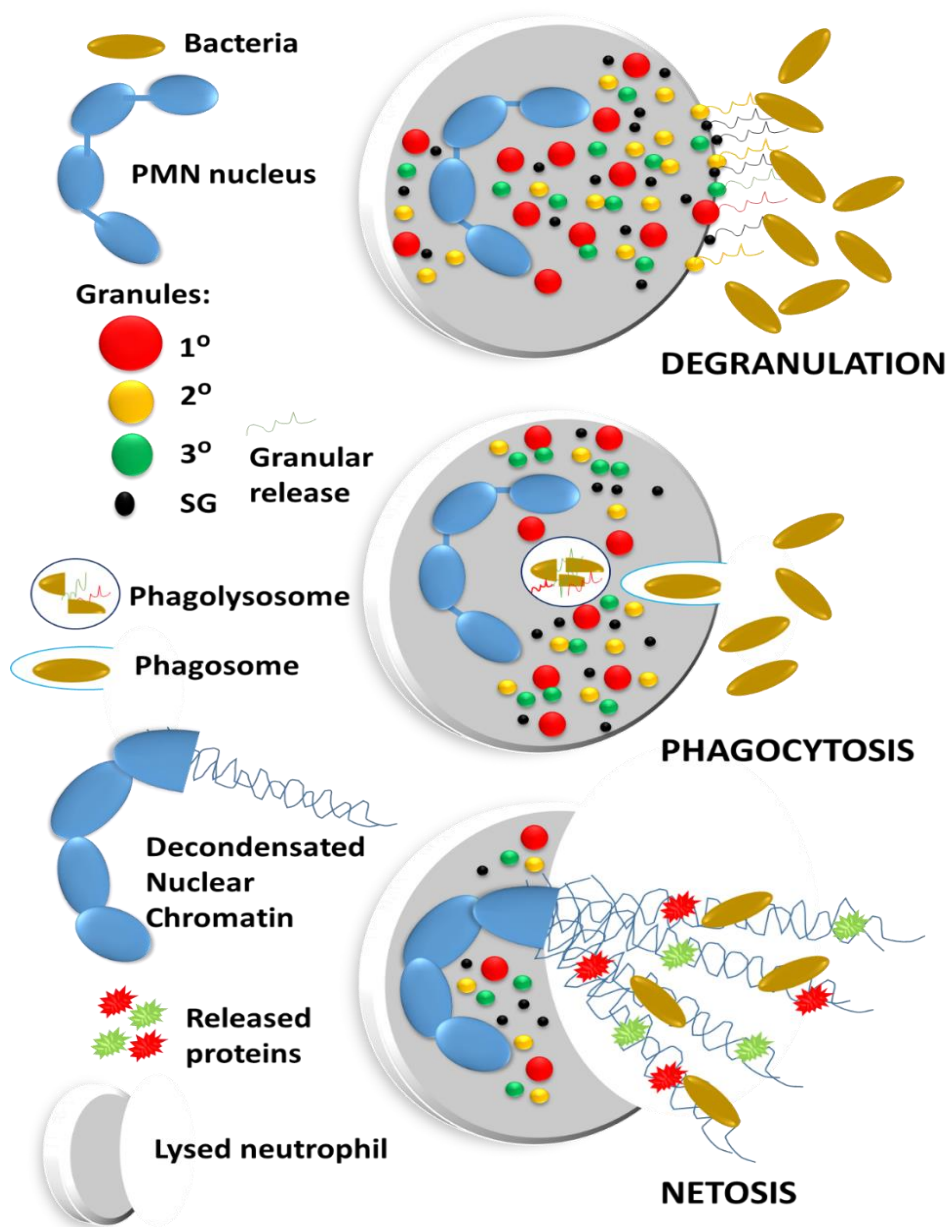


Figure 1.7. Three modes of operation of neutrophils. 1. Degranulation. Neutrophils contain different granules, including primary (red), secondary (yellow), tertiary (green) and secretory vesicles (SG; black). In response to bacterial infection, exocytosis of vesicles occurs in a process known as degranulation. Released proteins include MPO, defensins, elastase and lactoferrin. 2. Phagocytosis. Bacteria, either opsonized or not, are recognized by neutrophil Fc receptors and endocytosed into the phagosome. The phagosome fuses with the lysosome to form the phagolysosome. Here, vesicular release can occur as above to cause degradation of the bacteria. Phagocytosis is the most common mechanism employed by neutrophils. 3. NETosis. Neutrophils lyse and decondense their nuclear chromatin outside the cell. The backbones of the nets are formed from the chromatin DNA. Bacteria can be detected and trapped in these nets where, due to granular lysis, antimicrobial peptides can be deployed. NETosis is also known as programmed suicide. Adapted from Rosales (2017).

Interestingly, syncollin has been reported to be expressed within neutrophils, and specifically in their azurophilic granules (Bach *et al.*, 2006). As mentioned above, neutrophils also contain antimicrobial peptides. Examples of antimicrobial proteins (AMPs) will now be discussed in more detail.

1.13 ANTI-MICROBIAL PROTEINS

1.13.1 ZG16P

ZG16p, like syncollin, is located on the luminal surface of the pancreatic ZG membrane (Figure 1.8), and is also expressed in the goblet cells of the duodenum and colon. It is a 16-kDa secretory lectin and does not contain any transmembrane domains; rather, it associates with membranes via its lectin domain in a process believed to be facilitated by its surface electrostatics. ZG16p associates with particular membrane motifs, including sub-membranous matrices and cholesterol/glycosphingolipid-enriched microdomains in which it binds sulphated proteoglycans. These properties led to the proposal that ZG16p acts as a linker between the ZG matrix and ZG membrane microdomains (Rinn *et al.*, 2011; Kanagawa *et al.*, 2014).

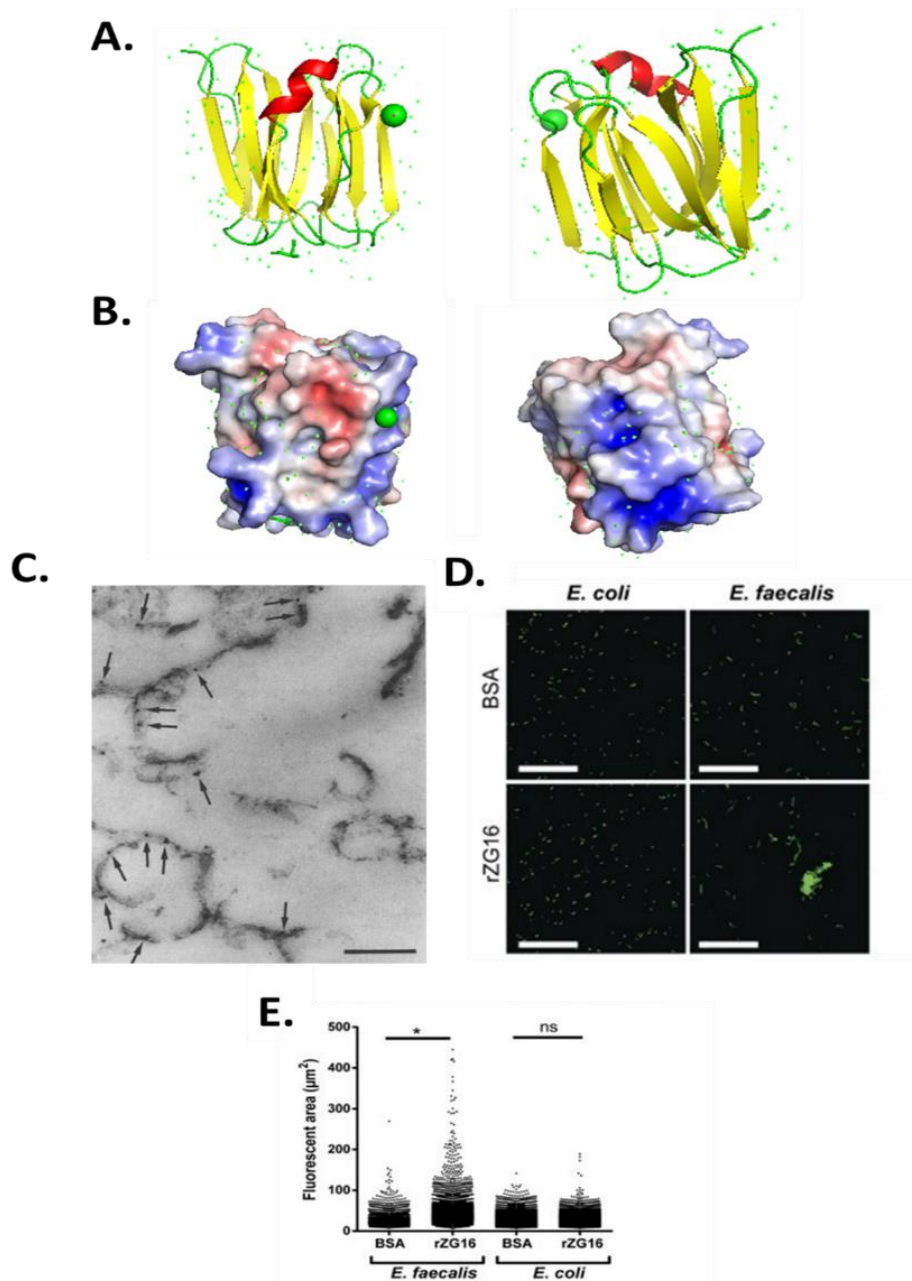


Figure 1.8. ZG16p structure and function. A. RCSB PDB: 3APA model of ZG16p displayed using PyMol. Colours are according to secondary structures: yellow: beta strand, red: alpha helix, green: loops. Small crosses surrounding ZG16p represent water molecules, and the green sphere represents a Cl⁻ ion. B. Electrostatic surface model of 3APA displayed using PyMol. Electrostatics were applied using the adaptive Poisson-Boltzmann solver (APBS) electrostatics plugin. C. Immunolocalization of ZG16p following lysis of ZGs. ZG16p can be seen associated with ZG membranes via immunogold particles, highlighted with black arrows (Kleene *et al.*, 1999). D. Gram-negative *E. coli* and Gram-positive *E. faecalis* stained with the dye Syto9. Bacteria were incubated with either bovine serum albumin (BSA) or ZG16p and subjected to fluorescence imaging. Aggregation could be observed in Gram-positive bacteria in the presence of ZG16p, but not BSA. E. Images were quantified using the programme ImarisTM to calculate the quantity of fluorescence per unit area; * p < 0.001 (Bergström *et al.*, 2016).

The crystal structure of ZG16p shows a predominantly beta-sheet structure. The protein contains a beta-prism fold of 3 beta-sheets, in which each sheet forms a 'Greek-Key' fold composed of 4 beta-strands (Figure 1.8A and B). In the C-terminal domain of the protein, there are 2 cysteine residues which form an intramolecular disulphide bond (Kanagawa *et al.*, 2011). Key features of the protein structure include a signal peptide, a conserved GG loop, an N-glycosylation site, and two conserved loops - binding and recognition loops (Rinn *et al.*, 2011).

It is thought that the interaction of ZG16p with membranes (Figure 1.8C) is initiated by its binding to sulphated proteoglycans, which it does via its lectin domain (carbohydrate binding motifs: GG...GSAID and GG...IRVNR) upon ZG formation. ZG16p is then apparently able to cross-link the proteoglycans and permit oligomerization of the matrix on the luminal side of the ZG membrane (Kumazawa-Inoue *et al.*, 2012). The protein is also believed to act as an essential scaffold, since the binding of ZG content proteins to ZG membranes is reduced by ~50% in the absence of ZG16p (Kleene *et al.*, 1999). Importantly, in addition to binding sulphated proteoglycans, ZG16p can also bind a similar carbohydrate: peptidoglycan (PGN).

PGN is found in bacterial membranes, predominantly in Gram-positive bacteria, where it forms the outer layer of the cell wall; however, it is also present to a lesser extent in Gram-negative bacteria beneath the outer membrane. ZG16p is able to bind to PGN and cause aggregation of Gram-positive bacteria (Figure 1.8D and E). This aggregation prevents the bacteria from penetrating the sub-membranous matrix and hinders their growth, allowing other bactericidal proteins to cause death (Bergström *et al.*, 2016). Hence, ZG16p has an anti-microbial role in addition to its involvement in ZG formation. This is especially important in the context of its expression in the goblet cells of the small intestine and colon. More recently, ZG16p has been shown to hinder colorectal cancer cell proliferation (Mito *et al.*, 2018), making this protein an important player in infection, inflammation and disease.

1.13.1.1 GREEK KEY MOTIF AND CRYSTALLINS

The Greek Key domain possessed by ZG16p, along with other AMPs, was originally identified in the crystallin family. Members of this family of proteins are found within the cytoplasm of cells in the eye, and they are known for their stability, Ca²⁺ binding and water solubility at high protein concentrations. In vertebrates, the crystallins can be divided into the α , β and γ -crystallins; in addition, there are the δ -crystallins, which are found in reptiles and birds (Basaglia and Di Luca, 1993). The Greek Key domains consists of four anti-parallel beta-sheets aligned via connecting loops in a 4123 topology, in which each sheet is connected to an adjacent sheet (Figure 1.9A; Brunsveld *et al.*, 2012). The structural similarities

between the various $\beta\gamma$ -crystallin family members (e.g. nitrollin and spherulin) are obvious in their crystal structures (Figure 1.9B-E). The structure of nitrollin provided an early indication of the oligomerization capabilities of the crystallins. Nitrollin is able to homo-dimerize through its N-terminal domain, in a process known as domain swapping, which is essential for the protein's conformation and stability (Aravind *et al.*, 2009). Spherulin is a protein from slime mould which, unlike nitrollin, does not oligomerize and exists in the form of a single-domain Greek Key motif. Importantly, the crystal structure of spherulin revealed that it was able to bind Ca^{2+} , leading to the hypothesis that the Greek Key motif, at least in some crystallins, acted to bind Ca^{2+} (Srivastava *et al.*, 2014). Intriguingly, given that both crystallins and syncollin interact with Ca^{2+} and show significant thermal stability, spherulin and nitrollin are predicted to be the closest structural homologues of syncollin (see below).

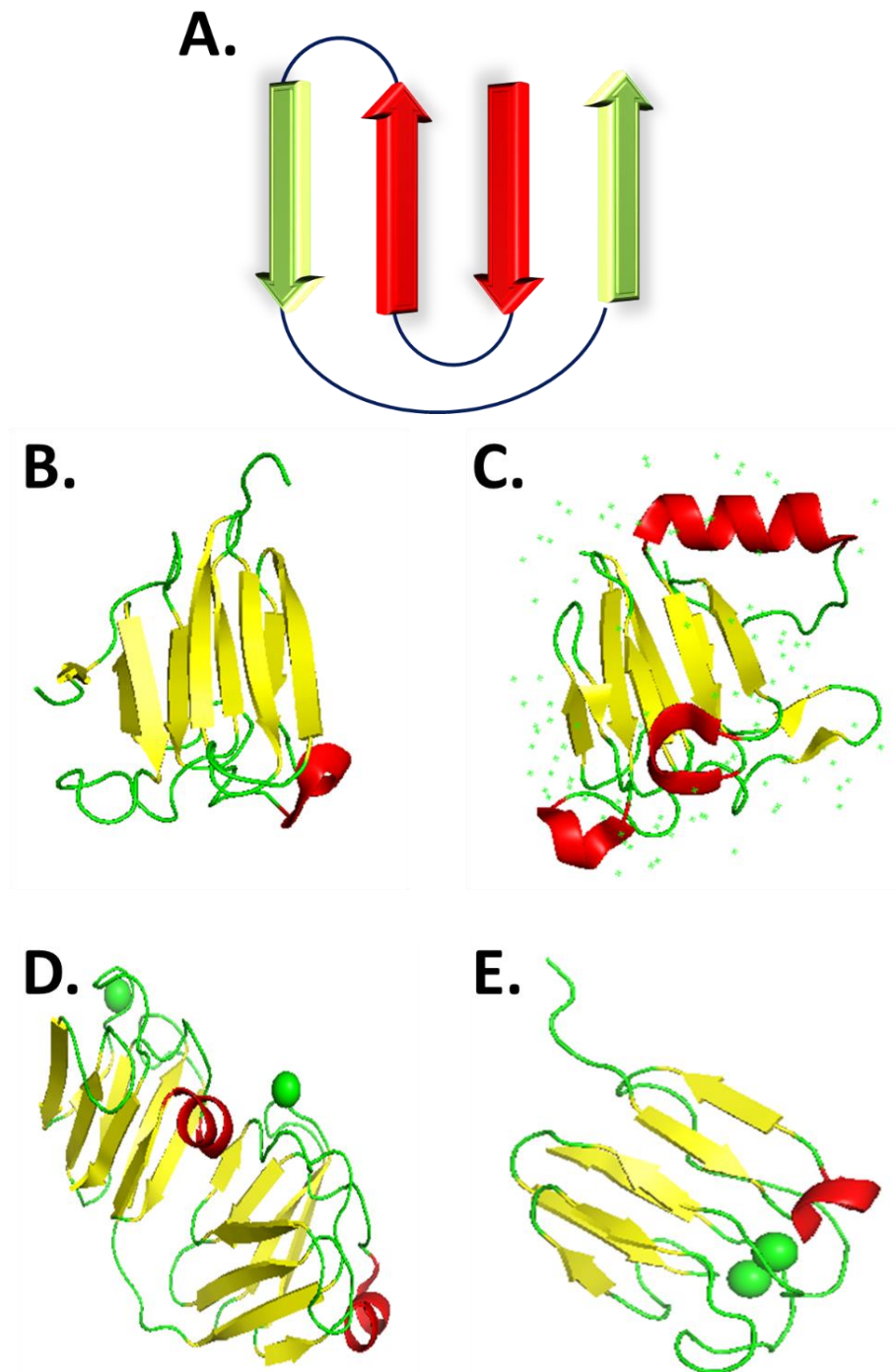


Figure 1.9. $\beta\gamma$ -crystallins. A. $\beta\gamma$ -crystallins adopt a Greek Key fold – a secondary structure composed of anti-parallel beta sheets connected by loops. B-E. Crystal structures from RCSB-PDB of the following proteins: spherulin - 1AG4 (B), nitrollin - 3ENU (C), γ -crystallin S (D), and M-crystallin-2K1W (E).

1.13.2 REGENERATING-ISLET DERIVED PROTEINS

Another class of antimicrobial proteins which adopt a predominantly beta-sheet structure (Figure 1.10A), is the regenerating-islet derived (Reg) protein family. Although not lectins themselves, unlike ZG16p, Reg family proteins have homology with C-type lectins in the sense they contain carbohydrate recognition domains and bind carbohydrates in a Ca^{2+} -sensitive manner (Lehotzky *et al.*, 2010). There are four subfamilies of Reg: RegI, RegII, RegIII, RegIV. In mice, the subfamilies can be further divided into α , β and γ . RegIII γ in mice is highly homologous to the protein HIP/PAP in humans, which is widely known to be up-regulated in inflammatory bowel disorders (Parikh *et al.*, 2012). For this reason, RegIII γ has been extensively investigated. It has been shown to be widely expressed in the small intestine, in epithelial cells including Paneth cells and enterocytes. RegIII γ has an N-terminal signal sequence and is secreted into the intestinal lumen, where it has specific antibacterial actions (Shin and Seeley, 2019).

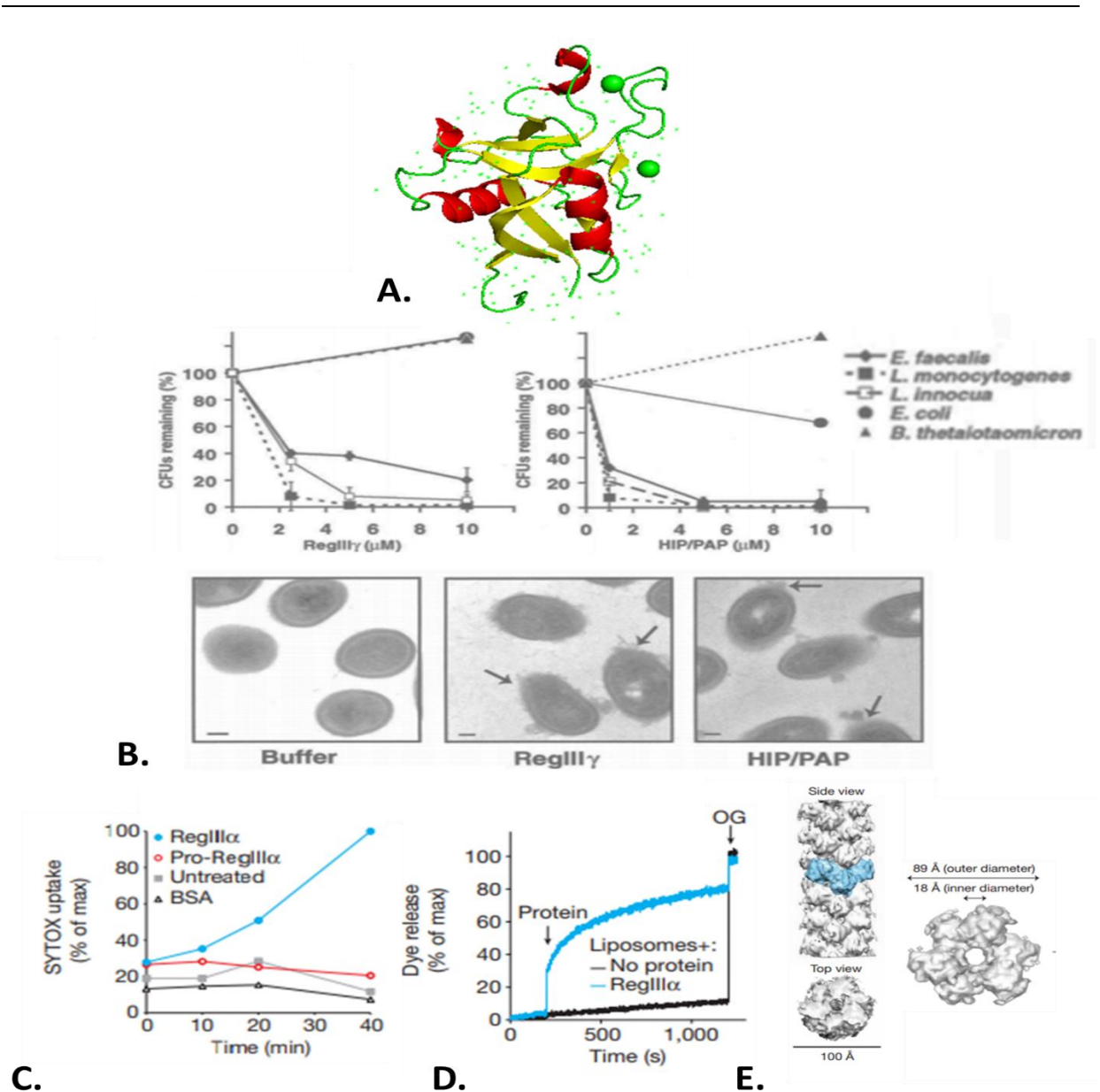


Figure 1.10. Bactericidal activity of RegIII. A. RegIII crystal structure. RCSB-PDB 4MTH RegIII α structure in PyMol with colouring according to secondary structure. B. RegIII γ is bactericidal. RegIII γ (left) or HIP/PAP (right) was added to various bacteria and CFU remaining monitored. Both RegIII γ and HIP/PAP killed Gram-positive but not Gram-negative bacteria in a concentration-dependent manner. TEM imaging after a 2-h incubation with 10 μ M RegIII γ or HIP/PAP revealed damage to and permeabilization of the bacterial cell surface (Cash *et al.*, 2006). C and D. RegIII α can permeabilize bacteria (C) and liposomes (D). C. *Listeria monocytogenes* was incubated in the presence of RegIII α , Pro-RegIII α , BSA or no protein and uptake of Sytox green dye was measured. Only in the presence of RegIII α was significant Sytox green uptake recorded (Mukherjee *et al.*, 2014). D. Carboxyfluorescein-filled liposomes were incubated with or without RegIII α and dye release monitored (Mukherjee *et al.*, 2014). E. Proposed oligomeric structure of RegIII. RegIII α hexamers (~10 nm diameter) are thought to form filamentous structures approximately 10 nm in diameter through post-translational modifications preventing unspecific toxicity to host membranes (Mukherjee *et al.*, 2014)

RegIII γ and α bind PGN with a dissociation constant of approximately 11 nM (Cash *et al.*, 2009; Lehotzky *et al.*, 2010). RegIII and HIP/PAP have selective carbohydrate-recognition domains for peptidoglycan, which are Ca²⁺-independent; in HIP/PAP, binding is thought to occur through an EPN motif (Lehotzky *et al.*, 2010). RegIII binding compromises the PGN layer of Gram-positive bacteria, causing the bacteria to become leaky and eventually lyse (Figure 1.10B and C); hence, RegIII is bactericidal. This lytic effect has been shown in various membrane permeability assays, involving, for example, stimulation of dye uptake into bacteria by RegIII α and of leakage of various dyes from reconstituted liposomes (Figure 1.10D; Mukherjee *et al.*, 2014). RegIII α is capable of forming hexamers on bacterial membranes through its binding to PGN. Upon binding, the protein's hydrophobic residues become embedded within the membrane, and there is an accompanying large-scale reorganisation of the protein's disulphide bonds, which changes the overall shape of the protein. These structural changes are then thought to result in the formation of a transmembrane pore, accounting for the observed membrane leakiness (Mukherjee *et al.*, 2014; Mukherjee and Hooper, 2015).

The pore-forming nature of RegIII, makes the protein potentially toxic to cells and it appears that post-translational modifications occur to render the protein less toxic upon its secretion. Site-specific cleavage of RegIII γ by trypsin converts it from inactive pro-RegIII into active RegIII. However, given that the intestine houses the majority of the microbiome, non-specific toxicity of RegIII is prevented through a post-translational modification, subsequent to pore formation, which results in the conversion of RegIII oligomers into filaments. These filaments do not interact efficiently with non-target bacteria or host membranes, and so further damage is prevented (Figure 1.10E; Mukherjee *et al.*, 2009, 2014). The activity of RegIII depends crucially on residue lysine 93. Mutation of this residue to alanine (K93A), was shown to reduce the action of RegIII α on both membranes and bacteria; in contrast, mutation of other positively-charged residues was without effect (Mukherjee *et al.*, 2014). It is believed that lysine 93 is orientated toward the lipid bilayer and mediates the binding of RegIII to its negatively charged surface. Negatively-charged lipids are required for RegIII α pore stability, and the K93A mutation reduces this stability. In addition, filament formation is also inhibited in the K93A mutant. Mutation of other positively-charged residues, such as arginine 166 to alanine, also resulted in reduced RegIII α membrane permeabilization. Further mutations in the carbohydrate-binding region of RegIII α also resulted in reduced toxicity.

In contrast to RegIII γ and α (and also HIP/PAP), RegIII β is able to bind Gram-negative bacteria through an interaction with lipopolysaccharide (LPS). Specifically, RegIII β binds to the carbohydrate moiety of

lipid-A, within LPS, to gain access to and permeabilize the membranes of Gram-negative bacteria (Miki *et al.*, 2012).

Taken together, the characteristics described above make RegIII a key antimicrobial peptide in the intestine. Further, some of the features of RegIII call to mind those of syncollin (e.g. oligomerization on membranes, the presence of intramolecular disulphide bonds and secretion into the gut). It is therefore tempting to speculate that these biochemical similarities might reflect similarities in function.

1.13.3 DEFENSINS

Defensin proteins form the largest known family of antimicrobial proteins. Although only 3-4 kDa in size, these proteins are capable of controlling the intestinal microbiome. They are found predominantly in the granules of leukocytes and are secreted from the Paneth cells of the small intestine, where their role in host defence is paramount. In addition, defensins are also found in epithelial cells and in other immune cells, such as phagocytes (Flaherty, 2012).

All defensins have a predominantly beta-sheet structure containing a triple beta-sheet fold (Figure 1.11A and B). Their structure is strongly dependent on disulphide bonds, and each protein contains six disulphide-bonded cysteines. All defensins are amphipathic, and contain non-polar amphipathic cores with highly polar N- and C-terminal regions. The defensin family can be sub-divided into the α - and β -defensins on the basis of the length of the peptide segment between the six cysteine residues (Bevins *et al.*, 1999). The expression pattern also differs between α - and β -defensins: α -defensins are stored in mature PMNs and Paneth cells as pro-peptides awaiting activation, whereas β -defensins are constitutively expressed in epithelial cells (Raj and Dentino, 2002; Ganz, 2003). Another subfamily, θ -defensins, are known to exist, but they are not expressed in humans.

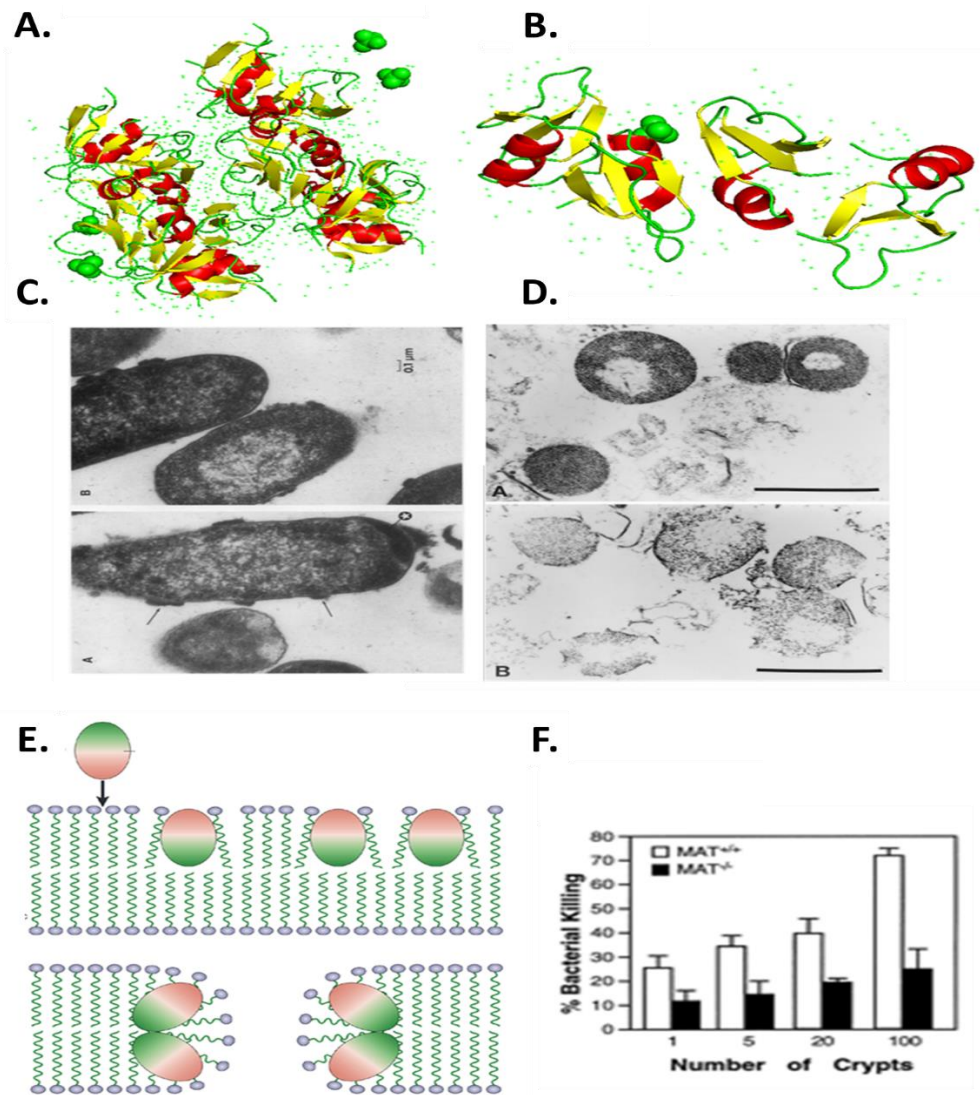


Figure 1.11. Anti-microbial actions of defensins. A, B. Crystal structures of human β -defensin 2. RCSB-PDB entries 1FD4 (A) and 1FD3 (B) displayed in PyMol, with colours representing secondary structure. C, D. Actions of defensins on Gram-negative (C) and Gram-positive (D) bacteria. C. *E. coli* ML35 were treated with defensin (HNP-1,2). Bacteria were sectioned and imaged by EM. Electron-dense material can be seen on the outer membrane (arrows). There are also obvious outer membrane deposits and lysis (top; Lehrer *et al.*, 1989). D. *S. aureus* were incubated in the absence (top) or presence (bottom) of defensin and imaged by EM. Scale bars, 5.1 μ m. Membrane disruption and lysis are seen in bacteria incubated with defensin (Shimoda *et al.*, 1995). E. Illustration of proposed defensin pore-forming action: the carpet worm-hole model. Amphipathic defensins are attracted to membranes via their highly positive face (red). Through electrostatic interaction with binding membrane components (LPS, teichoic acids) and exposed hydrophobic domains, defensins disturb the membrane and insert themselves, causing membrane strain. Multiple defensin proteins coat the membrane resulting in a carpet appearance. The membrane can therefore fold to be more energetically favourable with less strain and result in the formation of worm-holes (bottom). When this occurs on opposite sides of the membrane, pore formation occurs (Ganz, 2003). F. Matrilysin-deficient mice possess less antimicrobial activity (Wilson *et al.*, 1999).

Defensins comprise another AMP family, and they are also capable of forming oligomers, with monomers and dimers being predominantly found upon activation and release. However, it is still unknown whether the oligomeric state of the defensins facilitates their antimicrobial actions, although assemblies as large as octomers have been crystallized and modelled (Hoover *et al.*, 2000; Gan *et al.*, 2017).

Defensins are believed to locate their microbial targets initially through charge, using their highly polar N- and C-terminal regions, which contain clusters of cationic residues, predominantly arginine (Machado and Ottolini, 2015). Defensins are capable of binding to both Gram-negative bacteria via LPS and Gram-positive bacteria via polysaccharides, predominantly teichoic acid (Figure 1.11C and D). Consequently, they are bactericidal against a range of bacteria. The absence of zwitterionic lipids and cholesterol in bacterial membranes (unlike mammalian membranes) renders the defensins able to selectively kill to their prokaryote targets (Raj and Dentino, 2002).

Although it is not exactly clear how they do so, defensins are able to form pores and permeabilize bacteria membranes. The best model to date is thought to be the 'carpet wormhole' model (Figure 1.11E). Here, defensins are brought close to the bacterial membrane via electrostatic attraction, where they bind with LPS or teichoic acid, depending on the bacterial type. The proteins then accumulate on the membrane, forming a 'carpet-like' appearance. Because of their amphipathic nature, the defensins are able to manipulate the membrane and embed themselves within it, pulling the membrane around them and generating membrane strain. The membrane disturbances form 'worm-holes', resulting in pore formation and bacterial killing (Ganz, 2003). In addition to pore formation, many signalling cascades are also activated in response to the action of the defensins, resulting in the shut-down of DNA, RNA and protein synthesis. The antimicrobial activity of defensins occurs in the concentration range of 1-10 µg/mL (Ganz, 2003) with its minimum inhibitory concentration (MIC), defined as the minimum concentration of antibiotic or AMP required to inhibit bacterial growth, in the range of 1.4-250 µg/mL (Joly *et al.*, 2004). As with the other proteins described in this section, defensins can be toxic at excessive concentrations. This situation is thought to occur through the action of pro-inflammatory stimuli; hence, intracellular defensin levels are carefully monitored through protease-induced inactivation and degradation by host proteases (Prasad *et al.*, 2019).

Defensins are released from azurophilic neutrophil granules and from Paneth cells into the lumen of the small intestine (Kohlgraf *et al.*, 2010) in response to cytokines or microbial signals that occur in response to infection. The importance of the defensins in host defence can be seen in the phenotype of mice with homozygous disruption of the matrilysin gene. Matrilysin is a metalloprotease that

cleaves the defensin pro-peptide to produce the active form. The KO mice were found to be more susceptible to infection when challenged with bacteria and also possessed higher bacteria counts within the small intestine when compared to wild type mice (Figure 1.11F; Wilson *et al.*, 1999).

As with RegIII, there are clear similarities between the properties of defensins and syncollin, again suggesting that there might also be functional parallels.

1.14 AIMS AND OBJECTIVES

As discussed above, there is some evidence that syncollin might play a role in compound exocytosis in cells such as the pancreatic acinar cell. However, such a role cannot adequately explain why syncollin is present on the luminal side of the ZG membrane; why it is secreted into the pancreatic juice for delivery into the lumen of the small intestine; why it is also secreted from neutrophils; and why its expression changes in inflammatory diseases, such as inflammatory bowel diseases (IBD) and cancers. Further, syncollin has been shown to interact with biological membranes, forming oligomeric structures capable of permeabilizing membranes, and shares additional characteristics with other AMPs, as shown in Table 1.1.

This dissertation describes an exploration of a potential role for syncollin in host defence. My specific aims were:

1. To establish a robust method for purification of recombinant syncollin.
2. To determine the structural characteristics of recombinant syncollin and understand which residues are responsible for some of syncollin's physiological functions using mutational studies.
3. To assess the ability of syncollin to restrict bacterial growth.
4. To analyse syncollin expression in and secretion from neutrophils, and to determine how this secretion might be triggered in response to bacterial infection.

The results described in the following four chapters indicate that syncollin does indeed play a role in host defence, akin to that played by the other AMPs described above.

	Syncollin	ZG16p	RegIII	Defensin
Signal peptide	Yes	Yes	Yes	Yes
Length (amino acids)	134	140	175	40
Molecular weight (kDa)	16	16	19	4
Secondary structure	?	Predominantly beta-sheet Contains Greek-key motif	Beta-sheet 4 alpha helices	Beta-sheet + alpha helix
Function	Compound exocytosis	Secretory lectin – binds carbohydrates Sorts pancreatic enzymes	C-type lectin- binds carbohydrates Anti-microbial protein – acts on Gram-positive (RegIII gamma) and Gram-negative (RegIII beta) Involved in PI3K-AKT pathway	Anti-microbial protein – acts on Gram-positive and Gram-negative bacteria
Expression	Pancreas Duodenum Spleen Neutrophils Colon	Pancreas Duodenum Colon	Pancreas Intestine – Paneth cells Secretory granules and enterocytes	Epithelial cells Haematopoietic cells
Post translational modifications and disulphide bonding	Disulphide bonds	Disulphide bonds N-glycosylation site	Disulphide bonds Filament formation	Disulphide bonds ADP-ribosylation Phosphorylation
Binding partners	Syntaxin-2 GP-2 Cholesterol	Submembranous matrices Cholesterol Proteoglycans	Peptidoglycan (RegIII gamma) Teichoic acid (RegIII beta)	Glycosylated proteins
Oligomerization	Monomer Hexamer on membranes	Monomer	Monomer Hexamer on membranes Filament	Monomer Oligomeric 'nanonets' (human defensin 6)
Mechanism of action	Pore formation?	Binding sulphated proteoglycans	Binding peptidoglycan and permeabilization of bacterial membrane through pore formation (RegIII gamma)	Electrostatic interactions to bind bacterial membranes before permeabilization
Disease linkage	Pancreatic cancer Colitis-associated cancer IBD	Pancreatitis Colorectal cancer	Pancreatitis Pancreatic duct adenocarcinoma IBD	IBD Cancer (diverse)

Table 1.1. Summary of anti-microbial proteins discussed in Section 1.13 in comparison to syncollin.

2. SYNCOLLIN PURIFICATION AND BIOCHEMICAL CHARACTERIZATION

2.1 INTRODUCTION

Previous studies on the biochemical properties of syncollin were carried out on very small amounts of native protein (Edwardson *et al.*, 1997). My first aim, therefore, was to establish a robust method for the purification of recombinant syncollin, with a view to carrying out a thorough examination of the structural and functional properties of the protein.

As described in Chapter 1, syncollin has particular characteristics that needed to be considered when considering purification strategies. Firstly, although syncollin does not contain a transmembrane domain, it nevertheless behaves like a membrane protein in the sense that it requires a detergent to keep it in solution at neutral pH. Secondly, the protein contains seven cysteine residues and has been shown to contain disulphide bonds (An *et al.*, 2000); hence, the purification method must be able support disulphide bond formation. Thirdly, syncollin contains a signal sequence, which must be correctly processed and not expressed in the final form of the protein. Finally, although the monomeric form of syncollin has a molecular mass of only 16 kDa, the protein is able to oligomerize, potentially into hexamers (Geisse *et al.*, 2002). Hence, there is the possibility that purification might generate a

mixture of oligomeric states. To give myself the best chance of developing a successful purification method, I trialled purification in bacterial, insect and mammalian cells. In addition to testing protein yield and purity, I also screened for features that ought to be present in the correctly assembled protein: disulphide bond formation, ability to bind to syntaxin and ability to bind and permeabilize liposomes.

2.2 METHODS

2.2.1 BACTERIAL EXPRESSION

2.2.1.1 CLONING

All enzymes, buffers and reagents were from NEB or Sigma Aldrich, unless otherwise stated. Constructs for bacterial expression of syncollin-His₆ in the plasmid pTrcHis and syncollin-glutathione S-transferase (syncollin-GST) in pGEX-4T were kindly provided by J.M. Edwardson. For expression of syncollin with a tobacco etch virus (TEV)-cleavable His₈-tag, the pop2HA plasmid was used (kindly donated by M. Waterhouse). Syncollin-His₆ was amplified by polymerase chain reaction (PCR) using Vent polymerase and Extensor Master MixTM (Thermo) to incorporate restriction sites for NcoI and XhoI using forward primer: 5'- AATCCATGGGAGCTTGCCAGTG-3' and reverse primer 5'- AGTCTCGAGATAGCACTTGCCAGTAGAGG-3'. Syncollin-His₆ and pop2HA were then digested with NcoI and XhoI before ligation using DNA T4 ligase, transformation and Sanger sequencing.

For periplasmic expression of syncollin, the pMES4y plasmid was used (kindly donated by P. Miller). Syncollin-His₆ was amplified by PCR to incorporate restriction sites for PstI and BstEII using forward primer: 5'-AATCTGCAGGCTTGCCAGTGCCCGCA-3' and reverse primer 5'- AATGGTGACCATAGCACTTGCCAGTAGAGGCCAGAG-3'. Syncollin-His₆ and pMES4y were then digested with PstI and BstEII before ligation, transformation and Sanger sequencing.

2.2.1.2 BACTERIAL TRANSFORMATION AND PROTEIN EXTRACTION

Three bacterial strains were used in an attempt to optimize syncollin expression: BL21, T7 shuffle and Rosetta 2. For BL21 cells, approximately 200 µg of syncollin-His₆, syncollin-GST or syncollin-TEV-His₈-Avi was added to chemically-competent bacteria. Cells were incubated on ice for 30 min before delivery of a 42°C heat shock for 30 s. Cells were then incubated on ice for 5 min before addition of 1 mL 'super optimal broth with catabolite repression' (SOC) medium and incubation at 37°C for 1 h. Bacteria were pelleted by centrifugation at 12,000 rpm and plated onto Luria-Bertoni (LB) agar

containing 100 µg/mL ampicillin. After incubation at 37°C for 12 h, single colonies were picked from the plate and streaked onto fresh LB agar containing ampicillin, followed by incubation at 37°C for 12 h. Bacteria from the culture plate were then inoculated into 5-ml starter cultures of LB medium containing ampicillin, followed by incubation at 37°C, with orbital shaking at 240 rpm, before transfer into larger vessels. Protein production was induced at OD 0.7 by the addition of 0.1 mM isopropyl-β-D-thiogalactoside (IPTG), followed by incubation either at 37°C for 3 h or at 20°C overnight. Cells were pelleted by centrifugation at 5,000 rpm for 15 min, and the pellet was resuspended in 50 mM Tris-HCl, pH 8.0 containing cOmplete™ protease inhibitors, 1 mM phenylmethylsulphonyl fluoride (PMSF), DNase, and appropriate detergent. The cells were lysed mechanically using an Emulsiflex™ C5 with 2-3 strokes at a pressure of up to 15,000 psi. Lysed cells were normally centrifuged at 40,000 x g for 20 min and the supernatant was retained for protein preparation. For protein purification from inclusion bodies, the pellet was resuspended in 50 mM Tris-HCl, pH 8.0 containing 0.1 M NaCl, 10 mM Tris(2-carboxyethyl)phosphine (TCEP), 6 M guanidine hydrochloride (GnHCl), and protease inhibitors, followed by incubation at room temperature for 1 h with rotation. The lysate was then centrifuged at 40,000 x g for 1 h. The supernatant was collected and an attempt was made to refold the protein by dropwise addition into a 50 x volume of 50 mM Tris-HCl, pH 8.0 containing 0.1 M NaCl, 1 mM oxidized glutathione, 10 mM reduced glutathione and 0.5 M L-arginine. The protein was then purified by affinity chromatography (see below).

Transformation of T7 shuffle cells was as described for BL21 cells except that both plating onto LB agar and growth in liquid cultures involved incubation at 30°C rather than at 37°C. When the OD of the cultures reached 0.7, protein production was induced by addition of either 0.1 mM or 1 mM IPTG, followed by overnight incubation at temperatures between 20-37°C. Cell lysis, lysate clarification and purification of soluble protein was as described for BL21 cells.

Rosetta 2 cells were used for periplasmic expression of syncollin with the pMES4y syncollin-His₆ plasmid. Following heat-shock transformation, as described above, the cells were plated onto LB agar containing 100 µg/mL ampicillin, 35 µg/mL chloramphenicol and 1% (w/v) glucose, and the plates were incubated overnight at 37°C. After colony formation, a 5-mL starter culture was inoculated and incubated at 37°C for 16 h, with orbital shaking at 225 rpm. The starter culture was then poured into 1 L of LB medium containing 0.1% (w/v) glucose and 1 mM MgSO₄, followed by incubation at 37°C until the OD reached 0.6. IPTG (1 mM) was then added and the cultures were incubated at 28°C for 16 h. Cells were collected by centrifugation and the pellets were stored at -20°C for 3 h, followed by thawing and resuspension in TES buffer (0.2 mM Tris-HCl, pH 8.0 containing 0.5 M sucrose, 1 mM EDTA,

cOmplete™ protease inhibitors and 0.015% [w/v] dodecylmaltoside [DDM]). After a 16-h incubation at 4°C, with orbital shaking at 225 rpm, 30 mL of ice-cold TES4 buffer (40 mM Tris-HCl, pH 8.0 containing 0.1 M sucrose, 200 μM EDTA, 2 mg/mL DNase and 0.015% [w/v] DDM) was added before a further 1-h incubation at 4°C. Cell debris was removed by centrifugation at 12,500 x g for 10 min before further clarification by centrifugation at 40,000 x g for 30 min at 4°C. The clarified lysate was then loaded onto a HisTrap Excel™ column.

For all three strains described above, glycerol stocks were generated for routine inoculation of cultures. Cultures at approximate optical density (OD) 0.7-1.0 were mixed 1:1 with 20% (v/v) glycerol, before storage at -80°C. For inoculation, samples of glycerol stocks were added to 5-ml LB medium starter cultures containing appropriate selection antibiotics.

2.2.1.3 AFFINITY CHROMATOGRAPHY

Syncollin isolated from bacteria was either His-tagged (BL21, T7 shuffle, Rosetta 2) or GST-tagged (BL21 only). Clarified lysates containing syncollin-His₆ were filtered through a 0.2 μm polyethersuphone (PES) membrane filter and added either to a HisTrap Excel™ chromatography column for AKTA-Pure™ separation (GE Healthcare; using the manufacturer's recommended flow rates), or to Ni-NTA beads (Thermo) for batch incubation at 4°C for 3 h. Unbound proteins were removed using wash buffer (50 mM Tris-HCl, pH 8.0 containing 300 mM NaCl, 20 mM imidazole and 0.087% [w/v] DDM). (20 column volumes were used with the AKTA-Pure column). Syncollin-His₆ was eluted using 50 mM Tris-HCl, pH 8.0 containing 300 mM NaCl, 300 mM imidazole and 0.087% (w/v) DDM. Protein concentration was determined using Nanodrop™ analysis, and protein quality was assessed via the A260/280 ratio. For GST-syncollin, glutathione-Sepharose™ resin (Pierce) was used for batch production. Washing was as above, except in the absence of imidazole; for elution, 15 mM reduced glutathione was used in place of imidazole.

2.2.2 INSECT CELL EXPRESSION

2.2.2.1 CLONING

All enzymes, buffers and reagents were from NEB or Sigma Aldrich, unless otherwise stated. Generation of a Strep-tagged syncollin construct occurred in two stages. First, a linker and a TEV-protease site were added immediately downstream of syncollin. To achieve this, syncollin DNA (kindly donated by K. Zeiser) was amplified by PCR to include restriction enzyme sites for AgeI and NotI using forward primer: 5'-ATAACCGGTATGTCCCGCTGTGCCTGCTGTTGC-3' and reverse primer: 5'-

ATAGCGGCCGCGCCCTGGAAGTACAGGTTCTCGCCACCATAGCACTTGCAGTA-3'. Following sequence confirmation, two Strep-II tags were inserted downstream of the TEV site. These were amplified by PCR from a vector kindly donated by M. Debela, using forward primer: 5'-ATAGCGGCCGTTGGAGTCATCCT-3' and reverse primer: 5'-ATACCTGCAGGTCATCACTTCTCAAAGT-3' to incorporate NotI and SbfI restriction enzymes sites around the Strep-II tags for insertion downstream of syncollin. The resulting sequence is shown in Figure 2.1.

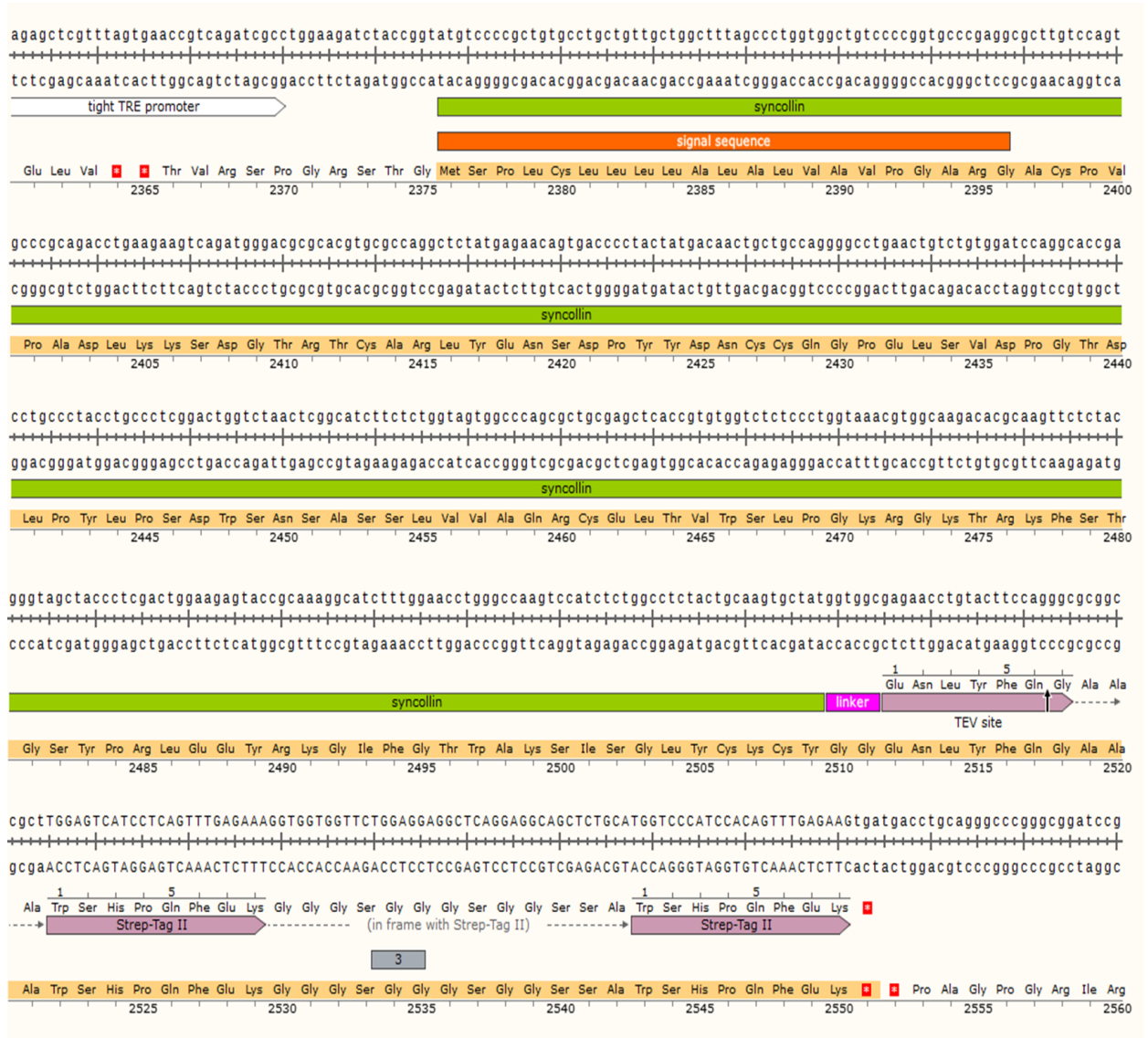


Figure 2.1. SnapGene schematic of Strep-tagged syncollin sequence. Recombinant rat syncollin was used containing the native signal sequence at the N-terminus, a linker, TEV protease site and two Strep-II tags.

For insect cell expression Strep-tagged syncollin was cloned into the pACEbacl plasmid (kindly donated by M. Synakewicz). The syncollin-Strep sequence was amplified by PCR to incorporate restriction sites

for EcoRI and BstBI using forward primer: 5'- AATGAATTCATGTCCCCGCTGTGCCTGCTGTTGCT-3' and reverse primer: 5'-CGCTTCGTCACTTCTCAAAGTGGATGGGACC-3'. Syncollin-Strep and pACEbac1 were then digested with EcoRI and BstBI before ligation and transformation into DH5 α as described above. After sequence confirmation, 1 ng of pFastbac-syncollin-Strep plasmid was used to transform DH10Bac competent cells. Transformed cells were plated onto agar containing 50 μ g/mL kanamycin, 7 μ g/mL gentamycin, 10 μ g/mL tetracycline, 200 μ g/mL 5-bromo-4-chloro-3-indolyl- β -D-galactopyranoside (X-Gal) and 40 μ g/mL IPTG. The plates were incubated for approximately 36 h until blue and white colonies appeared. White colonies were selected and inoculated into 2-mL LB cultures containing the above selection antibiotics but excluding X-Gal and IPTG, and incubated at 37°C for 16 h. Mini-preps (Qiagen), restriction digestion and agarose gel electrophoresis were performed, and samples containing bands at the correct size for both syncollin and the bacmid (2,300 base pairs) were selected for Sanger sequencing.

2.2.2.2 CELL CULTURE

Sf9 and Hi5 insect cell lines were kindly donated by M. Synakewicz. Both cell lines were cultured in suspension using InsectEXPRESS™ media (Gibco) at 27°C with rotation at 120 rpm. Sf9 and Hi5 cells were routinely passaged into 125-mL Ehrlenmeyer flasks when at 3×10^6 cell/mL and 5×10^6 cells/mL, respectively, to a density of 1×10^6 cells/mL. All cells were discarded at passage number 20 and fresh cell stocks thawed.

2.2.2.3 CELL TRANSFECTION

Sf9 cells were selected for transfection with syncollin-Strep and subsequent baculovirus generation. Cells were seeded into 50-mL Falcon tubes capped with breathable sterile adhesive membranes at 8×10^5 cells/tube in a 3-mL volume and incubated for 1 h at 27°C, with rotation at 120 rpm. In order to optimize expression, both CellFectin™ (Thermo) and polyethyleneimine (PEI) transfection reagents were trialled. Bacmid DNA (1 μ g) was added to 100 μ L of InsectXpress™ media in a sterile Eppendorf tube. In another tube, 8 μ L of CellFectin™ or 3 μ g of PEI was added to 100 μ L of InsectXpress™ media. The contents of the two tubes were then briefly mixed and incubated for 30 min at room temperature. The transfection mix was then added dropwise to cells and the cells were incubated for 5 days at 27°C, with rotation at 120 rpm. The cells were then centrifuged at 1,500 rpm and the supernatant containing the baculovirus was collected. A typical viral concentration was 1×10^9 viral particles/mL. For infection, Sf9 or Hi5 cells were seeded so as to be at 2×10^6 cells/mL on the day of infection, and 100 μ L of viral stock was added to a 25-mL culture. Cell density, viability and size were monitored daily. Cells were

cultured until cell viability reached 50% and cells swelled from 11 μm to $\sim 18.5 \mu\text{m}$, indicating infection (typically after 4-5 days). Initially, a time-course for syncollin expression was established. Cells were collected by centrifugation at 1,500 rpm for 5 min and both cell pellet and supernatant were collected.

2.2.2.4 PROTEIN PURIFICATION

Protein purification used the Strep-Tactin XT™ system (Figure 2.2). Strep-Tactin XT™, (engineered streptavidin attached to Sepharose™ beads; IBA), binds a twin Strep-II tag (WSHPNFEK-XXXXXXXXXXXX-WSHPNFEK) with picomolar affinity. Subsequently, the tagged protein can be eluted by addition of excess free biotin. After use, the Strep-Tactin XT™ beads can be regenerated for further use through addition of NaOH, which removes bound biotin. Successful regeneration can be visually shown through addition of 4'-hydroxyazobenzene-2-carboxylic acid (HABA), which binds regenerated Strep-Tactin XT™ resin and displays an orange to red colour shift.

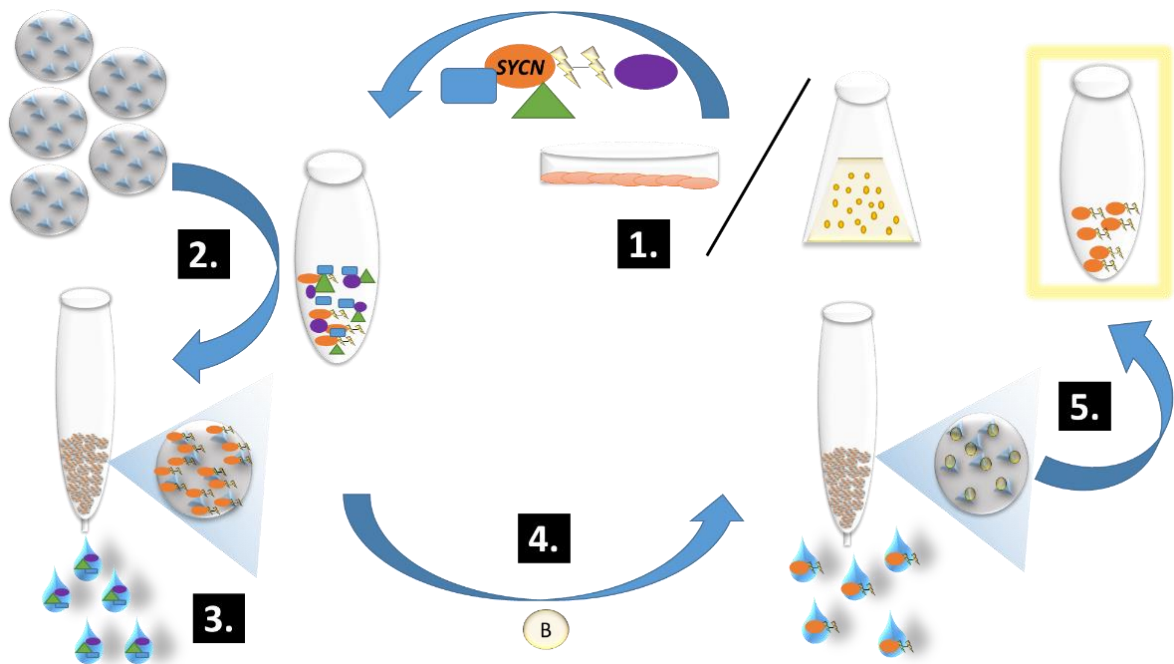


Figure 2.2. Strep-Tactin XT™ affinity chromatography. 1. Either cell lysate or culture supernatant containing syncollin-Strep is generated. 2. Strep-Tactin XT™ beads are incubated with lysates or supernatant to allow binding of the Strep-tag before thorough washing to remove contaminating proteins (3). Excess biotin is added to displace syncollin-Strep from the Strep-Tactin XT™ resin (4). Beads can then be regenerated using NaOH, to displace bound biotin, and HABA, to visually show successful regeneration (5).

For purification from the cell pellet, cells were frozen at -80°C and then thawed to room temperature. Cells were then incubated with lysis buffer (50 mM Tris-HCl containing 150 mM NaCl and 1% [w/v] (3-((3-cholamidopropyl)dimethylammonio)-1-propanesulfonate) (CHAPS) for 3 h at 4°C. Either cell lysate or clarified supernatant was then incubated for 3 h at 4°C with Strep-Tactin XT™ high-capacity resin at a 1:100 dilution (w/v), with shaking. Beads were then pelleted by centrifugation for 5 min at 13,000 rpm and 4°C, and the supernatant was discarded. The beads were resuspended in the relevant wash buffer supplemented with protease inhibitors and the relevant detergent, and loaded into an Econo-Pac™ disposable chromatography column (BioRad). The column was washed with 20 column volumes, and bound protein was eluted using 7 x 2 column volumes of relevant buffer containing 50 mM biotin. All fractions were analysed by SDS-PAGE, followed by Coomassie Blue staining or immunoblotting to assess syncollin yield and purity. Syncollin-Strep was then concentrated to 5 mg/mL or 120 µM (typically from 20 x T175 flasks) using 0.5-ml 10 kDa molecular mass cut-off (Amicon) concentrators. If further clarification was required, the protein was run on an S75 15/300 size exclusion column equilibrated with wash buffer, following the manufacturer's guidance for flow rate.

2.2.3 MAMMALIAN CELL EXPRESSION

2.2.3.1 CLONING

All enzymes, buffers and reagents were from NEB, unless stated. The syncollin-Strep sequence described above was cloned into a pcDNA3.1 backbone using primers 5'-AATAAGCTTATGTCCTCGCTGTGCCTGCTGTTGCT-3' and 5'-AATACCGGTTTCATCACTTCTCAAACGTGGATGGG-3' to incorporate HindIII and AgeI restriction sites. Syncollin-Strep was then ligated into the HindIII- and AgeI-cleaved pcDNA3.1 backbone. All digests and ligations were checked through the appearance of correctly-sized bands on 1% (w/v) agarose gels. Final constructs were then subjected to Sanger sequencing.

2.2.3.2 CELL CULTURE

Both adherent (tsA-201) and suspension (human embryonic kidney [HEK]-293F) cells were used for syncollin production. tsA-201 cells were grown in Dulbecco's Modified Eagle Medium (DMEM) high-glucose medium (Sigma) containing 10% (v/v) fetal bovine serum (FBS) and 1% (w/v) penicillin/streptomycin (Thermo) at 37°C in an atmosphere of 5% (v/v) CO₂/air. Cells were routinely passaged into 175 cm² flasks by trypsin-ethylenediaminetetraacetic acid (EDTA) dissociation when 80-90% confluent. HEK-293F cells were kindly donated by N.J. Rzechorzek and were grown in FreeStyle-

293™ medium (Gibco) at 37°C in an atmosphere of 8% (v/v) CO₂, with rotation at 125 rpm. Cells were routinely passaged into 125-mL Erlenmeyer flasks from densities of 1-2 x 10⁶ cells/mL down to 0.5 x 10⁶ cells/mL.

2.2.3.3 CELL TRANSFECTION

tsA-201 cells were transfected at 70-80% confluence. For each 175 cm² flask, 19 µg DNA, 58.2 µg PEI and 2 mL serum-free medium were combined, vortexed and then incubated for 10 min before addition to the cells. For HEK-293F cell transfection, cells were passaged to 0.5 x 10⁶ cell/mL 24 h before transfection. For 1 x 10⁶ cells, 1.2 µg DNA, 2.4 µg PEI and one tenth of the final volume of serum-free medium were combined, vortexed and incubated for 15 min before addition to the cells. For both tsA-201 and HEK-293F cells, transfected cells were incubated for 96 h before protein extraction.

2.2.3.4 PROTEIN PURIFICATION

Both cells and culture supernatant were collected for protein purification. For purifications from cells, the cells were centrifuged at 1,500 rpm for 4 min and then resuspended in a hypotonic lysis buffer (10 mM Tris-HCl, pH7.0 containing 2 mM EDTA, 1 mM PMSF, and protease inhibitors) and incubated for 20 min on ice. The cells were lysed using 30 strokes of a tight-fitting Dounce homogenizer. Cell debris was removed by centrifugation at 1,500 rpm for 2 min, before membranes were pelleted by centrifugation at 14,000 rpm for 15 min. The membranes were then solubilized in 4-(2-hydroxyethyl)-1-piperazineethanesulfonic acid- (HEPES)-buffered saline (HBS) containing 2% (w/v) DDM. Cell culture supernatant was centrifuged at 1,500 rpm to remove cell debris before analysis of protein content. For protein purification, the Strep-Tactin XT™ system was used as described above for insect cell expression.

2.2.4 PROTEIN ANALYSIS

2.2.4.1 SODIUM DODECYL SULPHATE-POLYACRYLAMIDE GEL ELECTROPHORESIS (SDS-PAGE)

Protein samples were heated for 5 min at 95°C in Laemmli buffer (1.14 g Tris base, 6 g SDS, 15 g sucrose, 7.5 ml 2-mercaptoethanol, and 1.5 ml bromophenol blue, made up to 50 ml with water). Sodium dodecyl sulphate polyacrylamide gel electrophoresis (SDS-PAGE) gels were cast with a 12.5% (w/v) acrylamide running gel (pH 8.8) and a 4% (w/v) stacking gel (pH 6.8) in Bio-Rad casting chambers. Electrophoresis was carried out at 110 V to allow the proteins to pass through the stacking gel and at 150 V once the proteins had entered the running gel. Separated proteins were transferred onto a

nitrocellulose membrane, using the semi-dry transfer method. The polyacrylamide gel was overlaid onto the nitrocellulose membrane that had been pre-soaked in semi-dry buffer (42.9 mM Tris base, 38.9 mM glycine, 0.038% [w/v] SDS) and placed in a Trans-Blot™ semi-dry blotter (BioRad). A 0.05-A current was then applied for 40 min. When the transfer was complete, the membrane was soaked in Ponceau S stain (0.19% [w/v] in 1% [v/v] acetic acid) to locate molecular mass markers. The membrane was blocked in 5% (w/v) milk powder in Tris-buffered saline (TBS; 200 mM Tris-HCl, pH 7.5, 1.5 M NaCl) containing 0.1% (v/v) Tween-20 (TBST) for 1 h. The membrane was incubated for 1.5 h at room temperature in primary antibody, diluted 1:1,000 in blocking solution, with agitation. (N.B. Syncollin was detected using either a mouse monoclonal antibody or a rabbit polyclonal antibody, as indicated). Membranes were then washed with TBST to remove excess antibody, and incubated in horseradish peroxidase- (HRP)-conjugated goat secondary antibody (BioRad), diluted 1:5,000, for 1 h, at room temperature. After three further washes, the immuno-positive bands were detected by enhanced chemiluminescence (ECL). Specifically, horseradish peroxidase was detected by a 5-min incubation in Super Signal West Pico™ (Thermo) before a 1-min exposure in a UVP Bioimager™. Samples of mouse pancreas (containing syncollin) were used as a positive control. To obtain these samples, a mouse pancreas was diced finely with scissors and mixed with radioimmunoprecipitation assay (RIPA) buffer (50 mM Tris-HCl, pH 8.0 containing 150 mM NaCl, 1% [v/v] Triton X-100, 0.5% [w/v] sodium deoxycholate and 0.1% [w/v] SDS), before homogenization by 4-5 strokes of a Dounce homogenizer. To remove debris, the cell lysate was centrifuged at 2,500 rpm for 5 min at 4°C in a bench-top centrifuge. The supernatant was then centrifuged at 14,000 rpm for 15 min at 4°C, and the pellet was resuspended in Laemmli buffer.

2.2.4.2 COOMASSIE BLUE STAINING

After SDS-PAGE, the gel was placed in a clean heat-proof plastic container and hot tap water was added for 3 x 3 min incubations, with agitation. Coomassie blue staining solution (1% [w/v] Coomassie G-250 (Thermo), 45% [v/v] methanol, 10% [v/v] glacial acetic acid and 44% [v/v] H₂O) was added to the gel, and the gel was briefly heated in a microwave oven (without boiling). The gel was incubated for 20 min at room temperature with agitation, before the staining solution was discarded. The gel was then destained in tap water, with an absorbent cloth in the container.

2.2.4.3 SILVER STAINING

After SDS-PAGE, the gel was incubated in fixative solution (40% [v/v] ethanol, 10% [v/v] acetic acid (v/v)) for 1 h, and then in incubation solution (30% [v/v] ethanol, 500 mM C₂H₃NaO₂, 8 mM Na₂S₂O₃,

0.52% [v/v] glutaraldehyde) for 1 h. The gel was then washed four times in water, and incubated in silver nitrate solution (6 mM AgNO₃, 0.2% [w/v] paraformaldehyde (PFA)) for 40 min. After silver impregnation, the gel was incubated in developer solution (24 mM Na₂CO₃, 0.2% [w/v] paraformaldehyde), until bands appeared (formaldehyde reduces silver ions to metallic silver). The reaction was stopped by addition of stop solution (40 mM EDTA).

2.2.4.4 PROTEIN QUALITY CONTROL

Two characteristics of syncollin were assessed after protein purification: the formation of disulphide bonds and the ability to bind syntaxin 2.

To check for the presence (or otherwise) of disulphide bonds, the protein was subjected to SDS-PAGE in the presence and absence of β-mercaptoethanol in the sample buffer. Immunoblotting was then carried out as described above.

To check for syntaxin binding, DH5α *E. coli* transformed with GST-tagged syntaxin 2 (C-terminal domain, residues 181-264) in the plasmid pGEX-4T (kindly donated by J.M. Edwardson) were grown in a 500-mL LB culture containing 100 µg/mL ampicillin. When an OD of 0.7 was reached, 1 mM IPTG was added and cells were incubated for a further 3 h. Cells were pelleted by centrifugation at 5,000 rpm for 15 min. The pellet was resuspended in 10 ml 50 mM HEPES, pH 7.6 containing 150 mM NaCl, protease inhibitors and 1% (v/v) Triton X-100, before sonication using a tip sonicator at medium power for 3 cycles of 30 s each, separated by 30-s pauses. The lysed cells were then pelleted by centrifugation at 14,000 rpm for 30 min. Clarified supernatant was incubated with glutathione-Sepharose™ as described above. The beads were washed with 10 bed volumes of HBS before addition of purified syncollin. After a 3-h incubation, the beads were again washed with 10 bed volumes of HBS. Syncollin was detected using SDS-PAGE followed by immunoblotting. As a negative control, GST (prepared as for GST-syntaxin 2) was used.

2.2.4.5 PROTEOLIPOSOME FORMATION FOR AFM IMAGING

A glass tube was washed briefly with chloroform, and then 0.3 mg L-α-PC (PC) and 0.1 mg 1,2-dioleoyl-sn-glycero-3-phospho-L-serine (PS; Avanti Polar lipids), both solubilized in chloroform, were added. The chloroform was evaporated in a stream of nitrogen gas until a lipid film formed on the bottom of the tube. 3-((3-cholamidopropyl)dimethylammonio)-1-propanesulfonate (CHAPS; Thermo) (1% w/v) was added and the mixture was vortexed to solubilize the lipids. Syncollin-Strep was added to produce

a 2:1 (w/w) ratio and the mixture was dialyzed against HBS for 3 days, with frequent buffer changes, to form proteoliposomes. Protein-free liposomes were prepared as a control.

2.2.4.6 AFM IMAGING

AFM imaging was carried out with the assistance of I. Mela and E. Santander. A proteoliposome suspension (20 μ l) was added to 1-cm diameter cleaved mica discs and incubated for 15 min at room temperature. The disc was then washed briefly 3-4 times using HBS. AFM imaging was carried out in fluid using a Bruker AXS FastScan DimensionTM atomic force microscope. All images were collected in tapping mode.

2.2.4.7 LIPOSOME BINDING ASSAY

Brain (total or polar) or a combination of lipids (PC: PS: cholesterol 3:1:2 ratio [w/w]; 2 mg total; Avanti Polar Lipids) dissolved in chloroform were added to a glass tube and the chloroform was evaporated using a stream of nitrogen gas. Lipids were hydrated overnight at 4°C with 500 μ L of water. The lipid suspension was sonicated with two 30-s pulses on a medium setting to produce liposomes. A further 500 μ L of 2X HBS at the appropriate pH was added, before 500 μ L of the liposome suspension was mixed with 10 μ L of syncollin-Strep (20 μ g/mL) and incubated for 30 min at 4°C, with agitation. A sample of the mixture was then added to 1.14 mL of 80% (w/v) sucrose in the appropriate buffer in 4-mL clear-walled, open-top centrifuge tubes. A further 1.14 mL of 50% (w/v) sucrose and then 1.14 mL of buffer alone were layered onto the 80% sucrose, and the tube was centrifuged at 115,000 x g for 2 h at 4°C in a 60Ti swing-out rotor using a Beckman CoulterTM ultracentrifuge. Fractions (500 μ L) were then taken carefully from the top of the tube and analysed by SDS-PAGE followed by immunoblotting using a rabbit polyclonal anti-syncollin antibody.

2.2.4.8 SYNCOLLIN OLIGOMERIZATION

Purified syncollin-Strep (0.3 mg/mL) was kept on ice, and samples were collected every other day for up to 14 days. Samples were added to Laemmli sample buffer before freezing at -20°C. For analysis, samples were thawed and incubated at 95°C for 15 min before being subjected to SDS-PAGE and immunoblotting using a polyclonal anti-syncollin antibody.

2.2.4.9 ERYTHROCYTE PERMEABILIZATION

Erythrocytes were isolated from the blood of healthy volunteers by members of the laboratory of Dr. M. Harper. Erythrocytes were centrifuged at 5,000 rpm for 2 min and the supernatant was removed to remove any remaining platelets and other unwanted cell types. The erythrocytes were washed three times in HBS and then resuspended in HBS. Samples (180 μ L) were added to EppendorfTM tubes in the relevant buffer. To assess permeabilization via measurement of haemoglobin release, syncollin-Strep at various concentrations in taurodeoxycholate (final concentration, 0.01% [w/v]) was added, and the samples were incubated for 90 min at 37°C before centrifugation at 5,000 rpm for 2 min. The supernatants were removed and added to round-bottomed wells in a clear 96-well plate. Absorbance was then measured at 414 nm. Triton X-100 (1% v/v) and buffer alone (plus taurodeoxycholate) were used as positive and negative controls, respectively. Haemoglobin release was expressed as a percentage of that caused by Triton X-100.

To image the erythrocytes after a 90-min incubation at 37°C, the erythrocytes (20- μ L samples) were added dropwise to poly-L-lysine-coated IbidiTM 18-well flat-bottomed clear plates. Plates were imaged using a ZeissTM confocal microscope with differential interference contrast (DIC) for location of the erythrocytes.

2.2.4.10 QUANTITATION OF LIPOSOME PERMEABILIZATION USING BCECF RELEASE

Brain total lipids (2 mg; Avanti Polar Lipids) in chloroform were added to a glass tube and the chloroform was evaporated using a stream of nitrogen gas. Lipids were hydrated for 2 h at room temperature with 500 μ L HBS, pH 6.7 containing 100 μ M 2',7'-bis-(2-carboxethyl)-5-(and-6)-carboxyfluorescein, acetoxymethyl ester (BCECF; Thermo) dye. The lipid suspension was sonicated with three 10-s pulses on a medium setting to produce liposomes. Filled liposomes were centrifuged at 114,000 x g for 1.5 h at 4°C in a Beckman CoulterTM ultracentrifuge. The supernatant was removed and the pellet was briefly washing with HBS, pH 8.1 to remove excess dye. The pellet was then resuspended in 500 μ L HBS, pH 8.1 and kept on ice in the dark. HBS, pH 8.1 (2 mL) was added to a glass cuvette in a fluorimeter. BCECF-loaded liposomes (20 μ L) were added to the cuvette and fluorescence (495 nm excitation, 535 nm emission) was monitored until the baseline stabilized (~ 50 seconds). Syncollin-Strep (20 μ L of a 0.45- 1.8 mg/mL solution), or elution buffer with or without 1% (w/v) Triton X-100, was then added to the cuvette and fluorescence recorded for ~200 s. For analysis, the fluorescence value for non-permeabilized liposomes was taken as the average of the last three

measurements before any addition. Further, all readings were baseline-subtracted. Triton X-100 was assumed to give 100% release. Data were plotted in GraphPad Prism™ and displayed as % release.

2.3 RESULTS

2.3.1 BACTERIAL EXPRESSION

2.3.1.1 BL21 CELLS

BL21 cells expressing syncollin-His₆ were mechanically lysed in a detergent-containing buffer, and the clarified lysate was incubated with Ni-NTA beads in order to extract the tagged protein. After extensive washing, protein was eluted with 100-400 mM imidazole. Typical elution profiles are shown in Figure 2.3A and B. Syncollin-His₆ ran as both a monomeric form at ~18 kDa and a more prominent oligomer at ~60 kDa. To confirm that the 60-kDa protein was syncollin and not a contaminating protein that non-specifically bound the anti-syncollin antibody, a TEV-cleavable His₆-tagged construct was generated and purified in the same way. Following TEV cleavage, a reduction in size was seen consistent with the removal of a ~5-kDa fragment from the oligomer (Figure 2.3C), confirming that the band did indeed represent syncollin. Interestingly, the oligomer eluted before the monomer (and was even present in the wash fraction containing 20 mM imidazole), indicating that it had a lower affinity for the Ni-NTA beads. Size exclusion chromatography was used to enhance the purity of the 60-kDa oligomer. The concentrated final product contained one contaminant at approximately 31 kDa (Figure 2.3D).

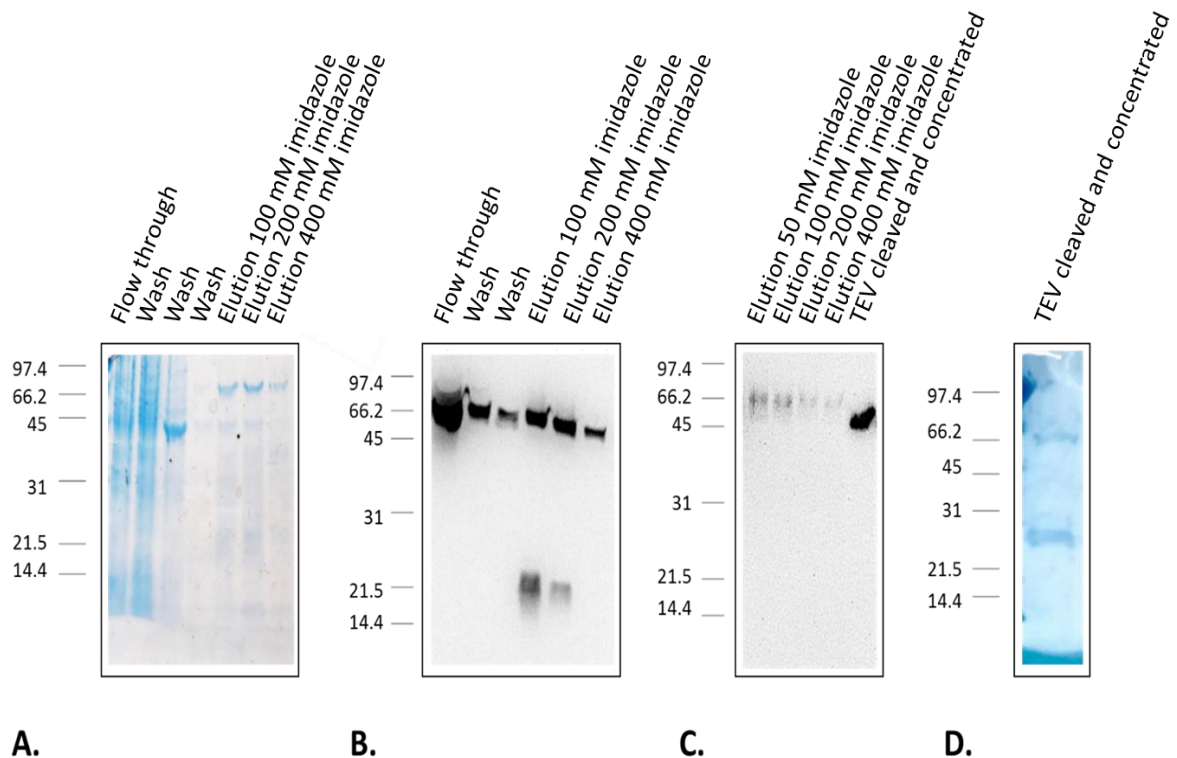


Figure 2.3. Purification of syncollin-His₆ from BL21 *E. coli*. A. Coomassie-stained gel of purified syncollin-His₆. Syncollin-His₆ was purified from BL21 cells and the cell lysate added to Ni-NTA beads for His₆ tag binding, with unbound protein in the flow-through before numerous wash steps to remove unbound protein. Elutions were then carried out with 100-400 mM imidazole. B. Immunoblot of the samples shown in A, using a polyclonal anti-syncollin antibody. C. Purification as in A, B, but using a TEV-cleavable Avi-tagged construct. Imidazole elutions are displayed on an anti-syncollin immunoblot in addition to protein following TEV cleavage and concentration. D. Coomassie-stained gel of TEV-cleaved concentrated protein following gel filtration. Standards are BioRad low-range molecular mass markers (kDa).

To assess whether the majority of purified syncollin from BL21 cells was soluble, the inclusion bodies were also blotted in addition to the imidazole elution fractions mentioned above (Figure 2.4A). It was evident that although soluble protein could be isolated, protein was also present in the insoluble inclusion body fraction. In an attempt to maximize the total yield of syncollin, the protein was purified from the inclusion bodies using the denaturant 6 M GnHCl, before protein refolding in a solution containing 1 mM oxidized glutathione, 10 mM reduced glutathione and 0.5 M L-arginine. This resulted in primarily one band at ~18 kDa and another at ~30 kDa (Figure 2.4B). The proportion of oligomeric states also differed depending on the scale of the bacterial purification, with protein in Figure 2.3 purified from 5 L of bacterial culture running primarily at 16 kDa and 60 kDa, and protein purified from 1 L of culture running at 16 kDa and 30 kDa (Figure 2.4).

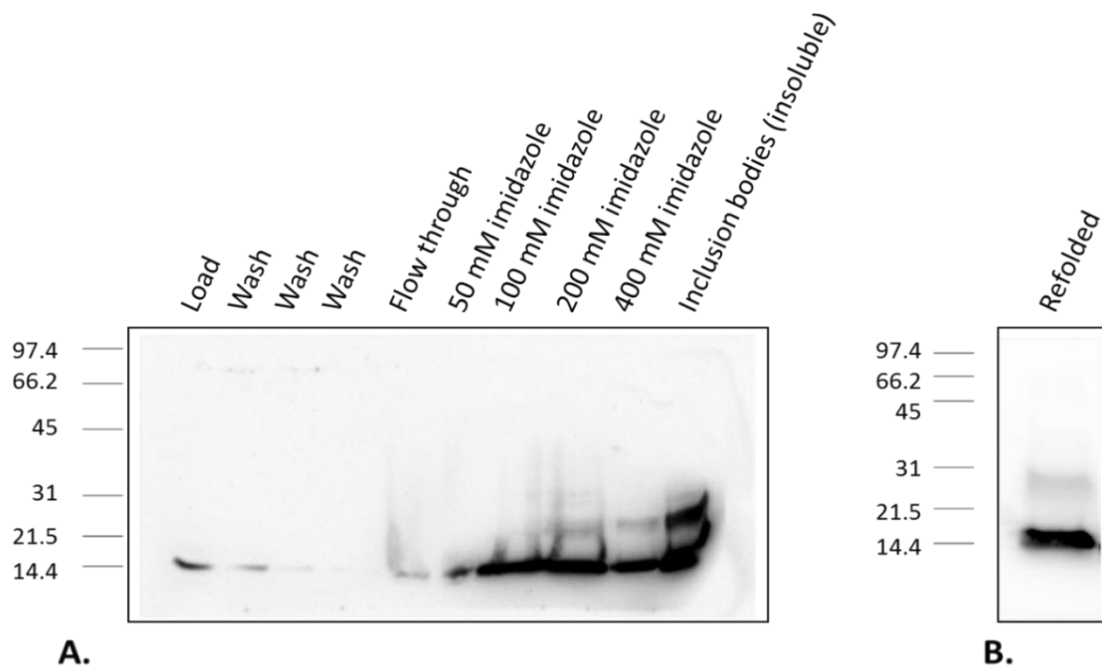


Figure 2.4. Purification of syncollin-His₆ purified from BL21 cells from inclusion bodies followed by refolding. A. Immunoblot showing a His₆-tagged syncollin purification as in Figure 2.3, along with a sample prepared from inclusion bodies, showing insoluble protein. B. Following denaturation of proteins in inclusion bodies, proteins were refolded using 1 mM oxidized glutathione, 10 mM reduced glutathione and 0.5 M L-arginine and immunoblotted using a polyclonal anti-syncollin antibody. Standards are BioRad low-range molecular mass markers.

To test for disulphide bond formation, a 'β-mercaptoethanol shift' assay was performed. The shift could be observed in the refolded protein but not in the unfolded denatured protein, confirming the presence of at least some disulphide bonds in the former sample, but not the latter (Figure 2.5).

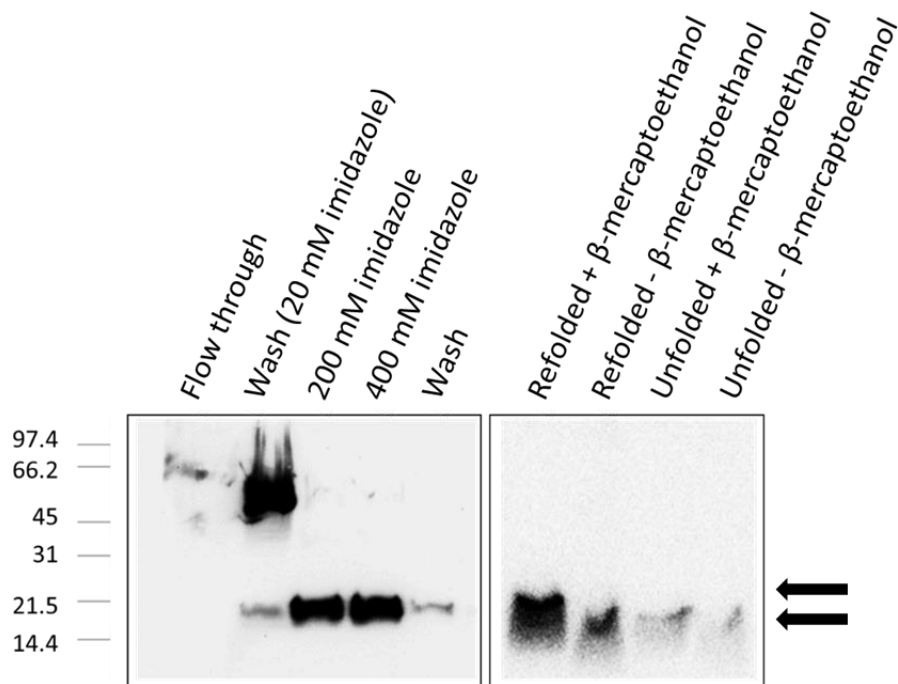


Figure 2.5. Refolding of syncollin-His₆ purified from BL21 inclusion bodies. Immunoblots using a polyclonal anti-syncollin antibody showing a His₆-tagged protein purification and imidazole elutions (left) from inclusion bodies, and (right) the β -mercaptoethanol shifts in unfolded guanidine-denatured protein compared with refolded protein in the presence and absence of β -mercaptoethanol. Standards are BioRad low-range molecular mass markers. Arrows indicate the shift in syncollin size.

2.3.1.2 T7 SHUFFLE CELLS

The purification of syncollin-His₆ was also trialled in T7 shuffle express cells. These cells have an oxidizing cytoplasm rather than the more typical reducing cytoplasm, thereby encouraging disulphide bond formation and correct protein folding (Lobstein *et al.*, 2012). T7 shuffle express cells require optimization for efficient protein production; hence, various temperatures, time courses and IPTG concentrations were tested, using BL21 expression as a comparator (Figure 2.6A). Unlike BL21 expression, where syncollin-His₆ was found in both soluble and insoluble fractions, T7 shuffle cells express the proteins predominantly in the cytoplasm and to a higher yield than in BL21 cells. For this system, induction at 30°C overnight in the presence of 0.1 mM IPTG gave optimal purification.

As can be seen in Figure 2.6B, contaminants were a problem with T7 shuffle expression, although gel filtration increased the purity of both monomeric and oligomeric forms (Figure 2.7). Various detergents were screened to optimize purity and yield (Table 2.1) with 0.015% (w/v) DDM being optimal, despite the presence of some contaminants that were too close in size to be removable by gel filtration.

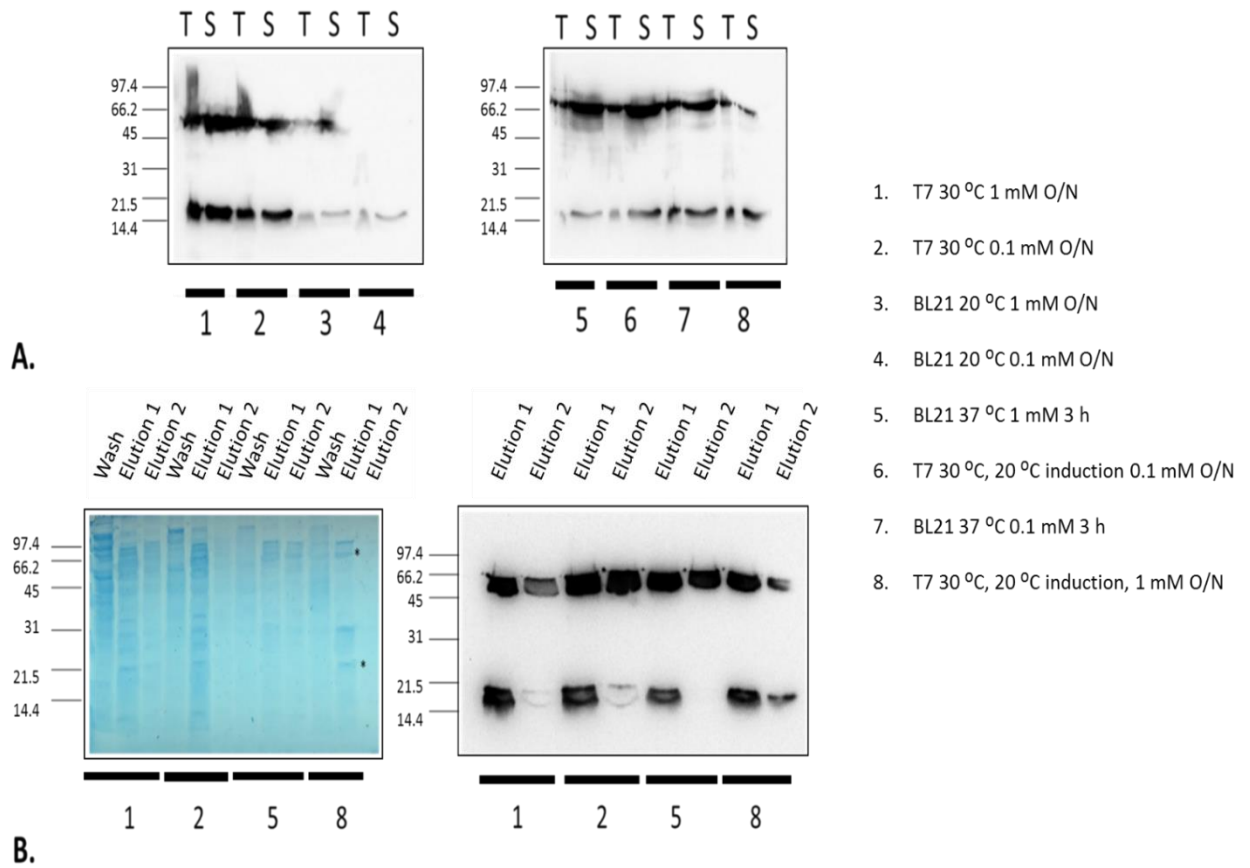


Figure 2.6. Optimization of syncollin-His₆ expression in T7 shuffle express cells. A. Immunoblots showing the results of trialed optimization conditions (listed on the right) in which bacteria type (T7 or BL21), temperature, IPTG concentration and induction time period were varied (ON, overnight). For each condition total (T) and soluble (S) syncollin are shown. B. Coomassie-stained gel (left) and syncollin immunoblot (right) of selected conditions 1, 2, 5 and 8. Elution 1, 100 mM imidazole; elution 2, 200 mM imidazole. A polyclonal anti-syncollin antibody was used for immunoblots. Standards are BioRad low-range molecular mass markers.

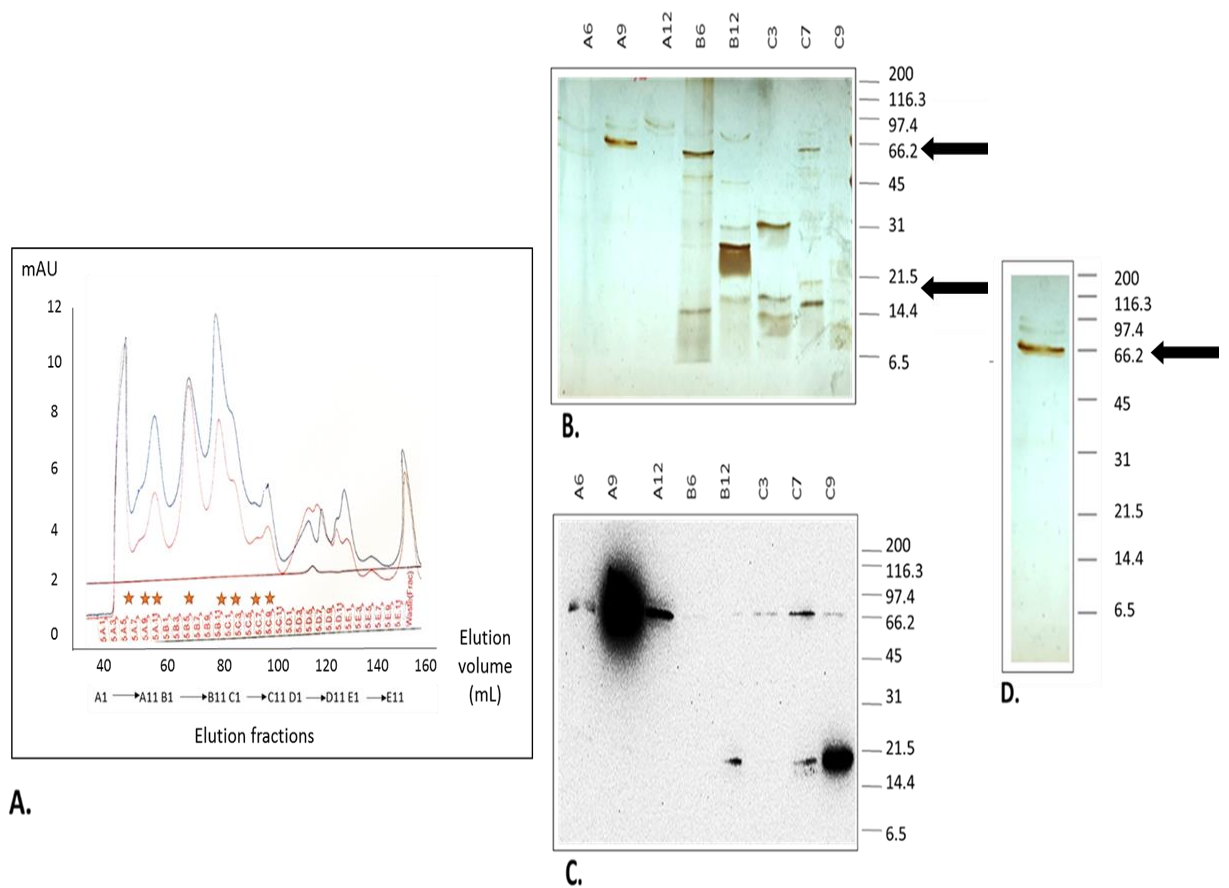


Figure 2.7. Gel filtration analysis of syncollin-His₆ isolated from T7 shuffle cells. A. Gel filtration size exclusion column 'S75 Increase' spectra from GE AKTA Unicorn™ software indicating absorbance at 280 nm (blue) and 260 nm (red). Orange stars indicate chosen elutions for silver stain gel (B) and syncollin immunoblot (C) as indicated above gels, representing the elution fractions collected from the fraction collector. Protein sizes corresponding to syncollin-His₆ monomer and oligomer are indicated by black arrows on the right of B. D. Example of a lane from a silver-stained gel of eluted syncollin-His₆. Standards are BioRad broad-range molecular mass markers. A polyclonal anti-syncollin antibody was used for immunoblots. Arrows indicate the location of syncollin bands.

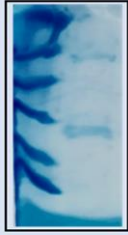

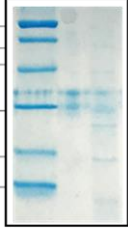

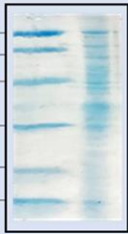

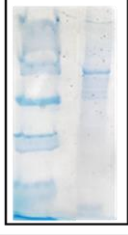

Condition Trialled	Coomassie	Western Blot (anti-syncollin)	Outcome
0.1 % Triton X-100			<ol style="list-style-type: none"> 1. Higher oligomeric band of syncollin seen but no monomer 2. Triton X-100 has a too high micelle size and concentrated upon protein concentration 3. Droplets could not form in crystal trials
0.1 % CHAPS			<ol style="list-style-type: none"> 1. Both monomer and oligomeric forms are present 2. Many other contaminants present
10% Glycerol			<ol style="list-style-type: none"> 1. Both monomeric and oligomeric forms are present 2. Worst purification for contaminants
0.015% DDM			<ol style="list-style-type: none"> 1. Predominantly monomeric form present 2. Contaminants present even following gel filtration column

Table 2.1. Optimization of detergent conditions for purification of syncollin-His₆ from T7 shuffle express cells. Standards are BioRad low-range molecular mass markers.

2.3.1.3 ROSETTA CELLS

In an attempt to reduce the number of contaminants present in samples of bacterially-expressed syncollin-His₆, I tested Rosetta periplasmic expression. Rosetta cells (DE3) are a strain of *E coli*, which are widely used due to improved recombinant protein expression and purity in comparison to BL21 (Tegel *et al.*, 2010). Proteins expressed in the bacterial periplasm contain an appropriate periplasm signal sequence, in this case PelB. The advantage of this system is that contaminating cytoplasmic proteins that are normally present after whole-cell lysis should be excluded. In addition, periplasmic expression is thought to increase efficiency of disulphide bond formation by removing the protein from

the reducing cytoplasm and also by facilitating bond catalysis of a thiol-disulphide exchange via the enzyme DsbA (Nakamoto and Bardwell, 2004).

Disappointingly, contaminants were still present after expression of syncollin-His₆ in Rosetta cells (Figure 2.8A), likely because of the requirement to include detergent in the isolation buffers to maintain protein solubility, which potentially results in general membrane lysis. In a trial of periplasmic expression in the absence of detergent, the protein precipitated and could be centrifuged out of solution (Figure 2.8B). It was concluded, therefore, that expression in T7 shuffle cells was the best option for purification from bacteria.

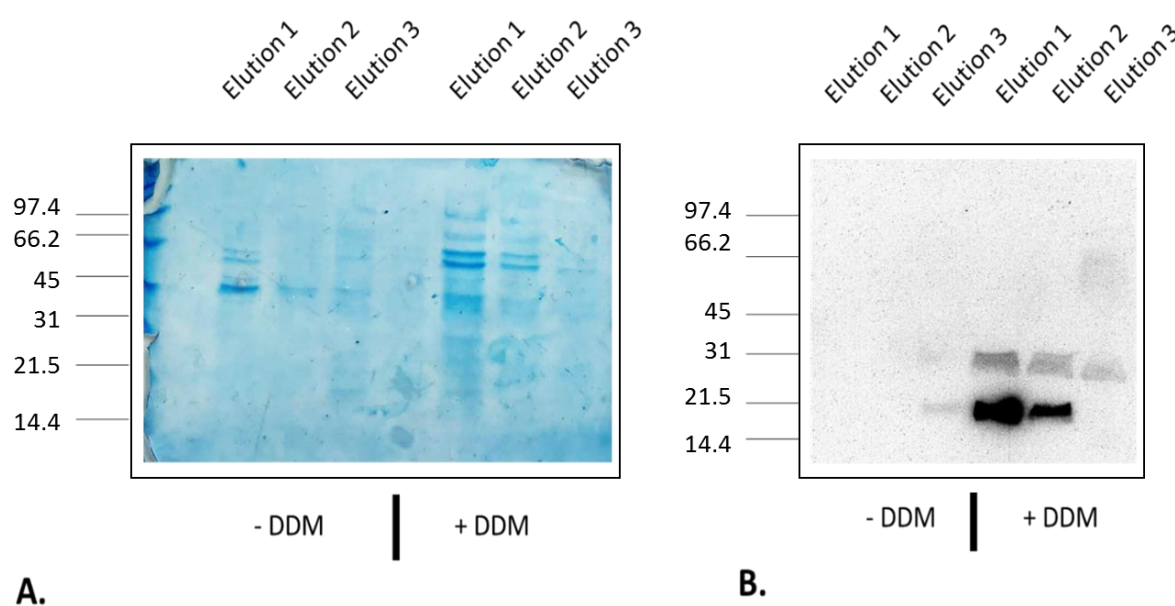


Figure 2.8. Periplasmic expression of syncollin-His₆ in Rosetta 2 cells. Syncollin-His₆ was transformed into Rosetta 2 bacteria. Following periplasmic expression and immobilization via a His₆ tag, elutions were made with imidazole (100-400 mM) in the presence and absence of detergent (DDM). Samples were analysed by Coomassie staining (A) and immunoblotting using a polyclonal anti-syncollin antibody (B). Standards are BioRad low-range molecular mass markers.

For protein quality control after bacterial expression, the ability of syncollin to bind syntaxin was tested. It was found that syncollin-His₆ expressed in T7 shuffle cells bound syntaxin poorly (Figure 2.9). For this reason, in addition to the lack of purity and the presence of various oligomeric states of the protein, bacterially expressed syncollin was ruled out as a purification approach for structural studies.

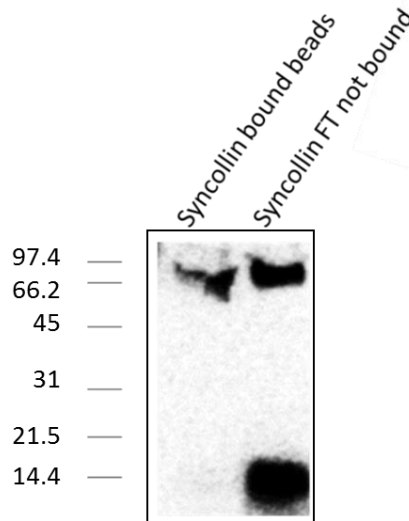


Figure 2.9. Binding of syncollin-His₆ to syntaxin 2. GST-syntaxin 2 was purified, and immobilized on glutathione-Sepharose™ beads. Syncollin-His₆ purified from T7 shuffle cells was incubated with syntaxin beads and the unbound protein (flow through: ‘Syncollin FT not bound’) retained. The beads were then washed and protein bound to the beads (‘Syncollin bound beads’) analysed by immunoblotting using a polyclonal anti-syncollin antibody, along with unbound protein. Standards are BioRad low-range molecular mass markers.

2.3.2 INSECT CELL EXPRESSION OF SYNCOLLIN

After bacterial expression of syncollin was ruled out, insect cell expression was trialled. Insect cells have been extensively optimized for secretory protein expression, resulting in the availability of cell lines such as Hi5 cells, which allow access to isomerase enzymes for disulphide bond formation and whose growth conditions require minimal media to reduce problems associated with the presence of protein contaminants (ThermoFisher Scientific, 2015).

Syncollin-Strep, a construct containing the native signal sequence, a linker, a TEV protease site and two StrepII tags (Figure 2.1) was expressed in insect cells using the bac-to-bac baculovirus transduction system, as illustrated in Figure 2.10. Briefly, syncollin-Strep (containing its native signal sequence) was cloned into pFastBacI and used to transform DH10Bac competent cells. Dh10Bac cells contain a baculovirus shuttle vector and a helper plasmid, which, after transformation with pFastBacI, trigger transposition of the cassette to generate a recombinant bacmid. This bacmid can then be extracted from DH10bacI and used to transfect Sf9 cells to generate a baculovirus, which can be amplified and used to drive protein expression in insect cells.

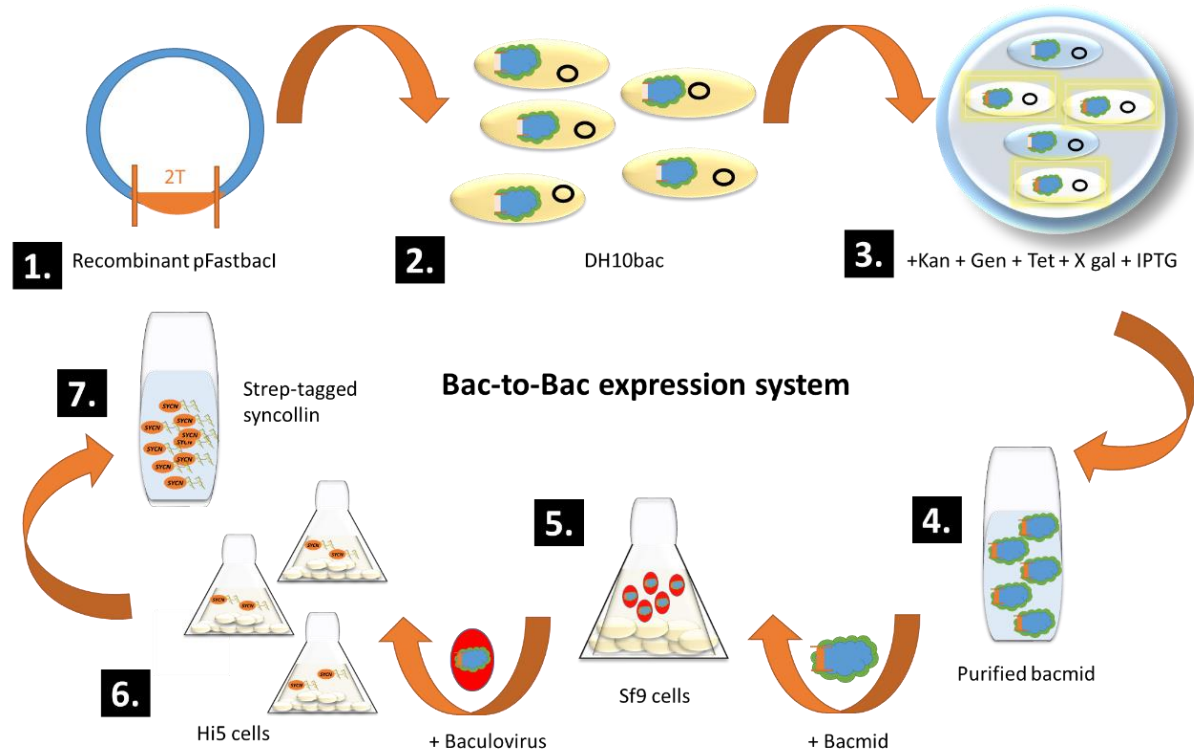


Figure 2.10. Schematic diagram of the bac-to-bac baculovirus purification system. Syncollin-Strep was cloned into a pFastbacl plasmid (1) for transformation into DH10bac cells (2). These cells contain the bacmid and a helper plasmid to facilitate the transposition. Selection occurs on plates as shown in (3) where, through the addition of X-Gal, white colonies are present if successful transposition occurs. Following a PCR reaction to ensure that syncollin-Strep DNA is present within the bacmid, the DNA is purified (4). The bacmid can now be used to transfect Sf9 insect cells using either PEI, CellFectin™ or another transfection reagent of choice. (5) These cells will now generate the baculovirus which will be secreted into the cell media. The baculovirus is collected and can now be used to infect further insect cell lines such as Hi5 (6) to begin a protein expression time-course. A typical time-course is 4-5 days; cells are lysed before the cell viability drops to below 50-60%. Purification using Strep-tactin XT™ beads is then carried out. Adapted from Sui *et al.* (2014).

Sf9 and Hi5 cells were used for generation of the baculovirus following transfection with the recombinant bacmid. It was also found that transfection with the recombinant bacmid using PEI gave a higher protein expression than with CellFectin™, so the former transfection reagent was used routinely (Figure 2.11A). In both cell lines, the optimum time for protein expression was ~4 days. At later time points, cell viability dropped to below 50%, although at this time point some protein had evidently been released into the cell medium following lysis (Figure 2.11B and C). Purified protein did however, appear to be disulphide-bonded (Figure 2.11D). After 3 or 4 days, syncollin-Strep expression was detected inside the cells but not in the culture supernatant (Figure 2.11E), indicating that minimal secretion had occurred. Hence, purification began with lysis of the cell pellet, and used the Strep-Tactin

XT™ affinity chromatography system. However, it proved difficult to produce contaminant-free syncollin-Strep, and so insect cell expression was abandoned.

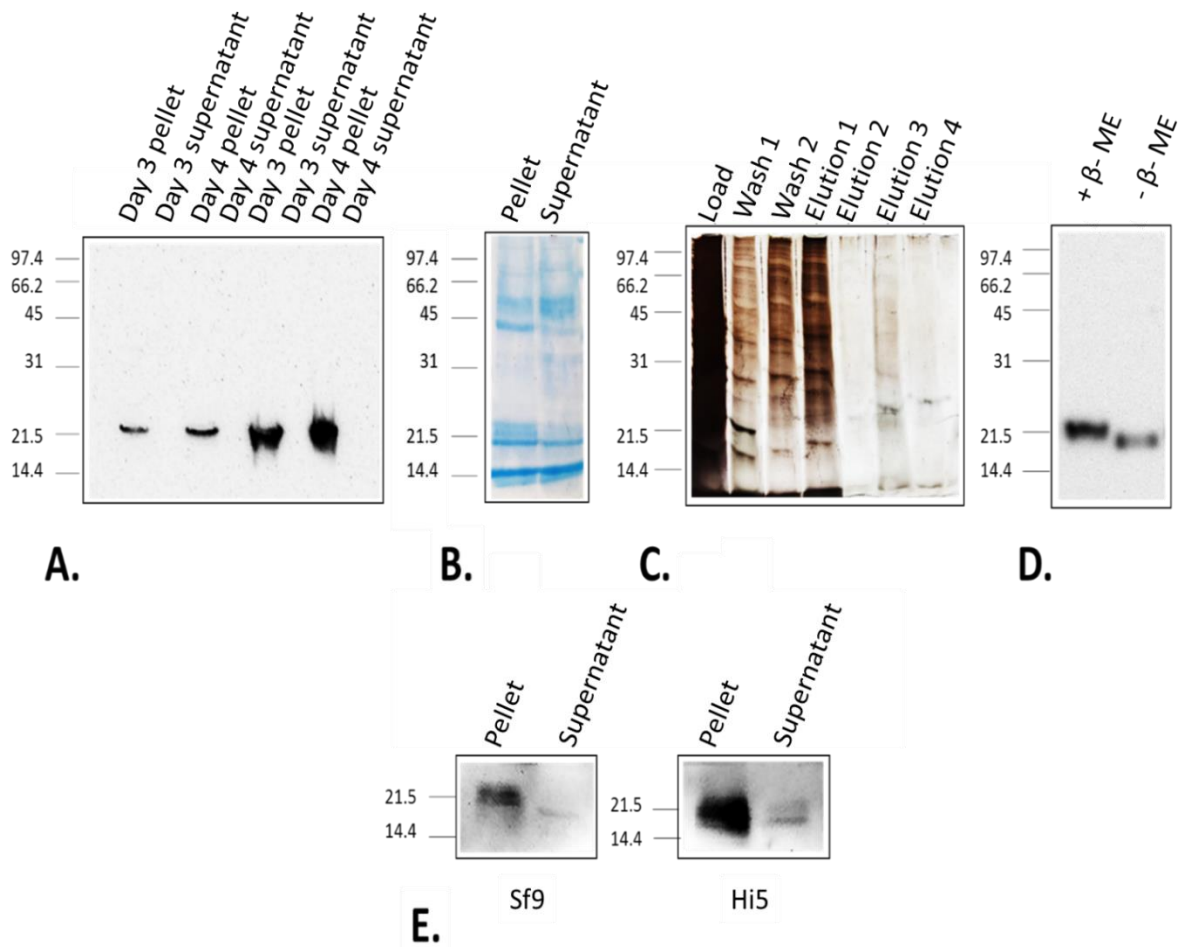


Figure 2.11. Insect cell expression of syncollin-Strep. A. Syncollin immunoblot. Baculovirus was generated in Sf9 cells through transfection of the recombinant bacmid DNA using either CellFectin™ (first 4 columns) or PEI (last 4 columns). Following addition of the baculovirus to Sf9 cells, cell pellets were lysed and culture supernatants were collected to assess syncollin-Strep expression. ‘Day 3’ and ‘Day 4’ refer to time after addition of the baculovirus. After day 4 the cell viability fell below 50% and so no further samples were taken. B. Coomassie-stained gel of the pellet and supernatant samples at day 4. C. Silver-stained gel of syncollin-Strep purification from the cell lysate of Sf9 cells. D. Immunoblot of an eluted sample of syncollin-Strep in the presence and absence of β-mercaptoethanol. E. Comparison of syncollin-Strep expression in Sf9 and Hi5 cells after 4 days of baculovirus infection. ‘Pellet’ refers to lysed cell pellet; ‘Supernatant’ refers to cell culture media. Standards are BioRad low-range molecular mass markers. A polyclonal anti-syncollin antibody was used for immunoblots.

2.3.3 MAMMALIAN CELL EXPRESSION

For purification of syncollin from mammalian cells, tsA-201 cells were transfected with syncollin-Strep in pcDNA3.1. Purification again used the Strep-Tactin XT™ system. As can be seen in Figure 2.12, following biotin elution of syncollin from Strep-Tactin XT™ beads, the protein ran at ~20 kDa in size and appeared as multiple bands on silver-stained gels and immunoblots. If contaminating proteins were present, gel filtration was carried out using a S75 size exclusion column, which yielded almost pure protein after combination of appropriate fractions and concentration (Figure 2.13).

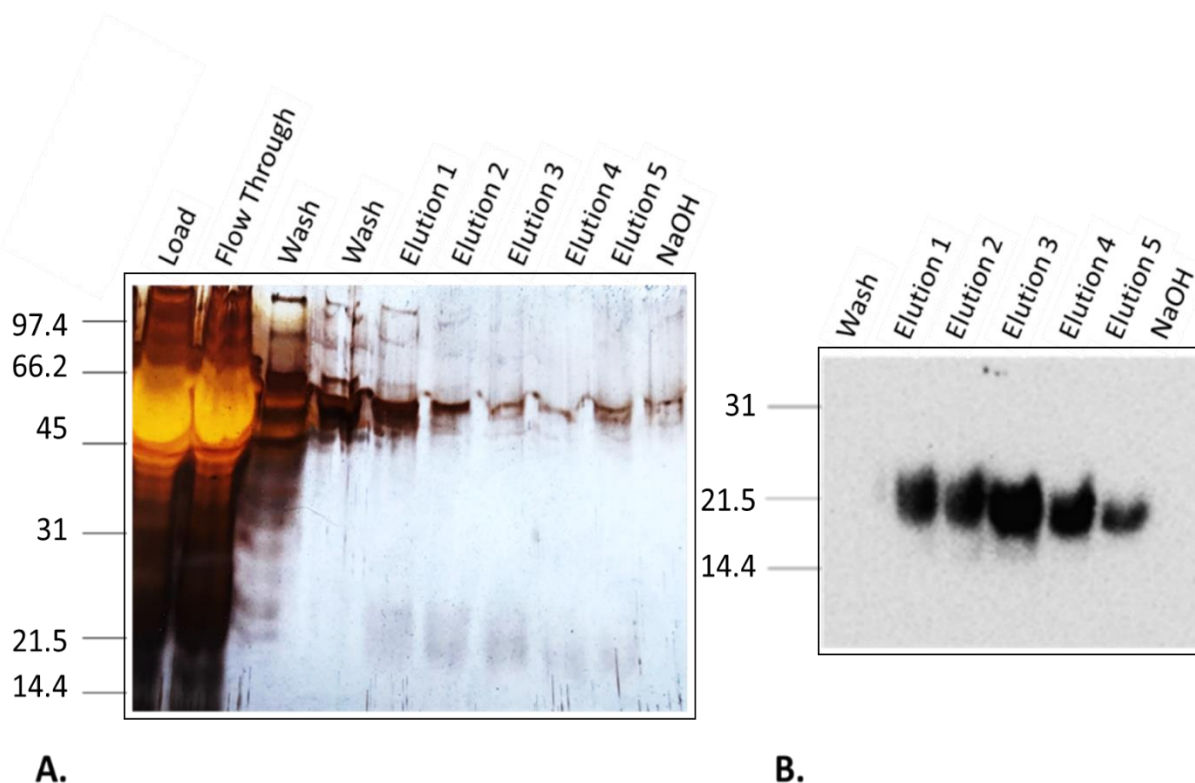


Figure 2.12. Elution of syncollin-Strep from Strep-Tactin XT™ beads. A. Silver stain showing the total cell supernatant added to Strep-Tactin XT™ beads ('Load'), the flow-through which did not bind to the beads ('Flow-through'), various wash fractions ('Wash'), elution fractions using 0.5 column volumes of 50 mM biotin in Buffer W ('Elution 1,2,...'), and the result of complete stripping of remaining bound protein using 10 mM sodium hydroxide ('NaOH'). B. Immunoblot using a polyclonal anti-syncollin antibody showing wash, elution and NaOH fractions from the silver-stained gel in A. Standards are BioRad low-range molecular mass markers.

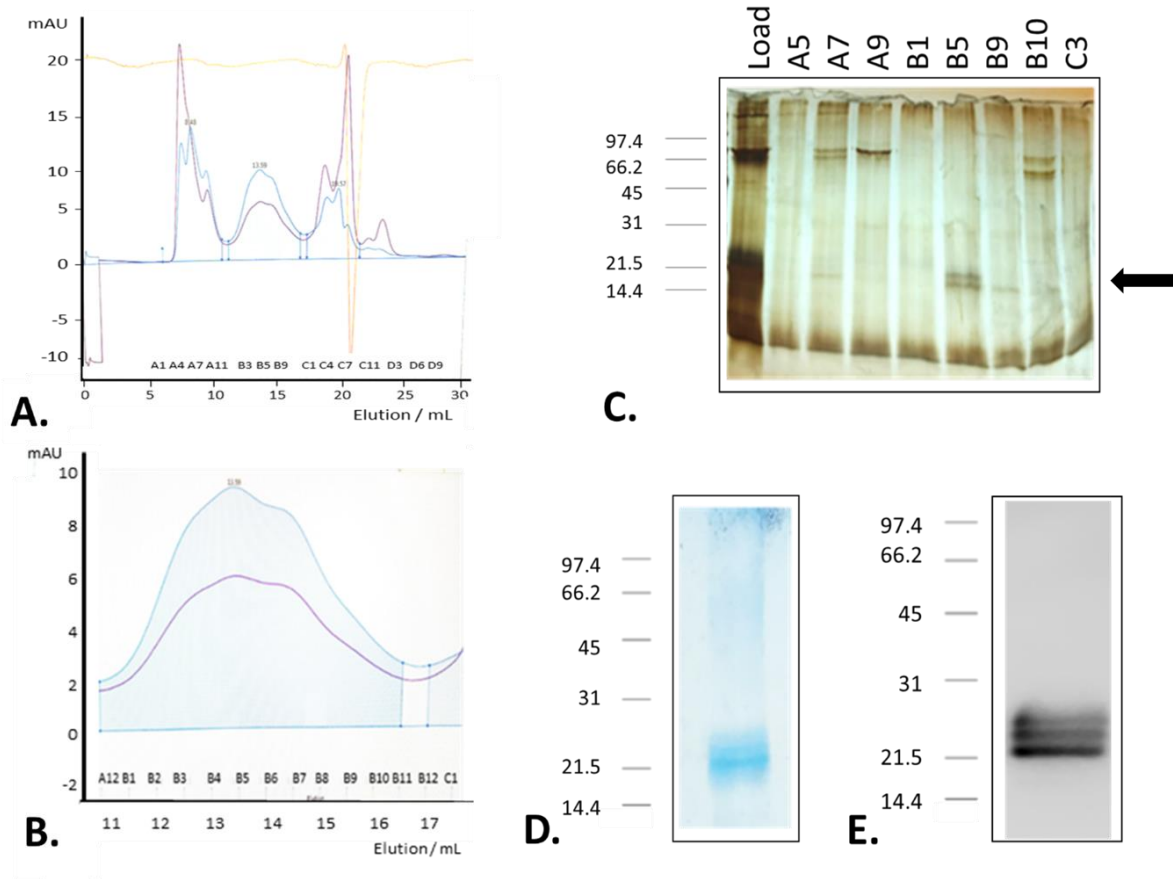


Figure 2.13. Behaviour of syncollin-Strep on gel filtration columns. A. Size exclusion gel filtration 'S75 Increase' column spectra showing fractional elutions using AKTA Unicorn™ software following Strep-tagged syncollin sample addition B. Zoomed-in peak from A showing syncollin-Strep double peak and fractions corresponding to lanes in silver stain C. D. Coomassie-stained gel of concentrated syncollin-Strep, using Amicon 10-kDa molecular mass cut-off concentrators (protein concentration, 2.5 mg/mL). E. Immunoblot of purified syncollin-Strep using a polyclonal anti-syncollin antibody, showing multiple bands on gel. Standards are BioRad low-range molecular mass markers. The arrow shows the location of the syncollin band.

Because of concerns related to the use of detergent-containing buffers for structural analysis of syncollin, a trial purification in the absence of detergent was carried out to determine whether the protein was soluble under this condition. As shown in Figure 2.14, the protein concentrations obtained in the absence of detergent were greatly reduced in both the eluted and concentrated fractions. Given that detergent (or a substitute) is clearly necessary to keep syncollin in solution, a screen of different detergents and other conditions with respect to purity, yield and micelle size was carried out. As shown in Table 2.2, the purest and most concentrated protein sample in a detergent with a low micelle size was obtained using 0.1% (w/v) CHAPS, a condition that was subsequently used routinely. As an alternative to the use of a detergent, 75 mM L-arginine was also trialled.

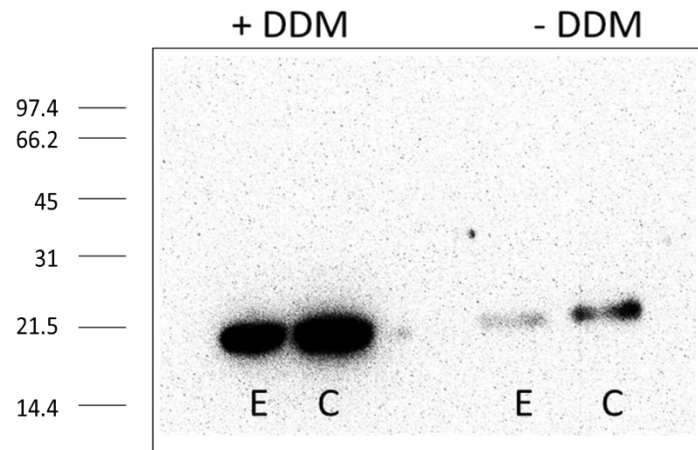


Figure 2.14. Immunoblot showing syncollin-Strep purified in the presence and absence of detergent (DDM). For each condition, elution (E) and concentrated (C) samples are shown. Standards are BioRad low-range molecular mass markers.

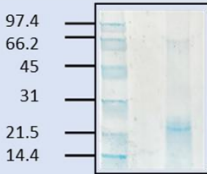
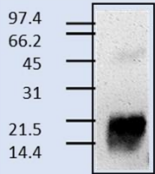
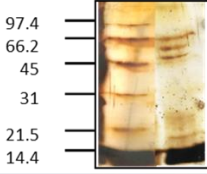
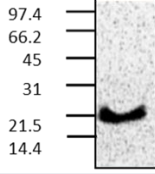
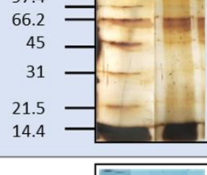
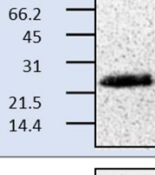
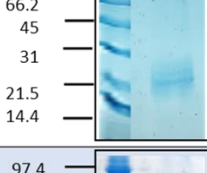
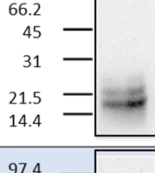
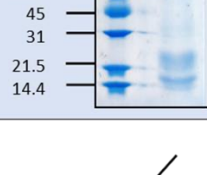
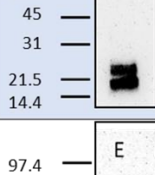

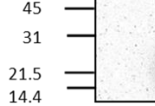

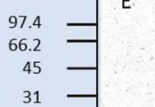
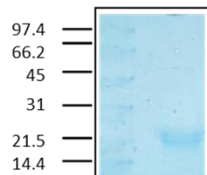
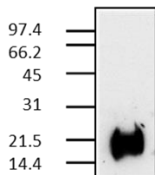
Condition Trialled	Micelle size (kDa)	Coomassie/ Silver Stain gel	Western Blot (anti-syncollin)	Outcome
0.015% DDM	70			<ol style="list-style-type: none"> Detergent has higher micelle size so concentrates in 10 kDa molecular weight cut off (MWCO) concentrator Higher molecular weight contaminant which can be removed through SEC Syncollin is a double band
0.3% NG	85			<ol style="list-style-type: none"> Many contaminants Lower yield Detergent has higher micelle size so concentrates in 10 kDa MWCO concentrator Syncollin is a single band
0.5% β-OG	25			<ol style="list-style-type: none"> Many contaminants Lower yield Syncollin is a single band
0.1% CHAPS	6			<ol style="list-style-type: none"> Pure sample No apparent contaminant seen Micelle size is small so passes through 10 kDa MWCO concentrator
0.2 M NDSB	-			<ol style="list-style-type: none"> Detergent free Close contaminant at approx. 16 kDa which did not separate on SEC
0.1 mM CaCl ₂	-			<ol style="list-style-type: none"> Protein known to bind calcium from literature Detergent-free No protein eluted, protein precipitated on beads
Syntaxin binding	-			<ol style="list-style-type: none"> Protein known to bind syntaxin Detergent free No protein eluted, protein precipitated on beads
75 mM L-Arginine	-			<ol style="list-style-type: none"> Detergent free No obvious contaminants seen After 24 hours increased spectrophotometer absorbance at >320 nm implying aggregation.

Table 2.2. Conditions trialled to facilitate the solubility of purified syncollin-Strep. Where protein precipitated on beads and did not elute, 'E' and 'B' are used to denote elution fraction and beads respectively. Standards are BioRad low-range molecular mass markers.

As for purifications from bacteria, a 'β-mercaptoethanol shift' assay was run to test whether syncollin-Strep purified from tsA-201 cells was disulphide bonded. The result shown in Figure 2.15 confirms the presence of disulphide bonds. The ability of syncollin-Strep purified from tsA-201 cells to bind syntaxin was also tested. As shown in Figure 2.16, syncollin-Strep bound to GST-syntaxin 2 (but not to GST alone) attached to GSH-Sepharose™ beads. Hence, at least some of the characteristics of the recombinant syncollin matched those of the native protein.

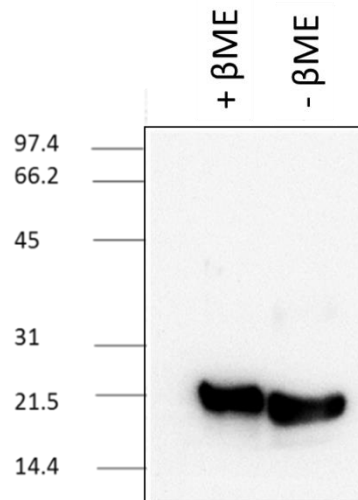


Figure 2.15. Immunoblots of syncollin-Strep purified from mammalian cells and run in the presence and absence of β-mercaptoethanol (βME) using a polyclonal anti-syncollin antibody. Standards are BioRad low-range molecular mass markers.

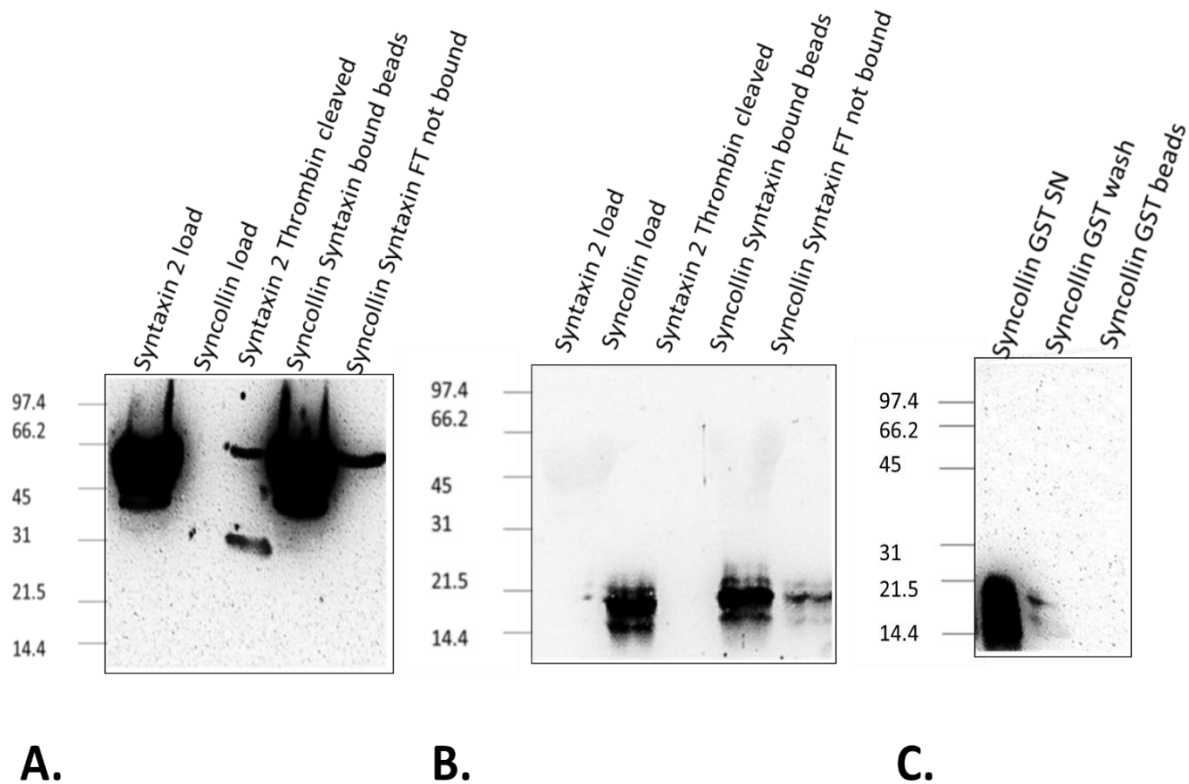


Figure 2.16. Binding of syncollin-Strep to syntaxin 2. Immunoblots using a polyclonal anti-syncollin antibody for either syntaxin 2 (A) or syncollin (B). GST-syntaxin 2 (C-terminal domain) was immobilized on glutathione-Sepharose™ ('Syntaxin 2 load') and washed to remove unbound proteins. Syncollin-Strep was also prepared ('Syncollin load'). To ensure that the protein detected was syntaxin 2, thrombin cleavage was carried out to remove the GST-tag ('Syntaxin 2 thrombin cleaved'). Syncollin-Strep was then added to immobilized syntaxin 2 and the beads were washed to remove unbound syncollin ('Syncollin syntaxin FT not bound'), syncollin-Strep bound to the beads was analysed ('Syncollin syntaxin bound beads'). As a control, the same experiment was carried out with GST alone rather than GST-syntaxin 2 (C). Here, syncollin-Strep remaining in the supernatant ('GST SN'), unbound protein washed from the beads ('Syncollin GST wash') and syncollin-Strep bound to the beads were analysed ('Syncollin GST beads'). Standards are BioRad low-range molecular mass markers.

In an attempt to scale up the production of syncollin-Strep, suspension cultures of HEK-293F cells were trialled. Surprisingly, syncollin-Strep was not secreted from HEK-293F in suspension; rather, all of the protein remained in the cell pellet (Figure 2.17A). Further, although syncollin could be purified from the cell pellet, the sample had many major contaminants and the protein yield was reduced (Figure 2.17B and C). For this reason, adherent tsA-201 cells were used for future syncollin-Strep purifications.

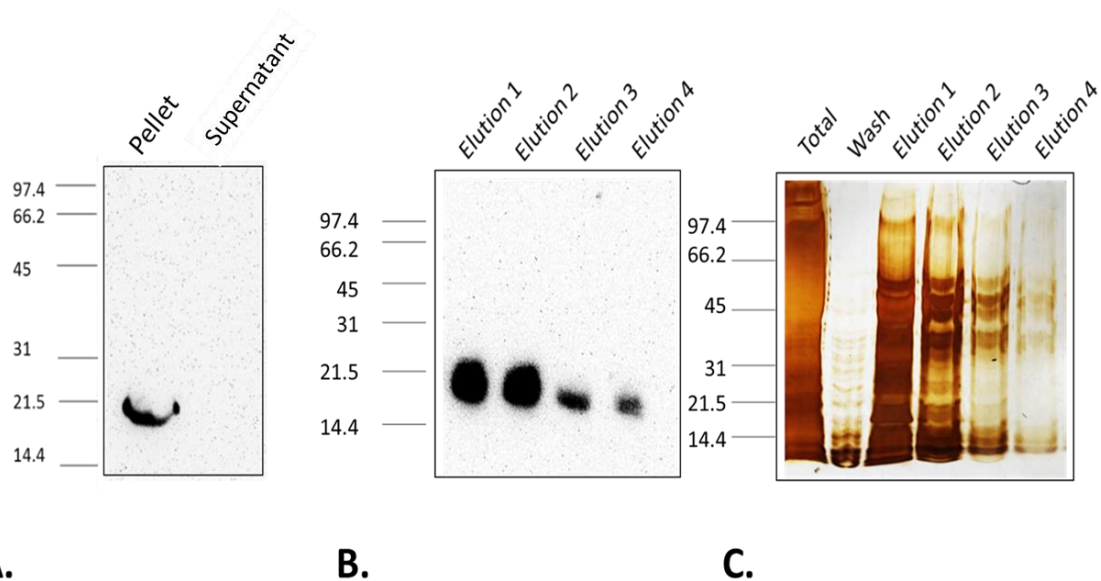


Figure 2.17. Purification of syncollin-Strep from HEK-293F cells in suspension HEK-293F. A. Following transfection with syncollin-Strep, HEK-293F cell pellets and supernatant were collected and immunoblotted. B. A cell lysate was incubated with Strep-Tactin XT™ beads and bound syncollin-Strep was eluted with successive 0.5 column volumes of 50 mM biotin ('Elution 1,2...'), followed by immunoblotting using a polyclonal anti-syncollin antibody. C. Silver-stained gel showing whole cell lysate following HEK-293F lysis ('Total'), wash fraction ('Wash') and the same 4 elution fractions shown in B (Elution 1,2...). Standards are BioRad low-range molecular mass markers.

Now a robust purification had been established for recombinant syncollin, several experiments were carried out to compare the behaviour of syncollin-Strep with that of native syncollin.

2.3.3.1 AFM IMAGING OF SYNCOLLIN ON LIPID BILAYERS

In order to investigate whether syncollin-Strep was capable of forming pore-like structures on lipid bilayers, as the native protein was reported to do (Geisse *et al.*, 2002), syncollin-Strep bound to supported lipid bilayers (PC/PS 3:1) was imaged under fluid by fast-scan AFM. As can be seen in Figure 2.18, circular 'beads-on-a-string' structures of various diameters were observed. Each circular 'necklace' ring structure appeared to consist of differing number of units with the peak diameter of the rings at ~10 nm and the peak height at ~2-3 nm. It is tempting to speculate based on these structures, syncollin is capable of forming pores and therefore, permeabilizing membranes.

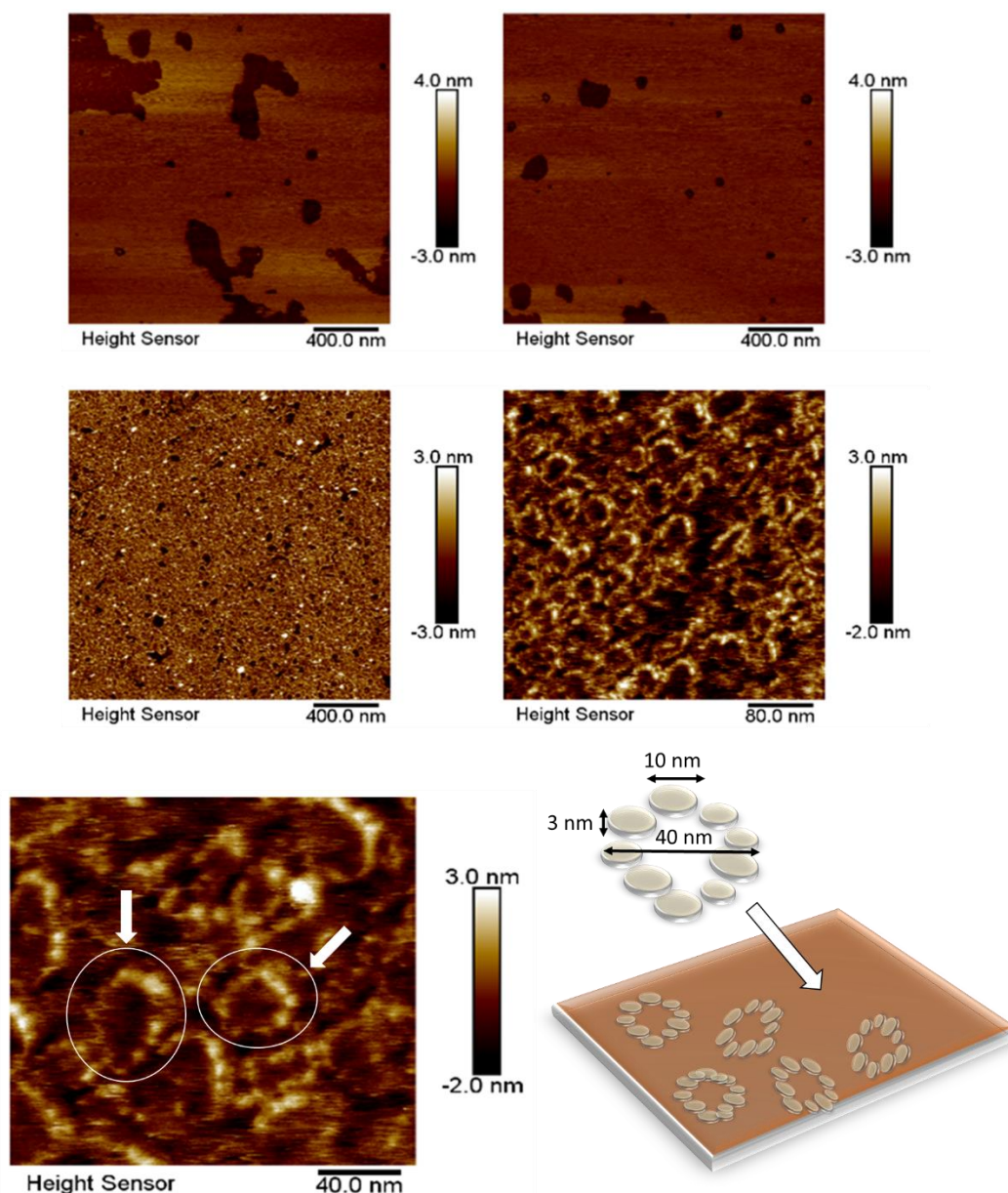


Figure 2.18. AFM imaging of syncollin-Strep in association with lipid bilayers. Upon addition of liposomes (without protein) to freshly cleaved mica, a continuous lipid bilayer was formed (top). Bilayers (PC/PS 3:1) containing syncollin-Strep were imaged in fluid tapping mode by fast-scan AFM (centre and bottom). A height scale is displayed to the right of each image. Circles and arrows are drawn to highlight 'necklace' ring structures which are further illustrated in the cartoon (bottom right), with average diameter and height measurements indicated.

2.3.3.2 BINDING OF SYNCOLLIN TO LIPOSOMES

To further assess the binding of syncollin to lipids, liposomes were incubated with purified syncollin-Strep and then floated on sucrose density gradients. As shown in Figure 2.19A, a 'fluffy' liposome layer could be observed. Liposomes of various compositions were incubated with syncollin: total brain lipids,

which included cholesterol; polar brain lipids, which did not; and L- α -PC and DOPS in the presence and absence of cholesterol. Fractions were collected from the top to the bottom of the gradient to assay for the presence of syncollin-Strep.

In all cases, syncollin-Strep ran as an oligomer (~80 kDa) on silver stained gels after incubation with liposomes, whereas the same protein had run as a monomer after purification (Figure 2.19B). Syncollin-Strep bound total brain lipids (90% of total) more avidly than polar brain lipids (74 % of total; Figure 2.19C). This difference is likely a result of the presence or absence of cholesterol, since when liposomes with defined composition were used, only 5% of the protein bound to liposomes without cholesterol whereas 30% bound to liposomes containing cholesterol (Figure 2.19D). This result demonstrates the importance of cholesterol for syncollin-Strep binding to liposomes, as had been shown previously for the native protein (Hodel *et al.*, 2001).

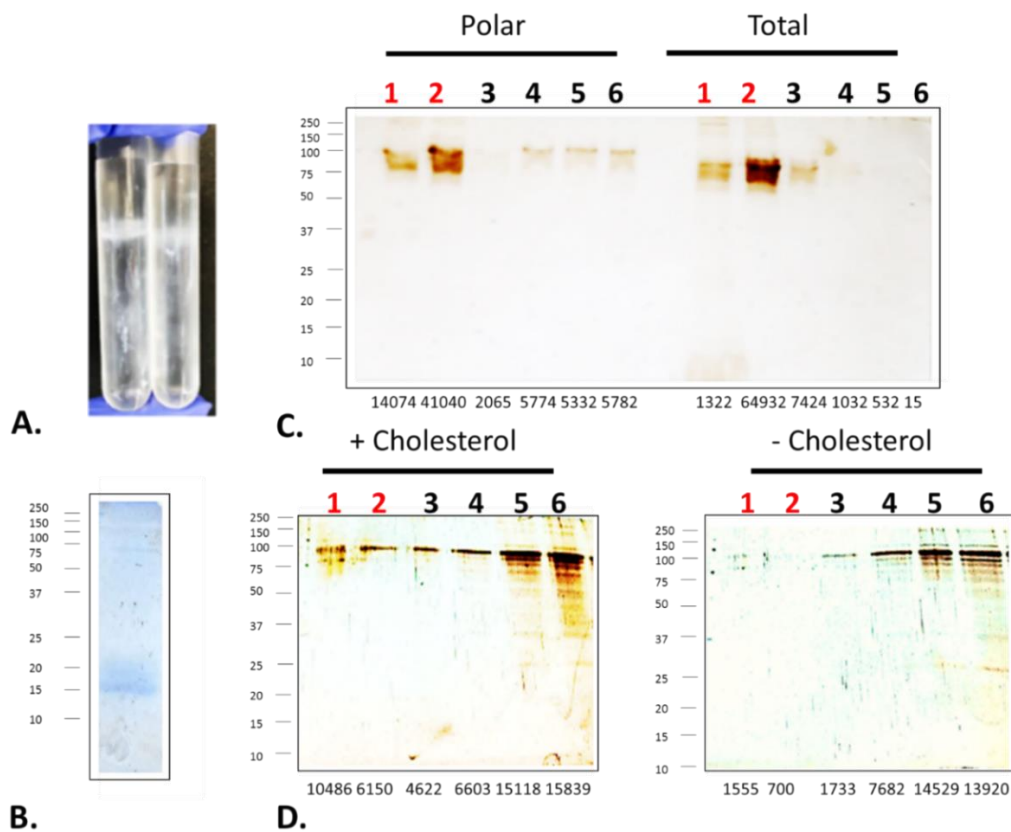


Figure 2.19. Syncollin binding to liposomes. A liposome/protein mix was floated on a sucrose density gradient via ultracentrifugation at 114,000 x g for 1.5 h at 4°C. Following ultracentrifugation, a 'fluffy' liposome layer was observed (A). Purified syncollin-Strep (B) was incubated with either brain lipids (polar and total) (C) or a combination of lipids (PS/PC \pm cholesterol) (D). Fractions were collected from the top (1) to the bottom (6) of the tubes, with fractions 1 and 2 containing the liposome layer (denoted by the red font). Fractions were then mixed with Laemmli sample buffer and subjected to SDS-PAGE and silver staining. (C, D) ImageJ™ was used to calculate the band intensities of syncollin-Strep which are displayed below each of the lanes.

2.3.3.3 SYNCOLLIN OLIGOMERIZATION

As syncollin-Strep appeared to oligomerize following incubation with liposomes of various compositions, a time-course of oligomerization was next assessed. Following purification, syncollin-Strep was stored on ice, and samples were collected every 2 days, added to Laemmli sample buffer and stored at -20°C until analysis by immunoblotting. The immunoblot for syncollin revealed that on day one the protein ran almost exclusively as a monomer at ~20 kDa, as seen previously following purification. However, an additional band at ~40 kDa appeared on days 3 and 5, and further bands at ~90-250 kDa appeared after 7 days, indicating that syncollin-Strep oligomerized progressively over several days (Figure 2.20). An alternative explanation could be syncollin aggregation as a result of partial unfolding causing an increase in molecular mass with time.

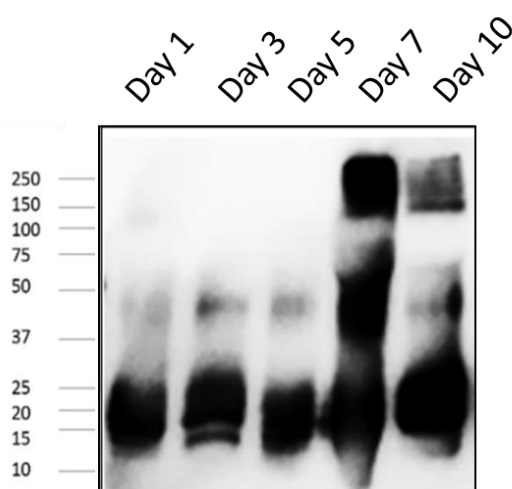


Figure 2.20 Time-course of oligomerization of syncollin-Strep. Syncollin-Strep was kept on ice for up to 10 days, and samples were collected approximately every 2 days. Samples were mixed with Laemmli sample buffer and stored at -20°C. All samples were thawed and incubated at 95°C for 15 min before analysis by SDS-PAGE and immunoblotting using a polyclonal anti-syncollin antibody. Standards are BioRad molecular mass markers (Precision Plus).

2.3.3.4 ERYTHROCYTE PERMEABILIZATION

To investigate whether syncollin-Strep was capable of permeabilizing membranes, haemoglobin release from erythrocytes was measured. Erythrocytes were incubated with various concentrations of syncollin-Strep for 90 min at 37°C. A concentration-dependent release of haemoglobin was seen, with ~35% of the total haemoglobin being released at the highest concentration of syncollin-Strep used (400 ng/ mL; Figure 2.21A). When erythrocytes were imaged by confocal microscopy, those incubated with the highest concentration of syncollin adopted a 'spiky' cell shape likely because of a collapse of

the plasma membrane around the cytoskeleton upon permeabilization (Figure 2.21B). These results demonstrate that syncollin-Strep retains the ability to permeabilize erythrocytes that was seen previously with native syncollin (Wäsle *et al.*, 2004).

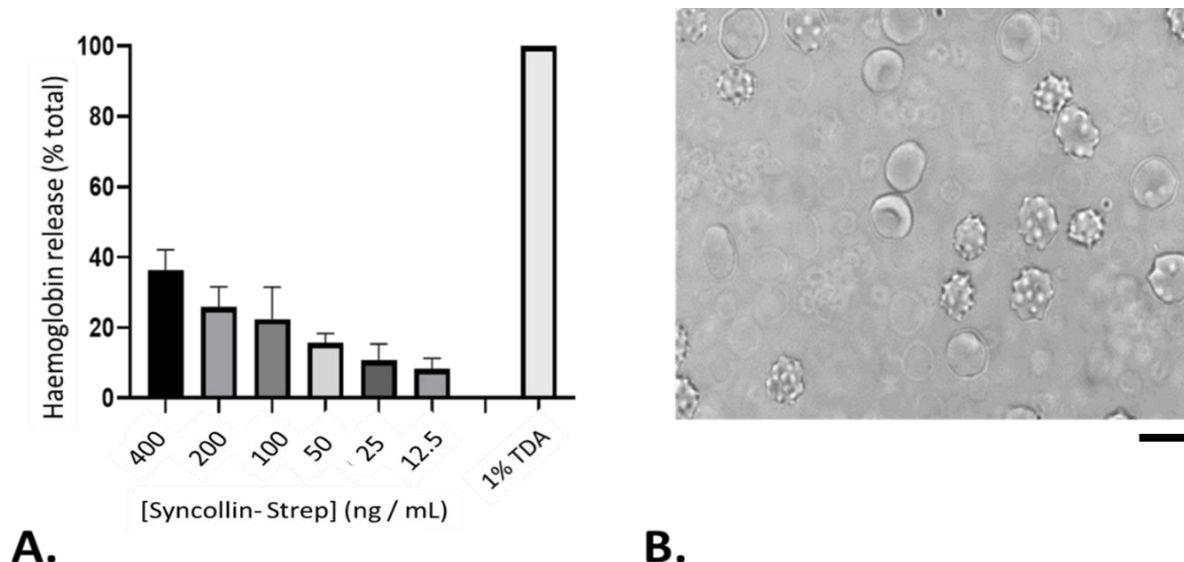


Figure 2.21 Permeabilization of erythrocytes by syncollin-Strep. A. Erythrocytes were incubated with syncollin-Strep for 30 min at 37°C. Haemoglobin release was then monitored via the absorbance of a cell supernatant at 414 nm. Taurodeoxycholate (1% [w/v]) addition was used to define 100% release, and data were expressed as % permeability. Syncollin-Strep concentrations are shown. Error bars are SD. B. DIC image of erythrocytes after incubation with syncollin-Strep. Scale bar 10 μ m.

2.3.3.5 LIPOSOME PERMEABILIZATION

As a second method to assess whether syncollin-Strep was capable of permeabilizing membranes, release of the dye BCECF from liposomes was measured. Here, an increase in fluorescence of BCECF would indicate permeabilization of liposomes to protons and, potentially, dye. BCECF, at 520 Da, is more than 100-fold smaller than haemoglobin (64 kDa) and responds more rapidly and sensitively to membrane disturbances. As BCECF has a pKa \sim 6.98, (Gdovin *et al.*, 2010) and its fluorescence is sensitive to changes in pH of approximately 1.0, pH 6.7 and 8.1 were selected as the internal and external pH, respectively. Liposomes containing BCECF were generated by sonication of a lipid suspension in HBS containing BCECF at pH 6.7. Liposomes were then pelleted by centrifugation, washed, resuspended in HBS at pH 8.1. Fluorescence was then measured in response to addition of syncollin-Strep at an excitation wavelength of 495 nm and an emission wavelength of emission 535 nm.

A rapid increase in fluorescence was observed even at the lowest concentration of syncollin-Strep added (0.45 mg/mL). Maximal release (~75% of total, defined by addition of Triton X-100) was observed following syncollin addition at 1.8 mg/mL. Neither internal buffer (HBS, pH 6.7) nor control elution buffer resulted in permeabilization of the liposomes (Figure 2.22A and B). Hence, syncollin-Strep permeabilized the liposomes in a concentration-dependent manner (Figure 2.22C).

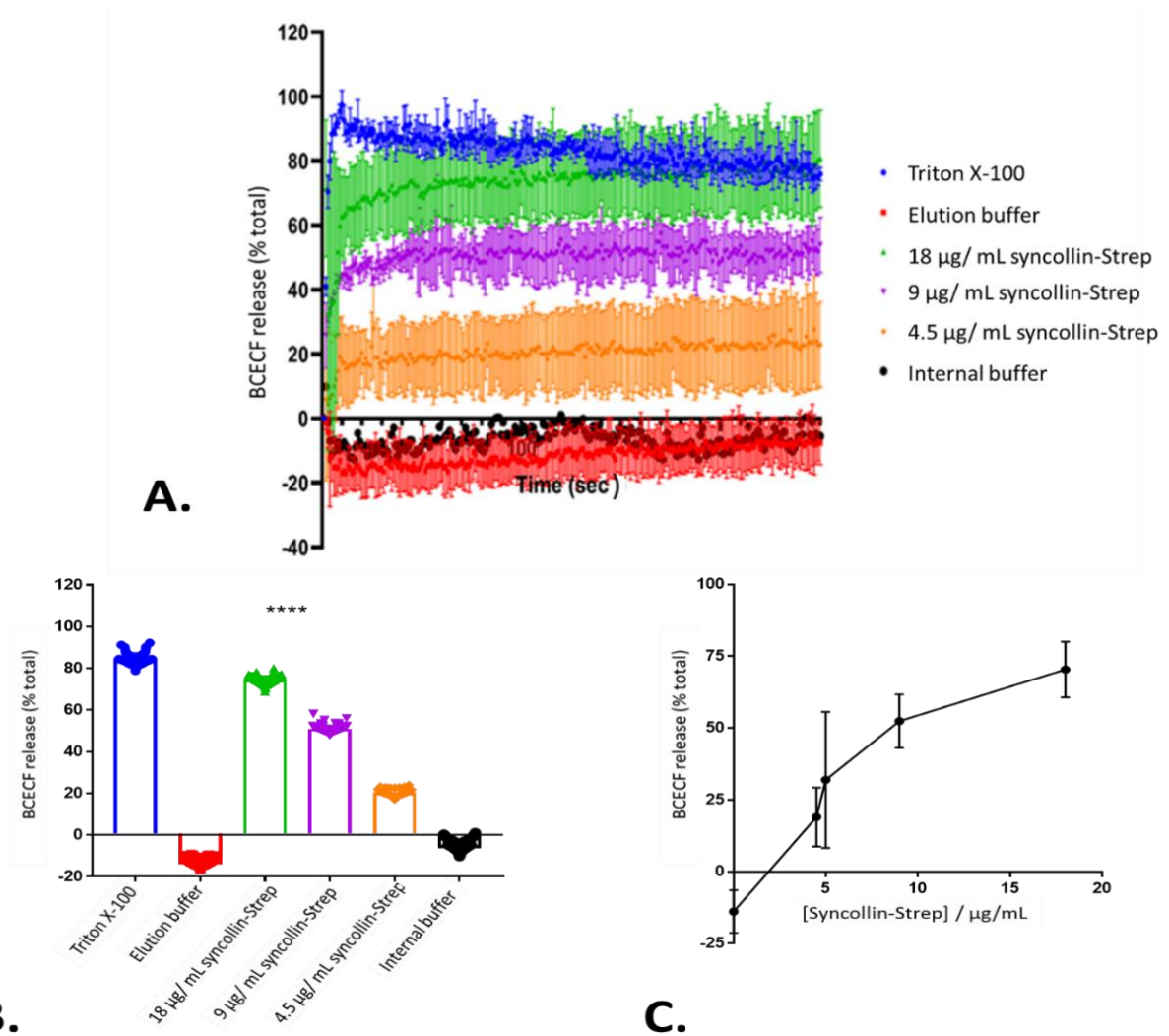


Figure 2.22 Permeabilization of liposomes by syncollin-Strep. Brain total lipids (2 mg) were dried under a nitrogen stream and rehydrated with HBS, pH 6.7 containing 100 µM BCECF for 2 h at room temperature. Liposomes were vortexed and then briefly sonicated before ultracentrifugation at 114,000 x g for 1.5 h. Pelleted liposomes were briefly washed with HBS, pH 8.1 before resuspension. Liposomes (20 µL) were added to 2 mL HBS, pH 8.1 in a 2-mL glass cuvette in a fluorimeter. The baseline was allowed to stabilize before addition of 20 µL syncollin-Strep (0.45 -1.8 mg/mL), elution buffer alone or Triton X-100. Syncollin-Strep concentrations shown are final concentrations. A. Time-course of BCECF release. Fluorescence was monitored (excitation 495 nm, emission 535 nm) for up to 200 s. Error bars are SD (n=3). Data were plotted using GraphPad Prism™. B. BCECF release triggered by syncollin-Strep. Data points from (A) between 50 and 150 s are displayed as a histogram using GraphPad Prism™. One-way ANOVA with Tukey's multiple comparison test was carried out between conditions. ****p<0.001 (for all syncollin concentrations). C. Dependence of BCECF release on syncollin-Strep concentration. Error bars are SD (n=3).

2.4 DISCUSSION

Establishing a robust purification of recombinant syncollin was important for the structural and functional studies described later in this dissertation. Previous purifications of syncollin were directly from rat acini. Hence, given the close homology between rat and human syncollin, rat syncollin was selected for recombinant protein purification.

Attempts to purify recombinant syncollin from bacterial, insect and mammalian cells were met with a number of challenges. For instance, when purified from bacteria, syncollin was not able to bind syntaxin, which the native protein is known to do, and also did not possess disulphide bonds without refolding in a redox-glutathione mix. Further, the oligomeric state of bacterially expressed syncollin differed according to the purification system, whereas it behaved as a monomer in mammalian and insect purifications. For these reasons, bacterial expression was not pursued.

When syncollin-Strep was expressed in mammalian cells, there was an evident requirement for detergent in order to keep the protein in solution. From homology modelling of its structure (see Chapter 3), it was anticipated that the protein contains two highly charged faces; hence it would not be surprising that a detergent might be needed to shield these faces in aqueous solution. It became apparent during testing of the various purification protocols that the absence of detergent or replacement of detergent with other agents such as glycerol, Ca²⁺ or syntaxin 2 was not sufficient to keep the protein soluble.

Finally (and interestingly), the behaviour of syncollin-Strep differed depending on whether the cells in which it is expressed were adherent or in suspension. When expressed in adherent tsA-201 cells, the protein (bearing its native signal sequence) was secreted into the supernatant, whereas the protein was retained within HEK-293F cells in suspension (and also in insect cells in suspension).

Despite the many attempts to increase protein yield, purification from adherent tsA-201 cell became the routine protocol, giving the purest sample and the highest yield among the conditions trialled, and showing evidence of disulphide bond formation and syntaxin 2 binding. Additionally, syncollin-Strep could bind to, oligomerize upon, and permeabilize membranes, mimicking the behaviour seen previously with the native protein. The number of syncollin monomers within oligomeric ring structures seen using AFM could not be quantified; however, additional AFM experiments in which syncollin could be pre-incubated with a monoclonal anti-syncollin antibody could facilitate quantification of the oligomeric complexes (Barrera *et al.*, 2005).

A typical yield of syncollin-Strep from 15 x T175 flasks was 0.1 ml of a ~5 mg/mL solution, and the buffer in which it was isolated was 10 mM sodium phosphate, pH 8.0 containing 0.1% (w/v) CHAPS. These samples were used in subsequent studies of the structural characteristics and function of the protein. All successful conditions which were trialled for syncollin expression are summarized in Table 2.3.

Cell	Chosen purification	Yield from 500 mLs	Contaminants
Adherent HEK cells (secreted)	0.1% CHAPS	~5 mg/mL	None visible
Adherent HEK cells (secreted)	75 mM L-arginine	~1.5 mg/mL	None visible
Bacterial T7 Shuffle cells	0.015% DDM	~1.5 mg/mL	>10
Insect Sf9 cells	0.1% CHAPS	~2 mg/mL	>5

Table 2.3. Table summarizing syncollin purification in mammalian, bacterial and insect cells. ‘Chosen purification’ indicates successful purification detergent/additive used for syncollin solubility. ‘Contaminants’ are protein bands observed on Coomassie-stained SDS-PAGE gels.

3. SYNCOLLIN STRUCTURAL CHARACTERISTICS

3.1 INTRODUCTION

3.1.1 PROTEIN STRUCTURE

Protein structure encompasses primary, secondary, tertiary and quaternary structure. Primary structure refers to the amino acid sequence, in which representatives of the 20 amino acids are joined together in a specific order via peptide bonds. Peptide bond formation involves the binding of the carboxyl group of one amino acid to the amine group of another, with the loss of a water molecule (Berg *et al.*, 2002). The amino acids that form the primary structure are able to interact with each other in ways that depend on their side chain. Most amino acids are non-polar and therefore do not interact with neighbouring peptide chains; however, some are reactive and it is these which begin to drive the folding of the primary structure to form the secondary structure (Lodish *et al.*, 2000). Interactions between protein chains can be either covalent, in the case of disulphide bonding, or non-covalent, involving ionic and hydrogen bonding, and van der Waals interactions. Cysteines are the only amino acids which are capable of forming intra-molecular covalent (disulphide) bonds, which are stronger than non-covalent bonds but weaker than peptide bonds. Disulphide bridges are important because

they can control the folding of the primary structure. Among the non-covalent bonds, ionic bonds (the strongest type) form between charged positive or negative side chains; hydrogen bonds form between partially charged polar amino acid side chains; and van der Waals interactions (the weakest type) form between hydrophobic amino acids. All of these types of bonding contribute to the folding of the primary structure (O'Connor and Adams, 2010). Another element that affects the primary structure of a protein is post-translational modification. These modifications (e.g. N-linked glycosylation) occur after the translation of the mRNA sequence into the peptide chain, and can be detected even as the amino acid sequence begins to emerge from the ribosome (Carter and Sheih, 2015).

The three-dimensional folding of the peptide chain as a result of the formation of inter-chain bonds determines the secondary structure of a protein. The two main types of secondary structure are the alpha-helix and the beta-sheet. Proteins can be composed predominantly of one or other type of structure, although more commonly both types co-exist. The existence of only two predominant secondary structures is a consequence of limited rotation of the planar peptide bond; with many repeated hydrogen bonds occurring between the peptide chains, only a limited number of continuous secondary structures are possible (Alberts *et al.*, 2002).

Once secondary structures are formed, folding continues to form the tertiary structure of the protein, which confers the overall 3D protein shape. In some cases, the folded polypeptide may interact stably with either identical or different partners (or both) to generate a quaternary structure (Figure 3.1).

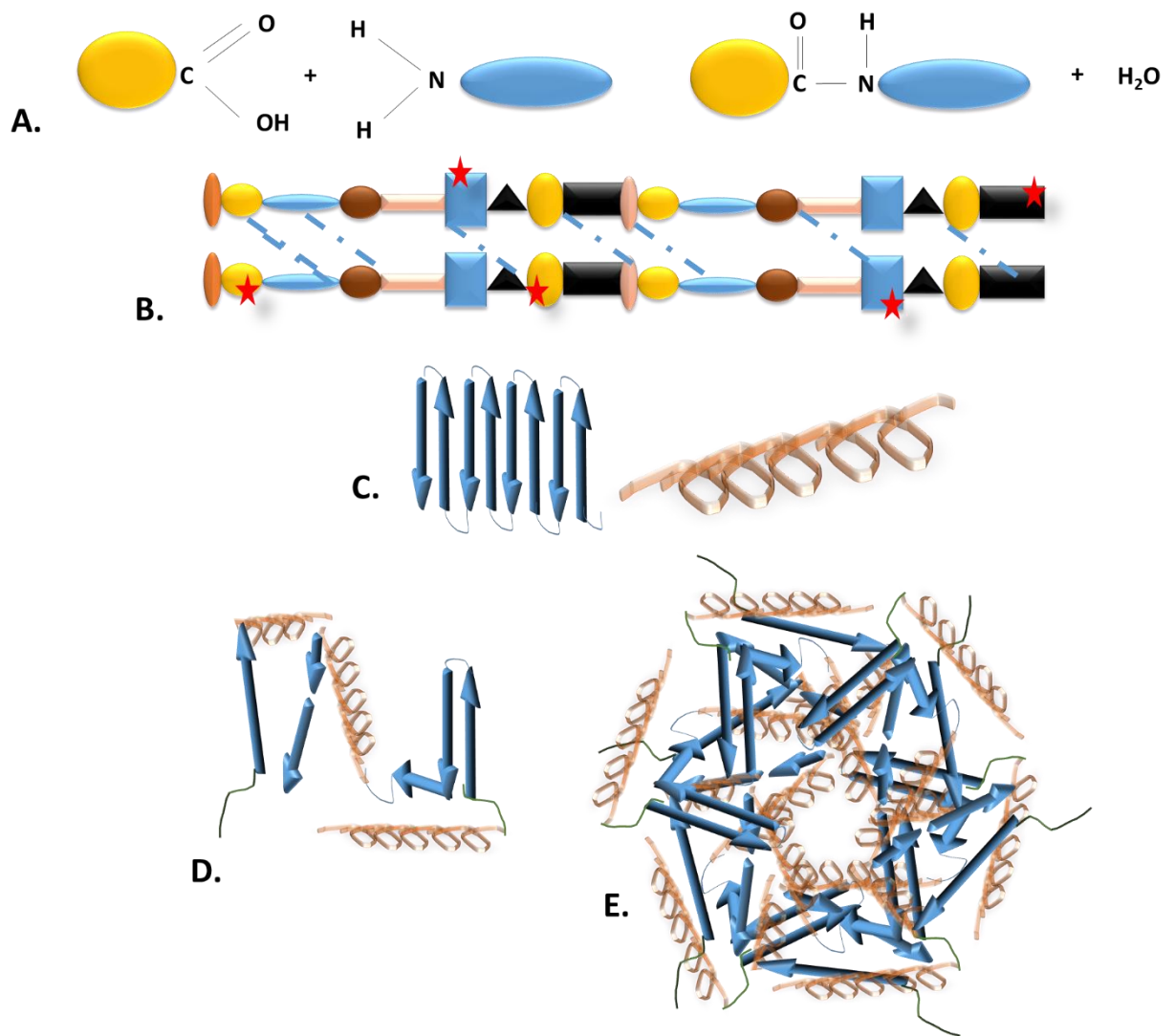


Figure 3.1. Protein structure. A. Peptide bond formation. A hydroxyl group from one amino acid reacts with an amino group in another. This, with the loss of water, results in peptide bond formation, a process that repeats to form the polypeptide chain. B. Primary protein structure. Amino acids are linked via peptide bonds, creating a chain of amino acids. Amino acids bind to other amino acids by hydrogen bond formation (blue dashed lines). In addition, proteins become post-translationally modified on certain amino acid residues (red stars). C. Disulphide, ionic and hydrogen bonds, and van der Waals and hydrophobic interactions lead to the folding of the protein, generating the secondary structure. Two main types of secondary structure are recognized: beta-sheets (left) and alpha-helices (right). D. Folding of the secondary structure generates the tertiary structure of the protein by transforming 2D folds into a 3D structure. E. If a protein has more than one polypeptide chain, this allows the formation of a quaternary structure. Adapted from Aryal, (2018).

3.1.2 STRUCTURE DETERMINATION

3.1.2.1 SECONDARY STRUCTURE AND CIRCULAR DICHROISM

Many aspects of protein structure are open to investigation. Knowledge of the primary structure could allow identification of particular motifs which, for example, might suggest post-translational modification sites. However, it is difficult to derive structural information from the primary structure, since protein folding relates to secondary structure onwards. Knowledge of the secondary structure of a protein can reveal key characteristics, for example whether conformational changes occur at the secondary structure level following ligand addition, or whether disulphide bonding contributes to folding (Lubrizol Life Science, 2019).

A commonly used technique for analysis of protein secondary structure is circular dichroism (CD). CD defines the difference in absorbance of a chiral molecule between left- and right-circularly polarized light. Depending on the absorbance wavelength, CD reveals the extent to which the secondary structure of a protein is alpha-helical, beta-sheet, random coil or a combination of all these features (Figure 3.2; Greenfield, 2006).

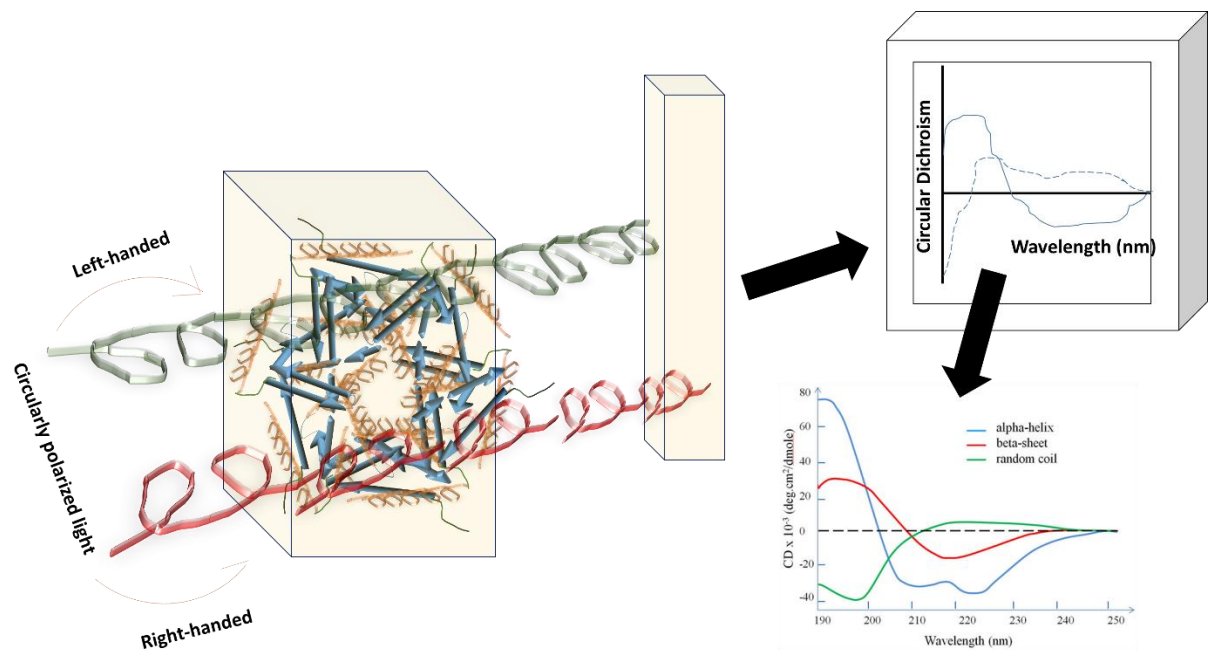


Figure 3.2. Circular dichroism. CD is the difference in absorbance between left-handed and right-handed circularly polarized light, which chiral molecules can display. In this instance, the chiral molecule is the protein, which is usually inserted into the CD spectrophotometer in a quartz cuvette to minimize background. Linearly polarized light is generated in the spectrophotometer, and a photoelastic modulator converts this into circularly polarized light. After passage through the optically active sample, the polarized light enters a photomultiplier tube detector which generates a high tension (HT) voltage and a signal spectrum which can be interpreted by a computer. The HT accommodates different wavelengths of light with different energies, and detects fluctuations caused by these different energies. It is important that the HT should not saturate, otherwise the noise increases significantly. The CD spectra of proteins display particular characteristics depending on their secondary structure. Alpha-helices (peaks at 190, 209 and 225 nm), beta-sheets (peaks at 190 and 218 nm) and random coils (peak at 200 nm) can all be distinguished. Adapted from Wei *et al.*, (2014); ISA, (2021).

Another approach to determining the extent a protein is folded, involves attempting to unfold it. Tryptophan and tyrosine have intrinsic fluorescence and, due to their hydrophobicity, are typically buried (and thereby shielded) within the core of a protein. When the protein is denatured either by heating or through addition of denaturants such as urea or GnHCl, an increase in the intrinsic fluorescence will indicate unfolding (Arntfield *et al.*, 1987).

Various approaches can be used to shed light on the tertiary and quaternary structures of proteins. Two of these approaches will be discussed here: X-ray crystallography and cryo-electron microscopy (cryo-EM).

3.1.2.2 X-RAY CRYSTALLOGRAPHY

The majority of structures within the protein data bank (PDB) were solved using X-ray crystallography, and this is still considered the best method both in terms of resolution and lack of size restriction. A major hurdle associated with the application of X-ray crystallography is that the proteins (obviously) have to be crystallized, to generate a uniform lattice of protein molecules. Crystallization requires a purified protein to be at a high enough concentration to come out of solution from its soluble state, a process that can be affected by many parameters, including pH, temperature and choice of precipitant. Successful crystallization requires a fine balance between under-saturation, super-saturation and precipitation. Protein crystals form during super-saturation in a nucleation region. Increasing the concentration of the protein or precipitant further, will likely result in precipitation. Similarly, if either are reduced in concentration, the protein will likely enter the metastable zone or enter an under-saturated state (Chirgadze, 2001). For this reason, crystal formation is often a limiting step in X-ray crystallography. The formation of crystals is typically carried out using vapour-drop or hanging-drop diffusion methods. Here, the protein sample is placed as a drop into a chamber with a reservoir of solution beneath it. The reservoir solution has a higher concentration of reagent compared to the drop and therefore, in order to establish equilibrium, water vapour will leave the drop into the reservoir, reducing its volume, thereby resulting in super-saturation and hopefully crystal formation (Hampton Research, 2020).

Once the crystals are formed, they are picked using a fine loop, and often plunge-frozen for prolonged data collection when exposed to the X-ray beam. X-rays are focussed and collimated to ensure that the beam is parallel, before being aimed at the crystal mounted on a flexible rotatable mount. Synchrotrons are often used as the X-ray source as they provide intense X-rays, allowing shorter exposure times, and thereby reducing crystal damage and increasing signal strength (Jeffrey, 2006).

When X-rays hit the crystal they are diffracted and detected usually by charge-couple device (CCD) detectors, which accelerate data collection. The diffraction pattern, which consists of a pattern of dots, can be converted into a plot of different X-ray intensities scattered at different angles and is the basis for structure determination. The solution of a crystal structure relies on the principles of Bragg's Law. Two pieces of information are required: intensity and phase angle (Martínez-Ripoll, 2021), as detailed in Figure 3.3. Intensity is established directly from the diffraction pattern using programmes such as DENZO. The difficulty lies in solving the phase problem, which is an indirect process. There are two main approaches: isomorphous replacement and molecular replacement, although other methods exist, including single/multiple isomorphous replacement (SIR/MIR) and single/multiple-wavelength

anomalous dispersion (SAD/MAD; Smyth and Martin, 2000). Isomorphous replacement involves soaking crystals in solutions containing heavy metals, such as mercury, which hopefully will bind to residues in the protein without altering its conformation. Diffraction data is then collected for both the un-soaked and soaked crystals and differences in the diffraction pattern can then be used to deduce where the heavy metal is bound within the protein structure. Various refinement programmes can then be applied to establish the phase angles. Alternatively, if a similar homologous structure already exists, molecular replacement can be used. Here, the intensity from the diffraction data can be combined with phases from a similar established structure to generate structure factors and therefore a model. This model structure can then be re-applied to the unknown structure, which can be further improved by various refinements. Although providing a more direct approach, molecular replacement is said to introduce more bias than isomorphous replacement and some consider this a disadvantage (Smyth and Martin, 2000; Taylor, 2010).

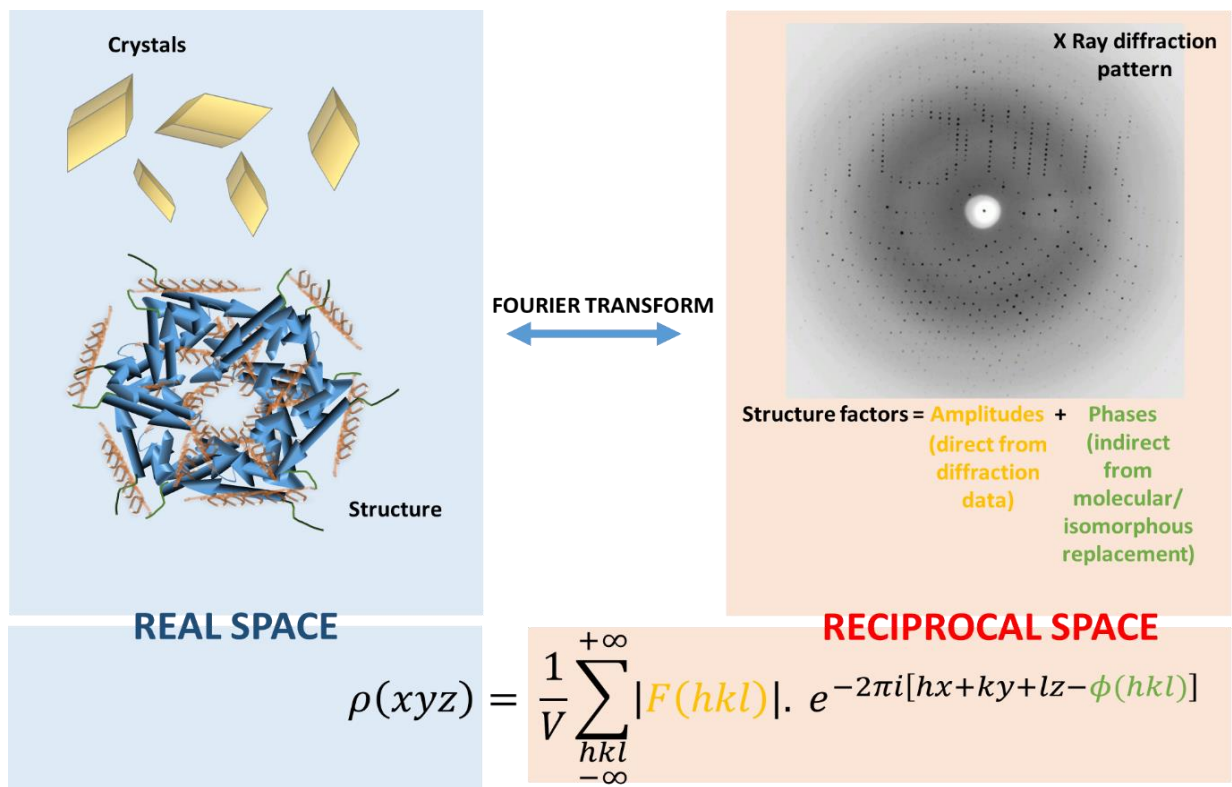


Figure 3.3. Origins of the phase problem in X-ray crystallography. Fourier transformation is used to relate the ‘real space’ (i.e. the structure and the crystals), to the ‘reciprocal space’ (i.e. the resulting diffraction pattern). In order to solve the structure in the ‘real space’, various parameters need to be determined, including the intensity shown in orange $F(hkl)$, which can be determined directly from the X-ray diffraction pattern, and the phase angles $\phi(hkl)$, which need to be determined indirectly by additional methods, including molecular and/or isomorphous replacement. Adapted from Martínez-Ripoll (2021).

Once the amplitude and phases are known, the structural factors can be calculated via fast Fourier transform. This generates an electron density map which acts as the scaffold for the structure to be built, before further refinement and final model building (Smyth and Martin, 2000).

3.1.2.3 CRYO-ELECTRON MICROSCOPY

Cryo-EM was established later than X-ray crystallography but is now evolving into the method of choice for determining protein structure. Cryo-EM arose out of transmission electron microscopy (TEM). TEM uses a beam of electrons, focused using electromagnetic lenses, which pass through a sample, interact with the molecules within it before being refracted and usually detected by a CCD detector. Electrons have a short wavelength, in comparison to photons, providing a much higher resolution than visible light. TEM has some disadvantages, including the risk that the electron beam may damage the sample and the requirement for the entire system to operate within a vacuum (Milne *et al.*, 2013).

With cryo-EM, the samples are spread across holes in a carbon film before being plunge-frozen in liquid nitrogen-cooled ethane. This rapid freezing results in water forming a disordered glass rather than signal-depleting crystalline or cubic ice. This method also provides greater protection of the sample from the electron beam as it requires a much weaker electron source compared with TEM. A major advantage of cryo-EM over X-ray crystallography is that crystals are not required. The protein molecules do not establish a preferential orientation or order on the grids; rather, they exist in many orientations (Broadwith, 2017; Dillard *et al.*, 2018). As with X-ray crystallography, image processing and refinement are key to the determination of the protein structure. This process begins with particle selection, where images are sorted based on structural features using various computer programmes such as SPIDER. The particles are then categorized into 'similar' particles which become clustered into groups and averaged, establishing various orientations of the protein while increasing the signal to noise ratio. This iterative process progresses through particle selection, 2D classification, projection angle determination and is continued with further refinement before 3D image reconstruction. 3D image reconstruction, as with X-ray crystallography, requires Fourier transformation. According to the central projection theorem, each of the 2D-projected images, will have 2D Fourier transform, and each of these 2D Fourier transforms is a section of the 3D Fourier transform of the total protein structure. Once the 3D Fourier transform sections are in place, a process known as Fourier inversion can then take place to generate a 3D map of the protein. Here, 3D reconstruction, classification and refinement can occur iteratively, as above, before model building can begin (Milne *et al.*, 2013).

X-ray crystallography often struggles with larger complexes because of the increased difficulty in forming crystals as a result of the increased flexibility of the structure. Cryo-EM has the opposite problem, in being able to accommodate larger complexes, but not smaller ones (<50 kDa) because of restrictions in resolution. Importantly, because the proteins are not crystallized, cryo-EM is capable of generating structures of proteins which are closer to their native state. Further, a lower concentration of protein is required for cryo-EM because it does not need to be concentrated so that it falls out of solution to form crystals; hence, sample preparation is more straightforward than for X-ray crystallography (Herzik *et al.*, 2019). Problems with cryo-EM include the fact that the particles are detected in unknown orientations, and the limitation in resolution resulting from the restriction of electron beam time so as to minimize sample damage (Carroni and Saibil, 2016).

3.1.3 PROBLEMATIC PROTEINS

Some proteins, despite lacking a transmembrane region, are not soluble in solution in the absence of a detergent. Syncollin is such a protein. Detergents cause complications in the application of both X-ray crystallography, because of interference with drop formation caused by a loss of surface tension in the drop diffusion system (Kaufmann *et al.*, 2006) and cryo-EM, because of an increase in background noise (Baker *et al.*, 2015). The use of nanodiscs presents a method by which normally detergent-requiring proteins may be stabilized in solution. Nanodiscs form when a polymer wraps around the phospholipid bilayer and excises segments which should, if the protein is over-expressed and bound or embedded in the membrane, contain the protein of interest. Diisobutylene maleic acid (DIBMA) can be used to generate nanodiscs from cell membranes. Specifically, cells over-expressing the protein of interest are lysed and membranes are incubated with DIBMA. The DIBMA-solubilized protein can then be purified using affinity chromatography (Oluwole *et al.*, 2017). If the protein of interest is known to form oligomers, a cross-linker such as disuccinimidyl suberate (DSS) can be added before membrane solubilization in an attempt to stabilize the oligomeric state prior to purification (Scheu *et al.*, 2010).

3.1.4 MUTATIONAL ANALYSIS

Once a protein structure is known, this provides a significant advance in the understanding of protein folding and may generate hypotheses regarding protein function. For many proteins, although a function can be initially hypothesized using functional assays and clarification with a structure, the mechanism of action of the protein cannot be fully understood without looking at the biochemical level to understand which residues are responsible. Mutational analysis therefore, provides a greater understanding of the mechanism of action of proteins.

Targets for mutational analysis in proteins differ depending on the protein and its role; however, there are particular residue types which are more likely involved in protein function and therefore more likely to be mutated, as will now be discussed.

3.1.5 PROTEIN-PROTEIN INTERACTION SURFACES AND HYDROPHOBIC RESIDUES

Protein-protein interactions (PPI) are vital for downstream signalling pathways such those involved in cell death and metabolism. Often with PPIs each protein's secondary structures are able to form small pockets or grooves which promote the binding of another protein (Sable and Jois, 2015). In order to assess the binding of two proteins at an interface, the free energy of binding is calculated. If the free energy of binding is reduced by 2 kcal/mol upon replacement of a particular residue by an alanine in one of these pockets, this is defined as a 'hot spot' (Morrow and Zhang, 2012). It is these hot spots which are at the protein-protein interface and which facilitate protein binding. The protein-protein interfaces are often highly hydrophobic, resulting in a lower free energy upon binding between the two proteins and consequent shielding from water; this is why the centre of hot-spots often contain key aromatic residues. Additionally, these residues are often more highly conserved between species than other surface residues (Sable and Jois, 2015).

Because of the high conservation among PPI surfaces, a database called the 'Interactome' has been established, which details protein-protein interactions and their interfaces. It should of course be borne in mind that mutating PPI residues can affect the structural integrity of the protein and produce alternative conformations. Further, the solubility of the protein may be affected through prevention of the PPI and exposure of additional hydrophobic residues (Jubb *et al.*, 2017).

Importantly, in addition to allowing interactions between different proteins, PPI interfaces can also mediate homo-oligomerization such as in the formation of ion channels or membrane-associated pore-promoting proteins (Stone and Deber, 2017).

3.1.6 ELECTROSTATIC AND POLAR RESIDUES

Other residues which are often mutated are charged and/or polar residues, which are involved in the formation of electrostatic interactions and, in the case of polar residues, hydrogen bonding. Depending on whether they are positively or negatively charged, charged residues can exert either repulsive or attractive forces on other nearby charged residues. As much as 25% of a protein can be composed of aspartate, glutamate, arginine and lysine residues, making electrostatics highly important with respect to protein structure and behaviour. Unlike hydrophobic residues, ionized residues are found on the

outer surface of proteins because is energetically unfavourable for them to be within the non-polar environment in the centre of the protein. This positioning renders them susceptible to conditions, such as pH or phosphorylation state. Electrostatic interactions can be important for downstream events such as cation binding, membrane recognition and signal transduction (Zhou and Pang, 2018).

3.1.7 CYSTEINE RESIDUES AND DISULPHIDE BRIDGES

It is well understood that formation of van der Waals, hydrophobic interactions and electrostatics are very important for protein stability. However, stability is dramatically improved (by up to 5-6 kcal/mol) through naturally occurring disulphide bridges (Zavodsky *et al.*, 2001). Cysteine residues are responsible for disulphide bridge formation, through the formation of reversible covalent cross links in the secondary structure of the proteins. Disulphide bridges are often highly conserved, and their role is vital for protein structure, through stabilization of monomeric and oligomeric forms of proteins. They may also be important functionally, for example in protein activity and catalysis. Folding facilitated by disulphide bond formation can also be required for exit of nascent polypeptide chains from the endoplasmic reticulum. It is still unconfirmed whether disulphide bond formation precedes protein folding or vice versa, but their importance with regard to protein structure is clear. Further, cysteine residues themselves, whether paired or not, can be essential for protein dimerization, metal co-ordination and thermal stability; hence, they are key targets for mutagenesis (Qui *et al.*, 2015). By way of background to my mutation studies on syncollin, described below, I shall now describe the results obtained using this approach on three example disulphide-containing proteins.

3.1.8 CYSTEINE MUTANTS

3.1.8.1 ABCG2

Members of the ATP Binding Cassette Superfamily G (ABCG) transport various molecules across the cell membrane and are well known for their role in protection against xenobiotic molecules; hence, they are known to contribute to multidrug resistance. The superfamily member ABCG2 exists as a homodimer stabilized by the presence of inter-molecular disulphide bonds. The homodimers proceed to form higher-order oligomers through various non-covalent interactions. When mutations were made to make an ABCG2 cysteine null mutant the transporter was found to be non-functional (Liu *et al.*, 2008). Further mutagenesis was used to explore whether the key disulphide bonds were intra- or inter-molecular. It was found that three cysteine residues, C284, C374 and C438, were required for intra-molecular disulphide bond formation. When these residues were mutated, homodimer

formation was prevented, and higher order oligomeric assembly and drug efflux activity were abolished. By contrast, mutation of the three cysteine residues that were responsible for inter-molecular disulphide bond formation, C592, C603, C608, did not prevent activity. It was therefore concluded that the intra-molecular disulphide bonds were essential for oligomerization and activity (Liu *et al.*, 2008).

3.1.8.2 HUMAN α GALACTOSIDASE A

Human α -galactosidase A is responsible for the removal of α -galactose from glycosphingolipids and can form homodimers. Each monomer is 50 kDa in size and contains two domains which consist of β/α -barrel and anti-parallel β -sheet structures (Qui *et al.*, 2015). There are twelve cysteine residues in each monomer, of which ten residues are involved in disulphide bond formation and two are free cysteines which contain unmodified sulphhydryl groups. When the ten bonding cysteine residues were mutated to serines, no protein expression occurred likely because of protein misfolding. However, when only one of these residues was mutated, C142, it was found that the secondary structure of the protein was disturbed, with a loss of part of the α -helix and a reduction in the thermal stability of the protein, resulting in a lower melting temperature. When the free cysteines, C90 and C174, were mutated, normal enzyme activity was seen, and the structure of the protein was similar to WT, as judged by CD spectroscopy. Interestingly, when the free cysteines were mutated to residues other than serine, an enhancement of enzyme activity up to two-fold was observed. It was concluded, therefore, that the 10 cysteines involved in disulphide bridge formation were essential for protein folding and enzyme activity, whereas the free cysteines, were more important for regulating activity rather than overall structure (Qui *et al.*, 2015; Andreotti *et al.*, 2010).

3.1.8.3 PANCREATITIS ASSOCIATED PROTEIN 2 (PAP2)

Pancreatitis associated protein 2 (PAP2) is a member of the Reg3 gene family and is classed as a C-type lectin type protein. It is responsible for the up-regulation of cytokines in macrophages via the NF κ B signalling cascade. PAP2 has three intra-chain disulphide bonds. Mutational studies identified that two of these bonds, present within the C-type lectin type domain (CTLTD), are critical to the function of the protein, whereas the third disulphide bond, also in the CTLTD, is not (Viterbo *et al.*, 2008). A 67% loss in PAP2 activity was observed following a double mutation of the key disulphide bonds present in the CTLTD. Additionally, PAP2 protein became non-functional on reduction of all disulphide bonds due to a reduction in signalling cascades and subsequent cytokine release from macrophages. The authors suggested that the bonds were responsible for stabilizing a beta-hairpin which is essential for PAP2

activity. Further, the disulphide bonds have been suggested to be important for maintaining structural integrity of PAP2 in harsh environments (Viterbo *et al.*, 2008).

From the above examples, it can be seen that there are many characteristics shared between ABCG2, Human A Galactosidase A and PAP2, including a predominantly beta-sheet structure, thermal stability and crucially the presence of disulphide bonds. I hypothesized that syncollin might share these features.

This chapter describes the use of modelling programmes to predict the structure of syncollin, an investigation of its secondary structure, and the determination of the structural characteristics of the syncollin monomer (secondary structure) and oligomer (quaternary structure). Further, a mutational study of syncollin was applied to understand the structural and functional importance of disulphide bonds and surface electrostatics.

3.2 METHODS

3.2.1 STRUCTURE PREDICTIONS

In order to guide subsequent experiments, the primary structure (amino acid sequence) of syncollin was used in an attempt to predict its tertiary structure. The sequence was entered into the following servers: iTasser, Pyre2, Robetta, Galaxy Web and Swissmodel. The best model in terms of Ramachandran score and E value was selected for each server, and the various models were aligned and overlaid in PyMol (Figure 3.4). A predicted Ca²⁺ binding site was identified using the iTasser Ion Ligand Binding site predictor and the residues selected were highlighted using PyMol. Predicted disulphide bonds based on proximity of cysteine residues were also displayed. Finally, hydrophobic residues (ala, gly, val, ile, leu and phe) were selected in PyMol and are displayed as sticks.

3.2.2 CIRCULAR DICHROISM SPECTROSCOPY

Syncollin-Strep was purified in 10 mM sodium phosphate, pH 8.0 containing 0.1% (w/v) CHAPS and diluted to 10 µM in the same buffer, before 300 µL was added to a 1-mm path-length quartz cuvette for analysis using a CD spectrophotometer (Applied Photophysics). Far-UV CD data were collected between 200 and 280 nm using a 1-mm path length and a 2-nm bandwidth, the range before the high tension (HT) voltage saturated. In some experiments a temperature ramp (25°C to 95°C) was applied, with 0.5 s per point. In other experiments dithioerythritol (DTE; 1 mM), GnHCl (6 M), or CaCl₂ (10 mM) were included in the buffer solution. In all cases, readings were corrected for the signal with the relevant buffer alone.

To calculate mean residual ellipticity calculations ($\text{deg.cm}^2\text{dmol}^{-1}$), the following equation was applied (Applied Photophysics, 2021):

$$[\theta_{MRW}] = \frac{100 \times \theta}{l \times [C] \times n}$$

where θ is the ellipticity in millidegrees, l is the path length in cm, c is the concentration of the sample in M and n is the number of residues.

3.2.3 X-RAY CRYSTALLOGRAPHY

Syncollin-Strep at concentrations in excess of 5.2 mg/mL was subjected to crystallization trials. Pre-formed 96-well plates containing various buffer solutions were used, at the laboratories of AstraZeneca (AZ; Cambridge). Droplets of syncollin (0.2 nL) were added to the multi-well plates using a Mosquito™ liquid handling robot. A clear plastic film was placed over the plate and any air bubbles between the plate and film were removed. The plate was then incubated at either 20°C or 4°C in a plate 'hotel' and imaged frequently using ROCK maker™ and ROCK imager™ programmes. Crystals were checked using both light and UV microscopy to ensure that they consisted of protein and not salt. Crystals were selected using fibre teeth and plunged into liquid nitrogen in preparation for imaging at the Diamond Light Source, Didcot.

3.2.4 SYNCOLLIN SEQUENCE HOMOLOGY

Syncollin (Rat UniProtKB - O35775) was inserted in WebLogo 3 and a sequence homology graphical logo generated (Crooks *et al.*, 2004).

3.2.5 SYNCOLLIN MUTANT GENERATION

Based on the predicted syncollin structure, syncollin cysteine mutants were generated by substituting a cysteine to a glycine either within predicted disulphide pairs or for free cysteines. The following mutants were thereby generated - Cys23Gly, Cys38Gly, Cys52Gly, Cys86Gly and Cys131Gly - and appropriate DNA sequences were synthesized using the Gene synthesis service (ThermoFisher). Additionally, charged mutants were generated by substituting arginine and lysine residues with alanine, to generate Lys9Ala, Lys10Ala, Arg76Ala and a triple mutant. Syncollin mutants were digested out of the ThermoFisher plasmid using restriction enzymes HindIII-HF and AgeI-HF (NEB) and ligated into HindIII-HF/AgeI-HF-digested pcDNA3.1. Transformation, mini-preps and Sanger sequencing were then carried out to check the constructs as previous.

3.2.6 SUSCEPTIBILITY TO DENATURATION

Syncollin-Strep was purified in 10 mM sodium phosphate, pH 8.0 containing 0.1% (w/v) CHAPS and used at a concentration of 10 μ M. The denaturation assay was carried out in a 96-well format using black clear-bottomed Corning™ 96-well plates. Protein was incubated with various concentrations of GnHCl from 0-6 M for 2 h at room temperature, with agitation. The intrinsic fluorescence of tryptophan and tyrosine residues was then measured at 360 nm using a ClarioStar™ plate reader (BMG labtech). Alternatively, protein at 10 μ M or 3.3 μ M was added to a spectrophotometer (Beckman) either in the presence or the absence of 6M GnHCl, and a fluorescence spectrum was recorded from 300-400 nm. Background fluorescence of the relevant buffer was subtracted from all data points.

3.2.7 DYNAMIC LIGHT SCATTERING

A lentivirally transfected syncollin-Strep cell line was generated to look at syncollin solubilization with DIBMA according to Elegheert *et al.* (2018). Briefly, this involved co-transfecting a lentivirus producer cell line (Lenti-X) with transfer (this contains syncollin-Strep, the transgene of interest), envelope and packaging plasmids required to make the lentiviral particles. The supernatant was then collected, which contained the lentivirus, following approximately 5 days and added to a mammalian cell line (tsA-201) for infection and transduction before expansion of the cell line.

Lentivirally-infected cell pellets containing syncollin-Strep were snap-frozen at -80°C. To prepare membranes, a 5-ml pellet was removed from -80°C storage and thawed on ice. The pellet was resuspended in 20 mL ice-cold membrane buffer (20 mM HEPES, pH7.4 containing 250 mM sucrose and cComplete™ protease inhibitors) and the cells were lysed by sonication on ice with a Soniprep™ tip sonicator (MSE), using 3 x 10 s bursts on a medium setting. After sonication, the cell suspension became visibly more translucent. The lysate was centrifuged at 13,000 x g for 15 min using a fixed-angle rotor to remove unbroken cells and nuclei. The supernatant was then removed and further centrifuged at 125,000 x g for 1 h at 4°C to produce a membrane pellet. The membrane pellet was diluted to 40 mg/mL in approximately 7 mL of ice-cold DIBMA buffer (20 mM Tris, pH 7.0 containing 150 mM NaCl and cComplete™ protease inhibitors). Lyophilized DIBMA (50 mg; Cube Biotech) was then added to 2 mL of the 40 mg/mL membrane suspension to give a final concentration of 2.5% (w/v) DIBMA. The solution instantly became transparent and was incubated 18 h at 4°C, with constant rotation. A DIBMA-solubilized membrane fraction (1 mL of a 40 mg/mL solution) was added to 200 μ L of Strep-Tactin XT™ slurry (50%) and incubated for 3 h at 4°C, with constant rotation. The beads were washed once with 200- μ L DIBMA buffer followed three further washes with 500 μ L. Syncollin-Strep

was then eluted using 10 mM biotin in DIBMA buffer, prepared by a 1:10 dilution from 100 mM biotin, pH 9.0, into DIBMA buffer, pH 7.0, to give a final pH between 7.4-7.5, required for DIBMA activity. Elution buffer (100 μ L) was added to the beads and incubated for 2 h at 4°C, with agitation. The beads were added to an Econo-Pac™ disposable chromatography column (BioRad) and the eluate was collected under pressure. The DIBMA-solubilized membrane were stored on ice at 4°C.

Dynamic light scattering (DLS) was carried out in the Biophysics Facility in Department of Biochemistry under the supervision of Dr. Katherine Stott. Syncollin in DIBMA was analysed using a Malvern Zetasizer Nano S™ running on settings for lipid detection after relevant buffer subtraction. Syncollin in DIBMA was compared with purified syncollin alone in 10 mM sodium phosphate, pH 8.0 containing 0.1% (w/v) CHAPS.

3.2.8 MEASUREMENT OF HYDRODYNAMIC RADIUS

For measurement of hydrodynamic radius, syncollin-green fluorescent protein (GFP) was used; this construct had been used previously for fluorescence imaging (Hays *et al.*, 2005). Syncollin-GFP was expressed in tsA-201 cells and cell pellets were frozen. Cells were lysed by incubation in ice-cold RIPA buffer for 30 min at 4°C, with agitation. Unlysed cells were pelleted by centrifugation at 100,000 x g for 30 min. Supernatant containing soluble syncollin-GFP was diluted 1,000-fold in phosphate-buffered saline, pH 7.0 (PBS) to give the lowest possible background reading in a Fluidity One-W™ instrument (Fluidic Analytics) whilst retaining a detectable signal for hydrodynamic radius. GST-syntaxin 2 was purified from transformed *E. coli* as described in Chapter 2. Syncollin-GFP was analysed either alone or together with GST-syntaxin 2, either in the absence of divalent cations or in the presence of 10 mM CaCl₂ or MgCl₂.

3.3 RESULTS

3.3.1 PREDICTED STRUCTURE OF SYNCOLLIN

Figure 3.4 shows the overlaid predicted structures of syncollin generated by a number of servers. Notably, the proteins nitrollin and spherulin, members of the $\beta\gamma$ -crystallin family, were identified as most likely to be structurally similar to syncollin. All of the models agree that syncollin is likely to contain anti-parallel beta sheets in the form of a Greek Key structure, in which each beta-sheet is connected via a loop. There are two predicted small alpha-helices, which appear on each side of the monomeric structure, and a central cavity through the centre of the protein. The protein also has a predicted Ca²⁺ binding site (magenta rods) on one face, embedded in a negatively charged pocket and

held in place through an anchoring small alpha-helix (yellow ring). The seven cysteine residues are arranged in three pairs with one individual lone cysteine, suggesting that there may be up to three disulphide bonds. The protein displays two contrasting faces - a highly negatively charged face and a highly positively charged face. Hydrophobic residues appear to line the central cavity (orange rods) (Figure 3.5).

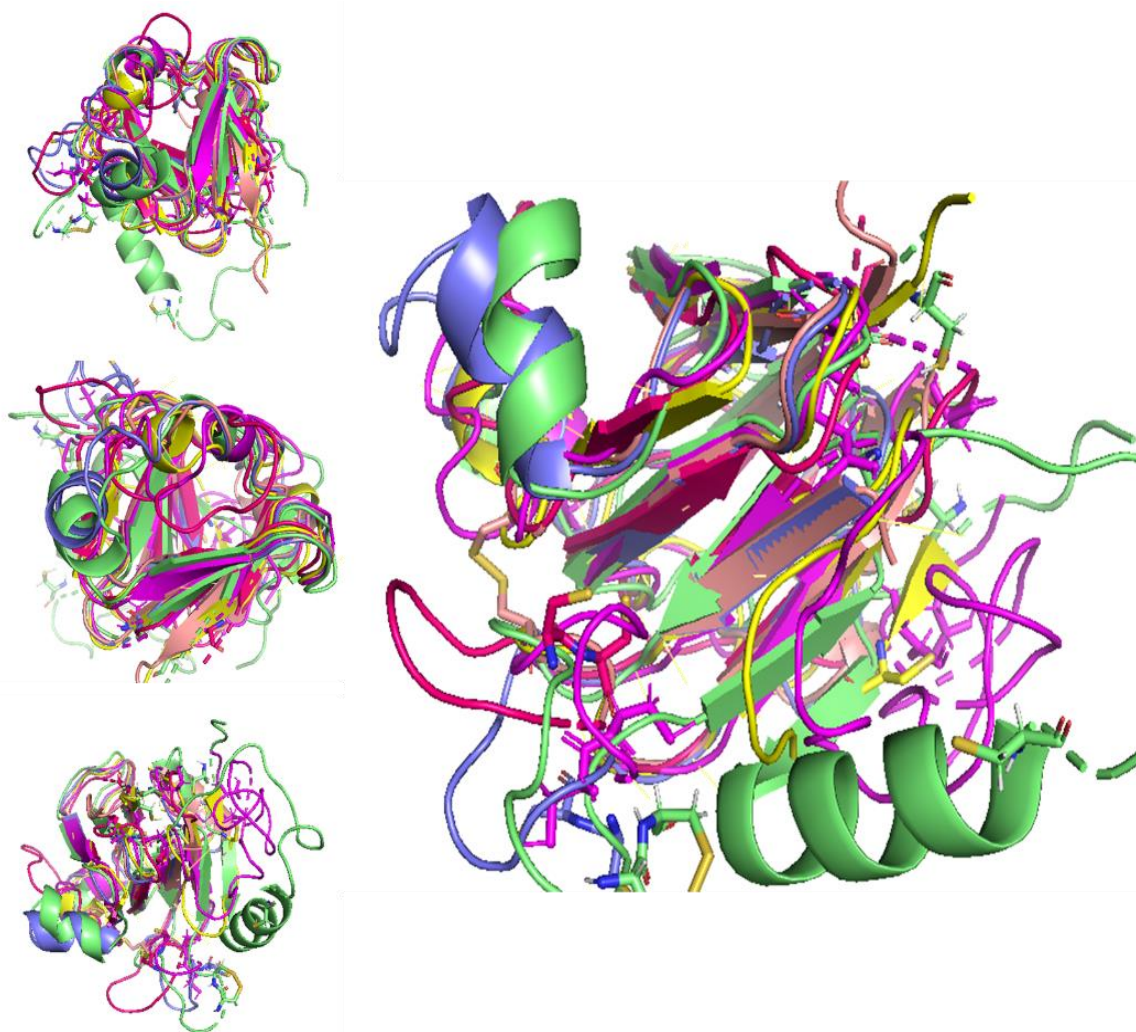


Figure 3.4. Predicted structure of syncollin based on sequence. Aligned and overlaid predicted structures from iTasser, Pyre2, Robetta, Galaxy Web and Swissmodel, selected based on Ramachandran score and E value. Each model is represented by a different colour and displays beta-sheets, alpha-helices and loops in ribbon format using PyMol. The four panels represent different orientations of the predicted syncollin monomer.

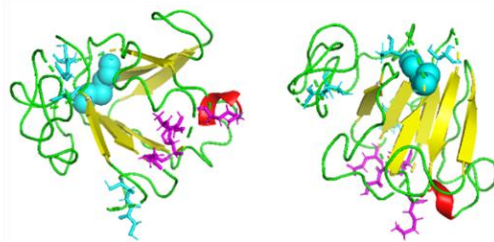
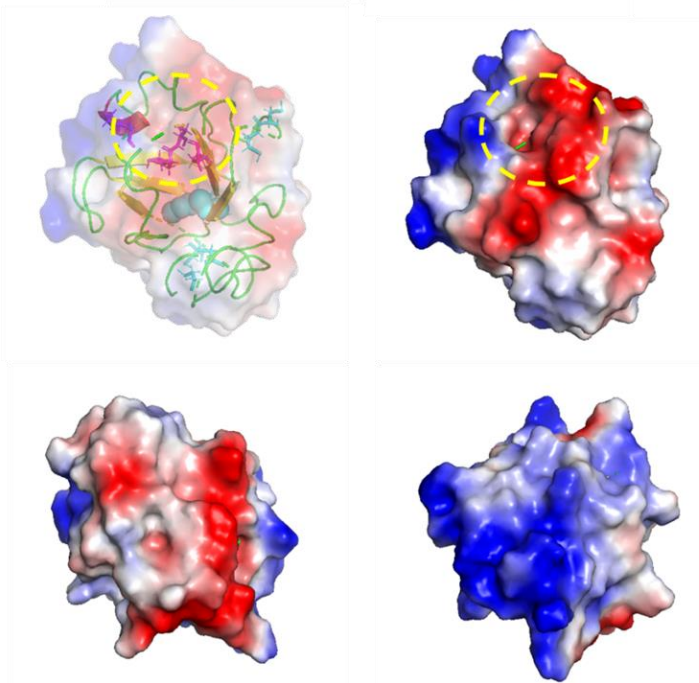
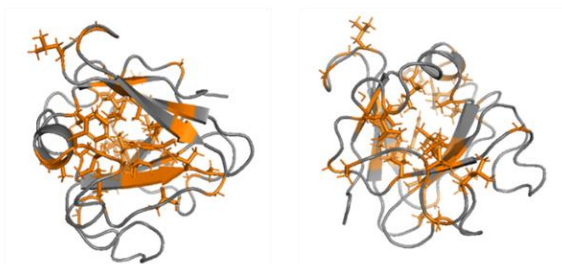
A.**B.****C.**

Figure 3.5. Predicted characteristics of the syncollin molecule. A. Best-fit model from Figure 3.4 illustrated in ribbon form, with beta-sheets in a 'Greek Key' motif displayed in yellow, alpha-helices in red, cysteine residues in cyan (with balloons demonstrating disulphide bonding) and a predicted Ca^{2+} binding site (using iTasser Ion Ligand Binding server) in magenta. B. Predicted electrostatic surface of syncollin with the predicted Ca^{2+} predicted binding site highlighted by the yellow dashed ellipse. Electrostatics were calculated using the APBS electrostatics plug-in in PyMol, with red demonstrating negative potential and blue demonstrating positive potential. C. Hydrophobic residue distribution shown in orange in the predicted syncollin monomer, with ala, gly, val, ile, leu and phe highlighted.

Just prior to submission of this dissertation, the DeepMind AlphaFold model, known for its coverage of 98.5% of human proteins with high-confidence structural predictions (Tunyasuvunakool *et al.*, 2021), became accessible via a public database. The predicted model for rat syncollin, is displayed in Figure 3.6.

The AlphaFold model predicts syncollin has a strongly beta-sheet structure, much like that seen previously (Figure 3.6A). The model shows three disulphide bonds between cysteine residues: 38 and 131, 86 and 133, and 23 and 53. A lone cysteine, residue 52, is also predicted (Figure 3.6 B and C). In addition to the similarity in structure, the new model predicted surface electrostatics much like those of the previous models, with both highly negatively and positively charged faces (Figure 3.6 D and E).

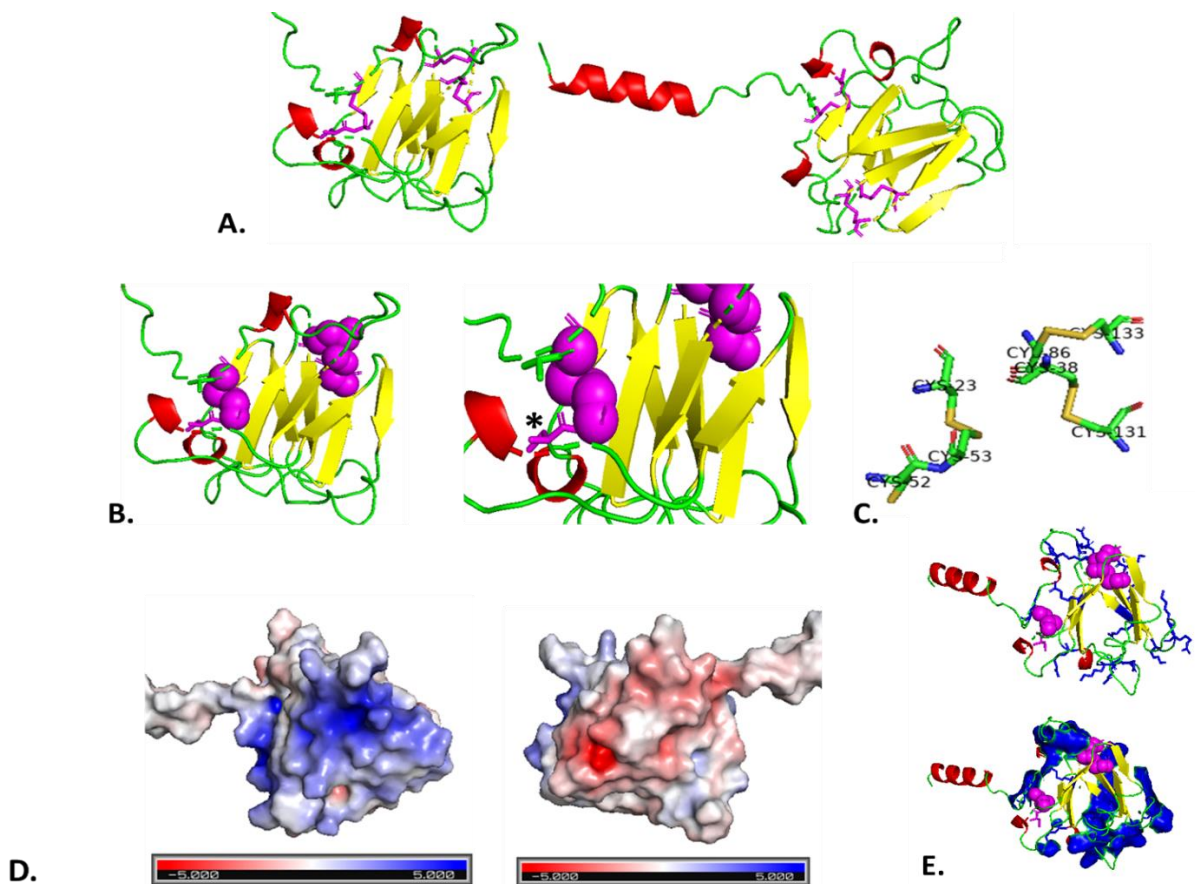


Figure 3.6. Syncollin structure predicted using the public database for DeepMind’s AlphaFold software. A. PyMol cartoon representations of syncollin with colouring representing secondary structure. B. Cysteine residues highlighted in magenta, and disulphide bridges displayed as spheres. The free cysteine residue is highlighted by an asterisk C. Stick representation displaying the orientation of cysteine residues shown in B. D. Surface electrostatics using the DPBS electrostatics plug-in in PyMol, with positively charged residues shown in blue and negatively charged residues shown in red. E. Basic residues highlighted as blue sticks (top) and blue surfaces (bottom). Note that the structure contains the signal sequence, which of course will not feature in the final structure.

3.3.2 CD SPECTROSCOPY

The CD spectrum of 10 μ M syncollin, in 10 mM sodium phosphate, pH 8.0 containing 0.1% CHAPS, had two peaks: a negative peak at approximately 218 nm, indicating beta-sheet secondary structure, and a positive peak at approximately 234 nm, indicating the presence of disulphide bonds (Figure 3.7A). The spectrum was collected over the range 210 nm to 280 nm because the HT saturated (at 1000 V; Figure 3.7B) at approximately 208 nm.

When the protein was subjected to a temperature ramp up to 90°C, both peaks were reduced in amplitude, although complete unfolding/denaturation did not occur (Figure 3.7C). The peak initially at 234 nm also appeared to shift rightwards with increasing temperature.

Addition of DTE and CaCl_2 (and analysis of the same sample on successive days) caused minimal change in the spectrum. In contrast, freeze-thawing of syncollin-Strep and, to a greater extent, addition of denaturant GnHCl caused reduction in the peak at 218 nm (Figure 3.7D). To explore this effect further, values for the 218-nm and 234 nm-peaks were plotted against temperature as mean residual ellipticity (for normalization). At both 218 nm and 234 nm, a larger decrease in amplitude with increasing temperature could be seen with DTE incubation, with minimal differences seen between protein alone, protein plus Ca^{2+} addition and protein plus GnHCl. Approximate melting temperatures were 63.0°C for the 218 nm peak and 58.5°C for the 234 nm peak (Figure 3.7 E and F).

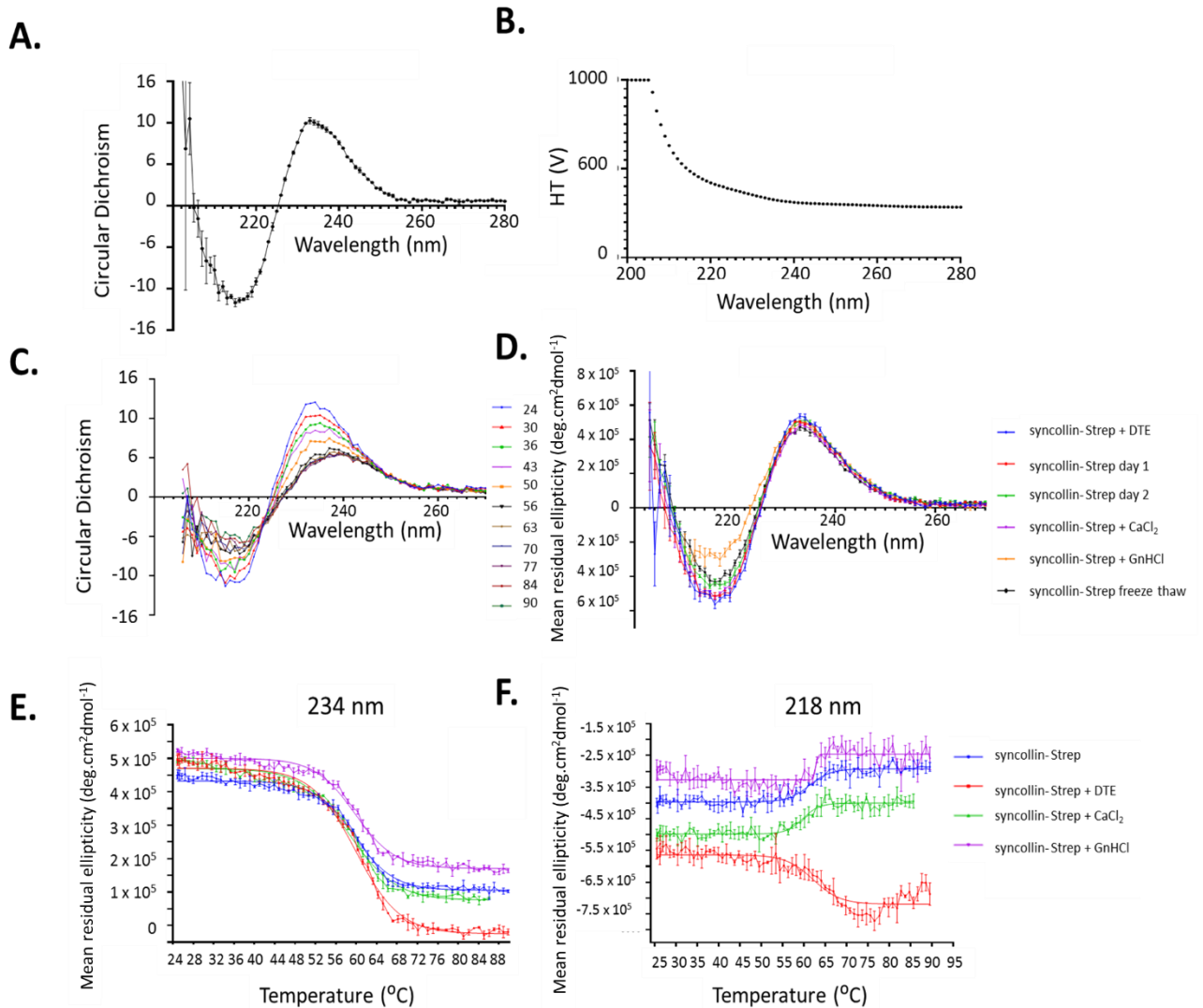


Figure 3.7. CD spectroscopy of syncollin. A. Syncollin-Strep, purified in 10 mM sodium phosphate, pH 8.0 containing 0.1% (w/v) CHAPS, was added to a 1-mm quartz cuvette. Two peaks are seen: a negative peak at 218 nm and a positive peak at 234 nm. Error bars are SD (n=3). B. HT data corresponding to the CD data in A. HT saturated at approximately 205 nm, and thereby defined the range 210-280 nm for readings. C. Syncollin-Strep was subjected to a temperature ramp from 24°C to 90°C. Different temperatures are represented by different colours. The time at each point was 0.5 s (n=3). D. Syncollin-Strep subjected to various conditions. Protein plus DTE (1 mM) in blue; protein on two different days in red and green; protein plus CaCl₂ (10 mM) in magenta; protein plus GnHCL (6 M) in orange; and protein thawed following -80°C storage in black. E, F. Mean residual molar ellipticity was calculated for normalized data for 234 nm and 218 nm wavelengths with increasing temperature for different conditions: protein alone; protein plus DTE; protein plus CaCl₂; and protein plus GnHCL (n=3). Curves were fitted using a GraphPad Prism™ non-linear regression fit.

3.3.3 X-RAY CRYSTALLOGRAPHY

In order to determine the structure of syncollin-Strep, X-ray crystallography was trialled. During various crystallography screens of syncollin-Strep in 10 mM sodium phosphate pH 8.0 containing 0.1% (w/v) CHAPS, some conditions resulted in protein crystal formation at concentrations in excess of 5.2 mg/mL (Figure 3.8). When exposed to an X-ray beam source (Diamond Light), the crystals diffracted to a resolution of 4.2 Å. Molecular replacement was trialled with syncollin using the most similar structures based on sequence homology (similarity only ~20%) however, this approach was unsuccessful. An attempt at phase solving was attempted through exposure of crystals to Sulfur-SAD beamlines at Diamond Light and also heavy metal soaking (mercury) of the crystals. However these trials were also unsuccessful and could not be efficiently optimized because of the low numbers of crystals generated.

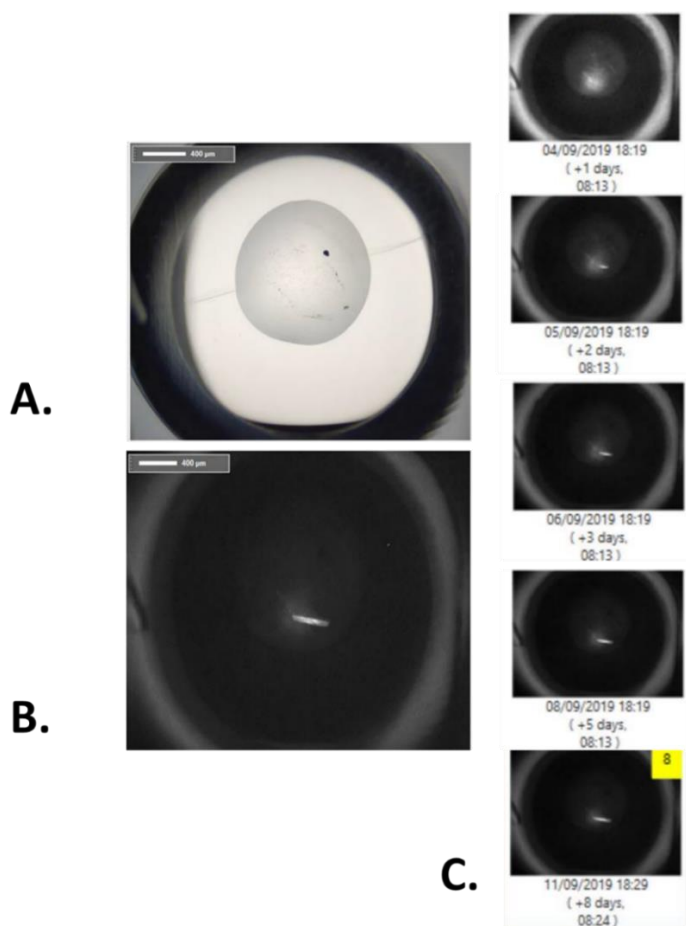


Figure 3.8. Crystallization of syncollin-Strep. Syncollin-Strep (5.2 mg/mL) was added to 96-well screening plates (AZ) and monitored for crystal formation. An example of one of the crystals formed is displayed here. Crystal formation could be seen using both light (A) and UV detection (B), indicating that the crystal was composed of protein and not salt. A time-course of crystal formation was collected for each crystal (C) and generally showed growth, in this case over 8 days. The crystal was removed on day 8.

3.3.4 SYNCOLLIN SEQUENCE HOMOLOGY

To assess further the importance of disulphide bonding and electrostatics on protein folding and function, mutational studies on syncollin-Strep were initiated based on the initial predicted structure shown in Figure 3.5. First, a sequence homology logo was generated to investigate whether there are any highly conserved residues in syncollin. From the logo generated, it was apparent that all cysteines in the protein were highly conserved (Figure 3.9). Charged residues - arginines, lysines, glutamate and aspartates - were also amongst the residues most highly conserved. Interestingly, the three aromatic tryptophans are fully conserved amongst species.

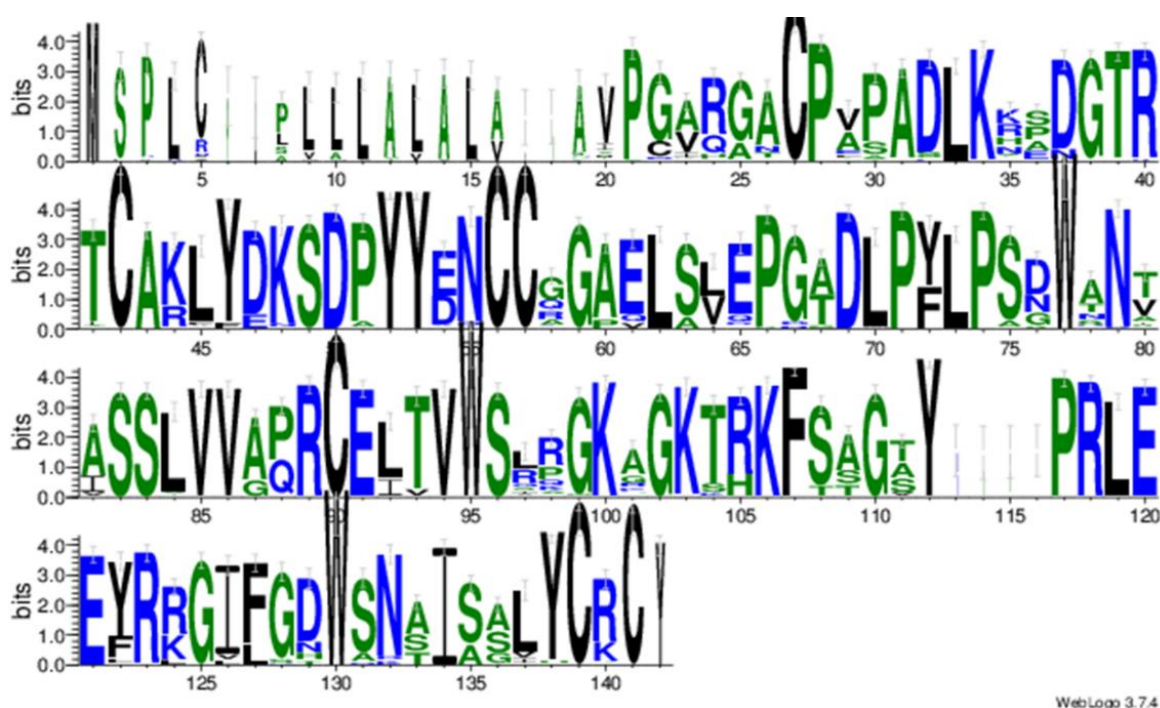


Figure 3.9: Syncollin homology logo. The sequence for rat syncollin was inserted into WebLogo and a sequence homology logo generated. The most conserved residues across species are represented by larger characters. Hydrophilic residues are shown in blue, neutral residues in green and hydrophobic residues in black.

3.3.5 DESIGN OF SYNCOLLIN MUTANTS

Based on the initial predicted modelled structure of syncollin-Strep, both cysteine mutants and positive charge mutants were designed. Cysteine mutants were designed so that they might interfere with predicted intra-molecular disulphide bonding or possible inter-molecular disulphide bond formation. The mutants chosen - C23G, C38G, C52G, C86G and C131G - are highlighted in cyan and labelled in bold text in Figure 3.10A. All remaining unselected cysteines are highlighted as orange sticks.

The predicted positively charged patch on the surface of syncollin-Strep is very large, making it difficult to home in on a small number of charged residues. I selected K9 and K10, which are adjacent, and R76, which appears within a strongly positive patch; these residues are highlighted in Figure 3.10B. A triple mutant was also constructed in an attempt to significantly reduce the overall positive charge of the patch.

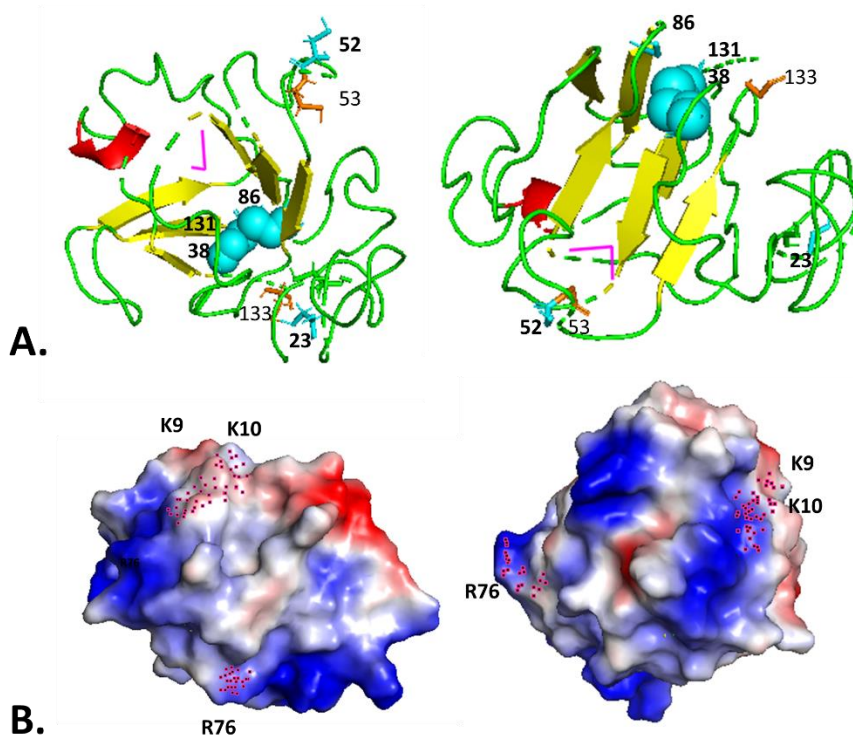


Figure 3.10. Design of syncollin mutants based on the predicted structure. A. Location of cysteine residues within the syncollin model. Cysteine residues mutated to glycine are shown in the modelled structure as cyan sticks and with cysteine residues labelled in bold. Cysteine residues which were not mutated are shown in orange and labelled in standard font. B. Location of positively charged mutations. Lysine and arginine residues which were mutated to alanine are shown with magenta dots on the electrostatic surface model of syncollin.

3.3.6 DISULPHIDE BOND SHIFT OF SYNCOLLIN CYSTEINE MUTANTS

Four of the five single-cysteine mutants - Cys23Gly (1), Cys38Gly (2), Cys52Gly (3), and Cys86Gly (4) were subjected to biochemical analysis. On a Coomassie-stained gel, all mutants (1-4) appeared to run at the same molecular mass (~20 kDa) as multiple bands, similar to the behaviour of WT syncollin-Strep (Figure 3.11A). Likewise, all mutants displayed a disulphide bond shift, as judged by comparison of mobilities in the presence and absence of β -mercaptoethanol (Figure 3.11B). Finally, all displayed a reduction in size of approximately 10 kDa upon incubation with 1.2 mg/mL trypsin for 30 min, as

reported previously (Figure 3.11C; An et al., 2000). Note that the additional band running at ~25 kDa in the plus-trypsin lanes is trypsin itself, which is detected by the anti-syncollin antibody.

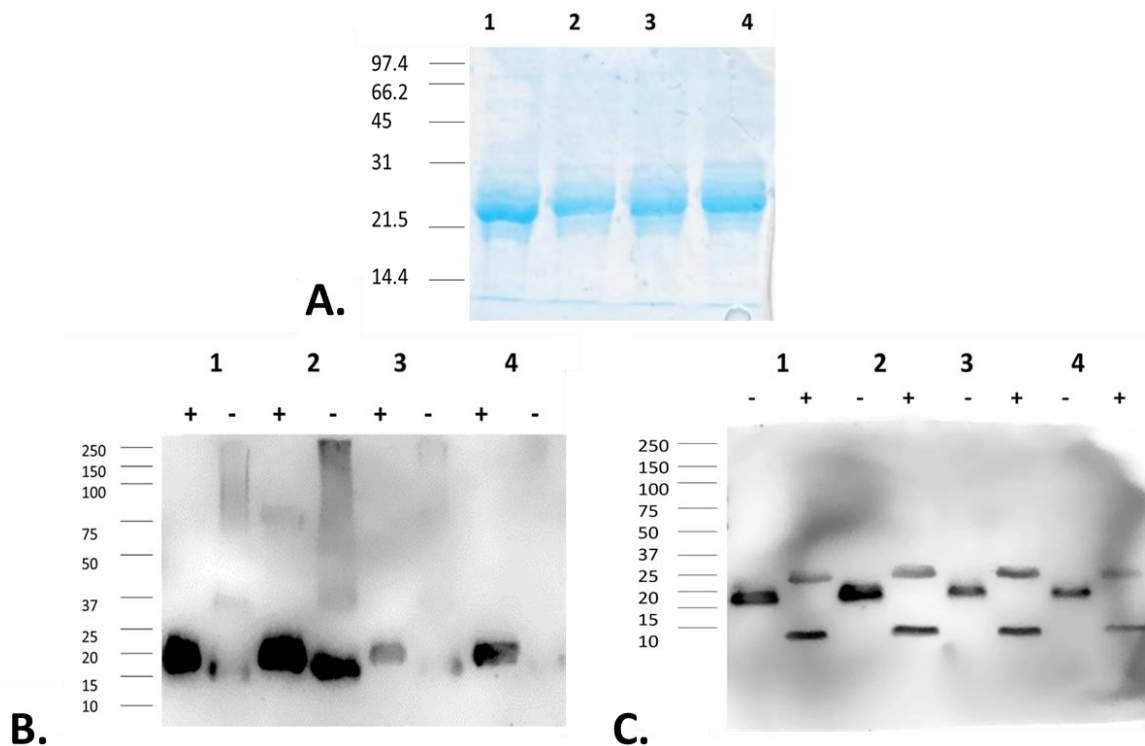


Figure 3.11. Biochemical properties of syncollin-Strep cysteine mutants Cys23Gly (1), Cys38Gly (2), Cys52Gly (3) and Cys86Gly (4). A. Cystine mutants were run on SDS-PAGE gels and stained using Coomassie blue. B. Cysteine mutants were run on SDS-PAGE gels in the presence (+) and absence (-) of the reducing agent β -mercaptoethanol and analysed by immunoblotting using a polyclonal anti-syncollin antibody. C. Mutants were run on SDS-PAGE gels after incubation in the absence (-) and presence (+) of trypsin and analysed by immunoblotting. Standards are BioRad low-range markers (A) or Precision Plus (B and C).

3.3.7 LIPOSOME PERMEABILIZATION BY SYNCOLLIN CYSTEINE MUTANTS

As shown in Chapter 2, WT syncollin-Strep is able to permeabilize brain liposomes and cause the release of encapsulated BCECF. Cysteine mutants 1-4 (above) also caused permeabilization of the brain liposomes, with values for BCECF release ranging between ~50% for mutant C38G and ~90% for mutant C23G, compared with a release of ~70% for WT-syncollin Strep (Figure 3.12A). The extent of BCECF release for all four mutants was significantly different from that given by elution buffer (Figure 3.12B), with mutants C38G, C52G and C86G also significantly lower than WT syncollin-Strep.

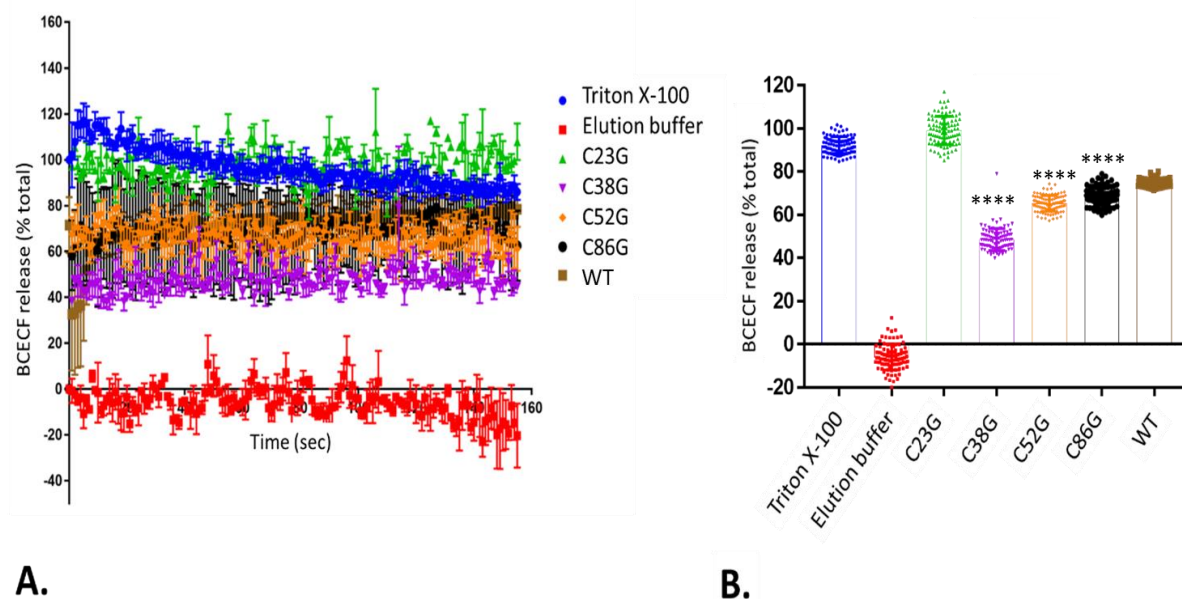


Figure 3.12. Brain liposome permeabilization and BCECF release by syncollin-Strep and cysteine mutants. A. BCECF release was monitored using fluorimetry. Negative (buffer) and positive controls (1% [v/v] Triton-X 100) were included. WT syncollin-Strep or syncollin cysteine mutants were added at 9 $\mu\text{g}/\text{mL}$. Data are shown as % release, assuming 100% release with Triton X-100. Error bars are SD (n=3). Data were plotted using GraphPad Prism™. B. Data points from A. between 50 s and 150 s are displayed as a histogram using GraphPad Prism™. One-way ANOVA with Tukey's multiple comparison test was carried out between conditions. All conditions were significantly different from buffer alone ($p < 0.0001$). **** $p < 0.0001$, compared with WT syncollin-Strep.

3.3.8 CD SPECTROSCOPY OF SYNCOLLIN CYSTEINE MUTANTS

CD spectroscopy was carried out with all five single-cysteine mutants. Spectra for all of the mutants displayed similarities with that for WT syncollin-Strep - a negative peak at ~ 217 nm, characteristic of a beta-sheet secondary structure, and a positive peak at ~ 234 nm indicating the presence of disulphide bonds (Figure 3.13).

To investigate the thermal stability of the mutants, temperature ramps were run from 25-90°C (Figure 3.13). Additionally, CD spectra at 25°C for WT and mutants were overlaid to investigate differences in peak amplitude (Figure 3.14A). It was apparent that there were increased 217-nm peak amplitudes for mutants C23G and C38G in comparison to WT. Likewise, there were increased 234-nm peak amplitudes for mutants C52G, C86G and C131G.

To quantify the changes in the CD spectra with temperature, CD values at 217 nm and 234 nm were plotted against temperature and the spans of the peaks were calculated (Figure 3.14B and C). C23G,

C38G and C86G displayed a four-fold greater reduction of the 217 nm peak with increasing temperature, in comparison to WT, and C52G showed an almost two-fold greater reduction than WT (Figure 3.14B). Minimal changes were seen in the 234-nm peak between the various constructs during the temperature ramp (Figure 3.14C).

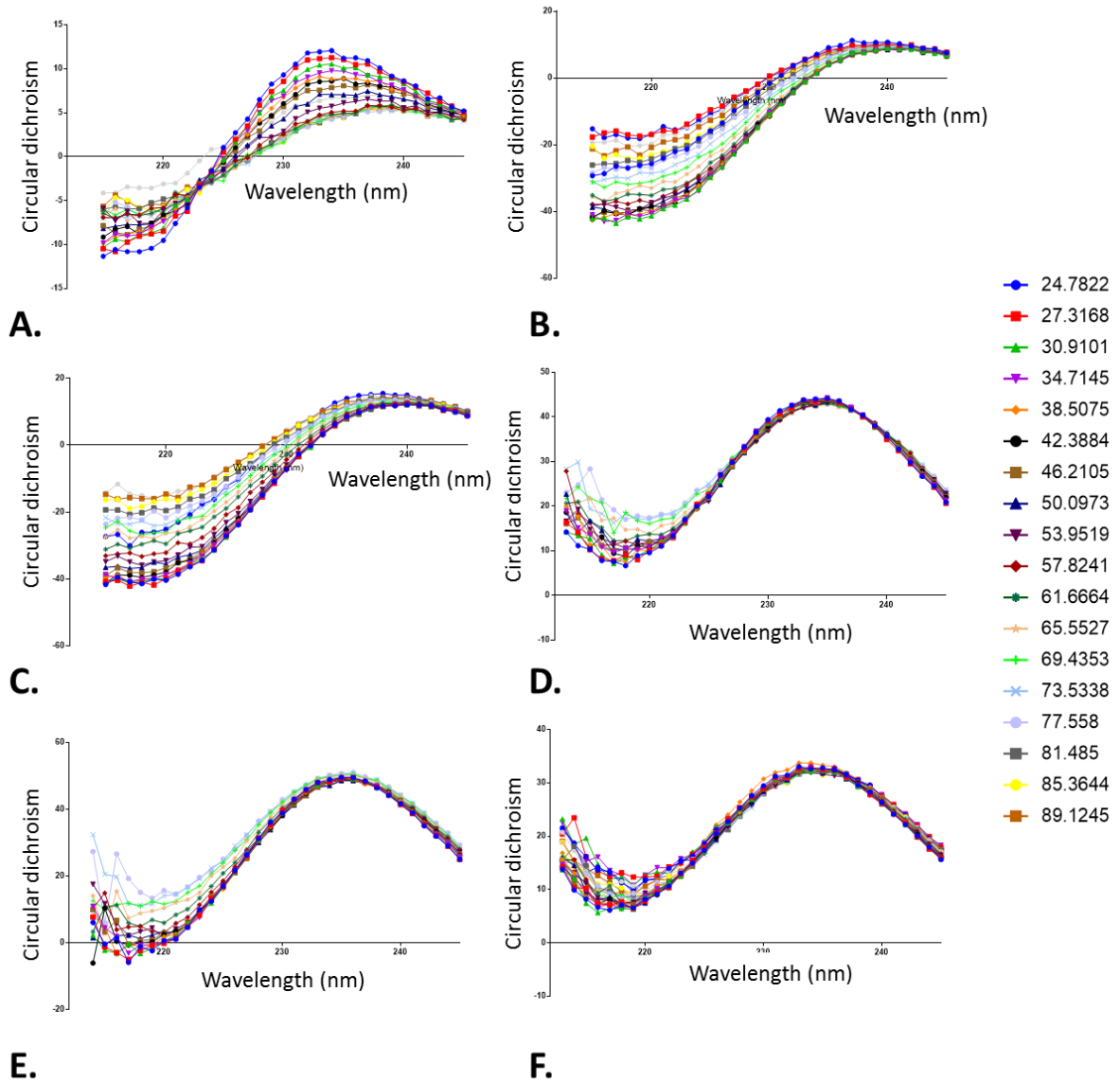


Figure 3.13. CD temperature ramps of syncollin-Strep and the cysteine mutants. CD spectroscopy was performed on WT syncollin-Strep (A), and on mutants C23G (B), C38G (C), C52G (D), C86G (E) and C131G (F). Protein (10 μ M) was added to 1 mm quartz cuvettes in 10 mM sodium phosphate, pH 8.0 containing 0.1% (w/v) CHAPS. Temperature ramps were performed between 25-90°C with temperatures displayed at the right. Three repeats were carried out for each temperature, with only one dataset shown for clarity. Data were plotted using GraphPad Prism™.

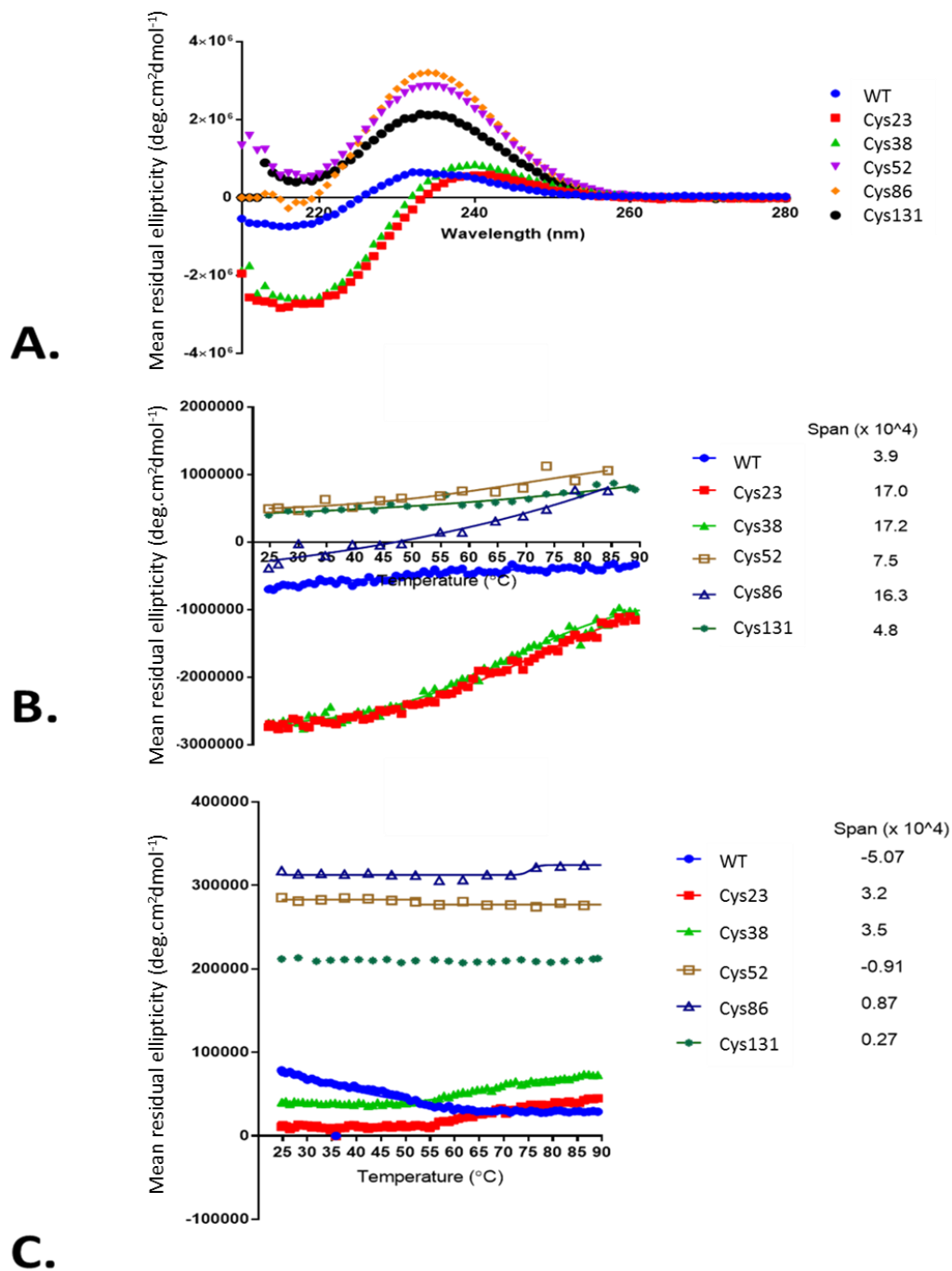


Figure 3.14. Changes in CD spectra with temperature. A. CD spectra for each cysteine mutant from Figure 3.13 were normalized to mean residual ellipticity and spectra were plotted for each mutant. B, C. CD was plotted against temperature for 2 wavelengths - 217 nm (B), 234 nm (C). Spans were calculated using GraphPad Prism™ and are shown at the right. Curves were plotted using GraphPad Prism™ and fitted by non-linear regression. Some mutants could not be fitted using non-linear regression and therefore are not depicted.

3.3.9 LIPOSOME PERMEABILIZATION BY SYNCOLLIN POSITIVE CHARGE MUTANTS

In addition to the cysteine mutants, positive charge mutants were also generated to investigate the importance of electrostatics on membrane binding and perturbation, measured via BCECF release from liposomes. The single mutants K9A, K10A, R76A and the triple mutant K9, 10, R76A all caused >20% permeabilization of the liposomes (Figure 3.15A), however all except the K9A single mutant resulted in a significant reduction in BCECF release compared to WT syncollin-Strep (Figure 3.15B).

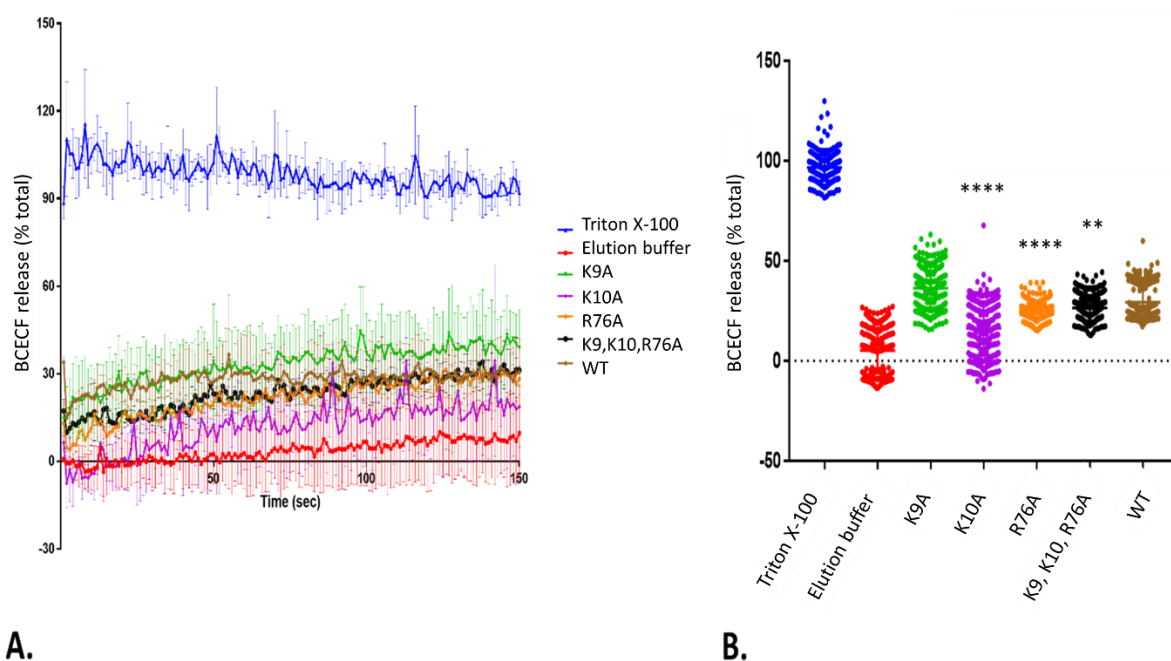


Figure 3.15. Liposome permeabilization by positive charge mutants. A. BCECF release was monitored using fluorimetry. Negative (elution buffer) and positive controls (1% [v/v] Triton X- 100) were included. WT syncollin-Strep or syncollin positive charge mutants were added at 4.5 $\mu\text{g}/\text{mL}$ to liposomes and fluorescence monitored. Data are shown as % release, assuming 100% release with Triton X-100. Error bars are SD (n=3). Data were plotted using GraphPad PrismTM. B. Histogram of data from (A) between 50 s and 150 s. One-way ANOVA with Tukey's multiple comparison test was carried out between conditions. For all conditions, $p < 0.0001$ compared with buffer alone. Mutants which were significantly lower than WT are displayed with asterisks ** $p < 0.005$, **** $p < 0.0001$.

3.3.10 SUSCEPTIBILITY TO DENATURATION

The stability of WT syncollin-Strep was next investigated through chemical unfolding of the protein using the denaturant GnHCl. Syncollin-Strep contains eight tyrosine and three tryptophan residues, which should fluoresce more strongly when exposed to solvent. Unfolding of the protein should therefore cause an increase in its fluorescence. Upon addition of 6 M GnHCl to syncollin-Strep, the

peak fluorescence increased from ~200 units to ~350 units, and the peak wavelength shifted from ~360 nm to ~350 nm (Figure 3.16). Further, when fluorescence at 365 nm was measured over a range of GnHCl concentrations, a concentration-dependent increase in fluorescence was seen.

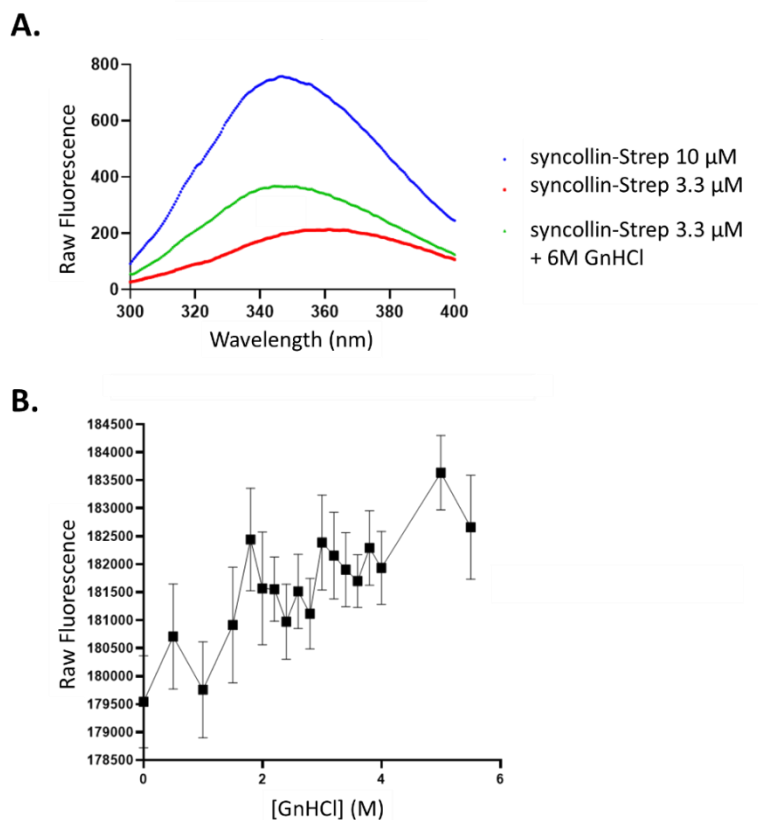


Figure 3.16. Denaturation of syncollin. A. Syncollin-Strep was used at either 10 μ M or 3.3 μ M. Fluorescence was measured between 300-400 nm, to detect increases in intrinsic tryptophan and tyrosine fluorescence upon unfolding. Syncollin-Strep was denatured by addition of 6 M GnHCl, and spectra were recorded. Typical traces are shown. B. Concentration dependence of denaturation. Syncollin-Strep (10 μ M) was incubated with varying concentrations of GnHCl from 0-6 M for 2 h at room temperature. Fluorescence was then recorded at 365 nm using a ClarioStar™ plate reader. Error bars are SD (n=5).

3.3.11 DIBMA PURIFICATION AND DLS

DLS was used to investigate whether syncollin-Strep can assemble on membranes and then be removed as an oligomer. A membrane fraction of lentivirally-infected HEK-293F cells expressing syncollin-Strep was solubilized in 2% (w/v) DIBMA (Figure 3.17A), and syncollin-Strep was purified using Strep-Tactin XT™ beads. As shown in Figure 3.17B and C, the majority of the protein was removed from the beads during washing rather than elution. (Note that the total wash volume was 3

mL, while the elution volume was only 100 μ L). To assess whether the protein was in DIBMA discs, DLS was carried out to determine the particle size. In the presence of DIBMA, the discs existed in two sizes - 33.2% at 269.9 nm in diameter and 66.8% at 41.65 nm (Figure 3.17D). This is in contrast to monomeric syncollin in CHAPS, which 99.5% of which exists at 16.63 nm in diameter (Figure 3.17E). The result of this experiment therefore suggests that larger particles are formed in DIBMA.

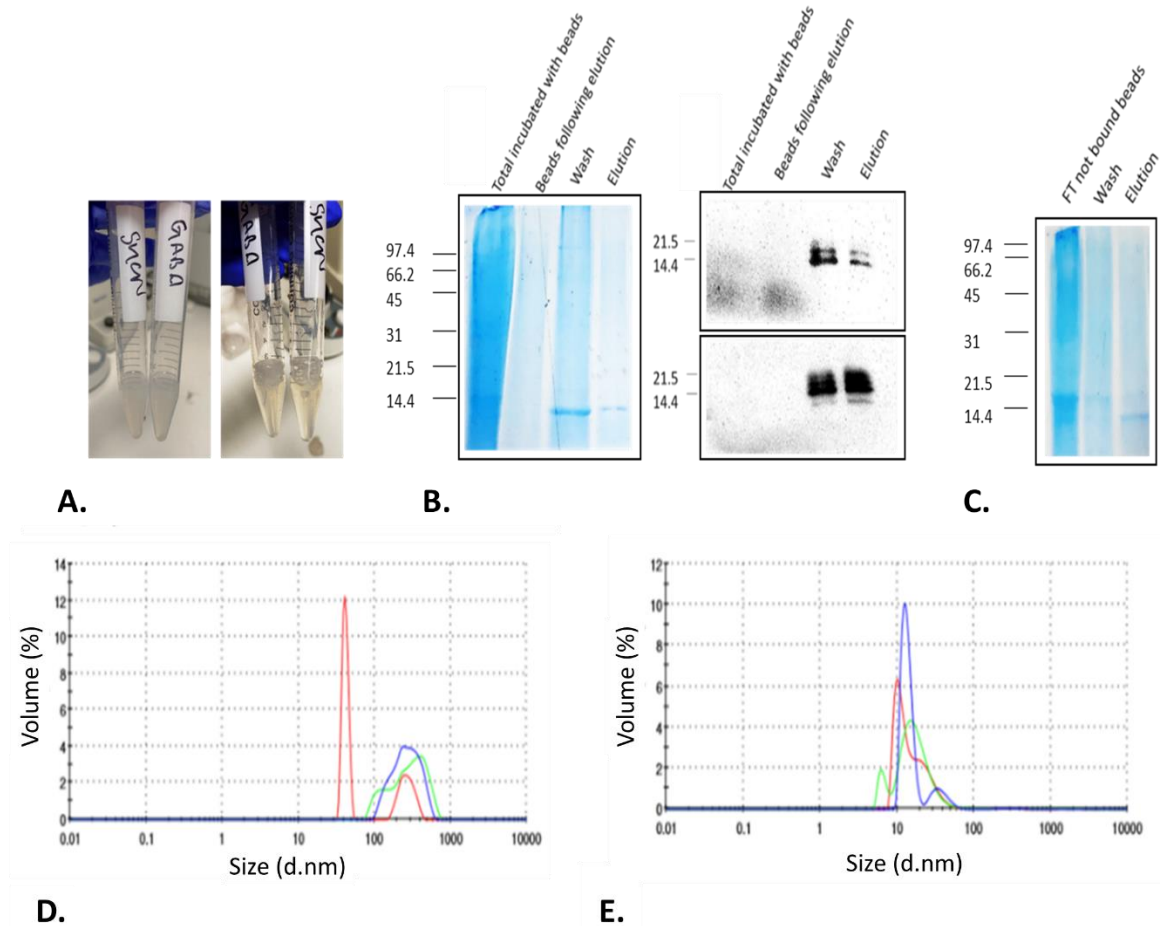


Figure 3.17. Syncollin solubilization with DIBMA. Membranes containing syncollin-Strep were prepared from lentivirally-infected HEK-293F cells. Membranes were resuspended to 40 mg/mL in DIBMA buffer (50 mM Tris, pH 7.0 containing 100 mM NaCl, protease inhibitors) and 2% [w/v] DIBMA) followed by incubation for 18 h at 4°C. A. Membrane fractions before (left) and after (right) DIBMA addition showing clarification caused by DIBMA. Membrane fractions were then incubated with Strep-Tactin XTTM resin for purification, as previous. B. SDS-PAGE analysis of various fractions from the purification: total added to beads (lane 1), beads following elution (lane 2), 3-mL wash fraction (lane 3) and 100- μ L elution fraction (lane 4). Proteins were detected either by Coomassie blue staining or immunoblotting, using a polyclonal anti-syncollin antibody. C. Repeat of B, but showing flow-through/unbound material (lane 1), 3-mL wash fraction (lane 2) and 100- μ L elution fraction (lane 3). Standards for B and C are BioRad low-range markers. D, E. DLS data from syncollin in DIBMA (D) and syncollin in CHAPS (E).

3.3.12 MEASUREMENT OF HYDRODYNAMIC RADIUS

The interaction of syncollin with syntaxin-2 has been shown to be affected by Ca^{2+} (Edwardson *et al.*, 1997). Given the predicted presence in syncollin of positively- and negatively-charged surfaces and the likely importance of electrostatics with respect to its function demonstrated above, I decided to test whether cation addition could affect the oligomerization of syncollin. I found that the hydrodynamic radius of syncollin-GFP alone was not significantly affected by addition of either Ca^{2+} or Mg^{2+} (Figure 3.18A); however, the radius of syncollin-GFP in combination with GST-syntaxin 2 was increased significantly by Ca^{2+} but not by Mg^{2+} (Figure 3.18B).

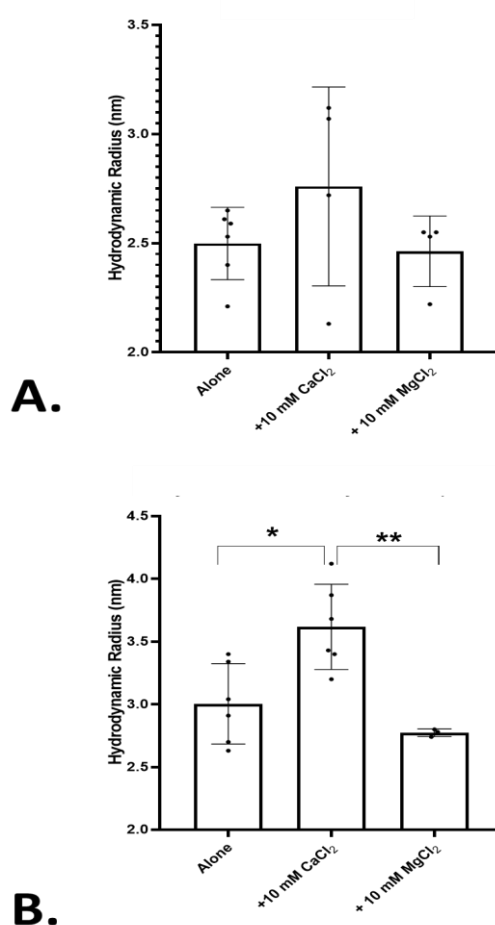


Figure 3.18. Hydrodynamic radius of syncollin-GFP. tsA-201 cells were transfected with syncollin-GFP and a cell lysate was generated using RIPA buffer and clarification by centrifugation. The cell lysate was added to a Fluidity One-W™ instrument after dilution 10,000-fold to reduce noise while producing a detectable signal. A. Syncollin-GFP either in the absence of divalent cation, or in the presence of either 10 mM CaCl_2 or 10 mM MgCl_2 . B. Syncollin-GFP plus 50 mM GST-syntaxin 2 cytoplasmic domain either in the absence of divalent cation, or in the presence of either 10 mM CaCl_2 or 10 mM MgCl_2 (n=4 or greater). *p<0.05; **p<0.01 by one-way ANOVA with Tukey's multiple comparison test. Error bars are SD (n=5).

3.4 DISCUSSION

Structure prediction based on primary sequence suggested that syncollin is likely to have a predominantly beta-sheet secondary structure in a Greek Key arrangement, similar to members of the $\beta\gamma$ -crystallin family members. Additionally, the predicted strong electrostatics of the surface of the protein (i.e. the presence of both positively- and negatively-charged patches) could potentially explain its interaction with negatively-charged membranes. Ca^{2+} may bind in a negatively-charged pocket and thereby affect the interaction of syncollin with syntaxin 2.

CD spectra had two peaks, a negative peak at 218 nm, indicating a beta-sheet structure, and a positive peak at 234 nm, indicating the presence of disulphide bonds, features also present in the $\beta\gamma$ -crystallins (Andley *et al.*, 1996). The predicted location of the cysteine residues within the protein, can accommodate up to three disulphide bonds in each monomer. This would explain the thermal stability of the protein seen in the CD heat-ramp experiment, where the protein did not fully denature even at high temperatures, and the resistance of the protein to GnHCl treatment. Further, the observation that the large 234-nm peak in the CD spectrum was reduced with temperature upon addition of the reducing agent DTE is also consistent with the presence of stabilizing disulphide bonds. Members of the $\beta\gamma$ -crystallin family are known to be particularly stable, a required feature, for example, in the extreme environment of the eye (Serebryany and King, 2014). The results described here suggest that syncollin shares this high stability.

Interestingly, the two peaks in the CD spectrum of syncollin-Strep displayed different melting temperatures, with the 234-nm peak having a lower melting temperature than the 218 nm peak. If protein folding were non-cooperative, one would expect to see the formation of an intermediate structure, where a conformational change and melting in the tertiary structure would precede the unfolding of the secondary structure. It is possible that the 218 nm peak represents the secondary beta-sheet structure of the protein, whereas the 234 nm peak, occurring as a result of the disulphide bonds, represents the tertiary conformation. If this were the case, it would make sense for the tertiary structure to have a lower melting temperature, and this might be expected given the structural contributions of the disulphide bonds. One other way of investigating this would be to collect CD data from the 250-340 nm range where aromatic tryptophan and tyrosine presence would be 'seen'. If these spectra displayed a similar melting temperature to that of the 234 nm peak, this would support the notion that this peak represents the tertiary structure of the protein, since exposure of aromatic residues during heat denaturation would occur in an altered tertiary structure. Likewise, the presence of a predicted free cysteine could result in inter-molecular disulphide bonding, which might contribute

to the 234-nm peak. To investigate this possibility, different spectra could be collected at different concentrations of the protein; the formation of oligomers would be concentration dependent, which ought to affect the behaviour of the 234-nm disulphide peak.

X-ray crystallography seemed the most appropriate method for the determination of the structure of syncollin. Syncollin-Strep (at >5.2 mg/mL) produced crystals under some trial conditions, which diffracted to a 4.2 Å resolution. The difficulty lay with proceeding from this stage to a structure. This problem can often be resolved through molecular replacement, where similar protein structures and folds can be used to solve the structure of an unknown protein. The issue with syncollin, was that the closest homology model had only ~20% sequence similarity, in contrast to the ~40% regarded as necessary for effective molecular replacement. Hence, this method could not be used. The next approach used was to try to solve the phase problem. To this end, both Sulfur-SAD beamline exposure and heavy metal (mercury) soaking of the crystals were explored. Unfortunately, either the signal was not strong enough after heavy metal addition and X-ray beam exposure, or the crystals dissolved at the highest concentrations of heavy metals used. A major hurdle encountered in developing these phase-solving methods was the poor availability of crystals to run trials. Typically from one purification, syncollin-Strep at 0.5 mgs which could be concentrated to 5 mg/mL, only a maximum of five crystals were observed in 4 x 96-well screens which was not compatible with effective optimization. However, the purification process was robust enough to provide material for functional assays described later in this dissertation.

Although the crystal structure of syncollin-Strep could not be solved, modelling was used to generate a predicted structure that allowed rational design of mutants in order to assess the importance of disulphide bonding and surface electrostatics with respect to the behavior of the protein. The cysteine mutants generated did not perform differently from WT in biochemical assays, and all mutants could permeabilize membranes. However, the cysteine mutants did demonstrate reduced thermal stability. Specifically, for mutants C23G, C38G and C86G, the beta-sheet 217-nm span over a temperature ramp increased 4-fold relative to WT, although the absolute CD values at 217 nm fell. Note that the melting curve for the mutants was not fully sigmoidal, and the shallow curves without a clear plateau could imply non-cooperative folding. The increase in span at 217 nm could imply increased beta-sheet folding. Alternatively, given that the negative peak for random coils is at ~200 nm, and considering that the CD spectra shown is an average of the secondary structure, the increase in span could be a result of an increase in random coils and a corresponding reduction in beta-sheets, resulting in a larger broader negative peak. The mutations did not change the span of the 234-nm disulphide peak over the temperature ramp, in comparison to WT. However, the spectra alone displayed differences in the

amplitude this peak, with clearly increased amplitudes for mutants C52G and C86G, for example. If the disulphide bonds affected by these mutations contribute to the tertiary structure of the protein then a conformational change which affects the tertiary structure might also affect the 234 nm peak.

When looking at the mutants which appear the most destabilized and bearing in mind the initial predicted structure, two observations are worthwhile. First, cysteine 23 is predicted to be a lone cysteine, and so the significant change observed in thermal stability could be as a result of disruption of inter-molecular disulphide bond and consequent prevention of oligomer formation. Second, the pairs C38 and C86, and C52 and C53 are within close enough proximity to enable intra-molecular disulphide bond formation. Hence, disrupting these bonds could result in alternative conformations of the protein, resulting in reduced thermal stability. Without the crystal structure, of course, one can only speculate on which disulphide bonds are formed. To surmount this problem, one could apply cysteine mapping using mass spectrometry, which should identify cysteine pairs and free cysteines.

Designing syncollin positive charge mutants was difficult because of the extensive nature of the positively charged surface. Mutations were targeted to likely key areas such as within a cluster (K9, K10), and within the most positively charged region (R76). A triple mutant encompassing all three residues was also produced in an attempt to reduce overall surface electrostatics. Impressively all of these mutants except K9A caused a reduction in the ability of syncollin-Strep to permeabilize liposomes. This reduced permeability could be interpreted as less syncollin membrane association or alternatively a reduction in the permeabilization capability of the protein. Regardless, this result shows the importance of electrostatics for the ability of syncollin to bind and/or perturb membranes.

To investigate syncollin oligomerization, purification of syncollin-Strep in nanodiscs was trialled. Syncollin was successfully solubilized from cell membrane in DIBMA nanodiscs, as judged by the sizes observed by DLS. Unfortunately, as reported previously (Dilworth *et al.*, 2021), DIBMA behaved as a 'sticky' polymer, attaching non-specifically to the Strep-Tactin XT™ resin and dissociating during washing steps, thereby hindering structural studies.

This chapter reveals details of the secondary structure of syncollin-Strep and highlights the importance of disulphide bonding and surface electrostatics for protein folding, stability and membrane interactions. Armed with this greater structural understanding, I initiated a functional approach, beginning with an assessment of the effect of syncollin on bacterial growth. These studies are described in Chapter 4.

4. ANTI-BACTERIAL ACTIONS OF SYNCOLLIN

4.1 INTRODUCTION

4.1.1 BACTERIAL MEMBRANE LANDSCAPE

One of the major differences between bacteria and mammalian cells is the presence of a cell wall in the former but not the latter. Indeed, bacteria can be categorized as either Gram-positive or Gram-negative based upon the structure of the cell wall. In Gram-positive bacteria there is a small periplasmic space between the plasma membrane and a thick multi-layered peptidoglycan (PGN) sheath that is 'laced' with teichoic and lipoteichoic acids (Figure 4.1). In contrast, Gram-negative bacteria have a wider periplasmic space that contains a thin single layer of PGN. Outside of this is an outer membrane which contains various porin proteins. The outer membrane is itself surrounded by a lipopolysaccharide (LPS) layer containing O-linked sugar residues (Silhavy *et al.*, 2010; Steward, 2019).

The bacterial cell wall provides structural integrity, enabling bacterial cells to survive internal osmotic pressure. Although the overall structure of the plasma membrane is similar in bacteria and mammalian

cells, the surface charge of the two cell types differs because of the different lipid compositions of the two membranes. Specifically, in mammalian membranes, anionic lipids are largely confined to the inner leaflet of the plasma membrane, whereas they are present in the outer leaflet in bacteria. Anionic lipids in bacterial membranes include cardiolipin and phosphatidylglycerol (PG); in contrast, mammalian cells contain more neutral lipids, such as cholesterol and PC (Epanand *et al.*, 2016; Sani *et al.*, 2015). The presence of a cell wall and the exposure of anionic lipids in bacteria has allowed the development of targeted and selective therapies. Further, the presence of PGN on the surface of Gram-positive bacteria and LPS in Gram-negative bacteria raises the possibility of additional selectivity between the two classes (Malanovic and Lohner, 2016).

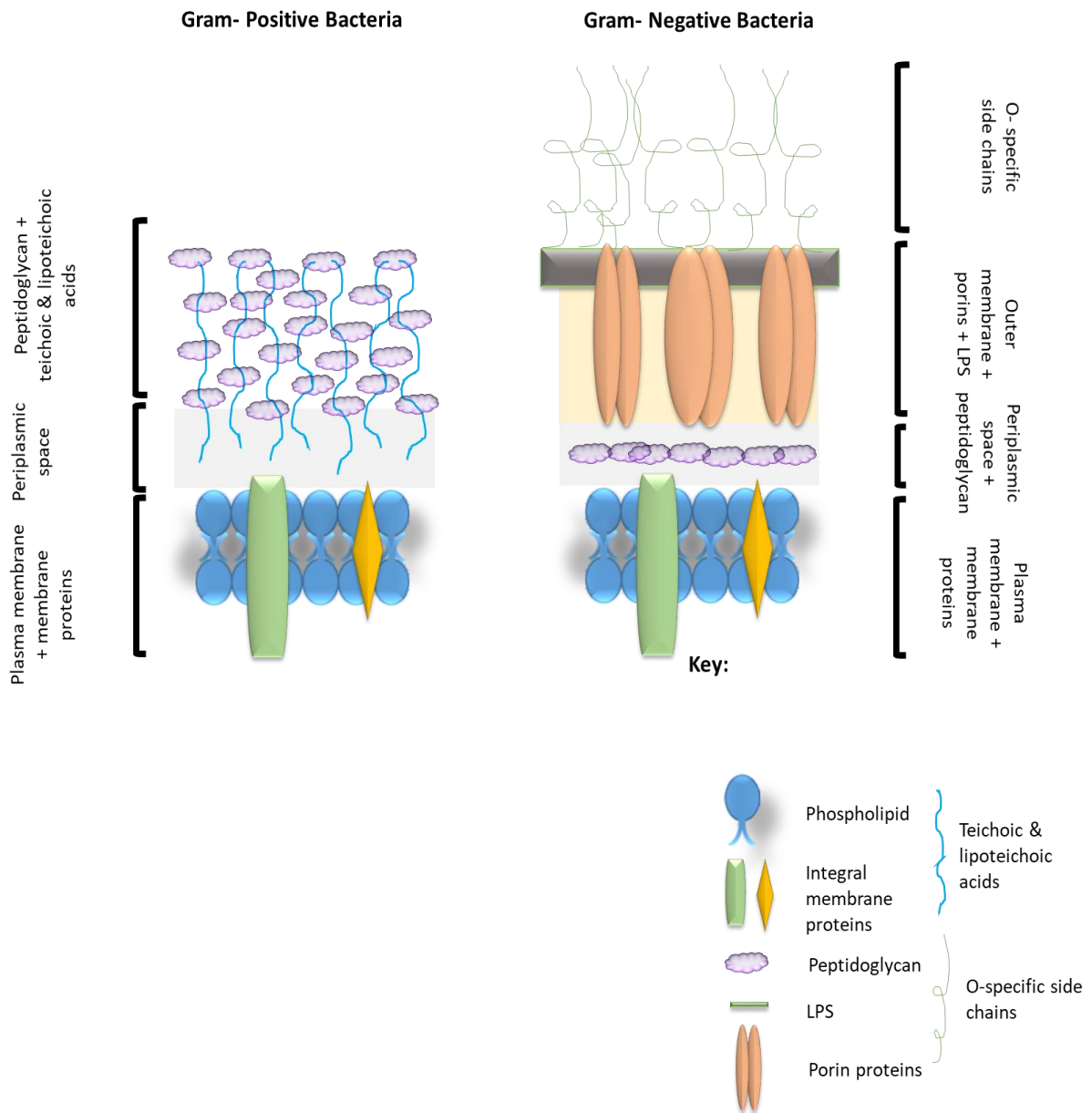


Figure 4.1. Schematic diagram illustrating the differences between Gram-positive and Gram-negative bacterial cell walls. Gram-positive bacteria (left) have a thick outer PGN layer containing various teichoic and lipoteichoic acids surrounding their plasma membrane. In contrast, Gram-negative bacteria, lack the outer PGN layer, and have instead a layer containing exposed O-linked sugars, surrounding an outer membrane containing porins and LPS. Inside of this membrane, within the periplasmic space, is a thin PGN layer that surrounds the plasma membrane. Adapted from Steward (2019).

4.1.2 MICROBES AND DISEASE

In the healthy state, microbes help the body to fight off unwanted infections and prevent disease. Many of these microbes are found in the gut, where they are known as enteric bacterial flora. In the gut, bacteria provide energy for intestinal epithelial cells through conversion of unabsorbed carbohydrates into short chain fatty acids; they are also involved in the maintenance of the innate and adaptive immune system (Sasaki and Klapproth, 2012). On the other hand, bacterially-induced infection, which can lead to inflammation, is a cause of or contributing factor to many different diseases. Some of these diseases are thought to be caused by commensal strains, whereas others are caused by clones that have become virulent (Rolhion and Chassaing, 2016).

4.1.2.1 ULCERATIVE COLITIS AND INFLAMMATORY BOWEL DISORDERS

Ulcerative colitis (UC) is a form of inflammatory bowel disease (IBD). The localization (in the large bowel) and symptoms (bloody diarrhoea and the presence of mucus) of UC are distinct from those of other types of IBD, such as Crohn's disease. Although the exact causative agent of UC is not known, and is the subject of much debate, bacterially-induced inflammation is thought to be a predominant factor. Potentially this would involve commensal bacteria gaining additional virulent properties, which prevents them from carrying out their normal roles. It is thought that bacteria cause UC in three stages: adherence to the gut mucosa and colonization, production of cytotoxins that enhance inflammation, and finally tissue invasion (Campieri and Gionchetti, 2001).

The intestinal mucosal barrier mitigates against bacterial colonization. Specifically, the epithelial cells of the gut are connected via tight junctions, which form a barrier to penetration. Further, mucin is secreted from the goblet cells of the epithelium and covers the colonic epithelium in a mesh-like layer, which, because of its negative charge among other features, attracts and captures bacteria. Mucin can also interact with other proteins and molecules involved in protein adhesion, thereby preventing bacterial colonization (Derrien *et al.*, 2010; France and Turner, 2017).

Unfortunately, in many cases of IBD there is an increase in levels of bacteria, including *Lactobacillus* and *Bifidobacterium* in active IBD patients (Bai and Ouyang, 2006) and *Clostridium* and *Bacteroides* in dextran sodium sulphate (DSS)-induced UC mouse models (Gkouskou *et al.*, 2014). One of the key roles of commensal strains, as mentioned above, is to convert carbohydrates into energy for use by the intestinal epithelial cells. It has been suggested that in UC energy depletion occurs through increased levels of sulphate-reducing bacteria, which generate hydrogen sulphide and thereby impair epithelial integrity (Rowan *et al.*, 2009). In addition, hydrogen sulphide is able to reduce the disulphide bonded

network formed between mucins in the mucin sheets, causing a reduction in barrier integrity (Ijssennagger *et al.*, 2016). The importance of epithelial barrier integrity is emphasized by the identification of IL-10, ECM-1 and cadherin-1 as UC susceptibility genes. Loss of function of these proteins is thought to result in impairment of anti-inflammatory pathways in addition to loss of barrier function (Kaur and Goggolidou, 2020).

4.1.2.2 COLITIS—ASSOCIATED CANCER

Another condition for which inflammation represents a hallmark is cancer. Colitis-associated cancer (CAC) is a colon cancer originating from UC, and contributes to colorectal cancer being the third most common malignancy worldwide (Grivennikov and Cominelli, 2016). As with colitis, the disruption of the epithelial barrier allows bacteria to penetrate, and in some cases these bacteria become virulent or conditionally pathogenic. Since the colon contains 70% of the body's microbiome, it is particularly susceptible to this effect. The stepwise progression towards CAC involves changes in gut microbiota, which directly or indirectly cause changes in the expression of oncogenes and tumour suppressors, including p53, K-Ras and STAT3. A bacterial strain which has been linked to CAC is *B. fragilis*, an enterotoxic species which among other roles is capable of cleaving E-cadherin, so disrupting the epithelial barrier and promoting β -catenin signalling to induce colitis. Wnt/ β -catenin signalling in healthy cells plays an important role in epithelial cell renewal; however, this pathway can be targeted in cancer to convert normal cells into rapidly proliferating malignant cells. Once the epithelial barriers are damaged and enhanced Wnt/ β -catenin signalling occurs, an inflammatory response is initiated, which alongside inactivation of Muc2 in the mucus layer results in further penetration of the epithelial barrier and exponential inflammation. Other hallmarks of cancer progression, such as DNA damage, can be induced by ROS produced by bacteria. Importantly, the initial disturbance in the gut microflora is thought to occur via genetic and dietary factors, and also environmental risk factors such as smoking, obesity and alcohol consumption, as with many cancers (Grivennikov, 2013; Muller *et al.*, 2020).

CAC is only one example of a colonic cancer that can be facilitated through bacterial infection; however, it is thought that 10-20% of all cancers stem from infections, showing the importance of robust maintenance of the microflora (De Flora and La Maestra, 2015).

4.1.3 ANTI-BACTERIAL DRUG ACTION

With diseases initiated by bacterial infection such as UC and CAC as extreme examples, prevention and treatment involve destruction of the pathological bacteria through use of antibiotics.

4.1.3.1 BACTERIAL GROWTH

Different bacteria require varying conditions (temperature, pH, nutrients, growth media and aeration) for optimal growth; however, all follow a similar growth pattern. Bacterial growth occurs asexually through binary fission and typically follows four phases, as illustrated in Figure 4.2. In the first (lag) phase, the cells are metabolically active, synthesizing proteins required for replication but not yet dividing; during this phase there is no significant increase in the optical density (OD) of the bacterial culture. Once the cells begin to divide, the bacteria enter the exponential (log) phase, where cells double in numbers over constant time intervals. Now the cells synthesize proteins required to keep division rates high, such as components of the DNA and RNA replication machinery. As the levels of nutrients in the medium diminish, growth slows until the number of actively dividing approaches the number of metabolically inactive and dying cells. This is the stationary phase where the growth curve 'plateaus'. When the number of dying cells becomes greater than the number dividing, OD falls. The dying bacteria lyse and release their nutrients and proteins into the media where they may be used by other bacteria. Now the levels of bacteria and the corresponding OD fall. Most antibiotics affect the bacteria in the exponential growth phase during which protein synthesis and RNA/DNA replication are at their highest, providing good targets for growth inhibition (Parker *et al.*, 2016).

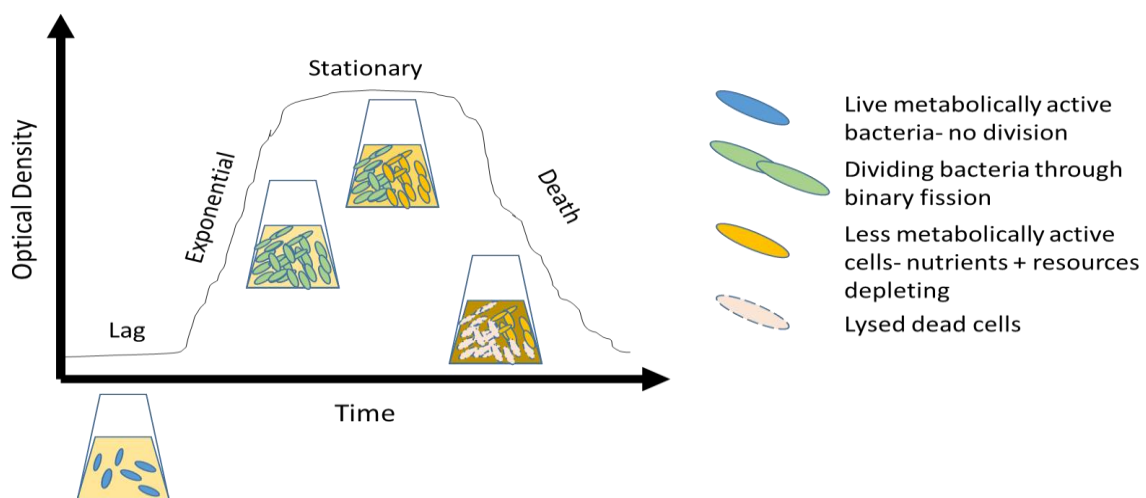


Figure 4.2. Schematic diagram of bacterial growth. Bacteria grown in a controlled culture all follow a similar predictable growth pattern reflecting division through asexual binary fission. Bacteria start in the lag phase, in which bacteria synthesize proteins required for replication, although no cell division occurs. In the exponential phase, the bacteria divide rapidly and there is extensive synthesis of proteins required for DNA and RNA synthesis. When growth becomes restricted because of limited resources and space, bacteria enter the stationary phase. Here, cells begin to die, although there are still some metabolically active cells, resulting in a plateau in cell numbers. Eventually, cell lysis and death causes a reduction in OD and bacterial contents are released into the medium.

4.1.3.2 ANTIBIOTIC CLASSES

Antibiotics may cause the elimination of the bacteria in one of two ways. Bactericidal agents directly kill the bacteria, whereas bacteriostatic agents slow bacterial growth, keeping them in the stationary phase to enable the immune system to eliminate them. Most antibiotics act on one of three bacterial targets: the cell wall or cell membrane, the nucleic acid synthetic machinery, or the protein synthetic machinery (Figure 4.3). In all three cases, the antibiotic exploits a qualitative difference between bacterial and mammalian cells. Consequently, there is a high degree of selective toxicity and side effects are usually minor (Kohanski *et al.*, 2010).

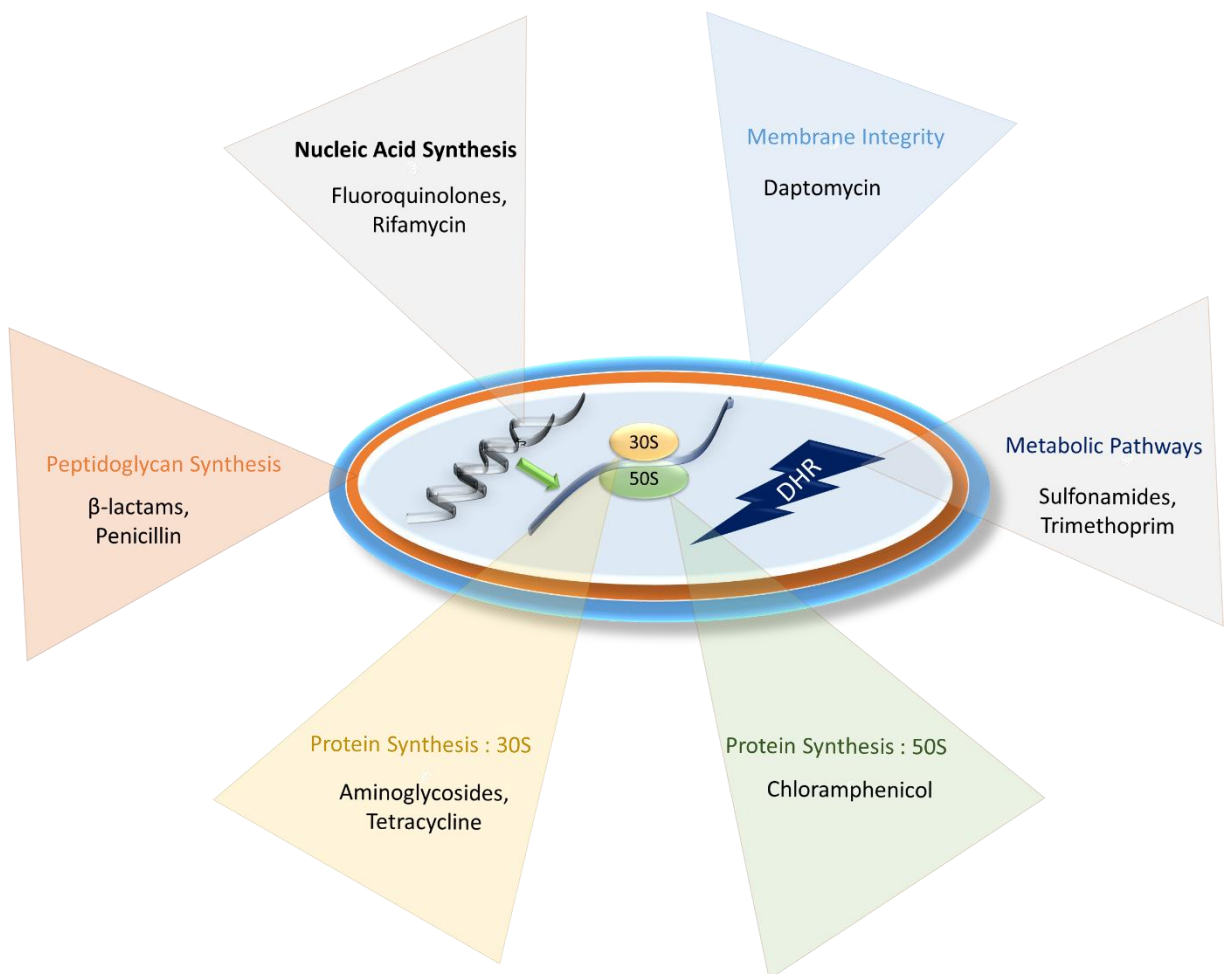


Figure 4.3. Diagram illustrating the various antibiotic targets. Targets are represented as differently coloured triangles indicating antibiotics that use this target. Targets include: PGN synthesis and membrane integrity, nucleic acid and protein synthesis (30S/50S ribosomal subunits) and metabolic pathways such as dihydrofolate reductase (DHR), required for thymidine synthesis. These targets may be attacked separately or in combination by the various antibiotics.

Antibiotics that inhibit the cell wall assembly target the synthesis of PGN, a crucial component of bacterial cell walls, especially in Gram-positive bacteria (see above). These antibiotics include members of the β -lactam family, with penicillin being the most widely used. β -lactam antibiotics inhibit PGN synthesis by preventing the final transpeptidation step, in which penicillin binding proteins (PBPs) cleave a D-alanyl-D-alanine peptide bond in the process of cross-linking two PGN chains, thereby conferring mechanical strength on the cell wall. Part of the β -lactam ring is structurally similar to D-alanyl-D-alanine and binds to the PBPs effectively irreversibly. As the cell wall is remodelled during cell division, β -lactams prevent new cell wall formation and the bacteria undergo osmotic lysis. β -lactams are therefore bactericidal (Zeng and Lin, 2013).

Membrane integrity is affected by the daptomycin class of antibiotics. Daptomycin is able to insert itself into the membrane, where it forms aggregates. These aggregates affect the fluidity and curvature of the bacterial membrane, making it more 'brittle' and creating holes that allow leakage of the cell contents. Hence, daptomycin is also bactericidal (Müller *et al.*, 2016).

Protein synthesis can be inhibited through the binding of various antibiotics to either the 30S or the 50S ribosomal subunit. Aminoglycosides, such as streptomycin, bind to the 30S subunit and cause a conformational change resulting in the inhibition of the initiation of translation and messenger RNA (mRNA) misreading. Aberrant proteins are produced, some of which enter the cell membrane and increase its permeability, causing cell death. The aminoglycosides are therefore also bactericidal. Tetracycline, also binds to the 30S subunit and prevents transfer ribonucleic acid (tRNA) attachment, inhibiting protein synthesis and having a bacteriostatic effect. Chloramphenicol and macrolide antibiotics bind to the 50S subunit. The former blocks translation by preventing peptide bond formation, whereas the latter preventing elongation of the nascent protein chain. Again, these antibiotics are bacteriostatic (Ruiz and Ramirez-Ronda, 1990).

Fluoroquinolones and rifamycins target DNA and RNA synthesis. These operate by inhibiting the action of two enzymes: DNA gyrase, responsible for the introduction of negative superhelical twists into the bacterial DNA, and topoisomerase IV, responsible for removal of interlinking daughter chromosomes, which permits their segregation into the two daughter cells following replication. Inhibition of nucleic acid synthesis by these compounds is irreversible, and they are therefore bactericidal (Pham *et al.*, 2019).

The final major class of antibiotics targets the synthesis of thymidine, a precursor required for DNA synthesis. Sulphonamides (e.g. sulphamethoxazole) and trimethoprim block successive steps in the

synthetic pathway of tetrahydrofolic acid by inhibition of the enzymes dihydropteroate synthase and dihydrofolate reductase, respectively. Their effects are reversible and they are therefore bacteriostatic (Capasso and Supuran, 2019; Smith and Powell, 2000).

4.1.3.3 ANTIBIOTIC RESISTANCE AND COMBINATION

Bacteria have evolved over time to become resistant to antibiotics, through mechanisms including target modification, gene mutations and post-translational modifications, hydrolysis of the drug (e.g. of β -lactams by the enzyme β -lactamase), efflux of the drugs out of the cells using efflux pumps (in Gram-negative bacteria) and reprogramming PGN synthesis (e.g. to overcome the effect of vancomycin; Munita and Arias., 2016). Resistance can sometimes be overcome using combination treatment with an 'antibiotic cocktail'. There are three possible ways in which the effects of two (say) antibiotics might interact. The effect might simply be additive. Alternatively, the combined effect might be greater than the sum of the two individual effects, described as a synergistic interaction. Or conversely, the antibiotics might oppose each other's effects, described as an antagonistic interaction. Synergy is seen, for example, when sulphamethoxazole and trimethoprim are combined (as cotrimoxazole), because the two drugs inhibit successive steps in the syntheses of tetrahydrofolate, as mentioned above (Minato *et al.*, 2018). In contrast, antagonism is often seen when a bacteriostatic and a bactericidal agent are combined. For example, the bactericidal effect of penicillin requires the cells to be actively dividing, a process that is prevented by tetracycline (Johansen *et al.*, 2000).

4.1.4 ANTI-BACTERIAL PROTEINS

Antibiotics have been developed for medical intervention in the treatment of bacterial infections. However, endogenous anti-bacterial or anti-microbial proteins (AMPs) are also mobilized in response to infection. Examples of these include RegIII and defensins, described in Chapter 1, whose expression increases in response to infection, and whose pore-forming properties can result in lysis of bacteria and the clearance of infection.

This chapter explores whether syncollin is able to bind to the bacterial membrane component PGN and whether syncollin has an effect on bacterial growth and membrane integrity (of either Gram-positive or Gram-negative bacteria). It also describes how the effect of syncollin interacts with those of typical bactericidal and bacteriostatic antibiotics and how syncollin affects the surface structure of bacteria.

4.2 METHODS

4.2.1 PEPTIDOGLYCAN BINDING ASSAY

Syncollin-Strep (100 μ L of a 0.33 mg/mL solution in 10 mM sodium phosphate buffer, pH 8.0, containing 0.1% [w/v] CHAPS) was incubated overnight at 4°C, with agitation, with various quantities of insoluble PGN (30-320 μ g; *Bacillus subtilis*, Sigma). Alternatively, 25 μ g PGN was incubated with various amounts of syncollin-Strep (7.8-15.6 μ g). In both experiments, PGN was precipitated by centrifugation at 13,000 rpm for 3 min at 4°C. The supernatants were retained and the PGN pellets were washed twice with ice-cold PBS, pH 7.4. Supernatants and pellets were resuspended in equal volumes of Laemmli sample buffer and analysed by SDS-PAGE and immunoblotting, using a polyclonal anti-syncollin antibody. To check that syncollin-Strep binding to PGN was specific, bovine serum albumin (BSA) was used at the same concentration as syncollin-Strep in the binding assay, and visualized on gels by Coomassie blue staining. To ensure that syncollin-Strep alone did not pellet, a control pull-down experiment, in the absence of PGN, was also included. In some assays, soluble PGN, produced by sonication of insoluble PGN (3 bursts of 10 s on medium intensity), was added in excess (100 μ g) to assess competition with insoluble PGN for binding to syncollin-Strep. Band intensities for syncollin-Strep (on immunoblots) and BSA (on Coomassie gels) were determined using ImageJ™ and are shown as histograms, produced using GraphPad Prism™.

4.2.2 BACTERIAL GROWTH CURVES

Lactococcus lactis (*L. lactis* NZ9000 Δ ImrA Δ ImrCD; Gram-positive) and *Escherichia coli* (*E. coli* DH5 α ; Gram-negative) were used for bacterial growth assays. *L. lactis* was grown in M17 media containing 0.5% (w/v) glucose under anaerobic conditions at 30°C, and *E. coli* was grown in LB broth, at 37°C, with shaking at 220 rpm. Bacteria were inoculated from glycerol stocks and cultures were grown for approximately 8 h until an OD of \sim 0.5 was reached. Bacterial growth curves were generated by quantification of absorbance using a plate reader for reading of a 96-well plate with a final volume of 100 μ L per well. Syncollin-Strep, at various concentrations up to 163 μ g/mL, was added in a 50- μ L volume to bacteria diluted to OD 0.01 and 0.02 for *E. coli* and *L. lactis*, respectively, before incubation as described above. A negative control, syncollin elution buffer (10 mM sodium phosphate buffer, pH 8.0, containing 0.1% [w/v] CHAPS and 50 mM biotin) and a positive control (40 μ g/mL ampicillin) were included. OD was measured at 600 nm for *L. lactis*, using a SpectraMax™ plate reader (Molecular Devices), and at 660 nm for *E. coli*, using a Clariostar™ plate reader. Plates were read every 30 min over an \sim 20-h period. Wells around the perimeter of the plates were not used and lids were left on the

plates during readings to prevent discrepancies due to evaporation. Each condition was repeated at least in triplicate in individual experiments, with independent repeats, and plate layouts altered in these repeats to rule out plate bias. Data and statistical analyses were carried out using GraphPad Prism™.

The antibiotics ampicillin and tetracycline were used in combination with syncollin-Strep to assess the effect of protein-antibiotic combinations on bacterial growth. Antibiotic concentrations were selected such that bacterial growth still occurred but at a significantly reduced rate compared with control. Selected ampicillin and tetracycline concentrations were 0.05 µg/mL and 2 µg/mL, respectively. Syncollin-Strep was used at final concentration of 300 µg/mL in these combination experiments. For some bacterial growth assays, the effect of divalent cation addition to syncollin was investigated. For these assays, MgCl₂ (10 mM) or CaCl₂ (10 mM) were incubated with syncollin-Strep for 30 min on ice prior to addition to the growth assay plates. In addition, for some assays, bovine pancreatic ribonuclease (RNase A) and soybean trypsin inhibitor were used (at 0.3 mg/mL) as protein controls.

4.2.3 STATISTICAL ANALYSIS OF BACTERIAL GROWTH CURVES

Absorbances at time zero were subtracted from all values to removal baseline differences between the various conditions so all data start from zero. Growth curves were displayed using GraphPad Prism™ following transformation by non-linear regression to generate a sigmoidal growth curve. Three growth parameters were derived from each curve: span, a measure of the increase in OD over the course of the curve, Hill slope, a measure of the gradient of the log phase of the curve, and T₅₀, where T₅₀ is the time taken for the curve to reach half of its maximal OD. To calculate Hill slope and T₅₀, the data were further normalized to % growth by setting the negative (buffer only) control as '100% growth'. This manipulation prevented the generation of ambiguous Hill slopes when the non-linear regression fit was applied. Data were presented as histograms, showing standard deviation. The statistical test used was a one-way ANOVA between the various syncollin-Strep concentrations. If the ANOVA was significant, either a Dunnett's multiple comparison was used for statistical significance between negative control (buffer alone) and other conditions or a Tukey's multiple comparison test for statistical significance between all conditions.

4.2.4 CHECKERBOARD ASSAY

Syncollin-Strep was diluted two-fold sequentially across a 96-well plate (from 0.18 mg/mL) and either ampicillin (from 0.004 mg/mL) or tetracycline (from 0.002 mg/mL) was diluted sequentially down the plate. *L. lactis* was then and incubated as described above. When the bacteria reached the plateau

phase of growth, absorbance (OD 600 nm) was measured. Minimum inhibitory concentrations (MIC) and fractional inhibitory concentration (FIC) were calculated according to Daly *et al.* (2017). Briefly, this involved determining the MIC for syncollin-Strep and antibiotic alone and also in combination for syncollin-Strep plus antibiotic, before application of the following equation:

$$FIC\ Index = \frac{MIC\ of\ Syncollin\ in\ combination}{MIC\ of\ Syncollin\ alone} + \frac{MIC\ of\ antibiotic\ in\ combination}{MIC\ of\ antibiotic\ alone}$$

The value of the FIC index was then used to interpret the nature of the interaction between syncollin-Strep and ampicillin or tetracycline as follows: synergistic (FIC \leq 0.5), additive (FIC 0.5-1), antagonistic (FIC \geq 1). Each type of interaction appears differently on a checkerboard plate, as shown in Figure 4.4.

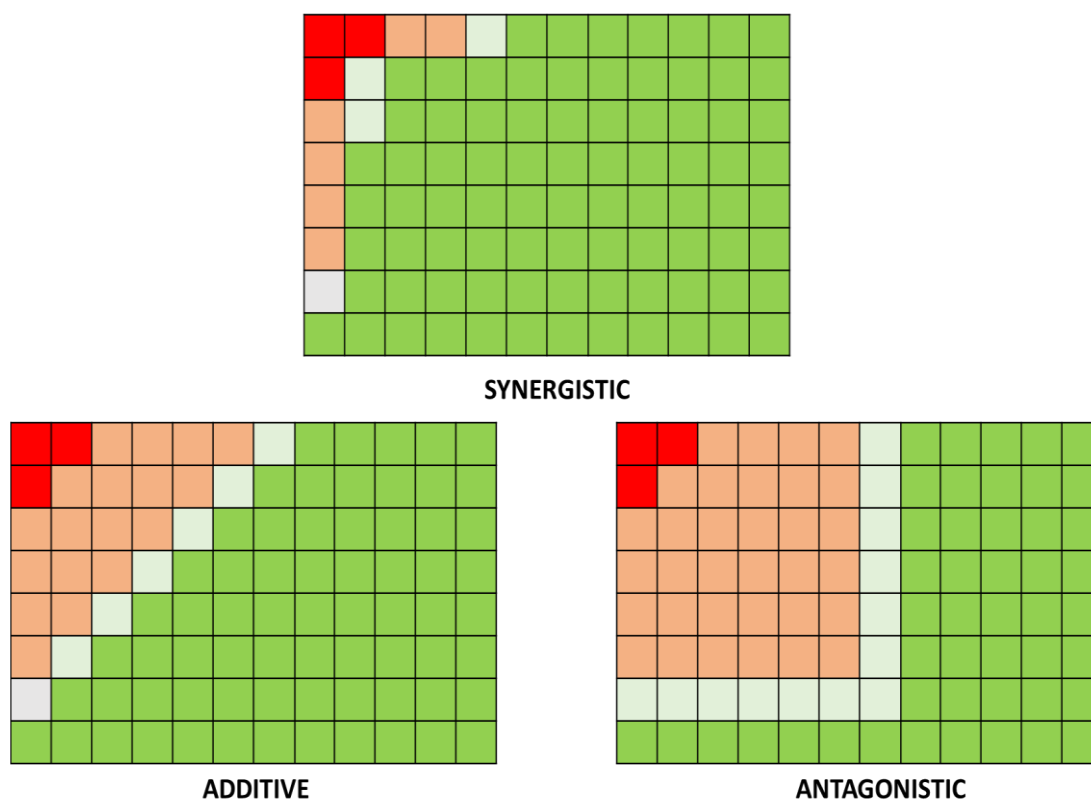


Figure 4.4. Checkerboard assay. Illustration of various checkerboard assay outcomes depending on FIC index values. Wells highlighted in green show bacterial growth, and growth inhibition is indicated in red. FIC Index values reveal the nature of the interaction between drug and protein. Possible interactions are: synergistic (FIC \leq 0.5), additive (FIC 0.5-1.0) and antagonistic (FIC \geq 1).

4.2.5 DETERMINATION OF BACTERIAL VIABILITY BY PROPRIDIUM IODIDE STAINING

E. coli and *L. lactis* were incubated with buffer alone, syncollin-Strep (0.3 mg/mL), ampicillin (0.05 µg/mL) or tetracycline (2 µg/mL). OD (*L. lactis*, 600 nm; *E. coli*, 660 nm) was monitored until bacteria reached the log phase (OD ~0.1) or the early plateau phase of growth (OD ~0.35 for *L. lactis* and ~2.2 for *E. coli*). Bacteria then were collected by centrifugation at 1,000 g for 2 min. Bacterial pellets were washed briefly with PBS and resuspended in PBS containing 1 µg/ml propidium iodide (PI) and 1 µg/ml 4',6'-diamidino-2-phenylindole dihydrochloride (DAPI). Resuspended bacteria were incubated in the dark for 20 min at room temperature and then added to poly-L-lysine coated 18-well flat imaging plates (Ibidi™) before confocal imaging. Confocal imaging settings were identical for all conditions for each bacterial strain. Raw images were incorporated into image composites using ImageJ™. Brightness was adjusted identically for all images within an experiment so that red and blue staining could be clearly identified. Red staining and red plus blue staining was quantified using set colour thresholding and area measurement using ImageJ™. The percentage of red (dead) cells relative to red plus blue (total) cells was then calculated. For each experiment, at least three images were analysed and a mean percentage dead cells was determined. Data from independent experiments were then combined. Statistical analysis used was one-way ANOVA with Dunnett's multiple comparisons to buffer control.

4.2.6 ATOMIC FORCE MICROSCOPY IMAGING OF BACTERIA FOLLOWING SYNCOLLIN TREATMENT

Samples (3 x 100 µL) were collected from bacterial growth plates after incubation with syncollin-Strep when the bacteria were in the plateau phase. Glass slides were incubated with 10% (w/v) poly-L-lysine in water for 30 min at room temperature. Poly-L-lysine was gently washed off by passing water over the surface before drying under a nitrogen stream. Bacterial samples were centrifuged at 5,000 rpm for 2 min and the pellets were gently washed with 10 mM sodium phosphate buffer, pH 8.0, before resuspension at a 500-fold dilution. Resuspended bacteria (20 µl) were then added to the poly-L-lysine-coated glass coverslips for 30 min at room temperature. AFM imaging under fluid was carried out by Dr. I. Mela, using a Bruker AXS FastScan Dimension™ instrument.

4.2.7 SCANNING ELECTRON MICROSCOPY (SEM) IMAGING OF BACTERIA FOLLOWING SYNCOLLIN TREATMENT

Coverslip coating differed for *L. lactis* and *E. coli* because of differential bacterial adherence. For *L. lactis*, 13-mm coverslips were washed with acetone for 5 min before coating with a 50:1 (v/w) acetone:Vectabond™ solution (Vector Laboratories) for 5 min. For *E. coli*, coverslips were washed with

water before coating with 0.1% (w/v) poly-L-lysine (Sigma) for 30 min at room temperature. Once coated, both sets of coverslips were washed three times with water and dried in a stream of nitrogen.

E. coli and *L. lactis* were incubated with buffer alone, or with syncollin-Strep, soybean trypsin inhibitor or RNase A (all at 0.3 mg/mL). Once in the plateau phase of growth, bacteria were removed and allowed to adhere to the coated coverslips for 30 min at room temperature. Coverslips were very briefly dipped twice in cold, de-ionized water to remove any buffer salts and then quickly plunge-frozen by dipping into liquid nitrogen-cooled ethane. Samples were transferred to liquid nitrogen-cooled brass inserts and freeze-dried overnight in a liquid nitrogen-cooled turbo freeze-drier (Quorum K775X). Samples were mounted on aluminium SEM stubs using conductive silver paint (TAAB) and sputter-coated with 20-nm gold using a Quorum K575X sputter coater. Samples were viewed using a FEI Verios 460 scanning electron microscope run at 1 keV and 25 pA probe current. Images were acquired in SE-mode using an Everhard-Thornley detector.

4.3 RESULTS

4.3.1 BINDING OF SYNCOLLIN TO PEPTIDOGLYCAN

To investigate syncollin binding to the bacterial membrane component PGN, syncollin-Strep (0.33 mg/ml) was incubated with various quantities of insoluble PGN (20-320 μ g), before pelleting of the PGN and quantitation of syncollin binding. As the mass of PGN increased, syncollin-Strep became increasingly associated with the pellet, with progressively less remaining in the supernatant (Figure 4.5A). All of the syncollin-Strep added was found in the pellet at the highest amount of PGN used (320 μ g). BSA was used as a control for non-specific binding to PGN. At least 70% of the BSA added remained in the supernatant irrespective of the amount of PGN present (Figure 4.5B). A control pull-down experiment was carried out in the absence of PGN. In this case, all of the syncollin-Strep remained in the supernatant, demonstrating that the protein was not pelleted by itself under the centrifugation conditions used (Figure 4.5C).

The same pattern was observed when different amounts of syncollin-Strep (7.8-15.6 μ g) were incubated with a fixed amount of insoluble PGN (25 μ g; Figure 4.6A). As the amount of syncollin-Strep fell, reducing amounts of protein were present in the supernatant, with protein detected only in the PGN pellet at 7.8 μ g syncollin-Strep.

To confirm that the binding of syncollin-Strep to insoluble PGN was specific, soluble PGN was included in the binding assay. The addition of 100 μ g soluble PGN caused an ~50% increase in the amount of

syncollin-Strep in the supernatant (Figure 4.6B), indicating that soluble and insoluble forms of PGN competed with each other for binding syncollin-Strep.

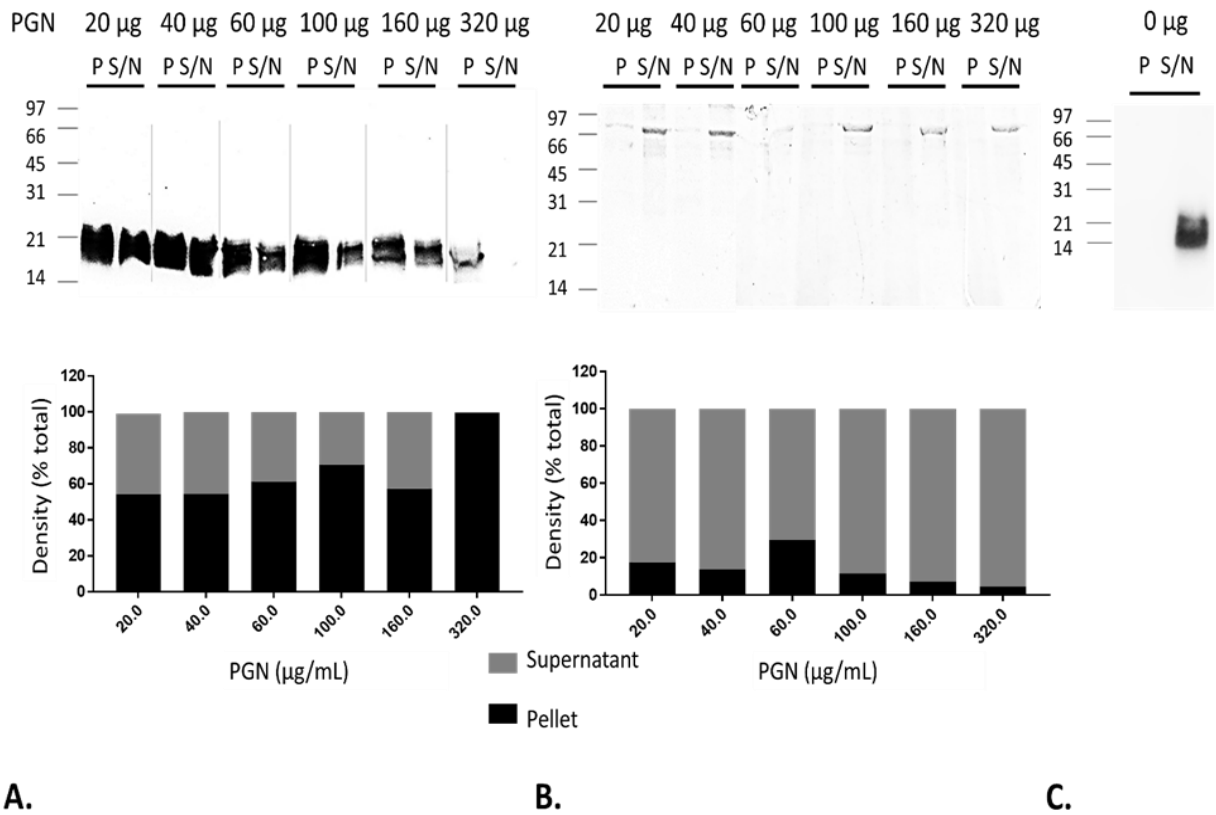


Figure 4.5. Syncollin binds to PGN (1). A. Syncollin-Strep (100 µl at 0.33 mg/mL) was incubated with various quantities of insoluble PGN (20-320 µg). PGN was precipitated by centrifugation and both pellet (P) and supernatant (S/N) were analysed by SDS-PAGE and immunoblotting, using a polyclonal anti-syncollin antibody. B. BSA was used as a negative control, and was detected using Coomassie staining. Band intensities were expressed as a percentage of the total protein for both syncollin-Strep and BSA and are displayed as histograms beneath each gel. C. Syncollin-Strep was centrifuged in the absence of PGN, as in A, as a control. Standards are BioRad low-range markers. Band intensities were calculated using ImageJ™ and plotted as histograms using Graph-Pad Prism™. The results shown representative of those from five experiments.

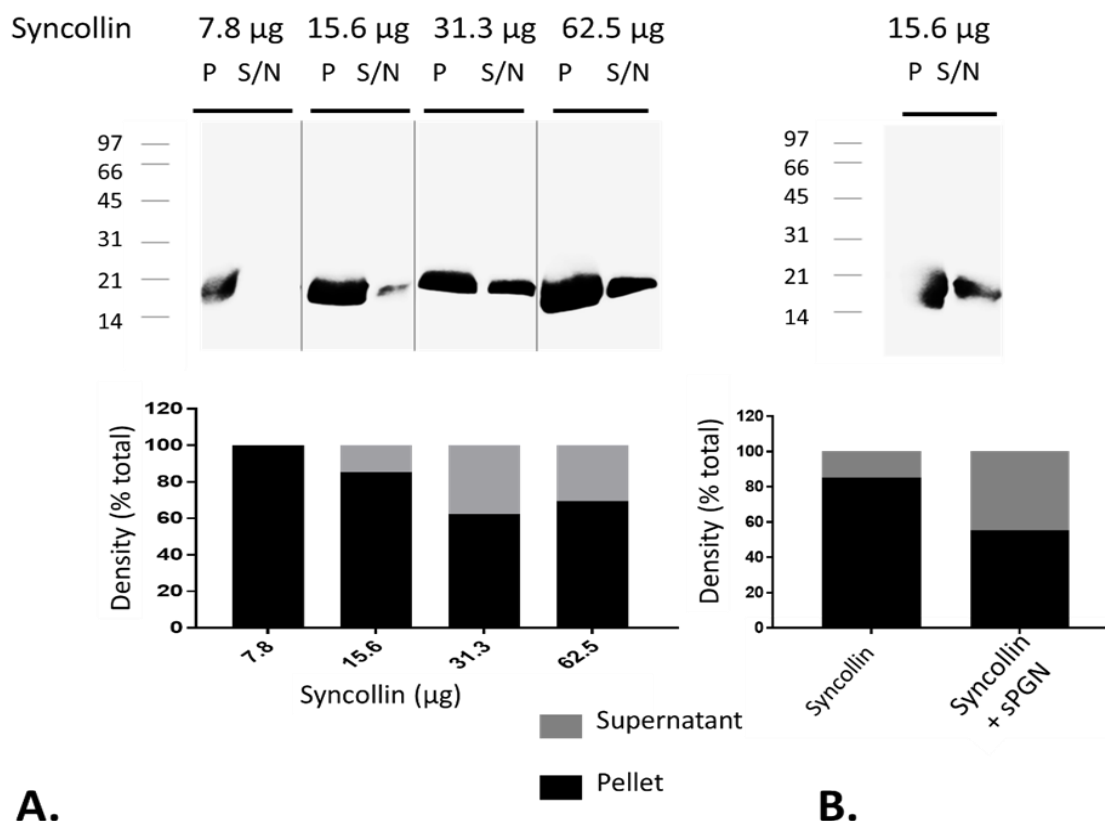


Figure 4.6. Syncollin binds to PGN (2). A. PGN (25 µg) was incubated with various quantities of syncollin-Strep (7.8-15.6 µg). Centrifugation and SDS-PAGE were carried out as in Figure 4.5. B. Syncollin-Strep (15 µg) was incubated with 25 µg PGN in the absence or presence of competing 100 µg soluble PGN. Band intensities were expressed as a percentage of the total protein for all conditions and are displayed as histograms beneath each of the blots. Standards are BioRad low-range markers. Band intensities were calculated using ImageJ™ and plotted as histograms using Graph-Pad Prism™.

4.3.2 EFFECT OF SYNCOLLIN ON BACTERIAL GROWTH

To investigate the effect of syncollin-Strep on bacterial growth, various concentrations of syncollin-Strep (0-163 µg/mL) were added to both Gram-positive *L. lactis* and Gram-negative *E. coli* in a 96-well plate format, and the increase in OD with time was used to generate growth curves. Three parameters were extracted from the growth curves: the span, indicating the number of bacteria, the T_{50} , indicating the time to reach 50% of the log phase maximal growth and the Hill slope, indicating the gradient and bacterial growth rate.

Increasing the concentration of syncollin-Strep in *L. lactis* (Figure 4.7A) resulted in a rightward shift of the growth curve, with 163 µg/mL syncollin-Strep causing a >200-min delay for bacteria to enter the exponential growth phase. This delay in growth start resulted in a significant increase in T_{50} at 163 µg/mL syncollin-Strep (Figure 4.7B). Other parameters of the growth curve were also affected at this concentration of syncollin-Strep, including a significantly reduced Hill slope and span (Figure 4.7C, D). By contrast, syncollin-Strep did not cause a rightward shift in the growth curve for *E. coli* (Figure 4.8A), with T_{50} values unaffected at all concentrations of the protein (Figure 4.8B). The only parameter which was significantly affected by syncollin-Strep addition was a reduction in the span of the growth curves, observed at syncollin-Strep concentrations greater than 81.5 µg/mL (Figure 4.8C). Unlike, *L. lactis* there was no pattern of reduced Hill slopes with increasing syncollin-Strep concentration (Figure 4.8D).

To ensure that the inhibition of bacterial growth seen in the presence of syncollin-Strep was not due simply to the presence of protein in the incubation media, the effect of two control proteins was examined. As shown in Figure 4.9, neither soybean trypsin inhibitor nor RNase A had any appreciable inhibitory effect on bacterial growth when added to the same concentration as syncollin-Strep (300 µg/mL).

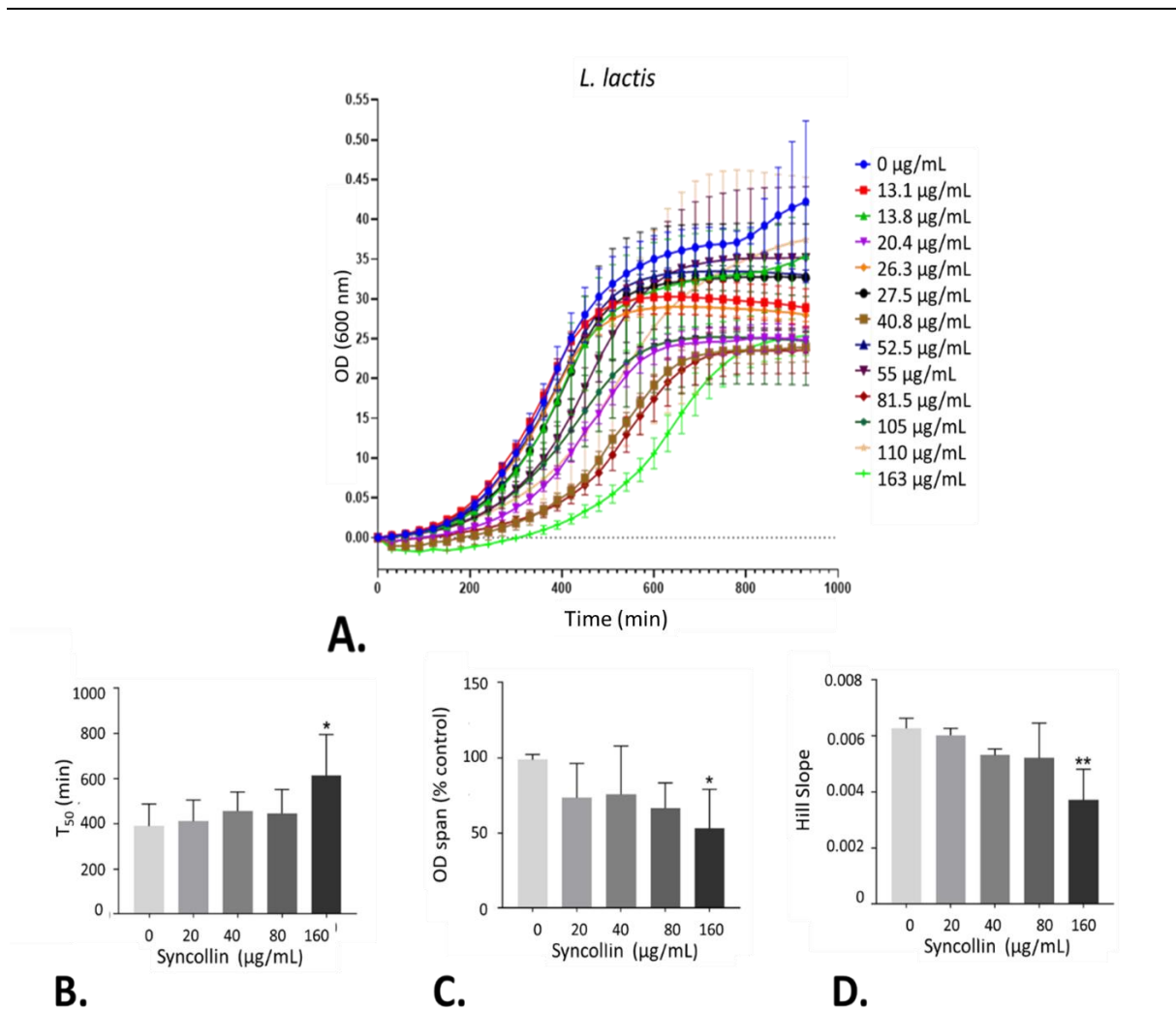


Figure 4.7. Effect of syncollin-Strep on the growth of *L. lactis*. A. Bacteria were incubated with various concentrations of syncollin-Strep, and OD was measured over a 20-h time-course. For each point, $n=3-6$, with error bars showing SD. Graphs were plotted and non-linear regression applied using GraphPad Prism™. B-D. T_{50} (B), span (C) and Hill slope (D) were calculated using GraphPad Prism™. One-way ANOVA was applied to the data. For $p < 0.05$, Dunnett's multiple comparisons test was applied for comparisons of each condition to buffer control. The results of these comparisons are shown above each histogram: * $p < 0.05$, ** $p < 0.01$. Where no asterisks are shown the differences are not significant. Data are from five repeat experiments. Error bars are SD.

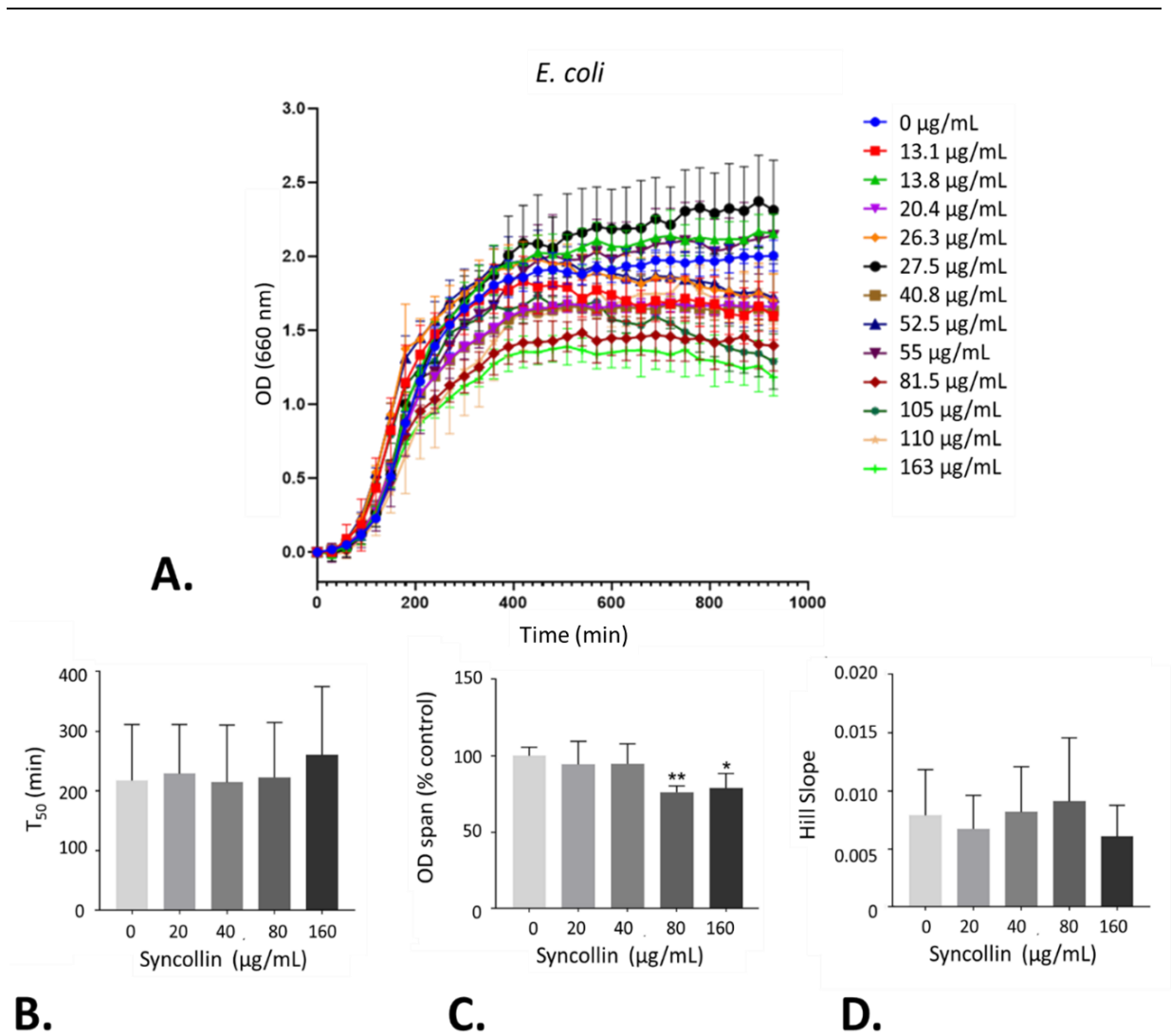


Figure 4.8. Effect of syncollin-Strep on the growth of *E. coli*. A. Bacteria were incubated with various concentrations of syncollin-Strep, and OD was measured over a 20-h time-course. For each point, $n=3-6$, with error bars showing SD. Graphs were plotted and non-linear regression applied using GraphPad Prism™. B-D. T_{50} (B), span (C) and Hill slope (D) were calculated using GraphPad Prism™. One-way ANOVA was applied to the data. For $p < 0.05$, Dunnett's multiple comparisons test was applied for comparisons of each condition to buffer control. The results of these comparisons are shown above each histogram: * $p < 0.05$, ** $p < 0.01$. Where no asterisks are shown the differences are not significant. Data are from five repeat experiments. Error bars are SD.

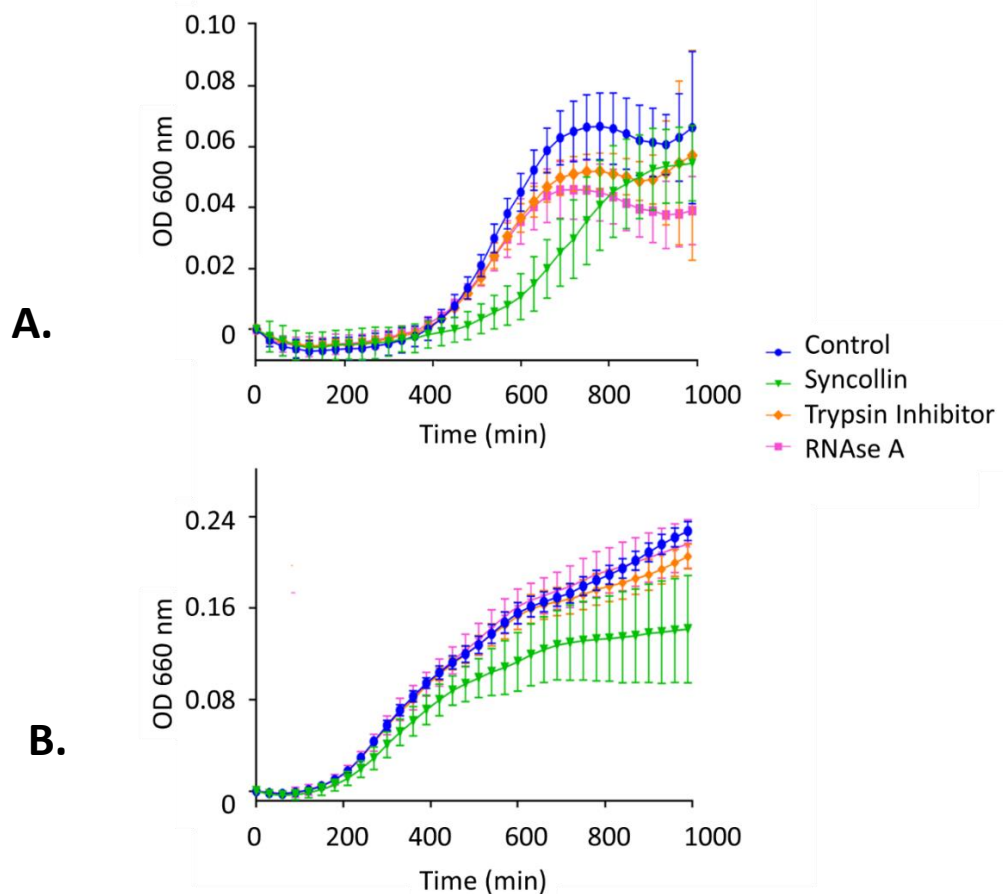


Figure 4.9. Control for the presence of protein in the bacterial growth assay. Bacterial growth curves for *L. lactis* (A) and *E. coli* (B) were generated in the presence of syncollin-Strep, soybean trypsin inhibitor and RNase A (all at 300 $\mu\text{g}/\text{mL}$). OD at 600 nm (*L. lactis*) or 660 nm (*E. coli*) was measured every 30 min over a 20-h time-course. Error bars are SD ($n=5$) and data are representative of 3 repeat experiments.

4.3.3 EFFECT OF SYNCOLLIN ON BACTERIAL GROWTH IN COMBINATION WITH ANTIBIOTICS

To investigate the effects of syncollin in combination with antibiotics on bacterial growth, ampicillin and tetracycline were used alone and in combination with syncollin-Strep in the bacterial growth assay, using both *L. lactis* and *E. coli*. Antibiotic concentrations for ampicillin (0.05 $\mu\text{g}/\text{mL}$) and tetracycline (2 $\mu\text{g}/\text{mL}$) were selected so a clear reduction in, but not total inhibition of, bacterial growth was seen.

For *L. lactis*, addition of syncollin-Strep or either antibiotic alone (Figure 4.10 A and B) did not result in a significant reduction in span (Figure 4.10C). However, following addition of syncollin-Strep in combination with either ampicillin or tetracycline, a significant reduction in span was observed. No significant changes were observed in T_{50} values for any of the syncollin-Strep/antibiotic combinations (Figure 4.10D).

For *E. coli*, a significant reduction in span could be observed following addition of either ampicillin (Figures 4.11A and C) or tetracycline (Figures 4.11B and C). However, there was no further significant reduction in span or T_{50} following combination of syncollin-Strep with either antibiotic (Figure 4.11C and D).

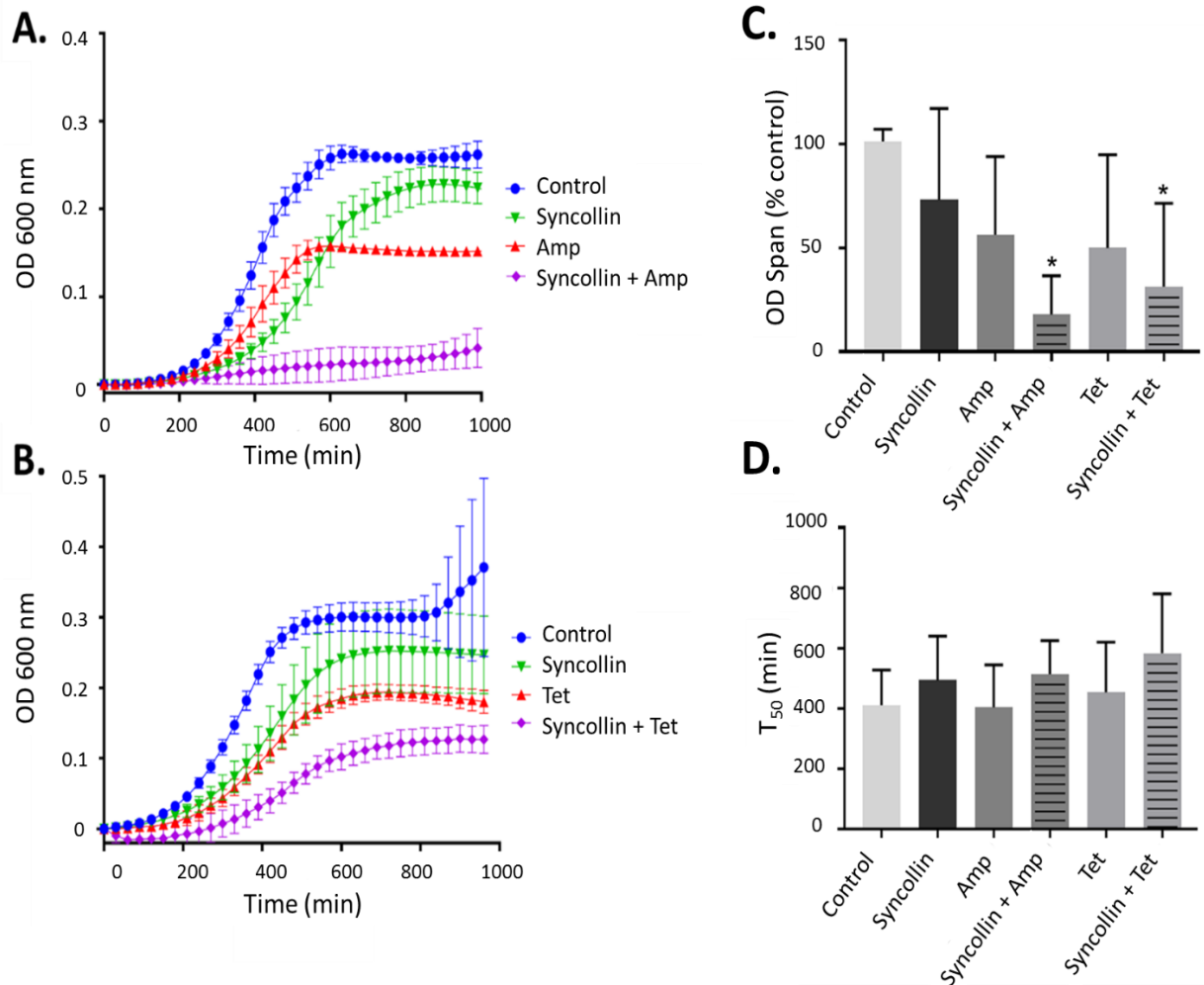


Figure 4.10. Effect of syncollin-Strep on the growth of *L. lactis* in combination with antibiotics. A, B. Bacteria were incubated with syncollin-Strep (118 $\mu\text{g}/\text{mL}$), ampicillin (0.05 $\mu\text{g}/\text{mL}$) and tetracycline (2 $\mu\text{g}/\text{mL}$), alone or in combination, and OD was measured over an ~ 18 -h time-course. For each point, $n=4$, with error bars showing SD. Graphs were plotted and non-linear regression applied using GraphPad PrismTM. C, D. Statistical analysis of the bacterial growth curves following addition of syncollin-Strep (300 $\mu\text{g}/\text{mL}$) either alone or in combination with antibiotics ampicillin (0.05 $\mu\text{g}/\text{mL}$) and tetracycline (2 $\mu\text{g}/\text{mL}$) following addition to *L. lactis*. Span and T_{50} were calculated using GraphPad PrismTM. One-way ANOVA was applied to the data. For a p value $p < 0.05$, Tukey's multiple comparisons test was applied for comparisons of all conditions. The results of these comparisons are shown above each histogram, using asterisks to denote the p value: * $p < 0.05$. Where no asterisks are shown the differences are not significant. Data are from five repeat experiments. Error bars are SD.

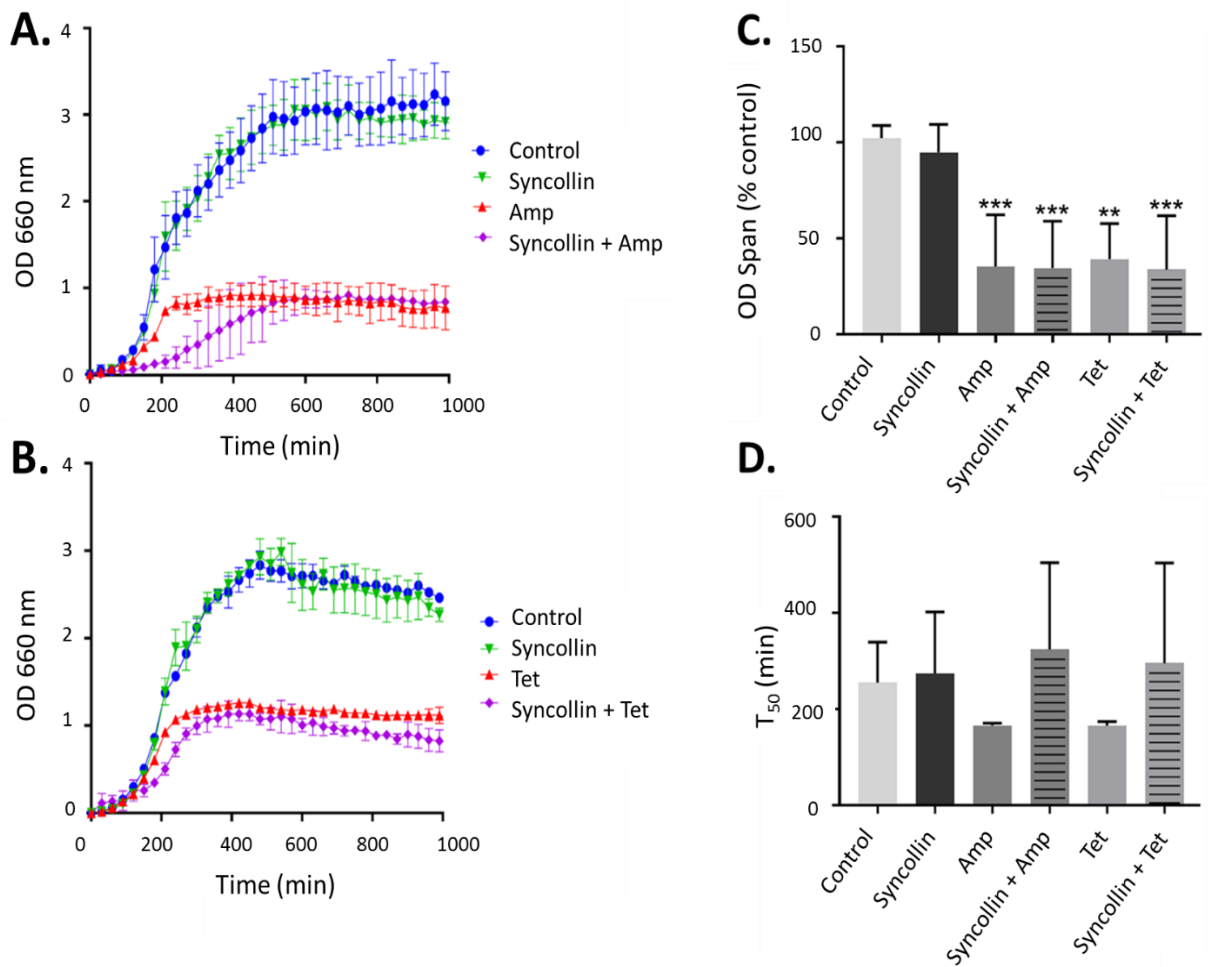


Figure 4.11. Effect of syncollin-Strep on the growth of *E. coli* in combination with antibiotics. A, B. Bacteria were incubated with syncollin-Strep (118 $\mu\text{g}/\text{mL}$), ampicillin (0.05 $\mu\text{g}/\text{mL}$) and tetracycline (2 $\mu\text{g}/\text{mL}$), alone or in combination, and OD was measured over an ~ 18 -h time-course. For each point, $n=4$, with error bars showing SD. Graphs were plotted and non-linear regression applied using GraphPad PrismTM. C, D. Statistical analysis of the bacterial growth curves following addition of syncollin-Strep (300 $\mu\text{g}/\text{mL}$) either alone or in combination with antibiotics ampicillin (0.05 $\mu\text{g}/\text{mL}$) and tetracycline (2 $\mu\text{g}/\text{mL}$) following addition to *E. coli*. Span and T_{50} were calculated using GraphPad PrismTM. One-way ANOVA was applied to the data. For a p value $p < 0.05$, Tukey's multiple comparisons test was applied for comparisons of all conditions. The results of these comparisons are shown above each histogram, using asterisks to denote the p value: ** $p < 0.01$ *** $p < 0.001$. Where no asterisks are shown the differences are not significant. Data are from five repeat experiments. Error bars are SD.

4.3.4 CHECKERBOARD ASSAY OF SYNCOLLIN/ANTIBIOTIC INTERACTIONS

To further investigate the effect of combining syncollin with antibiotics, checkerboard assays were carried out. To clarify the results, visual schematic representations are shown of each checkerboard

assay plate with conditional formatting to visualise no growth- red to growth- green (Figure 4.12), full data are shown in Appendix A1. The mean FIC index value for *L. lactis* with syncollin-Strep plus ampicillin was 0.712, which suggests an additive relationship (Fig 4.12A). The mean FIC index value for syncollin-Strep plus tetracycline was 0.75, indicating too an additive relationship (Fig 4.12B).

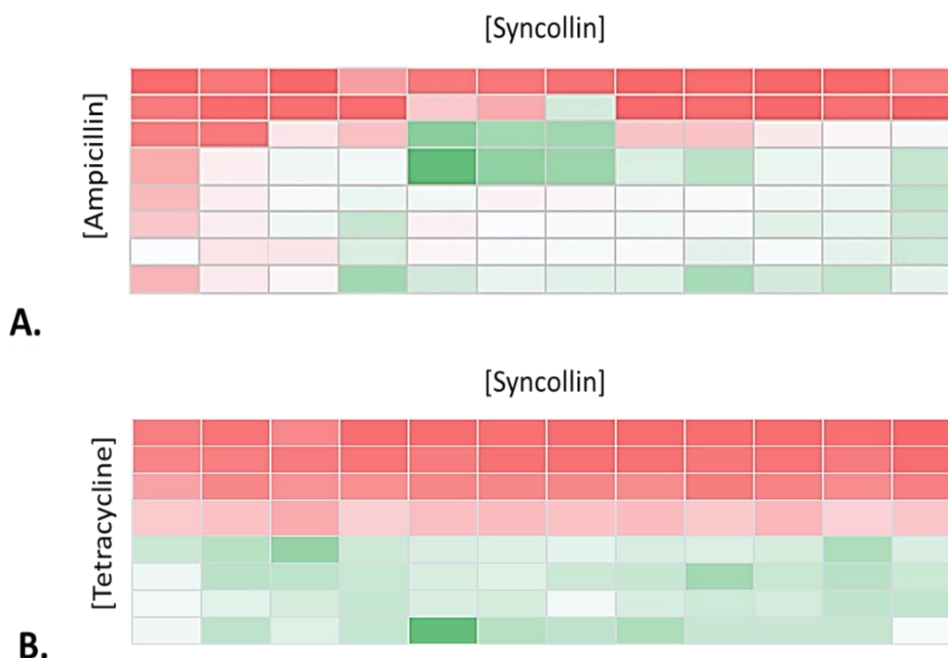


Figure 4.12. Checkerboard assay to investigate the interaction between syncollin-Strep and antibiotics on *L.lactis*. Sequential two-fold dilutions of syncollin-Strep (from 0.2 mg/mL) were made horizontally across the plate, and two-fold dilutions of antibiotic (ampicillin, from 0.004 mg/mL; tetracycline, from 0.002 mg/mL) were made vertically down the plate. OD for *L. lactis* was measured at the plateau phase of the growth curve. Schematics are shown for simplicity with data visually represented by conditional formatting with red shading indicating no growth and green shading representing maximal growth. A. Syncollin-Strep plus ampicillin (plateau phase; n=3). B. Syncollin-Strep plus tetracycline (plateau phase; n=3).

4.3.5 DETERMINATION OF BACTERIAL VIABILITY BY PROPIDIUM IODIDE STAINING

As an alternative method to visualize viability, propidium iodide (PI) staining was carried out. PI is not membrane permeant, and therefore can only enter and stain bacteria if their membranes are compromised following cell death. Hence, staining provides a useful visual measure of viability.

Bacterial growth assays were set up using buffer only, syncollin-Strep, ampicillin or tetracycline. Bacteria were collected both in the log phase (OD 0.1) and in the plateau phase of growth. Bacteria

were briefly centrifuged and washed in PBS before resuspension in PBS containing PI and DAPI (both at 1 µg/mL).

Neither *L. lactis* nor *E. coli* displayed high levels of PI-staining in the log phase under any of the treatment conditions (Figure 4.13A-C). However, in the plateau phase of growth, ampicillin, but not tetracycline, resulted in a significant increase in PI uptake by both *L. lactis* and *E. coli* (Figure 4.13D-F). Syncollin-Strep also resulted in significant PI uptake by *E. coli* however, but not by *L. lactis*. Additionally, an increase in the number of filamentous bacteria was observed in ampicillin- and syncollin-Strep-treated *E. coli*, and these filamentous forms were also stained by PI.

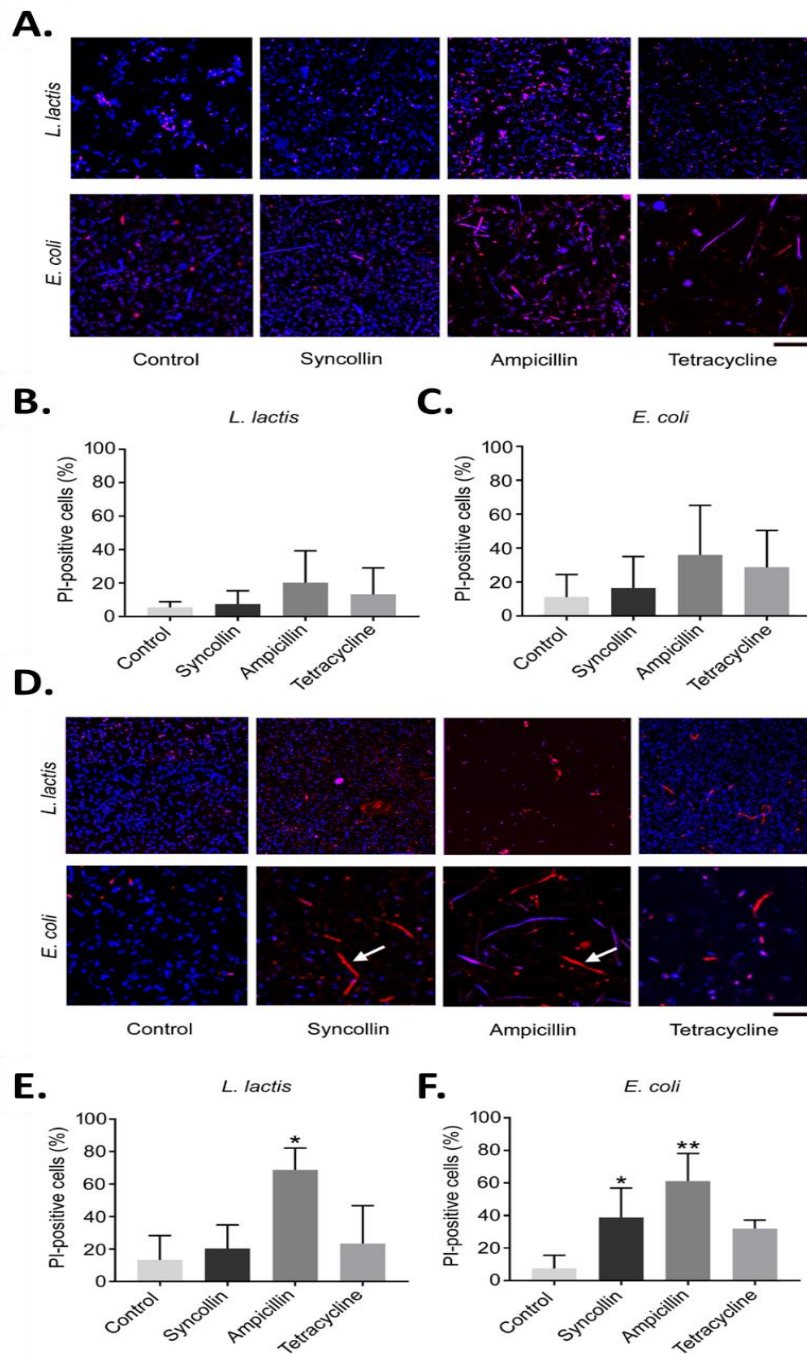


Figure 4.13. Effect of syncollin-Strep addition on bacterial viability. Bacteria were incubated with buffer alone, syncollin-Strep (300 $\mu\text{g/ml}$), ampicillin (0.05 $\mu\text{g/ml}$) or tetracycline (2 $\mu\text{g/ml}$). When bacteria reached the log phase (A-C) or the early plateau phase of growth (D-F), they were briefly washed before incubation in PBS containing propidium iodide (1 $\mu\text{g/ml}$; red) and DAPI (1 $\mu\text{g/ml}$; blue) and imaged by confocal microscopy. A, D, Representative images for the various conditions. Filamentous forms of bacteria are indicated by arrows. Scale bars, 20 μm . Quantitative image analysis (B, C, E and F) for both growth stages are shown as histograms from four repeat experiments using one-way ANOVA with Dunnett's multiple comparisons. * $p < 0.05$; ** $p < 0.01$. Error bars are SD.

4.3.6 ATOMIC FORCE MICROSCOPY IMAGING OF BACTERIAL SURFACES

AFM imaging was used to assess the integrity of *E. coli* pre-incubated with syncollin-Strep. Bacteria were incubated with either buffer alone or with syncollin-Strep (0.3 mg/mL) for 2 h before imaging. As shown in Figure 4.14A, control images reveal classic rod-shaped bacteria. By contrast, bacteria incubated with syncollin-Strep (Figure 4.14B) had a 'rounded up' appearance, with an increase in height from ~ 800 nm (buffer-treated) to ~ 2.6 μm (syncollin-Strep-treated). Interestingly, bacteria treated with syncollin-Strep were also difficult to image by AFM because of the propensity of the AFM tip to stick to the bacterial surface. It proved to be impossible to image *L. lactis* by AFM, because the bacteria did not adsorb to poly-L-lysine-coated glass, and Vectabond™ coating resulted in too much noise for AFM imaging.

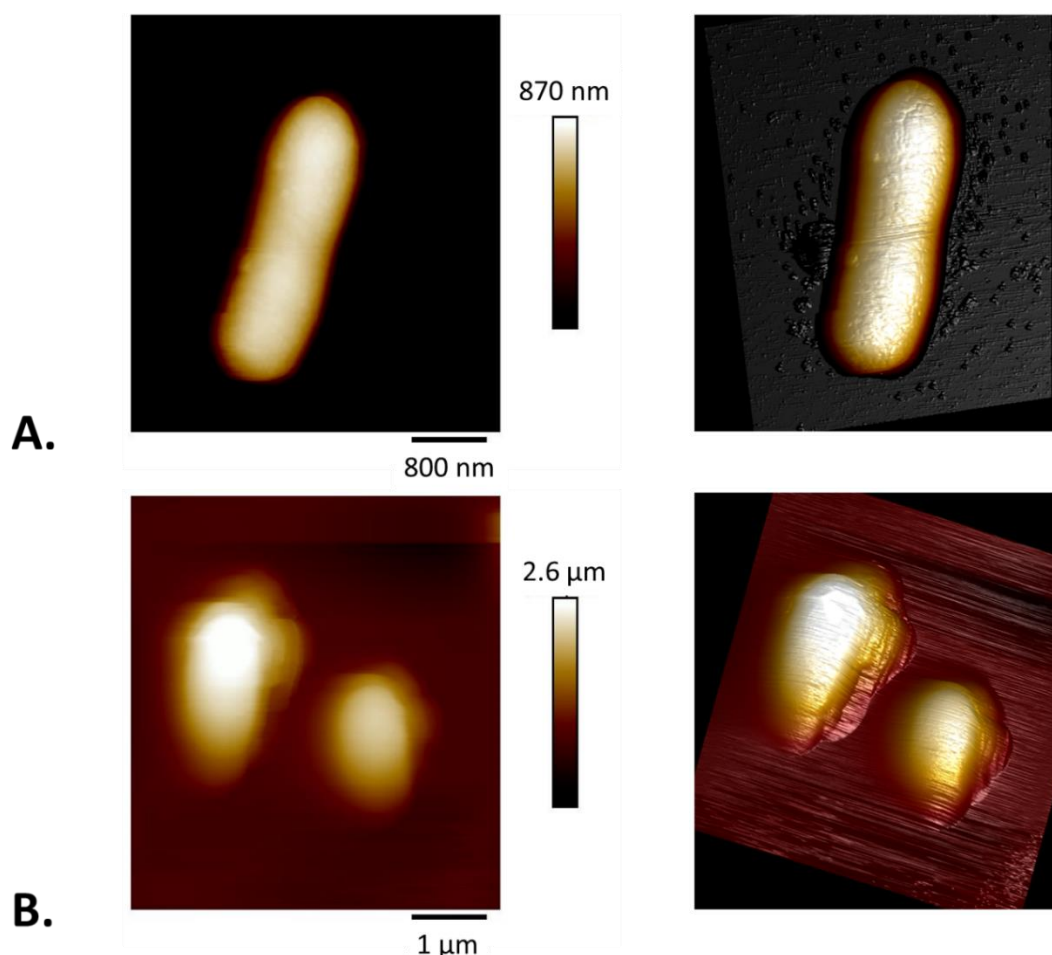


Figure 4.14. AFM analysis of the effects of syncollin-Strep on the structure of *E. coli*. Bacteria were either pre-incubated with elution buffer (A) or syncollin-Strep (B) before AFM imaging. Height images are shown on the left with 3D-image reconstructions shown on the right. Bacteria were adsorbed onto poly-L-lysine-coated glass coverslips and imaged using fast-scan AFM in fluid. Imaging was carried out by Dr. I. Mela.

4.3.7 DETERMINATION OF BACTERIAL VIABILITY USING SCANNING ELECTRON MICROSCOPY (SEM)

To further visualize the bacterial membranes, SEM imaging was carried out on bacteria pre-incubated with syncollin, or with the control proteins soybean trypsin inhibitor or RNase A (all at 0.3 mg/ml). Control (buffer only) images reveal smooth-surfaced spherical (*L. lactis*) and rod-shaped structures (*E. coli*; Figure 4.15). In contrast, both *L. lactis* and *E. coli* treated with syncollin-Strep (300 µg/mL) were mis-shapen and rough-surfaced, with large aggregates observable in both cases. On the other hand, soybean trypsin inhibitor and RNase A caused only a minor increase in surface disturbance of both types of bacteria.

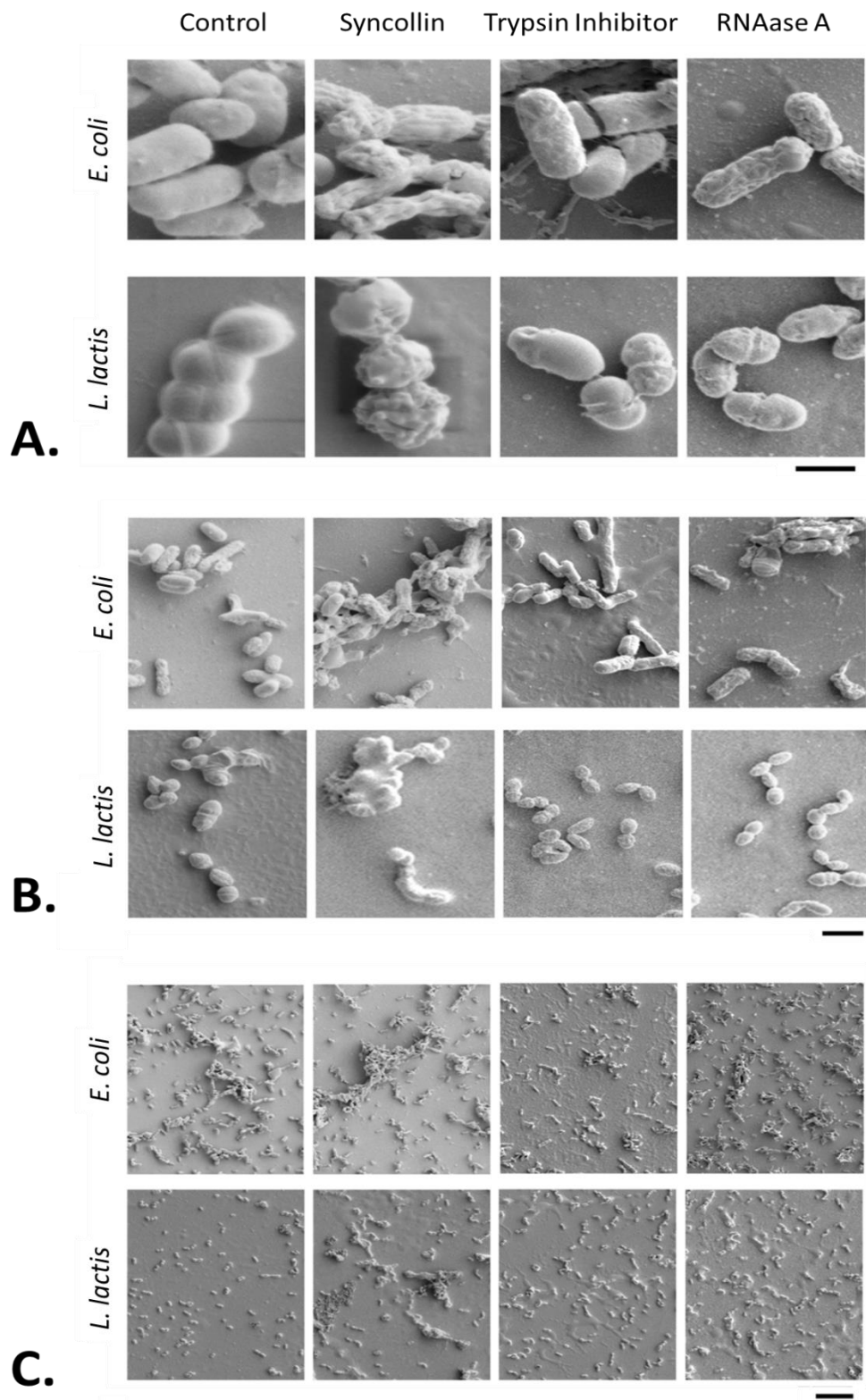


Figure 4.15. SEM analysis of the effects of syncollin-Strep on bacterial structure. Bacteria (*E. coli* and *L. lactis*) were incubated in either buffer alone or in buffer containing either syncollin-Strep, soybean trypsin inhibitor or RNase A (0.3 mg/ml) before SEM imaging. Representative images are shown at different scale bars of 1 μm (A), 2 μm (B) or 10 μm (C). Images are representative of those from three experiments.

4.4 DISCUSSION

The results presented in this Chapter demonstrate that syncollin hinders the growth of Gram-positive (*L. lactis*) and Gram-negative (*E. coli*) bacteria, reducing the viability of the latter in the plateau phase of growth. SEM imaging showed that syncollin also causes obvious structural damage to the bacterial capsule in both *L. lactis* and *E. coli*, and AFM imaging confirmed this effect in the case of *E. coli*. Syncollin has two properties that are likely to be involved in its antibacterial activity – the ability to bind to PGN, as shown here in my study, and the ability to permeabilize biological membranes (Wäsle *et al.*, 2004) and lipid bilayers (Geisse *et al.*, 2002), as also demonstrated in Chapter 2. I suggest that the slowing of the growth of *L. lactis* (but not *E. coli*) in log phase might be caused primarily through binding to the exposed PGN-based cell wall in the former, whereas the permeabilization of the *E. coli* (but not *L. lactis*) in the plateau phase might be caused by an action of syncollin on the membranes of the Gram-negative bacterium. Further studies will be required to confirm this suggestion.

Bacterial growth curves and checkerboard assays were used to investigate the interactions between syncollin and standard antibiotics: ampicillin (bactericidal) and tetracycline (bacteriostatic). In the case of *L. lactis*, syncollin in combination with either ampicillin or tetracycline resulted in a greater reduction in the span of the growth curve than was seen with either protein or antibiotic alone. This effect could also be observed in checkerboard assays, where an additive relationship was seen between syncollin and both antibiotics.

My observation that syncollin binds to PGN begs the question of why it is not inactivated through association with sulphated proteoglycans in the pancreatic ZG (mentioned in Chapter 1). It is worth pointing out that only about 60% of the total granular syncollin is membrane-associated, with the remaining 40% existing free in the ZG lumen (Hodel *et al.*, 2001). This free pool is likely to escape interaction with the sulphated proteoglycans. Further, even the membrane associated pool of syncollin might become liberated when exposed to the increase in pH that occurs upon ZG exocytosis.

As discussed in Chapter 1, syncollin shares features with other small antimicrobial polypeptides that are known to play roles in host defence in the gut, including ZG16p, RegIII and members of the defensin family. These features include a predominantly beta-sheet structure, the presence of intramolecular disulphide bonds, and in some cases the ability to form homo-oligomers. Given these structural similarities, it is reasonable to propose that syncollin is a previously unidentified member of the antimicrobial protein superfamily. It is known that pancreatic juice has antibacterial activity

(Rubinstein *et al.*, 1985), which is likely to be important not only for the control of the bacterial flora of the upper intestine, but also for protection of the pancreas itself from infection.

As mentioned in Chapter 1, syncollin is also expressed in (and secreted from) neutrophils (Bach *et al.*, 2006), again consistent with a role in host defence. Indeed, the authors of this previous paper speculated that syncollin might have an antibacterial effect, but were unable to demonstrate this property. I suggest that this failure might have been a result of the elaborate method used to prepare native syncollin (removal from the ZG membrane at high pH followed by selective precipitation in an aggregated state after dialysis to neutral pH; An *et al.*, 2000). The physiological relevance of the presence of syncollin in human neutrophils is explored in Chapter 5.

5. SYNCOLLIN NEUTROPHIL EXPRESSION AND BACTERIAL INTERACTION

5.1 INTRODUCTION

5.1.1 NEUTROPHIL GRANULES AND EXOCYTOSIS

Neutrophils contain four different types of granule, which are formed during different stages of differentiation. During degranulation of the neutrophils, primary, secondary, tertiary granules and secretory vesicles are released. Primary (azurophilic) granules, formed at the promyelocyte stage, are the main type of granule, which release antimicrobial proteins and participate in phagocytosis; their contents include proteins such as MPO (see Chapter 1), defensins, which permeabilize microbial membranes and neutrophil elastase, which degrades the extracellular matrix (ECM). Specific granules, formed at the myelocyte and metamyelocyte stages, form the secondary and tertiary granules, respectively. The secondary granules contain lactoferrin, which has an antimicrobial action, collagenase, which degrades the ECM, and NADPH oxidase, which generates ROS. Tertiary granules, also known as gelatinase granules, contain gelatinase, which degrades the ECM, and arginase-1, which inhibits T cell proliferation. Finally, the secretory vesicles contain β 2-integrins, which promote neutrophil apoptosis, and formylated bacterial peptides, which act as pro-inflammatory mediators.

Note that other proteins exist within the neutrophil granules, and play essential roles, in addition to those detailed above (Selders *et al.*, 2017; Cassatella *et al.*, 2019).

Exocytosis in neutrophils is thought to involve various SNARE proteins, including syntaxins 4 and 6 on the plasma membrane, and synaptobrevin 2 and SNAP-23 on secondary and tertiary granules, along with the small GTPase Rab 27. The majority of these exocytotic events are believed to occur via compound exocytosis, which fulfils the requirement for rapid degranulation upon stimulation. Eosinophils, another member of the white blood cell family, are also known to undergo compound exocytosis while serving their function in host defence (Logan *et al.*, 2006).

Neutrophils are well established as essential cells in the innate immune system; however, they have also been found to be important in adaptive immunity, through interactions with various other cells, including dendritic cells, lymphocytes and natural killer cells. Consequently, neutrophils are considered to be key immune cells that bridge the gap between the two immune systems (Rosales *et al.*, 2017). The antimicrobial actions of neutrophils depend on the combined operations of the various proteins present within their granules.

Syncollin has been shown previously to be expressed within neutrophils, and was proposed to be expressed in the primary azurophilic granules. This chapter describes the expression and localization of syncollin within neutrophils, and its behaviour upon activation triggered either by a chemical mediator or by exposure to a bacterial challenge.

5.2 METHODS

5.2.1 NEUTROPHIL ISOLATION

Human blood was collected by members of the lab of Dr. M. Harper using citrate-coated collection tubes. Neutrophils were either kindly donated by R. Riddle, I. Ivenov, J. Davis of the Harper lab, or isolated from blood by myself. Blood (25 mL) was layered gently onto Histopaque-1077™ (15 mL) in 50-mL Falcon™ tubes so that two distinct layers were formed. The tubes were centrifuged at 1,450 rpm for 30 min with low acceleration and deceleration settings. The layer above the red blood cell fraction, containing mononuclear cells, was aspirated off leaving the remaining erythrocyte layer (approximately 10 mL for 20 mL of blood). The erythrocyte layer was then diluted with an equal volume of Hanks' Balanced Salt Solution (HBSS) without Ca²⁺ or Mg²⁺. The erythrocyte/HBS suspension was then further diluted with an equal volume of 2% (w/v) dextran at room temperature. The mixture was gently mixed by inversion and left to rest for 30 min at room temperature to allow the erythrocytes to

sediment. The top layer without erythrocytes was collected and mixed with an equal volume of HBSS without Ca^{2+} or Mg^{2+} before centrifugation at 1,150 rpm for 5 min, with medium acceleration and deceleration settings. The supernatant was gently removed, leaving a white neutrophil pellet. This pellet was then resuspended in 5 mL Roswell Park Memorial Institute (RPMI) medium containing 10% (v/v) FBS and penicillin/streptomycin, and the cells were counted using a haemocytometer.

5.2.2 IMMUNOFLUORESCENCE

Sterile fibronectin (10 ng/mL) was added to 18-well flat-bottomed imaging dishes (Ibidi™) and left to incubate for 2 h at 30°C. Fibronectin was then removed and the wells were washed twice with sterile PBS, pH 7.0, and dried in air. Neutrophils ($\sim 2 \times 10^6$ cells/mL in a 30- μL volume) were added to the plates and left to settle at 37°C for 30 min. The medium was then aspirated and the cells were fixed by incubation in sterile 4% (w/v) PFA for 20 min at room temperature. The PFA was then removed and the wells were gently washed three times with 30 μL PBS, taking care to avoid detaching cells. To permeabilize cells, 30 μL of 0.1% (v/v) Triton X-100 was added to each well, followed by incubation for 5 min. Triton X-100 was removed using three gentle PBS washes. Neutrophil Fc receptors are a major site for non-specific binding in neutrophil cells and these were therefore blocked by incubation with 10 $\mu\text{g}/\text{mL}$ Fc-Receptor block (BD) in PBS containing 1% (w/v) BSA for 1 h at room temperature. Primary antibodies were diluted in PBS containing 1% (w/v) BSA (according to the concentrations in Table 5.1) and then added to each well for overnight incubation at 4°C. Primary antibody was aspirated and wells were washed gently three times with PBS, taking care not to dislodge adhered cells. Secondary antibody, again in PBS containing 1% (w/v) BSA (see Table 5.1), was added to each well for 2 h at room temperature in the dark. In addition to secondary antibody, Hoechst 33342 (Thermo; 1 mg/mL in PBS) was diluted to 1 $\mu\text{g}/\text{mL}$ and added for detection of nuclei. Secondary antibody and Hoechst were then aspirated from cells and the wells were gently washed three times with PBS. A drop of immersion oil (Ibidi™) was added to each well, and the plates were kept in the dark at 4°C before imaging. Control wells (exposed to secondary antibody alone) were included to ensure that any signal detected was not due to non-specific binding of the secondary antibody. Samples were imaged using a Leica SP5 confocal microscope with constant exposure time, brightness and contrast adjustments for each experiment.

Protein Name	Host	Dilution	Supplier
Primary Antibodies:			
Syncollin (Antibody B)	Rabbit	1/50	Kindly donated by JM.Edwardson
MPO (light chain A-5)	Mouse	1/100	Santa Cruz Biotechnology
Neutrophil Elastase (G-2)	Mouse	1/100	Santa Cruz Biotechnology
Defensin-3 (D-3)	Mouse	1/100	Santa Cruz Biotechnology
CD11b (M1/70)	Mouse	1/100	Thermo Fisher eBioscience
CD15 (HI98)	Mouse	1/100	Thermo Fisher eBioscience
CD14 (61D3)	Mouse	1/100	Thermo Fisher eBioscience
Secondary Antibodies/ Conjugated Antibodies:			
MPO- FITC (MPO455-8E6)	Mouse	1/200	Thermo Fisher eBioscience
F(ab') ₂ -Goat anti-Rabbit IgG (H+L) Secondary Antibody, FITC	Rabbit	1/1000	Thermo Fisher eBioscience
F(ab') ₂ -Goat anti-Mouse IgG (H+L) Secondary Antibody, APC	Mouse	1/1000	Thermo Fisher eBioscience
Other dyes			
DAPI (1 mg/mL)	-	1/1000	Thermo Fisher
Propidium Iodide (1 mg/mL)	-	1/1000	Thermo Fisher

Table 5.1: Summary of antibodies (primary and secondary) used for neutrophil immunofluorescent studies. Host, supplier and dilution used are shown.

5.2.3 NEUTROPHIL ACTIVATION

For activation of neutrophils, either fMLP peptide (Merck) or *E. coli* were used. For fMLP activation, after adherence of the neutrophils, cells were incubated in RPMI medium containing 10% (v/v) FBS, penicillin/streptomycin and 200 nM fMLP for 30 min at 37°C. The neutrophils visibly spread and became more flattened as a result of activation. For *E. coli*-induced activation, neutrophils were incubated for 30 min at 37°C in an *E. coli* at OD 0.01 in RPMI.

5.2.4 ANALYSIS OF NEUTROPHIL ACTIVATION BY IMMUNOBLOTTING

fMLP (200 nM) was added to a neutrophil suspension (5×10^6 cells/mL) for 30 min at 37 °C. After fMLP activation, neutrophils were gently centrifuged at 5,000 rpm for 3 min with a medium-brake setting to prevent unspecific activation. Neutrophil pellets were then resuspended in Laemmli sample buffer. Supernatants were collected and proteins precipitated using methanol-chloroform. Here, 400 μ L of methanol was added to 100 μ L of neutrophil supernatant, followed by 100 μ L chloroform and 300 μ L of water, with vortexing after each addition. Samples were then centrifuged at 14,000 x g for 2 min. The top (aqueous) layer was removed before addition of a further 400 μ L methanol and subsequent vortexing. Samples were again centrifuged at 14,000 x g for 3 min and the methanol was removed from the precipitated protein pellet, which was resuspended in an equal volume of Laemmli sample buffer. Samples were analysed by SDS-PAGE and immunoblotting using a polyclonal anti-syncollin antibody.

5.2.5 IMAGING OF NEUTROPHILS AFTER ACTIVATION BY BACTERIAL INFECTION

E. coli at OD 1.5 was added in 30- μ L volumes to poly-L-lysine-coated 18-well flat-bottomed imaging dishes (Ibidi™) and allowed to adhere for 30 min at 37°C. Medium was then removed before addition of 30 μ L of freshly isolated neutrophils at 1.6×10^6 cells/mL followed by incubation at 37°C for 45, 90 and 180 min. At each time point, medium was removed from a well and the cells were fixed by incubation in 4% (w/v) PFA for 15 min at 37°C. Triton X-100 (0.1% [v/v]) was then added to permeabilize the cells. Cells were washed twice with PBS before addition of blocking buffer (PBS containing 10% [v/v] FBS, 3% [w/v] BSA and Fc-Receptor blocker) followed by incubation overnight at 4°C. Cells were then incubated overnight at 4°C with primary antibodies (rabbit polyclonal anti-syncollin diluted 1:50; mouse monoclonal anti-MPO diluted 1:100). Wells were washed three times with PBS before addition of secondary antibodies (fluorescein isothiocyanate- [FITC]-conjugated anti-rabbit, diluted 1:500); allophycocyanin- [APC]-conjugated anti-mouse, diluted 1:500) and DAPI dye (diluted 1:500) and incubation for 2 h at room temperature in the dark. Samples were then imaged using confocal microscopy.

5.3 RESULTS

5.3.1 SYNCOLLIN LOCALIZATION

Neutrophils were isolated from human blood and either lysed in RIPA buffer to prepare a cell lysate for immunoblotting or attached to plates for immunofluorescence imaging. Immunoblotting showed that syncollin was expressed in neutrophils as a heat-resistant ~66 kDa oligomer (Figure 5.1). For

immunofluorescence imaging, neutrophils were fixed in 4% (w/v) PFA and permeabilized in 0.1% (v/v) Triton X-100. After numerous washes, neutrophils were added to a blocking buffer containing Fc-receptor inhibitor and then incubated with polyclonal anti-syncollin antibody overnight at 4°C. Neutrophils were then incubated with FITC-conjugated secondary antibody and Hoechst dye. The Hoechst dye revealed the polymorphonuclear nuclei of neutrophils, and DIC imaging revealed a cell size of approximately 10 μm . Syncollin staining revealed a punctate distribution throughout the cytoplasm (Figure 5.1).

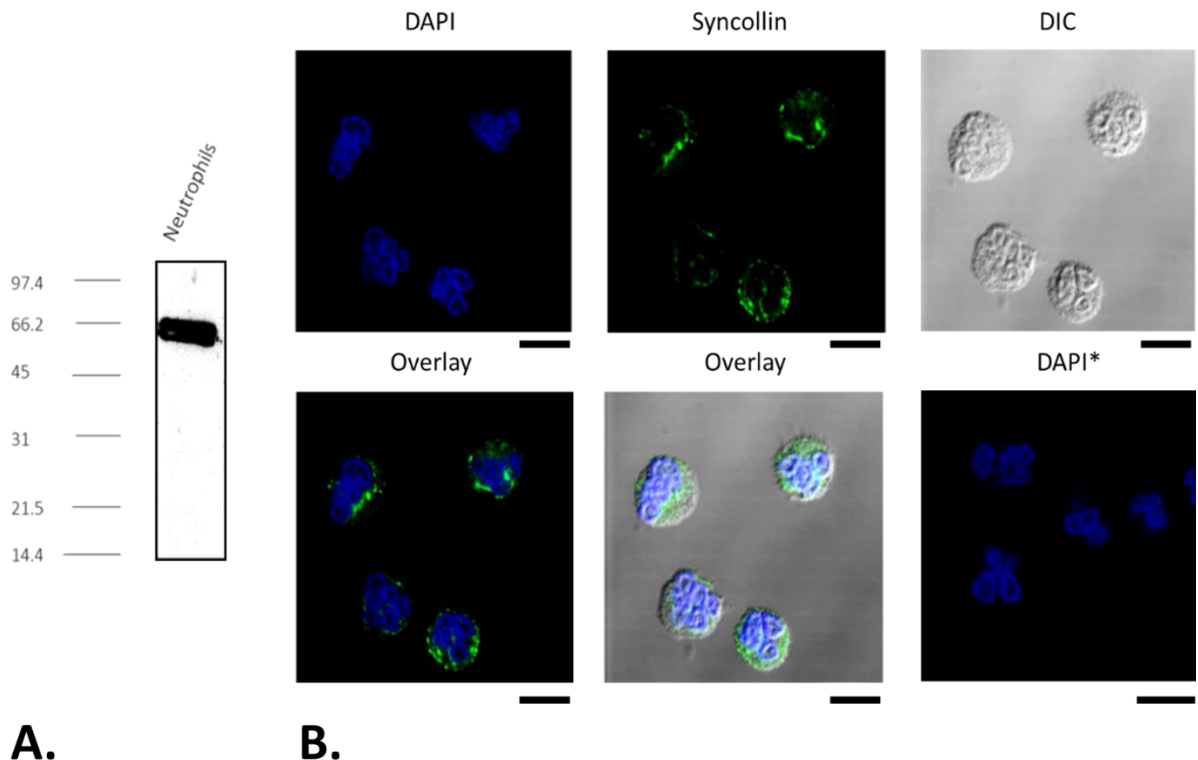


Figure 5.1. Syncollin expression in isolated human neutrophils. A. Immunoblot for syncollin. Neutrophils were lysed in RIPA buffer to generate a cell lysate. Laemmli sample buffer was then added to neutrophil lysates before incubation at 95°C. Samples were subjected to SDS-PAGE and immunoblotted for syncollin. Standards were BioRad low-range markers. B. Immunofluorescence detection of syncollin in neutrophils. Syncollin was detected using a polyclonal anti-syncollin antibody and an FITC-conjugated secondary antibody. Samples were imaged by confocal microscopy. FITC was imaged using a 488 nm laser and is displayed in green. Hoechst dye (labelling nuclei) was detected using a 418 nm laser and is displayed in blue. DIC imaging was also carried out, and all three images were overlaid. Samples exposed to DAPI and secondary antibody alone (DAPI*) were included to control for non-specific antibody binding. All images were processed using ImageJ Fiji™. Scale bars, 8 μm .

5.3.2 SYNCOLLIN GRANULAR LOCALIZATION

In order to determine the localization of syncollin in the various types of granule in the neutrophils, I used immunofluorescence detection of syncollin and co-staining of markers of the various granule types: MPO (primary, azurophilic), CD15 (secondary), CD11b (tertiary) and CD14 (secretory). All proteins displayed punctate staining indicating a granular location. With the primary azurophilic and secondary granules, there was limited co-staining for syncollin and MPO and CD15, arguing against a predominant localization in primary and secondary granules (Figure 5.2). Some degree of co-localization with syncollin could be observed with both the tertiary vesicle marker CD11b and the secretory vesicle marker CD14 (arrows, Figure 5.2B). However, neither marker showed complete overlap with syncollin, suggesting that syncollin is not uniquely localized in a particular granule type.

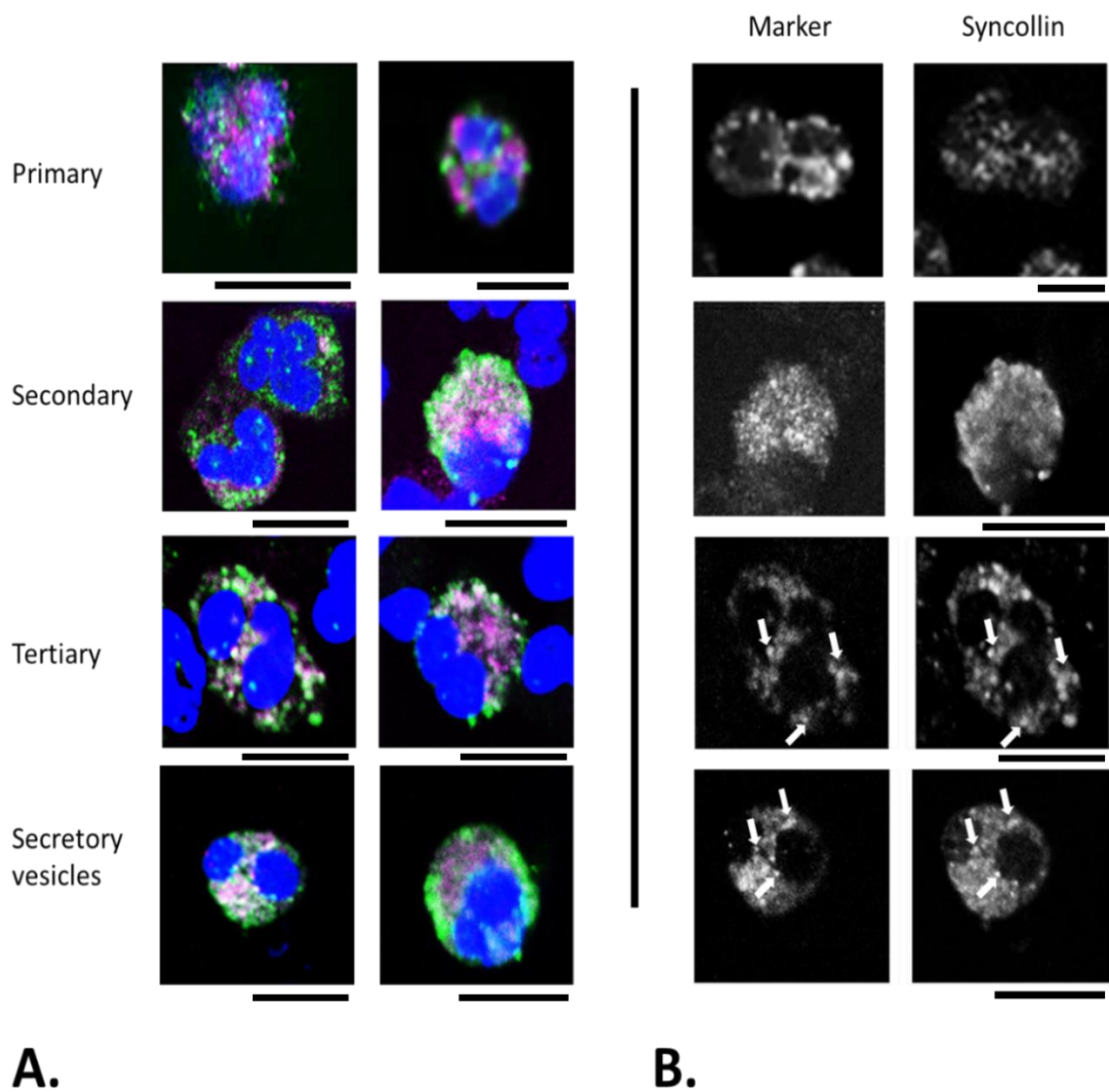


Figure 5.2. Granular localization of syncollin. A. Neutrophils were prepared for immunofluorescence as described in the caption to Figure 5.1. Primary antibodies to syncollin and either MPO (primary granule marker), CD15 (secondary granule marker), CD11b (tertiary granule marker) or CD14 (secretory granule marker) primary antibodies were incubated overnight at 4°C with fixed and permeabilized neutrophils. Secondary antibodies for syncollin (rabbit FITC-conjugated) and granule markers (mouse APC-conjugated) were then incubated with the neutrophils for 2 h at room temperature. DAPI dye was added to identify nuclei. Scale bars, 8 μm. Images were overlaid using ImageJ Fiji™ with the colour scheme: DAPI; blue, syncollin; green, granule marker; magenta. Scale bars, 8 μm. B. Neutrophils from A were separated into the separate image channels for both the granule marker (left) and syncollin (right). Arrows indicate granule co-localization. Scale bars, 8 μm.

5.3.3 SYNCOLLIN MOBILITY UPON NEUTROPHIL ACTIVATION

Following confirmation of the expression and apparent granular localization of syncollin in neutrophils, I next looked for any changes in syncollin localization upon neutrophil activation in response to addition of 200 nM fMLP. Activation caused a change in the shape of the neutrophils, causing them to become less uniformly round and more flattened (Figure 5.3). Syncollin staining also changed from a uniform punctate distribution within the cytoplasm to a more membrane-localized distribution, with a reduced fluorescence intensity.

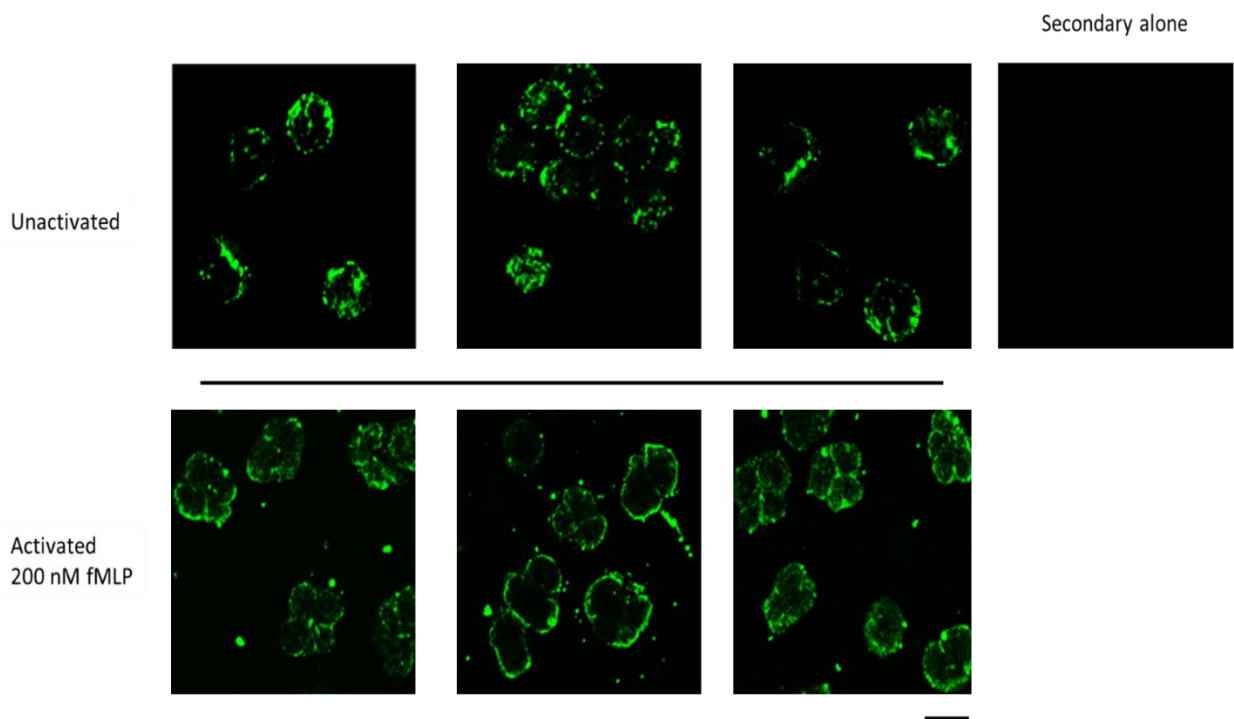


Figure 5.3. Effect of activation on syncollin staining in neutrophils. Neutrophils were activated by incubation with 200 nM fMLP for 30 min at 37°C. Antibody incubation, and image acquisition and processing was as described in the caption to Figure 5.1. The inclusion of samples exposed to secondary antibody alone was to control for non-specific antibody binding and is shown as 'secondary alone'. Scale bar, 8 μ m.

Building on the observation that syncollin became more localized at the plasma membrane in response to neutrophil activation, and the previous report that syncollin is secreted under this condition (Bach *et al.*, 2006), syncollin fluorescence intensity of individual granules was recorded before and after activation by fMLP. As a control for secretion of granular proteins from activated neutrophils, MPO staining was also quantified. As shown in Figure 5.4, the fluorescence intensity of both syncollin and MPO fell after a 30-min activation. In addition, pellets and supernatants were collected from resting

and activated neutrophils and immunoblotted for syncollin (Figure 5.5). Consistent with the immunofluorescence result, the syncollin level in the neutrophil pellet fell from 30% of total in resting neutrophils to 17% of total in activated neutrophils, with a corresponding increase in the supernatant from 70% to 83% of total.

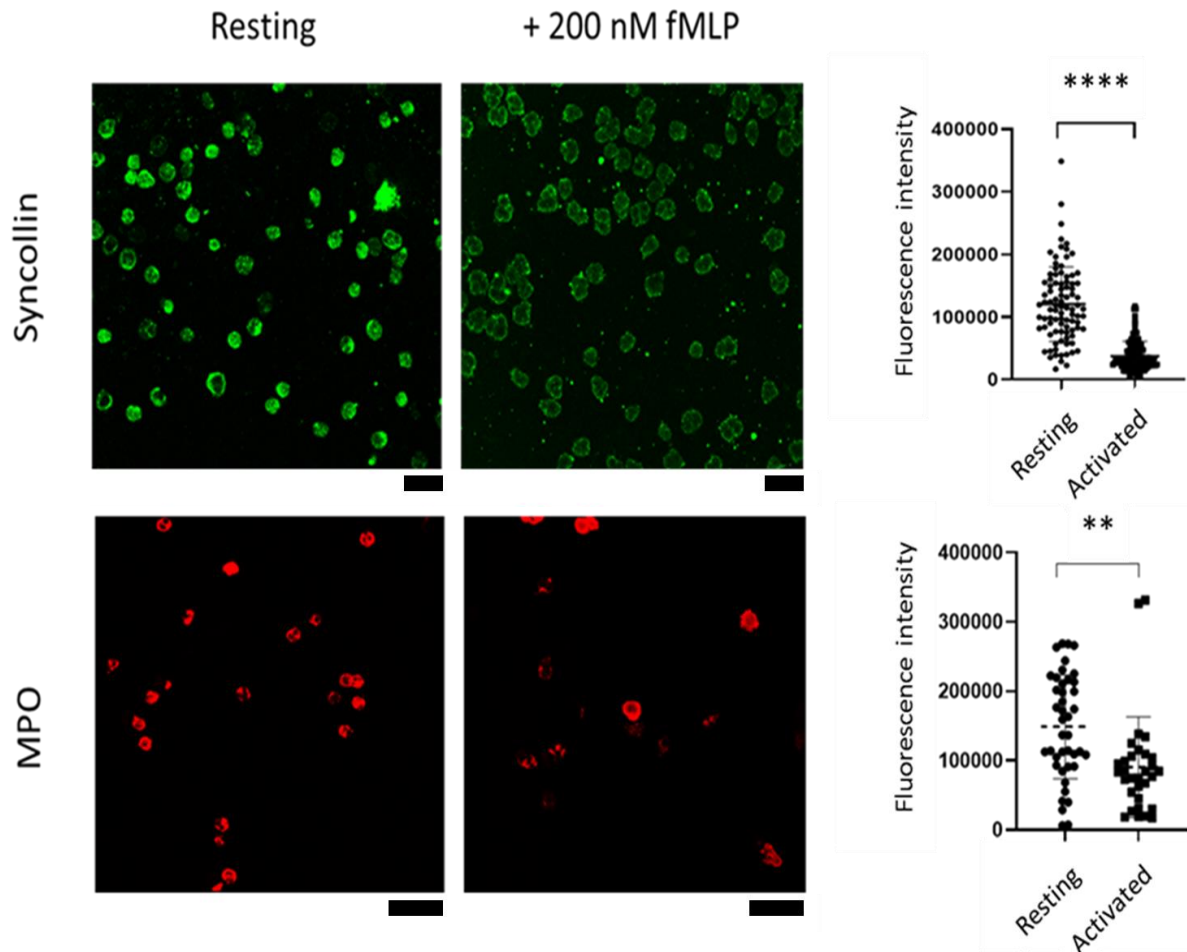


Figure 5.4. Quantitation of syncollin secretion from activated neutrophils. Immunofluorescence analysis was carried out as described in the caption to Figure 5.1. Fluorescence intensity for both syncollin and MPO was determined in resting and fLMP-activated cells using ImageJ Fiji™. Each cell was defined and fluorescence intensity was quantified. Raw intensities were then plotted using GraphPad Prism™. Intensities for resting and activated neutrophils were compared using Student's t-test where **** denotes $p < 0.0001$ and ** denotes $p < 0.05$. Scale bars, 24 μm .

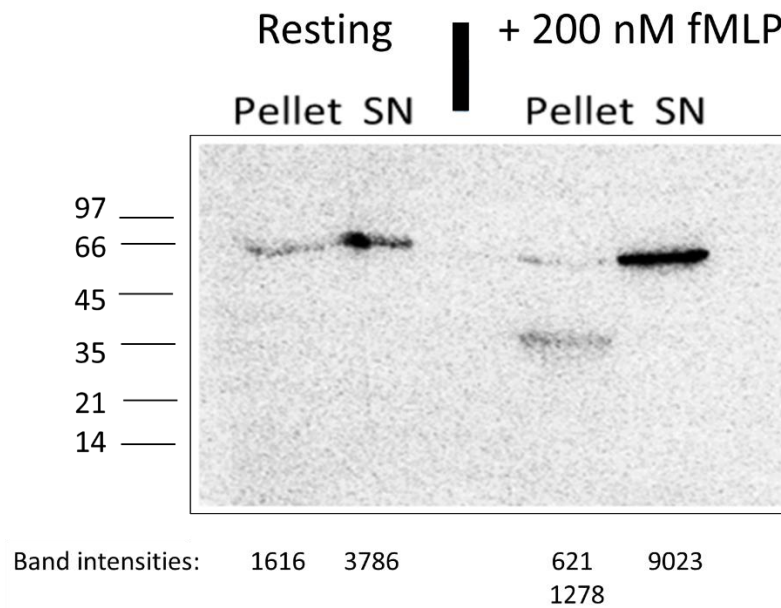


Figure 5.5. Immunoblot analysis of syncollin release from activated neutrophils. Neutrophils were activated by incubation with 200 nM fMLP for 30 min at 37°C before centrifugation. Pellets and precipitated supernatants ('SN') were subjected to SDS-PAGE and immunoblotting using a polyclonal anti-syncollin antibody. Resting neutrophils (left) were compared with activated neutrophils (right). Band intensities were calculated using ImageJ™. Standards are BioRad low-range markers.

5.3.4 NEUTROPHIL NET STRUCTURES

Up to this point, activation of neutrophils has been triggered by fMLP. Since it has been shown in Chapter 4 that syncollin is capable of hindering bacterial growth, I decided next to investigate neutrophil activation in response to the presence of bacteria, in attempt to mimic a bacterial infection *in vitro*.

Neutrophils were allowed to adhere to fibronectin-coated imaging plates and a sample of *E. coli* was then added. The neutrophils were then fixed, permeabilized and subjected to immunofluorescence analysis. Neutrophil extracellular trap (NET) formation began to occur after a 45-min incubation with *E. coli*, with extracellular staining observed for defensin, MPO and neutrophil elastase following their release via degranulation (Figure 5.6). The NETs themselves became stained with Hoechst dye; this was expected, given that the NETs contain de-condensed neutrophil DNA. Interestingly, syncollin was also present in the NETs, along with the proteins mentioned above.

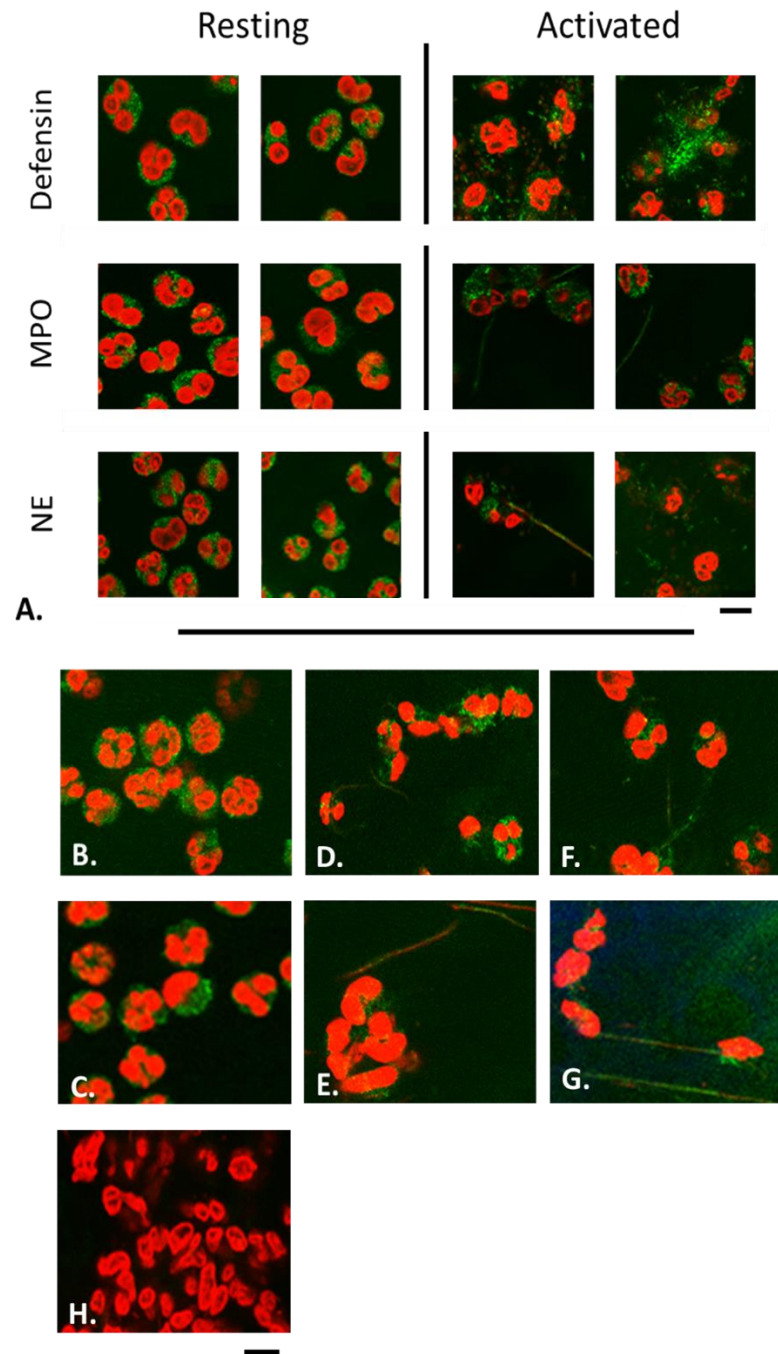


Figure 5.6. *E. coli*-activated neutrophil immunofluorescence. Neutrophils were isolated and prepared for immunofluorescence as described in the caption to Figure 5.1. Following adherence to fibronectin-coated imaging dishes, *E. coli* was added and incubated at 37°C for 45 min. Cells were then fixed and permeabilized. A. In addition to syncollin, other granular proteins were stained for, including defensin, myeloperoxidase (MPO) and neutrophil elastase (NE), with resting neutrophils shown on the left and *E. coli*-activated neutrophils on the right B, C. Syncollin in resting neutrophils. D-G. Syncollin in activated neutrophils. Granular proteins are shown in green and Hoechst dye is shown in red. H. Secondary antibody alone control. Scale bars, 8 μm , applied in ImageJ Fiji™.

5.3.5 BINDING OF SYNCOLLIN-STREP TO BACTERIA

Chapter 4 reported the inhibitory actions of syncollin-Strep on bacterial growth, and it was suggested that syncollin-Strep must bind to the bacterial capsule to mediate its inhibitory action. To look for this binding, syncollin-Strep was incubated with *L. lactis* and *E. coli* for 3 h at 4°C. Bacteria were then pelleted by centrifugation and washed three times with PBS. Bacteria were then added to imaging dishes (Ibidi™) and incubated with a polyclonal anti-syncollin antibody for 2 h at room temperature. Bacteria were washed before addition of FITC-conjugated secondary antibody and DAPI. DAPI staining revealed the presence of the bacteria (Figure 5.7), and syncollin could be seen bound to the surface of both types of bacterium, consistent its ability to bind to PGN and to restrict bacterial growth.

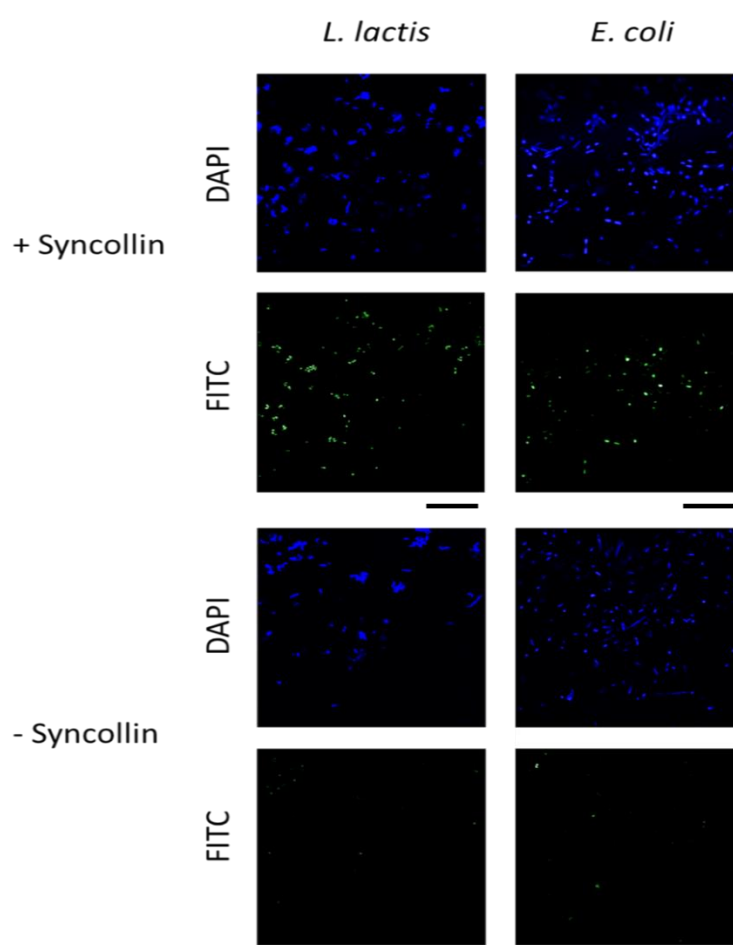


Figure 5.7 Syncollin-Strep binds the bacterial surface. Purified syncollin-Strep (0.05 mg/mL) was incubated with bacteria (*L. lactis* and *E. coli*) for 3 h at 4°C. As a control bacteria were incubated with elution buffer in the absence of syncollin-Strep. Bacteria were subsequently washed and incubated with a polyclonal anti-syncollin primary antibody followed by FITC-conjugated secondary antibody and DAPI. Scale bars, 20 µm.

5.3.6 BACTERIA AND NEUTROPHIL CO-STAINING

Having shown that both *L. lactis* and *E. coli* become decorated with recombinant syncollin-Strep, I next asked whether syncollin released from activated neutrophils would also bind to the bacteria. *E. coli* were allowed to adhere to fibronectin-coated imaging dishes, and neutrophils (20 μ L at 3.6×10^6 cells/mL) were added. At various times, between 30 min and 2 h, cells were fixed, permeabilized and subjected to immunofluorescence imaging. Although some NET formation could be observed at 30 min, a majority of the NETs appeared at 120 min (Figure 5.8). MPO was clearly visible on the NET surface and also within the nuclei of the neutrophils. Consistent with the results described above, syncollin could also be seen in association with the bacteria.

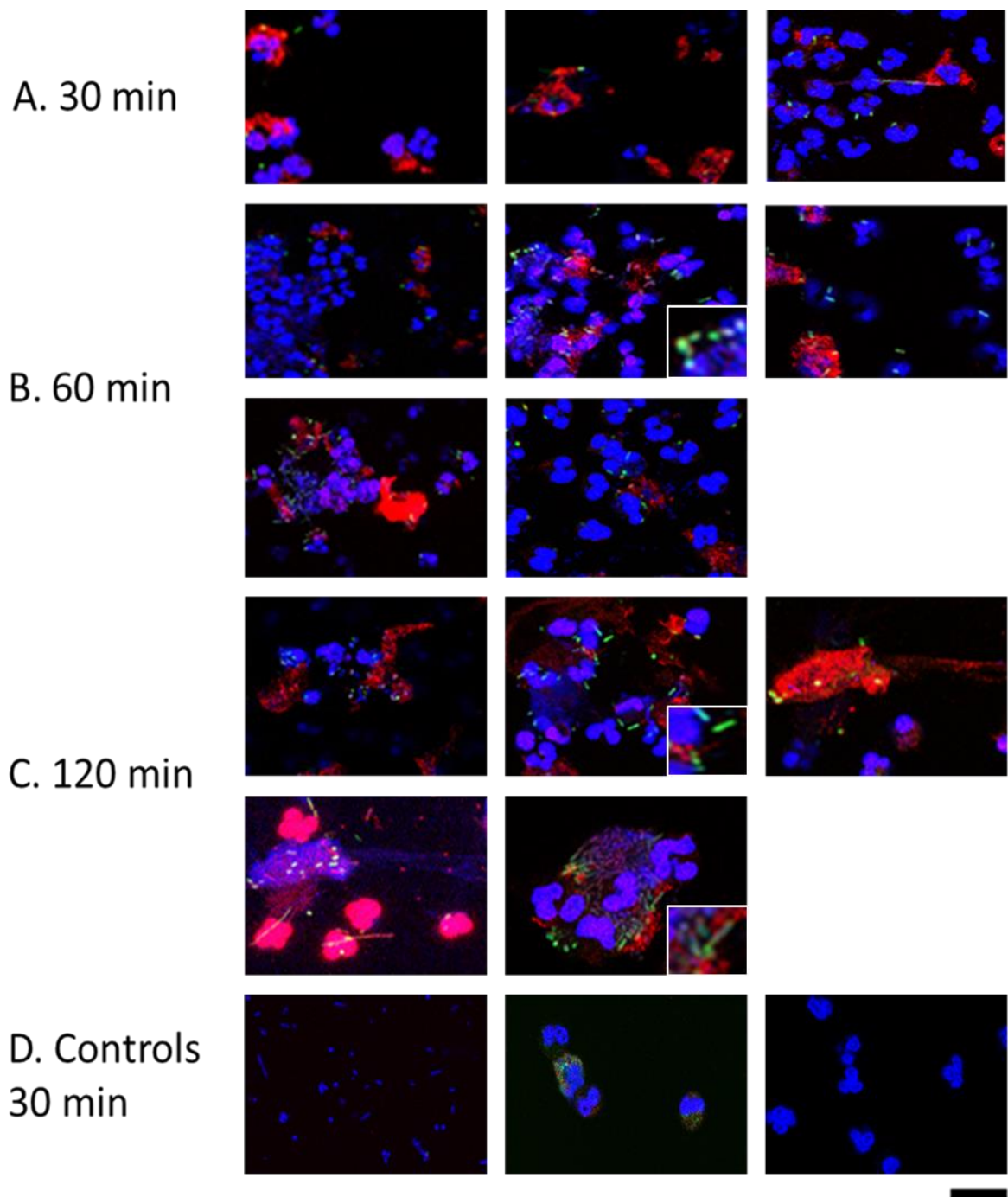


Figure 5.8 Decoration of bacteria by syncollin secreted by activated neutrophils. Neutrophils were added to adherent *E. coli* and subjected to immunofluorescence as described in the caption to Figure 5.1. Images were taken after 30 (A), 60 (B) and 120 (C) min of activation. Syncollin was detected using a polyclonal primary antibody followed by an FITC-conjugated secondary antibody. MPO was detected using a monoclonal primary antibody followed by an APC-conjugated secondary antibody. Hoechst dye was added to detect neutrophils and bacteria. Control images (D) show (left to right) bacteria alone, neutrophils alone and bacteria plus neutrophils with secondary antibody alone. Insets display a higher magnification of the image to highlight the bacteria. Images were overlaid using ImageJ Fiji™. Colours are: syncollin, green; MPO, red; Hoechst, blue. Scale bar, 20 μm .

5.4 DISCUSSION

It has been reported previously (Bach *et al.*, 2006) that syncollin is expressed in neutrophils, likely in the azurophilic granules, and it is released upon neutrophil activation, which hinted at a role in host defence. This chapter confirms and extends these previous findings.

Syncollin is expressed in neutrophils as a higher order oligomer (>60 kDa) which stains in a granular punctate manner. The use of confocal imaging and immunoblotting confirms that the protein is secreted from the neutrophils upon activation. My results suggest that the protein does not co-localize with MPO in the azurophilic granules, but rather and has a greater co-localization with CD11b and CD14 in the tertiary and secretory vesicles. Part of the difficulty involved in assigning a precise localization arises due to limitations in resolution. Limitations in resolution could be resolved through the use of higher-resolution microscopy such as total internal reflection fluorescence microscopy.

Upon activating of neutrophils with bacteria, syncollin decorated the NETs, and also bound to the bacterial surface. Bacteria could also be decorated with recombinant syncollin-Strep. On the basis of these results and those described in Chapter 4, it is tempting to speculate that in a physiological setting, syncollin is released from the neutrophils in response to a bacterial challenge, and then binds to bacteria to produce an anti-microbial effect.

6. FINAL COMMENTS

I have shown that syncollin is an exceptionally stable protein with a CD spectrum consistent with a predominantly beta-sheet structure. Its high stability, conferred in part by the presence of disulphide bonds, is likely significant, given that it is secreted into the pancreatic duct, where it will encounter a cocktail of proteases and bile salts. I have also confirmed that recombinant Strep-tagged syncollin forms oligomers and assembles on lipid bilayers in the form of ring-shaped structures, consistent with the ability of the native protein to permeabilize biological membranes (Wäsle *et al.*, 2004) and lipid bilayers (Geisse *et al.*, 2002). Syncollin is predicted to have a large positively charged patch on its surface, and reduction of this charges significantly impairs its ability to disrupt bilayers.

Importantly, I have shown that syncollin binds to PGN and hinders the growth of Gram-positive (*L. lactis*) and Gram-negative (*E. coli*) bacteria, reducing the viability of the latter in the plateau phase of growth. Syncollin also causes obvious structural damage to the bacterial capsule in both *L. lactis* and *E. coli*. I suggest that the slowing of the growth of *L. lactis* (but not *E. coli*) in log phase might be caused primarily through binding to the exposed PGN-based cell wall in the former, whereas the permeabilization of the *E. coli* (but not *L. lactis*) in the plateau phase might be caused by an action of

syncollin on the membranes of the Gram-negative bacterium. Further studies will be required to confirm this suggestion.

Syncollin knockout mice are viable and fertile, although gut physiology and sensitivity to bacterial challenge have not been addressed. Intriguingly, syncollin shares features with other small antimicrobial polypeptides that are known to play roles in host defence in the gut, including ZG16p, RegIII and members of the defensin family (Bergström *et al.*, 2016; Cash *et al.*, 2006; Raj and Dentino, 2002). These features include a predominantly beta-sheet structure, the presence of intramolecular disulphide bonds, and in some cases the ability to form homo-oligomers. Given that many antibacterial polypeptides are known to be secreted into the gut, it is perhaps unlikely that the absence of just one (syncollin) would cause an obvious gut phenotype. Signs of abnormality in the pancreas of the knockout mice were detected, including an increase in the numbers of ZGs within the acinar cells and a reduction in the number of individual exocytotic events (Wäsle *et al.*, 2005). Could it be that a component of the exocytotic machinery ‘moonlights’ as an antibacterial protein? At present, I cannot rule this out, although it is worth pointing out that compound exocytosis continues at a reduced rate in the knockout mice, rather than being completely abolished. Further, compound exocytosis occurs in several other cell types (e.g. mast cells; Klein and Sagi-Eisenberg, 2019) that do not express syncollin. It is clear that syncollin is a major component of the protein matrix lining the luminal surface of the ZG membrane. It is therefore possible that its absence in the knockout mouse causes structural abnormalities that perturb the function of the membrane during exocytosis.

It has been shown previously that syncollin is expressed in, and secreted from, neutrophils (Bach *et al.*, 2006), consistent with a role in host defence. Indeed, the authors of this previous paper speculated that syncollin might have an antibacterial effect, but were unable to demonstrate this property. I suggest that this failure might have been a result of the elaborate method used to prepare native syncollin (removal from the ZG membrane at high pH followed by selective precipitation in an aggregated state after dialysis to neutral pH; An *et al.*, 2000). It is possible, for example, that membrane permeabilization by syncollin might require oligomerization on the target membrane, and that pre-formed oligomers are inactive. The time-dependent oligomerization seen in my experiments is consistent with this notion. Significantly, I have shown that syncollin secreted from neutrophils, in response to activation either by fMLP or by exposure to *E. coli*, binds to NETs and coats the bacteria. It may then go on to produce the antibacterial effects seen in my *in-vitro* experiments.

There are some observations which still require explanation, such as the role of syncollin in disease. In DSS-induced colitis, expression of syncollin was found paradoxically to decrease, unlike another AMP, RegIII, which was found to increase (Li *et al.*, 2014). Conversely, in pancreatic cancer the protein was

found to be secreted and into the serum (Makawita *et al.*, 2013). It has been shown that in experimental DSS-induced UC and CAC gut tissues become damaged, including the crypts (Shan *et al.*, 2021; Sun *et al.*, 2020), where syncollin is thought to be localized. Likewise, in pancreatic cancer, the acinar cells can become damaged (Murtaugh and Keefe, 2015; Storz, 2017) and as a result, could release this abundant protein into the serum.

Further research into the mechanism of action of syncollin would be greatly facilitated by a crystal structure. A crystal structure would provide a greater understanding of how the protein oligomerizes, how it interacts with membranes and other bacterial targets, and identify the location of the key disulphide bonds that contribute to its thermal stability. For further work on host defence, it would be beneficial to trial syncollin addition to other Gram-positive and Gram-negative bacterial strains to see if similar patterns of behaviour are observed as were seen with *L. lactis* and *E. coli*. A greater understanding of how syncollin behaves once released from neutrophils could be achieved using co-cultures of various cell types; for example, co-culturing of intestinal cells, neutrophils and bacteria would mimic a bacterial challenge in the gut. Finally, real-time monitoring of syncollin release using immunofluorescence would provide significant new information.

Antibiotic resistance is dramatically on the rise, and many conventional antibiotics are becoming ineffective, for example in the case of methicillin-resistant *Staphylococcus aureus* (MRSA). Hence, there is an urgent need for new mechanisms for killing harmful bacteria. It is possible that natural AMPs might be mobilized in the fight against drug-resistant bacteria; hence, an increase in our understanding of the mechanisms underlying the action of these AMPs is crucial. Future studies on the antibacterial actions of syncollin might therefore become therapeutically relevant.

7. REFERENCES

Alam P, Bousset L, Melki R, Otzen DE. α -synuclein oligomers and fibrils: a spectrum of species, a spectrum of toxicities. *J Neurochem*. 2019 Sep;150(5):522-534. doi: 10.1111/jnc.14808. Epub 2019 Aug 2. PMID: 31254394.

Alberts B, Johnson A, Lewis J, et al. *Molecular Biology of the Cell*. 4th edition. New York: Garland Science; 2002. Transport from the Trans Golgi Network to the Cell Exterior: Exocytosis. Available from: <https://www.ncbi.nlm.nih.gov/books/NBK26892/>

Alonso MA, Millán J. The role of lipid rafts in signalling and membrane trafficking in T lymphocytes. *J Cell Sci*. 2001 Nov;114(Pt 22):3957-65. PMID: 11739628.

An SJ, Hansen NJ, Hodel A, Jahn R, Edwardson JM. Analysis of the association of syncollin with the membrane of the pancreatic zymogen granule. *J Biol Chem*. 2000 Apr 14;275(15):11306-11. doi: 10.1074/jbc.275.15.11306. PMID: 10753942.

Andley UP, Mathur S, Griest TA, Petrash JM. Cloning, expression, and chaperone-like activity of human alphaA-crystallin. *J Biol Chem*. 1996 Dec 13;271(50):31973-80. doi: 10.1074/jbc.271.50.31973. PMID: 8943244.

Andreasen M, Lorenzen N, Otzen D. Interactions between misfolded protein oligomers and membranes: A central topic in neurodegenerative diseases? *Biochim Biophys Acta*. 2015 Sep;1848(9):1897-907. doi: 10.1016/j.bbamem.2015.01.018. Epub 2015 Feb 7. PMID: 25666871.

Andreotti G, Guarracino MR, Cammisa M, Correr A, Cubellis MV. Prediction of the responsiveness to pharmacological chaperones: lysosomal human alpha-galactosidase, a case of study. *Orphanet J Rare Dis*. 2010 Dec 7;5:36. doi: 10.1186/1750-1172-5-36. PMID: 21138548; PMCID: PMC3016270.

Applied Photophysics. Circular Dichroism units and conversions. 2021. Available at: <https://www.photophysics.com/circular-dichroism/chirascan-technology/circular-dichroism-spectroscopy-units-conversions/>

Aravind P, Suman SK, Mishra A, Sharma Y, Sankaranarayanan R. Three-dimensional domain swapping in nitrocollin, a single-domain beta-gamma-crystallin from *Nitrosospira multiformis*, controls protein conformation and stability but not dimerization. *J Mol Biol*. 2009 Jan 9;385(1):163-77. doi: 10.1016/j.jmb.2008.10.035. Epub 2008 Oct 19. PMID: 18976659.

Arntfield, S., Ismond, M. And Murray, E. Use of intrinsic fluorescence to follow the denaturation of vicilin, a storage protein from *Vicia faba*. *International Journal of Peptide and Protein Research* . 1987. 29: 9-20. <https://doi.org/10.1111/j.1399-3011.1987.tb02225.x>

Aroso M, Agricola B, Hacker C, Schrader M. Proteoglycans support proper granule formation in pancreatic acinar cells. *Histochem Cell Biol*. 2015 Oct;144(4):331-46. doi: 10.1007/s00418-015-1339-x. Epub 2015 Jun 24. PMID: 26105026.

Aryal S. Protein structure- primary, secondary, tertiary and quaternary. *Microbe notes*. 2018. Available at: <https://microbenotes.com/protein-structure-primary-secondary-tertiary-and-quaternary/>

Bach JP, Borta H, Ackermann W, Faust F, Borchers O, Schrader M. The secretory granule protein syncollin localizes to HL-60 cells and neutrophils. *J Histochem Cytochem*. 2006 Aug;54(8):877-88. doi: 10.1369/jhc.5A6792.2006. Epub 2006 Mar 3. PMID: 16517980.

Bai AP, Ouyang Q. Probiotics and inflammatory bowel diseases. *Postgrad Med J*. 2006;82(968):376-382. doi:10.1136/pgmj.2005.040899

Baker MR, Fan G, Serysheva II. Single-particle cryo-EM of the ryanodine receptor channel in an aqueous environment. *Eur J Transl Myol*. 2015;25(1):35-48. doi: 10.4081/ejtm.2015.4803. PMID: 25844145; PMCID: PMC4381806.

Barrera NP, Ormond SJ, Henderson RM, Murrell-Lagnado RD, Edwardson JM. Atomic force microscopy imaging demonstrates that P2X2 receptors are trimers but that P2X6 receptor subunits do not oligomerize. *J Biol Chem*. 2005 Mar 18;280(11):10759-65. doi: 10.1074/jbc.M412265200. Epub 2005 Jan 18. PMID: 15657042.

Basaglia F, Di Luca D. A comparative study of vertebrate eye lens crystallins using isoelectric focusing and densitometry. *Comp Biochem Physiol B*. 1993 Nov;106(3):575-86. doi: 10.1016/0305-0491(93)90134-q. PMID: 8281753.

Benham AM. Protein secretion and the endoplasmic reticulum. *Cold Spring Harb Perspect Biol*. 2012 Aug 1;4(8):a012872. doi: 10.1101/cshperspect.a012872. PMID: 22700933; PMCID: PMC3405867.

Berg JM, Tymoczko JL, Stryer L. Biochemistry. 5th edition. New York: W H Freeman; 2002. Available from: <https://www.ncbi.nlm.nih.gov/books/NBK21154/>

Bergström JH, Birchenough GM, Katona G, Schroeder BO, Schütte A, Ermund A, Johansson ME, Hansson GC. Gram-positive bacteria are held at a distance in the colon mucus by the lectin-like protein ZG16. *Proc Natl Acad Sci U S A*. 2016 Nov 29;113(48):13833-13838. doi: 10.1073/pnas.1611400113. Epub 2016 Nov 14. PMID: 27849619; PMCID: PMC5137749.

Bernal-Conde LD, Ramos-Acevedo R, Reyes-Hernández MA, Balbuena-Olvera AJ, Morales-Moreno ID, Argüero-Sánchez R, Schüle B, Guerra-Crespo M. Alpha-Synuclein Physiology and Pathology: A Perspective on Cellular Structures and Organelles. *Front Neurosci*. 2020 Jan 23;13:1399. doi: 10.3389/fnins.2019.01399. PMID: 32038126; PMCID: PMC6989544.

Bervers EM, Williamson PL. Getting to the Outer Leaflet: Physiology of Phosphatidylserine Exposure at the Plasma Membrane. *Physiol Rev*. 2016;96(2):605-645. doi:10.1152/physrev.00020.2015

Bevins CL, Martin-Porter E, Ganz T. Defensins and innate host defence of the gastrointestinal tract. *Gut*. 1999 Dec;45(6):911-5. doi: 10.1136/gut.45.6.911. PMID: 10562592; PMCID: PMC1727760.

Bonifacino JS, Glick BS. The mechanisms of vesicle budding and fusion. *Cell*. 2004 Jan 23;116(2):153-66. doi: 10.1016/s0092-8674(03)01079-1. PMID: 14744428.

Branzk N, Papayannopoulos V. Molecular mechanisms regulating NETosis in infection and disease. *Semin Immunopathol*. 2013 Jul;35(4):513-30. doi: 10.1007/s00281-013-0384-6. Epub 2013 Jun 4. PMID: 23732507; PMCID: PMC3685711.

Broadwith P. Explainer: What is cryo-electron microscopy. *Chemistry World*. 2017. Available at: <https://www.chemistryworld.com/news/explainer-what-is-cryo-electron-microscopy/3008091.article>

Brunsveld L, Crain J, Heddle JG. Amino acids, peptides and proteins. Volume 37. Royal Society of Chemistry. 2012. Available from: <https://pubs.rsc.org/en/content/ebook/978-1-84973-406-6>

Campieri M, Gionchetti P. Bacteria as the cause of ulcerative colitis. *Gut*. 2001 Jan;48(1):132-5. doi: 10.1136/gut.48.1.132. PMID: 11115835; PMCID: PMC1728175.

Capasso C, Supuran CT. Dihydropteroate synthase (Sulfonamides) and Dihydrofolate reductase inhibitors. *Bacterial resistance to antibiotics- From molecules to Man, 2019: 163-172.* doi.org/10.1002/9781119593522.ch7

Carr CM, Munson M. Tag team action at the synapse. *EMBO Rep*. 2007 Sep;8(9):834-8. doi: 10.1038/sj.embor.7401051. PMID: 17767192; PMCID: PMC1973957.

Carr CM, Rizo J. At the junction of SNARE and SM protein function. *Curr Opin Cell Biol*. 2010 Aug;22(4):488-95. doi: 10.1016/j.ceb.2010.04.006. Epub 2010 May 12. PMID: 20471239; PMCID: PMC2923694.

Carroni M, Saibil HR. Cryo electron microscopy to determine the structure of macromolecular complexes. *Methods*. 2016 Feb 15;95:78-85. doi: 10.1016/j.ymeth.2015.11.023. Epub 2015 Nov 27. PMID: 26638773; PMCID: PMC5405050.

Carter M, Sheih J. Chapter 15- Biochemical Assays and intracellular signalling. Guide to research techniques in neuroscience (second edition). 2015. 331-345. ISBN: 9780128005118.

Cash HL, Whitham CV, Behrendt CL, Hooper LV. Symbiotic bacteria direct expression of an intestinal bactericidal lectin. *Science*. 2006 Aug 25;313(5790):1126-30. doi: 10.1126/science.1127119. PMID: 16931762; PMCID: PMC2716667.

Cassatella MA, Östberg NK, Tamassia N, Soehnlein O. Biological Roles of Neutrophil-Derived Granule Proteins and Cytokines. *Trends Immunol*. 2019 Jul;40(7):648-664. doi: 10.1016/j.it.2019.05.003. Epub 2019 May 30. PMID: 31155315.

Chen X. Protein composition and biogenesis of the pancreatic zymogen granules. *Pancreapedia: Exocrine pancreas knowledge base*. 2018. doi: 10.3998/panc.2018.16

Chirgadze D. Protein crystallisation in action. University of Cambridge. 2001. Available at: <https://www.researchgate.net/profile/Mohamed-Mourad-Lafifi/post/How-to-continue-from-precipitation-cluster-to-get-protein-crystals/attachment/59d6449e79197b807799fd83/AS%3A449397134761988%401484156034784/ddownloa/Proteine+Crystallisation-in-action.pdf>

Cooper GM. *The Cell: A Molecular Approach*. 2nd edition. Sunderland (MA): Sinauer Associates; 2000. Available from: <https://www.ncbi.nlm.nih.gov/books/NBK9839/>

Crooks GE, Hon G, Chandonia JM, Brenner SE. WebLogo: a sequence logo generator. *Genome Res*. 2004 Jun;14(6):1188-90. doi: 10.1101/gr.849004. PMID: 15173120; PMCID: PMC419797.

Daly SM, Sturge CR, Greenberg DE. Inhibition of Bacterial Growth by Peptide-Conjugated Morpholino Oligomers. *Methods Mol Biol*. 2017;1565:115-122. doi: 10.1007/978-1-4939-6817-6_10. PMID: 28364238; PMCID: PMC5497461.

De Flora S, La Maestra S. Epidemiology of cancers of infectious origin and prevention strategies. *J Prev Med Hyg*. 2015;56(1):E15-E20. Published 2015 Jun 10.

Derrien M, van Passel MW, van de Bovenkamp JH, Schipper RG, de Vos WM, Dekker J. Mucin-bacterial interactions in the human oral cavity and digestive tract. *Gut Microbes*. 2010 Jul;1(4):254-268. doi: 10.4161/gmic.1.4.12778. Epub 2010 Jun 23. PMID: 21327032; PMCID: PMC3023607.

Dillard RS, Hampton CM, Strauss JD, Ke Z, Altomara D, Guerrero-Ferreira RC, Kiss G, Wright ER. Biological Applications at the Cutting Edge of Cryo-Electron Microscopy. *Microsc Microanal*. 2018 Aug;24(4):406-419. doi: 10.1017/S1431927618012382. PMID: 30175702; PMCID: PMC6265046.

Dilworth MV, Findlay HE, Booth PJ. Detergent-free purification and reconstitution of functional human serotonin transporter (SERT) using diisobutylene maleic acid (DIBMA) copolymer. *Biochim Biophys Acta Biomembr*. 2021 Jul 1;1863(7):183602. doi: 10.1016/j.bbmem.2021.183602. Epub 2021 Mar 18. PMID: 33744253; PMCID: PMC8111416.

Dolai S, Liang T, Cosen-Binker LI, Lam PLL, Gaisano HY. Regulation of Physiologic and Pathologic Exocytosis in Pancreatic acinar cells. *Pancreapedia American Pancreatic Association*. 2012 doi: 10.3998/panc.2012.12

Edwardson JM, An S, Jahn R. The secretory granule protein syncollin binds to syntaxin in a Ca²⁺(+)-sensitive manner. *Cell*. 1997 Jul 25;90(2):325-33. doi: 10.1016/s0092-8674(00)80340-2. PMID: 9244306.

Elegheert J, Behiels E, Bishop B, Scott S, Woolley RE, Griffiths SC, Byrne EFX, Chang VT, Stuart DI, Jones EY, Siebold C, Aricescu AR. Lentiviral transduction of mammalian cells for fast, scalable and high-level production of soluble and membrane proteins. *Nat Protoc*. 2018 Dec;13(12):2991-3017. doi: 10.1038/s41596-018-0075-9. PMID: 30455477; PMCID: PMC6364805.

Epand RM, Walker C, Epand RF, Magarvey NA. Molecular mechanisms of membrane targeting antibiotics. *Biochim Biophys Acta*. 2016 May;1858(5):980-7. doi: 10.1016/j.bbamem.2015.10.018. Epub 2015 Oct 26. PMID: 26514603.

Falke M, Victor J, Wördehoff MM, Peduzzo A, Zhang T, Schröder GF, Buell AK, Hoyer W, Etkorn M. α -Synuclein-derived lipoparticles in the study of α -Synuclein amyloid fibril formation. *Chem Phys Lipids*. 2019 May;220:57-65. doi: 10.1016/j.chemphyslip.2019.02.009. Epub 2019 Feb 28. PMID: 30826264; PMCID: PMC6451039.

Flaherty DK. *Immunology for Pharmacy*. Mosby. 2012. Chapter 2- Innate Immunity: 15-22. Available at: <https://www.sciencedirect.com/science/article/pii/B9780323069472100021>

France MM, Turner JR. The mucosal barrier at a glance. *J Cell Sci*. 2017 Jan 15;130(2):307-314. doi: 10.1242/jcs.193482. Epub 2017 Jan 6. PMID: 28062847; PMCID: PMC5278669.

Gan W, Schneidman D, Zhang N, Ma B, Nussinov R. Probing Oligomerized Conformations of Defensin in the Membrane. *Methods Mol Biol*. 2017;1529:353-362. doi: 10.1007/978-1-4939-6637-0_18. PMID: 27914061; PMCID: PMC6484831.

Ganz T. Defensins: antimicrobial peptides of innate immunity. *Nat Rev Immunol*. 2003 Sep;3(9):710-20. doi: 10.1038/nri1180. PMID: 12949495.

Gdovin MJ, Zamora DA, Ravindran CR, Leiter JC. Optical recording of intracellular pH in respiratory chemoreceptors. *Ethn Dis*. 2010 Winter;20(1 Suppl 1):S1-33-8. PMID: 20521382; PMCID: PMC4068026.

Geisse NA, Wäsle B, Saslowsky DE, Henderson RM, Edwardson JM. Syncollin homo-oligomers associate with lipid bilayers in the form of doughnut-shaped structures. *J Membr Biol*. 2002 Sep 15;189(2):83-92. doi: 10.1007/s00232-002-1005-9. PMID: 12235484.

Gkouskou KK, Deligianni C, Tsatsanis C, Eliopoulos AG. The gut microbiota in mouse models of inflammatory bowel disease. *Front Cell Infect Microbiol*. 2014;4:28. Published 2014 Feb 28. doi:10.3389/fcimb.2014.00028

Greenfield NJ. Using circular dichroism spectra to estimate protein secondary structure. *Nat Protoc*. 2006;1(6):2876-90. doi: 10.1038/nprot.2006.202. PMID: 17406547; PMCID: PMC2728378.

Grivennikov SI. Inflammation and colorectal cancer: colitis-associated neoplasia. *Semin Immunopathol*. 2013 Mar;35(2):229-44. doi: 10.1007/s00281-012-0352-6. Epub 2012 Nov 16. PMID: 23161445; PMCID: PMC3568220.

Grivennikov SI, Cominelli F. Colitis-Associated and Sporadic Colon Cancers: Different Diseases, Different Mutations? *Gastroenterology*. 2016 Apr;150(4):808-10. doi: 10.1053/j.gastro.2016.02.062. Epub 2016 Feb 26. PMID: 26924087.

Hampton Research. Drop Ratio. 2020. Crystallization reading. Available at: <https://hamptonresearch.com/blog-drop-ratio-190.html>

Hansen NJ, Antonin W, Edwardson JM. Identification of SNAREs involved in regulated exocytosis in the pancreatic acinar cell. *J Biol Chem*. 1999 Aug 6;274(32):22871-6. doi: 10.1074/jbc.274.32.22871. PMID: 10428873.

Hays LB, Wicksteed B, Wang Y, McCuaig JF, Philipson LH, Edwardson JM, Rhodes CJ. Intragranular targeting of syncollin, but not a syncollinGFP chimera, inhibits regulated insulin exocytosis in pancreatic beta-cells. *J Endocrinol*. 2005 Apr;185(1):57-67. doi: 10.1677/joe.1.05934. PMID: 15817827.

Hecker N, Sharma V, Hiller M. Convergent gene losses illuminate metabolic and physiological changes in herbivores and carnivores. *Proc Natl Acad Sci U S A*. 2019 Feb 19;116(8):3036-3041. doi: 10.1073/pnas.1818504116. Epub 2019 Feb 4. PMID: 30718421; PMCID: PMC6386725.

Johansen HK, Jensen TG, Dessau RB, Lundgren B, Frimodt-Møller N. Antagonism between penicillin and erythromycin against *Streptococcus pneumoniae* *in vitro* and *in vivo*, *Journal of Antimicrobial Chemotherapy*, 2000. 46(6): 973–980, <https://doi.org/10.1093/jac/46.6.973>

Herzik MA Jr, Wu M, Lander GC. High-resolution structure determination of sub-100 kDa complexes using conventional cryo-EM. *Nat Commun*. 2019 Mar 4;10(1):1032. doi: 10.1038/s41467-019-08991-8. PMID: 30833564; PMCID: PMC6399227.

Heuck AP, Savva CG, Holzenburg A, Johnson AE. Conformational changes that effect oligomerization and initiate pore formation are triggered throughout perfringolysin O upon binding to cholesterol. *J Biol Chem*. 2007 Aug 3;282(31):22629-37. doi: 10.1074/jbc.M703207200. Epub 2007 Jun 5. PMID: 17553799.

Hodel A, An SJ, Hansen NJ, Lawrence J, Wäsle B, Schrader M, Edwardson JM. Cholesterol-dependent interaction of syncollin with the membrane of the pancreatic zymogen granule. *Biochem J*. 2001 Jun 15;356(Pt 3):843-50. doi: 10.1042/0264-6021:3560843. PMID: 11389693; PMCID: PMC1221912.

Hoover DM, Rajashankar KR, Blumenthal R, Puri A, Oppenheim JJ, Chertov O, Lubkowski J. The structure of human beta-defensin-2 shows evidence of higher order oligomerization. *J Biol Chem*. 2000 Oct 20;275(42):32911-8. doi: 10.1074/jbc.M006098200. PMID: 10906336. https://www.xtal.iqfr.csic.es/Cristalografia/parte_05_6-en.html

Hummer BH, Maslar D, Soltero-Gutierrez M, de Leeuw NF, Asensio CS. Differential sorting behavior for soluble and transmembrane cargoes at the trans-Golgi network in endocrine cells. *Mol Biol Cell*. 2020 Feb 1;31(3):157-166. doi: 10.1091/mbc.E19-10-0561. Epub 2019 Dec 11. PMID: 31825717; PMCID: PMC7001476.

Ijssennagger N, van der Meer R, van Mil SWC. Sulfide as a Mucus Barrier-Breaker in Inflammatory Bowel Disease? *Trends Mol Med*. 2016 Mar;22(3):190-199. doi: 10.1016/j.molmed.2016.01.002. Epub 2016 Feb 3. PMID: 26852376.

InformedHealth.org. The innate and adaptive immune systems. Institute for Quality and Efficiency in Health Care (IQWiG); 2006-2010 Dec 7. Available from: <https://www.ncbi.nlm.nih.gov/books/NBK279396/>

ISA. The AU-CD Beam line on Astrid 2. ISA Aarhus University. Available at: https://www.isa.au.dk/facilities/astrid2/beamlines/au-cd/AU-CD_3.asp

James DJ, Martin TF. CAPS and Munc13: CATCHRs that SNARE Vesicles. *Front Endocrinol (Lausanne)*. 2013;4:187. doi:10.3389/fendo.2013.00187

Janeway CA Jr, Travers P, Walport M, et al. *Immunobiology: The Immune System in Health and Disease*. 5th edition. New York: Garland Science; 2001. Principles of innate and adaptive immunity. Available from: <https://www.ncbi.nlm.nih.gov/books/NBK27090/>

Jeffrey P. X-Ray data collection course. Princeton Education. 2006. (6). Available at: <http://xray0.princeton.edu/~phil/Facility/Guides/XrayDataCollection.html>

Johnson BB, Heuck AP. Perfringolysin O structure and mechanism of pore formation as a paradigm for cholesterol-dependent cytolysins. *Subcell Biochem*. 2014;80:63-81. doi:10.1007/978-94-017-8881-6_5

Joly S, Maze C, McCray PB Jr, Guthmiller JM. Human beta-defensins 2 and 3 demonstrate strain-selective activity against oral microorganisms. *J Clin Microbiol*. 2004 Mar;42(3):1024-9. doi: 10.1128/JCM.42.3.1024-1029.2004. PMID: 15004048; PMCID: PMC356847.

Jubb HC, Pandurangan AP, Turner MA, Ochoa-Montaño B, Blundell TL, Ascher DB. Mutations at protein-protein interfaces: Small changes over big surfaces have large impacts on human health. *Prog Biophys Mol Biol*. 2017 Sep;128:3-13. doi: 10.1016/j.pbiomolbio.2016.10.002. Epub 2016 Nov 29. PMID: 27913149.

Kalus I, Hodel A, Koch A, Kleene R, Edwardson JM, Schrader M. Interaction of syncollin with GP-2, the major membrane protein of pancreatic zymogen granules, and association with lipid microdomains. *Biochem J*. 2002 Mar 1;362(Pt 2):433-42. doi: 10.1042/0264-6021:3620433. PMID: 11853552; PMCID: PMC1222404.

Kanagawa M, Liu Y, Hanashima S, Ikeda A, Chai W, Nakano Y, Kojima-Aikawa K, Feizi T, Yamaguchi Y. Structural basis for multiple sugar recognition of Jacalin-related human ZG16p lectin. *J Biol Chem*. 2014 Jun 13;289(24):16954-65. doi: 10.1074/jbc.M113.539114. Epub 2014 Apr 30. PMID: 24790092; PMCID: PMC4059138.

Kanagawa M, Satoh T, Ikeda A, Nakano Y, Yagi H, Kato K, Kojima-Aikawa K, Yamaguchi Y. Crystal structures of human secretory proteins ZG16p and ZG16b reveal a Jacalin-related β -prism fold. *Biochem Biophys Res Commun*. 2011 Jan 7;404(1):201-5. doi: 10.1016/j.bbrc.2010.11.093. Epub 2010 Nov 24. PMID: 21110947.

Kaufmann TC, Engel A, Rémygy HW. A novel method for detergent concentration determination. *Biophys J*. 2006 Jan 1;90(1):310-7. doi: 10.1529/biophysj.105.070193. Epub 2005 Oct 7. PMID: 16214861; PMCID: PMC1367029.

Kaur A, Goggolidou P. Ulcerative colitis: understanding its cellular pathology could provide insights into novel therapies. *J Inflamm (Lond)*. 2020;17:15. Published 2020 Apr 21. doi:10.1186/s12950-020-00246-4

Kleene R, Dartsch H, Kern HF. The secretory lectin ZG16p mediates sorting of enzyme proteins to the zymogen granule membrane in pancreatic acinar cells. *Eur J Cell Biol*. 1999 Feb;78(2):79-90. doi: 10.1016/S0171-9335(99)80009-0. PMID: 10099930.

Klein O, Sagi-Eisenberg R. Anaphylactic Degranulation of Mast Cells: Focus on Compound Exocytosis. *J Immunol Res*. 2019 Mar 18;2019:9542656. doi: 10.1155/2019/9542656. PMID: 31011586; PMCID: PMC6442490.

Kohanski MA, Dwyer DJ, Collins JJ. How antibiotics kill bacteria: from targets to networks. *Nat Rev Microbiol*. 2010 Jun;8(6):423-35. doi: 10.1038/nrmicro2333. Epub 2010 May 4. PMID: 20440275; PMCID: PMC2896384.

Kohlgraf KG, Pingel LC, Dietrich DE, Brogden KA. Defensins as anti-inflammatory compounds and mucosal adjuvants. *Future Microbiol*. 2010 Jan;5(1):99-113. doi: 10.2217/fmb.09.104. PMID: 20020832; PMCID: PMC2820878.

Kondo M. Lymphoid and myeloid lineage commitment in multipotent hematopoietic progenitors. *Immunol Rev*. 2010 Nov;238(1):37-46. doi: 10.1111/j.1600-065X.2010.00963.x. PMID: 20969583; PMCID: PMC2975965.

Kumazawa-Inoue K, Mimura T, Hosokawa-Tamiya S, Nakano Y, Dohmae N, Kinoshita-Toyoda A, Toyoda H, Kojima-Aikawa K. ZG16p, an animal homolog of β -prism fold plant lectins, interacts with heparan sulfate proteoglycans in pancreatic zymogen granules. *Glycobiology*. 2012 Feb;22(2):258-66. doi: 10.1093/glycob/cwr145. Epub 2011 Sep 23. PMID: 21948871.

Lehotzky RE, Partch CL, Mukherjee S, Cash HL, Goldman WE, Gardner KH, Hooper LV. Molecular basis for peptidoglycan recognition by a bactericidal lectin. *Proc Natl Acad Sci U S A*. 2010 Apr 27;107(17):7722-7. doi: 10.1073/pnas.0909449107. Epub 2010 Apr 9. PMID: 20382864; PMCID: PMC2867859.

Lehrer RI, Barton A, Daher KA, Harwig SS, Ganz T, Selsted ME. Interaction of human defensins with *Escherichia coli*. Mechanism of bactericidal activity. *J Clin Invest*. 1989 Aug;84(2):553-61. doi: 10.1172/JCI114198. PMID: 2668334; PMCID: PMC548915.

Li J, Zhou R, Zhang J, Li ZF. Calcium signaling of pancreatic acinar cells in the pathogenesis of pancreatitis. *World J Gastroenterol*. 2014;20(43):16146-16152. doi:10.3748/wjg.v20.i43.16146

Liang K, Wei L, Chen L. Exocytosis, Endocytosis, and Their Coupling in Excitable Cells. *Front Mol Neurosci*. 2017 Apr 19;10:109. doi: 10.3389/fnmol.2017.00109. PMID: 28469555; PMCID: PMC5395637.

Liu Y, Yang Y, Qi J, Peng H, Zhang JT. Effect of cysteine mutagenesis on the function and disulfide bond formation of human ABCG2. *J Pharmacol Exp Ther*. 2008 Jul;326(1):33-40. doi: 10.1124/jpet.108.138115. Epub 2008 Apr 22. PMID: 18430864; PMCID: PMC2632310.

Lobstein J, Emrich CA, Jeans C, Faulkner M, Riggs P, Berkmen M. SHuffle, a novel *Escherichia coli* protein expression strain capable of correctly folding disulfide bonded proteins in its cytoplasm. *Microb Cell*

Fact. 2012 May 8;11:56. doi: 10.1186/1475-2859-11-56. Erratum in: *Microb Cell Fact.* 2016;15(1):124. PMID: 22569138; PMCID: PMC3526497.

Lodish H, Berk A, Zipursky SL, et al. *Molecular Cell Biology*. 4th edition. New York: W. H. Freeman; 2000. Available from: <https://www.ncbi.nlm.nih.gov/books/NBK21532/>

Logan MR, Lacy P, Odemuyiwa SO, Steward M, Davoine F, Kita H, Moqbel R. A critical role for vesicle-associated membrane protein-7 in exocytosis from human eosinophils and neutrophils. *Allergy*. 2006 Jun;61(6):777-84. doi: 10.1111/j.1398-9995.2006.01089.x. PMID: 16677249.

Logsdon CD, Ji B. The role of protein synthesis and digestive enzymes in acinar cell injury. *Nat Rev Gastroenterol Hepatol.* 2013 Jun;10(6):362-70. doi: 10.1038/nrgastro.2013.36. Epub 2013 Mar 19. PMID: 23507798; PMCID: PMC3902846.

Lubrizol Life Science. Protein Structure. 2019. Available at: https://lubrizolcdmo.com/wp-content/uploads/2019/10/TB-8-Protein-Structure_lowres.pdf

Machado LR, Ottolini B. An evolutionary history of defensins: a role for copy number variation in maximizing host innate and adaptive immune responses. *Front Immunol.* 2015 Mar 18;6:115. doi: 10.3389/fimmu.2015.00115. PMID: 25852686; PMCID: PMC4364288.

Mackie RI. Mutualistic fermentative digestion in the gastrointestinal tract: diversity and evolution. *Integr Comp Biol.* 2002 Apr;42(2):319-26. doi: 10.1093/icb/42.2.319. PMID: 21708724.

Maekawa M, Yang Y, Fairn GD. Perfringolysin O Theta Toxin as a Tool to Monitor the Distribution and Inhomogeneity of Cholesterol in Cellular Membranes. *Toxins (Basel).* 2016 Mar 8;8(3):67. doi: 10.3390/toxins8030067. PMID: 27005662; PMCID: PMC4810212.

Makawita S, Dimitromanolakis A, Soosaipillai A, Soleas I, Chan A, Gallinger S, Haun RS, Blasutig IM, Diamandis EP. Validation of four candidate pancreatic cancer serological biomarkers that improve the performance of CA19.9. *BMC Cancer.* 2013 Sep 3;13:404. doi: 10.1186/1471-2407-13-404. PMID: 24007603; PMCID: PMC3847832.

Malanovic N, Lohner K. Antimicrobial Peptides Targeting Gram-Positive Bacteria. *Pharmaceuticals (Basel).* 2016;9(3):59. Published 2016 Sep 20. doi:10.3390/ph9030059

Martínez-Ripoll M. Crystallography-Cristolografia. 2021. CSIS. Available at: https://www.xtal.iqfr.csic.es/Cristalografia/parte_05_7-en.html

Mayadas TN, Cullere X, Lowell CA. The multifaceted functions of neutrophils. *Annu Rev Pathol.* 2014;9:181-218. doi: 10.1146/annurev-pathol-020712-164023. Epub 2013 Sep 16. PMID: 24050624; PMCID: PMC4277181.

Messenger SW, Falkowski MA, Groblewski GE. Ca²⁺-regulated secretory granule exocytosis in pancreatic and parotid acinar cells. *Cell Calcium.* 2014;55(6):369-375. doi:10.1016/j.ceca.2014.03.003

Miki T, Holst O, Hardt WD. The bactericidal activity of the C-type lectin RegIII β against Gram-negative bacteria involves binding to lipid A. *J Biol Chem.* 2012 Oct 5;287(41):34844-55. doi: 10.1074/jbc.M112.399998. Epub 2012 Aug 15. PMID: 22896700; PMCID: PMC3464586.

Milne JL, Borgnia MJ, Bartesaghi A, Tran EE, Earl LA, Schauder DM, Lengyel J, Pierson J, Patwardhan A, Subramaniam S. Cryo-electron microscopy--a primer for the non-microscopist. *FEBS J.* 2013 Jan;280(1):28-45. doi: 10.1111/febs.12078. Epub 2012 Dec 17. PMID: 23181775; PMCID: PMC3537914.

Minato, Y., Dawadi, S., Kordus, S.L. et al. Mutual potentiation drives synergy between trimethoprim and sulfamethoxazole. *Nat Commun.* 2018 9, 1003. <https://doi.org/10.1038/s41467-018-03447-x>

Mito A, Nakano Y, Saitoh T, Gouraud SSS, Yamaguchi Y, Sato T, Sasaki N, Kojima-Aikawa K. Lectin ZG16p inhibits proliferation of human colorectal cancer cells via its carbohydrate-binding sites. *Glycobiology.* 2018 Dec 1;28(1):21-31. doi: 10.1093/glycob/cwx088. PMID: 29069492.

Moon Y, Jun Y. The Effects of Regulatory Lipids on Intracellular Membrane Fusion Mediated by Dynamin-Like GTPases. *Front Cell Dev Biol.* 2020 Jun 24;8:518. doi: 10.3389/fcell.2020.00518. PMID: 32671068; PMCID: PMC7326814.

Morgan A, Burgoyne RD, Barclay JW, Craig TJ, Prescott GR, Ciuffo LF, Evans GJ, Graham ME. Regulation of exocytosis by protein kinase C. *Biochem Soc Trans.* 2005 Dec;33(Pt 6):1341-4. doi: 10.1042/BST20051341. PMID: 16246114.

Monie, Tom. A Snapshot of the Innate Immune System. *The Innate Immune System.* University of Cambridge. 2017:1-40. doi: 10.1016/B978-0-12-804464-3.00001-6.

Morrow JK, Zhang S. Computational prediction of protein hot spot residues. *Curr Pharm Des.* 2012;18(9):1255-65. doi: 10.2174/138161212799436412. PMID: 22316154; PMCID: PMC3807665.

Mukherjee S, Hooper LV. Antimicrobial defense of the intestine. *Immunity.* 2015 Jan 20;42(1):28-39. doi: 10.1016/j.immuni.2014.12.028. Epub 2015 Jan 1. PMID: 25607457.

Mukherjee S, Partch CL, Lehotzky RE, Whitham CV, Chu H, Bevins CL, Gardner KH, Hooper LV. Regulation of C-type lectin antimicrobial activity by a flexible N-terminal prosegment. *J Biol Chem.* 2009 Feb 20;284(8):4881-8. doi: 10.1074/jbc.M808077200. Epub 2008 Dec 18. PMID: 19095652; PMCID: PMC2643518.

Mukherjee S, Zheng H, Derebe MG, Callenberg KM, Partch CL, Rollins D, Propheter DC, Rizo J, Grabe M, Jiang QX, Hooper LV. Antibacterial membrane attack by a pore-forming intestinal C-type lectin. *Nature.* 2014 Jan 2;505(7481):103-7. doi: 10.1038/nature12729. Epub 2013 Nov 20. PMID: 24256734; PMCID: PMC4160023.

Muller M, Hansmann F, Arnone D, Choukour M, Ndiaye NC, Kokten T, Houlgatte R, Peyrin-Biroulet L. Genomic and molecular alterations in human inflammatory bowel disease-associated colorectal cancer. *United European Gastroenterol J.* 2020 Jul;8(6):675-684. doi: 10.1177/2050640620919254. Epub 2020 Apr 8. PMID: 32268844; PMCID: PMC7437079.

Müller A, Wenzel M, Strahl H, Grein F, Terrens N, Saaki V, Kol B, Siersma T, Bandow JE, Sahl HG, Schneider T, Hamoen LW. Daptomycin interferes with fluid lipid domains. *Proceedings of the National Academy of Sciences.* 2016. 113(45) E7077-7086. doi: 10.1073/pnas.1611173113

Munita JM, Arias CA. Mechanisms of Antibiotic Resistance. *Microbiol Spectr.* 2016;4(2):10.1128/microbiolspec.VMBF-0016-2015. doi:10.1128/microbiolspec.VMBF-0016-2015

Murtaugh LC, Keefe MD. Regeneration and repair of the exocrine pancreas. *Annu Rev Physiol.* 2015;77:229-49. doi: 10.1146/annurev-physiol-021014-071727. Epub 2014 Oct 24. PMID: 25386992; PMCID: PMC4324082.

Nakamoto H, Bardwell JC. Catalysis of disulfide bond formation and isomerization in the *Escherichia coli* periplasm. *Biochim Biophys Acta.* 2004 Nov 11;1694(1-3):111-9. doi: 10.1016/j.bbamcr.2004.02.012. PMID: 15546661.

Nicolson GL. The Fluid-Mosaic Model of Membrane Structure: still relevant to understanding the structure, function and dynamics of biological membranes after more than 40 years. *Biochim Biophys Acta.* 2014;1838(6):1451-1466. doi:10.1016/j.bbamem.2013.10.019

Noordstra I, Akhmanova A. Linking cortical microtubule attachment and exocytosis. *F1000Res.* 2017 Apr 12;6:469. doi: 10.12688/f1000research.10729.1. PMID: 28491287; PMCID: PMC5399970.

O'Connor CM, Adams, JU. *Essentials of Cell Biology.* Cambridge, MA: NPG Education, 2010. Available at:<https://uta.pressbooks.pub/cellphysiology/front-matter/about-this-project/>

Oluwole AO, Danielczak B, Meister A, Babalola JO, Vargas C, Keller S. Solubilization of Membrane Proteins into Functional Lipid-Bilayer Nanodiscs Using a Diisobutylene/Maleic Acid Copolymer. *Angew Chem Int Ed Engl.* 2017;56(7):1919-1924. doi:10.1002/anie.201610778

Opekarová M, Tanner W. Specific lipid requirements of membrane proteins--a putative bottleneck in heterologous expression. *Biochim Biophys Acta.* 2003;1610(1):11-22. doi:10.1016/s0005-2736(02)00708-3

Palfreyman MT, Jorgensen EM. Roles of SNARE proteins in synaptic vesicle fusion. Molecular mechanisms of neurotransmitter release. Humana Press. Totowa NJ. 2008: 35-59 doi: 10.1007/978-1-59745-481-0

Pandol SJ. The Exocrine Pancreas. Colloquim series on integrated systems physiology: from molecule to function. Morgan & Claypool Life Sciences; 2010;3(1):1-64. *Digestive Enzymes.* Available from: <https://www.ncbi.nlm.nih.gov/books/NBK54127/>

Parikh A, Stephan AF, Tzanakakis ES. Regenerating proteins and their expression, regulation and signaling. *Biomol Concepts.* 2012 Feb;3(1):57-70. doi: 10.1515/bmc.2011.055. Epub 2011 Nov 10. PMID: 22582090; PMCID: PMC3348543.

Parker N, Schneegurt M, Tu AHT, Lister P, Forster BM. *Microbiology.* OpenStax. 2016. Available at; <https://openstax.org/books/microbiology/pages/9-1-how-microbes-grow>

Peña-Blanco A, García-Sáez AJ. Bax, Bak and beyond - mitochondrial performance in apoptosis. *FEBS J.* 2018 Feb;285(3):416-431. doi: 10.1111/febs.14186. Epub 2017 Sep 4. PMID: 28755482.

Pham TDM, Ziora ZM, Blaskovich MAT. Quinolone antibiotics. *Medchemcomm.* 2019;10(10):1719-1739. Published 2019 Jun 28. doi:10.1039/c9md00120d

Pichot R, Watson RL, Norton IT. Phospholipids at the interface: current trends and challenges. *Int J Mol Sci.* 2013;14(6):11767-11794. Published 2013 Jun 3. doi:10.3390/ijms140611767

Pineda A, Burré J. Modulating membrane binding of α -synuclein as a therapeutic strategy. *Proc Natl Acad Sci U S A*. 2017 Feb 7;114(6):1223-1225. doi: 10.1073/pnas.1620159114. Epub 2017 Jan 26. PMID: 28126719; PMCID: PMC5307480.

Prasad SV, Fiedoruk K, Daniluk T, Pikel E, Bucki R. Expression and Function of Host Defense Peptides at Inflammation Sites. *Int J Mol Sci*. 2019 Dec 22;21(1):104. doi: 10.3390/ijms21010104. PMID: 31877866; PMCID: PMC6982121.

Qui H, Honey DM, Kingsbury JS, Park A, Boudanova E, Wei RR, Pan CQ, Edmunds T. Impact of cysteine variants on the structure, activity, and stability of recombinant human α -galactosidase A. *Protein Sci*. 2015 Sep;24(9):1401-11. doi: 10.1002/pro.2719. Epub 2015 Jul 14. PMID: 26044846; PMCID: PMC4570535.

Raj PA, Dentino AR. Current status of defensins and their role in innate and adaptive immunity. *FEMS Microbiol Lett*. 2002 Jan 2;206(1):9-18. doi: 10.1111/j.1574-6968.2002.tb10979.x. PMID: 11786250.

Revelo NH, Ter Beest M, van den Bogaart G. Membrane trafficking as an active regulator of constitutively secreted cytokines. *J Cell Sci*. 2019 Oct 10;133(5):jcs234781. doi: 10.1242/jcs.234781. PMID: 31601617.

Rinn C, Aroso MM, Schrader S. The secretory lectin ZG16p. *Pancreapedia: Exocrine Pancreas Knowledge Base*. 2011. doi: 10.3998/panc.2011.17

Röder PV, Wu B, Liu Y, Han W. Pancreatic regulation of glucose homeostasis. *Exp Mol Med*. 2016 Mar 11;48(3):e219. doi: 10.1038/emm.2016.6. PMID: 26964835; PMCID: PMC4892884.

Rolhion N, Chassaing B. When pathogenic bacteria meet the intestinal microbiota. *Philos Trans R Soc Lond B Biol Sci*. 2016 Nov 5;371(1707):20150504. doi: 10.1098/rstb.2015.0504. PMID: 27672153; PMCID: PMC5052746.

Rosales C, Lowell CA, Schnoor M, Uribe-Querol E. Neutrophils: Their Role in Innate and Adaptive Immunity 2017. *J Immunol Res*. 2017;:9748345. doi: 10.1155/2017/9748345. Epub 2017 Nov 7. PMID: 29238732; PMCID: PMC5697120.

Rossjohn J, Polekhina G, Feil SC, Morton CJ, Tweten RK, Parker MW. Structures of perfringolysin O suggest a pathway for activation of cholesterol-dependent cytolysins. *J Mol Biol*. 2007;367(5):1227-1236. doi:10.1016/j.jmb.2007.01.042

Rowan FE, Docherty NG, Coffey JC, O'Connell PR. Sulphate-reducing bacteria and hydrogen sulphide in the aetiology of ulcerative colitis. *Br J Surg*. 2009 Feb;96(2):151-8. doi: 10.1002/bjs.6454. PMID: 19160346.

Rubinstein E, Mark Z, Haspel J, Ben-Ari G, Dreznik Z, Mirelman D, Tadmor A. Antibacterial activity of the pancreatic fluid. *Gastroenterology*. 1985 Apr;88(4):927-32. doi: 10.1016/s0016-5085(85)80009-3. PMID: 3882511.

Ruiz NM, Ramírez-Ronda CH. Tetracyclines, macrolides, lincosamides & chloramphenicol. *Bol Asoc Med P R*. 1990 Jan;82(1):8-17. PMID: 2180420.

Sable R, Jois S. Surfing the Protein-Protein Interaction Surface Using Docking Methods: Application to the Design of PPI Inhibitors. *Molecules*. 2015 Jun 23;20(6):11569-603. doi: 10.3390/molecules200611569. PMID: 26111183; PMCID: PMC6272567.

Sani MA, Henriques ST, Weber D, Separovic F. Bacteria May Cope Differently from Similar Membrane Damage Caused by the Australian Tree Frog Antimicrobial Peptide Maculatin 1.1. *J Biol Chem*. 2015;290(32):19853-19862. doi:10.1074/jbc.M115.643262

Sasaki M, Klapproth JM. The role of bacteria in the pathogenesis of ulcerative colitis. *J Signal Transduct*. 2012;2012:704953. doi: 10.1155/2012/704953. Epub 2012 Apr 24. PMID: 22619714; PMCID: PMC3348635.

Scheu PD, Liao YF, Bauer J, Kneuper H, Basché T, Uden G, Erker W. Oligomeric sensor kinase DcuS in the membrane of *Escherichia coli* and in proteoliposomes: chemical cross-linking and FRET spectroscopy. *J Bacteriol*. 2010 Jul;192(13):3474-83. doi: 10.1128/JB.00082-10. Epub 2010 May 7. PMID: 20453099; PMCID: PMC2897680.

Schwarz DS, Blower MD. The endoplasmic reticulum: structure, function and response to cellular signaling. *Cell Mol Life Sci*. 2016 Jan;73(1):79-94. doi: 10.1007/s00018-015-2052-6. Epub 2015 Oct 3. PMID: 26433683; PMCID: PMC4700099.

Selders GS, Fetz AE, Radic MZ, Bowlin GL. An overview of the role of neutrophils in innate immunity, inflammation and host-biomaterial integration. *Regen Biomater*. 2017;4(1):55-68. doi:10.1093/rb/rbw041

Serebryany E, King JA. The $\beta\gamma$ -crystallins: native state stability and pathways to aggregation. *Prog Biophys Mol Biol*. 2014 Jul;115(1):32-41. doi: 10.1016/j.pbiomolbio.2014.05.002. Epub 2014 May 14. PMID: 24835736; PMCID: PMC4438767.

Shan D, Zheng J, Klimowicz A, Panzenbeck M, Liu Z, Feng D. Deep learning for discovering pathological continuum of crypts and evaluating therapeutic effects: An implication for in vivo preclinical study. *PLoS One*. 2021 Jun 14;16(6):e0252429. doi: 10.1371/journal.pone.0252429. PMID: 34125849; PMCID: PMC8202954.

Shimoda M, Ohki K, Shimamoto Y, Kohashi O. Morphology of defensin-treated *Staphylococcus aureus*. *Infect Immun*. 1995 Aug;63(8):2886-91. doi: 10.1128/iai.63.8.2886-2891.1995. PMID: 7622209; PMCID: PMC173392.

Shin JH, Seeley RJ. Reg3 Proteins as Gut Hormones? *Endocrinology*. 2019 Jun 1;160(6):1506-1514. doi: 10.1210/en.2019-00073. PMID: 31070724; PMCID: PMC6542482.

Silhavy TJ, Kahne D, Walker S. The bacterial cell envelope. *Cold Spring Harb Perspect Biol*. 2010 May;2(5):a000414. doi: 10.1101/cshperspect.a000414. Epub 2010 Apr 14. PMID: 20452953; PMCID: PMC2857177.

Silvius JR. Role of cholesterol in lipid raft formation: lessons from lipid model systems. *Biochim Biophys Acta*. 2003 Mar 10;1610(2):174-83. doi: 10.1016/s0005-2736(03)00016-6. PMID: 12648772.

Slochower DR, Wang YH, Tourdot RW, Radhakrishnan R, Janmey PA. Counterion-mediated pattern formation in membranes containing anionic lipids. *Adv Colloid Interface Sci*. 2014;208:177-188. doi:10.1016/j.cis.2014.01.016

Smith CL, Powell KR. Review of the sulfonamides and trimethoprim. *Pediatr Rev.* 2000 Nov;21(11):368-71. PMID: 11077020.

Smyth MS, Martin JH. X-ray crystallography. *Mol Pathol.* 2000 Feb;53(1):8-14. doi: 10.1136/mp.53.1.8. PMID: 10884915; PMCID: PMC1186895.

Srivastava SS, Mishra A, Krishnan B, Sharma Y. Ca²⁺-binding motif of $\beta\gamma$ -crystallins. *J Biol Chem.* 2014 Apr 18;289(16):10958-10966. doi: 10.1074/jbc.O113.539569. Epub 2014 Feb 24. PMID: 24567326; PMCID: PMC4036236.

Steward K. Gram positive vs Gram negative. *Technology Networks Immunology and Microbiology.* 2019. Available at: <https://www.technologynetworks.com/immunology/articles/gram-positive-vs-gram-negative-323007>

Stone TA, Deber CM. Therapeutic design of peptide modulators of protein-protein interactions in membranes. *Biochim Biophys Acta Biomembr.* 2017 Apr;1859(4):577-585. doi: 10.1016/j.bbamem.2016.08.013. Epub 2016 Aug 28. PMID: 27580024.

Storz P. Acinar cell plasticity and development of pancreatic ductal adenocarcinoma. *Nat Rev Gastroenterol Hepatol.* 2017 May;14(5):296-304. doi: 10.1038/nrgastro.2017.12. Epub 2017 Mar 8. PMID: 28270694; PMCID: PMC6036907.

Study.com. Glycoprotein Function in the Cell Membrane. 2016. Available at: <https://study.com/academy/lesson/glycoprotein-function-in-the-cell-membrane.html>.

Subczynski WK, Pasenkiewicz-Gierula M, Widomska J, Mainali L, Raguz M. High Cholesterol/Low Cholesterol: Effects in Biological Membranes: A Review. *Cell Biochem Biophys.* 2017;75(3-4):369-385. doi:10.1007/s12013-017-0792-7

Summers C, Rankin SM, Condliffe AM, Singh N, Peters AM, Chilvers ER. Neutrophil kinetics in health and disease. *Trends Immunol.* 2010 Aug;31(8):318-24. doi: 10.1016/j.it.2010.05.006. PMID: 20620114; PMCID: PMC2930213.

Sun Y, Hu A, Fan S, Wei L, Aden CM, Gao L, Wang Y. Dextran sulfate sodium salt corrupted colonic crypts declined the smooth muscle tension in mouse large intestine. *bioRxiv.* 2020 Jan 1.

Tan S, Hooi SC. Syncollin is differentially expressed in rat proximal small intestine and regulated by feeding behavior. *Am J Physiol Gastrointest Liver Physiol.* 2000 Feb;278(2):G308-20. doi: 10.1152/ajpgi.2000.278.2.G308. PMID: 10666056.

Taylor GL. Introduction to phasing. *Acta Crystallogr D Biol Crystallogr.* 2010 Apr;66(Pt 4):325-38. doi: 10.1107/S0907444910006694. Epub 2010 Mar 24. PMID: 20382985; PMCID: PMC2852296.

Tegel H, Tourle S, Ottosson J, Persson A. Increased levels of recombinant human proteins with the *Escherichia coli* strain Rosetta(DE3). *Protein Expr Purif.* 2010 Feb;69(2):159-67. doi: 10.1016/j.pep.2009.08.017. Epub 2009 Sep 4. PMID: 19733669.

ThermoFisher Scientific. Protein expression handbook. Gibco education series. 2015. Available at: <https://www.thermofisher.com/content/dam/LifeTech/global/Forms/PDF/protein-expression-handbook.pdf>

Tunyasuvunakool K, Adler J, Wu Z, Green T, Zielinski M, Židek A, Bridgland A, Cowie A, Meyer C, Laydon A, Velankar S, Kleywegt GJ, Bateman A, Evans R, Pritzel A, Figurnov M, Ronneberger O, Bates R, Kohl SAA, Potapenko A, Ballard AJ, Romera-Paredes B, Nikolov S, Jain R, Clancy E, Reiman D, Petersen S, Senior AW, Kavukcuoglu K, Birney E, Kohli P, Jumper J, Hassabis D. Highly accurate protein structure prediction for the human proteome. *Nature*. 2021 Jul 22. doi: 10.1038/s41586-021-03828-1. Epub ahead of print. PMID: 34293799.

van Kessel KP, Bestebroer J, van Strijp JA. Neutrophil-Mediated Phagocytosis of *Staphylococcus aureus*. *Front Immunol*. 2014 Sep 26;5:467. doi: 10.3389/fimmu.2014.00467. PMID: 25309547; PMCID: PMC4176147.

Viterbo D, Bluth MH, Lin YY, Mueller CM, Wadgaonkar R, Zenilman ME. Pancreatitis-associated protein 2 modulates inflammatory responses in macrophages. *J Immunol*. 2008 Aug 1;181(3):1948-58. doi: 10.4049/jimmunol.181.3.1948. PMID: 18641332.

Wäsle B, Edwardson JM. The regulation of exocytosis in the pancreatic acinar cell. *Cell Signal*. 2002 Mar;14(3):191-7. doi: 10.1016/s0898-6568(01)00257-1. PMID: 11812646.

Wäsle B, Hays LB, Rhodes CJ, Edwardson JM. Syncollin inhibits regulated corticotropin secretion from AtT-20 cells through a reduction in the secretory vesicle population. *Biochem J*. 2004 Jun 15;380(Pt 3):897-905. doi: 10.1042/BJ20031726. PMID: 15040787; PMCID: PMC1224234.

Wäsle B, Turvey M, Larina O, Thorn P, Skepper J, Morton AJ, Edwardson JM. Syncollin is required for efficient zymogen granule exocytosis. *Biochem J*. 2005 Feb 1;385(Pt 3):721-7. doi: 10.1042/BJ20041064. PMID: 15462671; PMCID: PMC1134747.

Wei Y, Thyparambil AA, Latour RA. Protein helical structure determination using CD spectroscopy for solutions with strong background absorbance from 190 to 230nm. *Biochim Biophys Acta*. 2014;1844(12):2331-2337. doi:10.1016/j.bbapap.2014.10.001

Weng N, Thomas DDH, Groblewski GE. Pancreatic acinar cells express vesicle-associated membrane protein 2- and 8-specific populations of zymogen granules with distinct and overlapping roles in secretion. *J Biol Chem*. 2007 Mar 30;282(13):9635-9645. doi: 10.1074/jbc.M611108200. Epub 2007 Feb 1. PMID: 17272274.

Westphal D, Dewson G, Czabotar PE, Kluck RM. Molecular biology of Bax and Bak activation and action. *Biochim Biophys Acta*. 2011 Apr;1813(4):521-31. doi: 10.1016/j.bbamcr.2010.12.019. Epub 2010 Dec 30. PMID: 21195116.

Westphal D, Kluck RM, Dewson G. Building blocks of the apoptotic pore: how Bax and Bak are activated and oligomerize during apoptosis. *Cell Death Differ*. 2014 Feb;21(2):196-205. doi: 10.1038/cdd.2013.139. Epub 2013 Oct 25. PMID: 24162660; PMCID: PMC3890949.

Williams JA, Yule DI. Chapter 50- Stimulus secretion coupling in pancreatic acinar cells. *Physiology of the Gastrointestinal tract*. 2012. (5)1361-1398 ISBN: 9780123820266,

Wilson CL, Ouellette AJ, Satchell DP, Ayabe T, López-Boado YS, Stratman JL, Hultgren SJ, Matrisian LM, Parks WC. Regulation of intestinal alpha-defensin activation by the metalloproteinase matrilysin in innate host defense. *Science*. 1999 Oct 1;286(5437):113-7. doi: 10.1126/science.286.5437.113. PMID: 10506557.

Wu LG, Hamid E, Shin W, Chiang HC. Exocytosis and endocytosis: modes, functions, and coupling mechanisms. *Annu Rev Physiol.* 2014;76:301-31. doi: 10.1146/annurev-physiol-021113-170305. Epub 2013 Nov 20. PMID: 24274740; PMCID: PMC4880020.

Yipp BG, Kubes P. NETosis: how vital is it? *Blood.* 2013 Oct 17;122(16):2784-94. doi: 10.1182/blood-2013-04-457671. Epub 2013 Sep 5. PMID: 24009232.

Zavodszky M, Chen CW, Huang JK, Zolkiewski M, Wen L, Krishnamoorthi R. Disulfide bond effects on protein stability: designed variants of *Cucurbita maxima* trypsin inhibitor-V. *Protein Sci.* 2001 Jan;10(1):149-60. doi: 10.1110/ps.26801. PMID: 11266603; PMCID: PMC2249841.

Zeng X, Lin J. Beta-lactamase induction and cell wall metabolism in Gram-negative bacteria. *Front Microbiol.* 2013 May 22;4:128. doi: 10.3389/fmicb.2013.00128. PMID: 23734147; PMCID: PMC3660660.

Zhou HX, Pang X. Electrostatic Interactions in Protein Structure, Folding, Binding, and Condensation. *Chem Rev.* 2018 Feb 28;118(4):1691-1741. doi: 10.1021/acs.chemrev.7b00305. Epub 2018 Jan 10. PMID: 29319301; PMCID: PMC5831536.

8. APPENDIX

		[Syncollin]											
A.	[Ampicillin]	0.0829	0.0855	0.0823	0.0947	0.0865	0.0856	0.0844	0.0824	0.0829	0.0817	0.0826	0.087
		0.0865	0.083	0.0837	0.0827	0.1053	0.0979	0.1368	0.0823	0.0827	0.0822	0.0846	0.0823
		0.0874	0.0865	0.1122	0.1035	0.1708	0.1578	0.1591	0.1045	0.1039	0.1134	0.116	0.1208
		0.0984	0.1148	0.1226	0.122	0.1879	0.1665	0.162	0.1324	0.1472	0.1263	0.1226	0.1427
		0.1015	0.1139	0.117	0.125	0.1221	0.1158	0.1164	0.1202	0.1174	0.122	0.1262	0.1448
		0.1052	0.1144	0.1229	0.1412	0.1152	0.118	0.1191	0.1215	0.1197	0.1292	0.1264	0.1397
		0.1178	0.112	0.112	0.1335	0.1162	0.1189	0.1205	0.1188	0.1279	0.1197	0.1276	0.1381
		0.1008	0.1139	0.1162	0.1578	0.136	0.1259	0.1291	0.1308	0.1559	0.1352	0.1432	0.1268
	B.	[Tetracycline]	0.0851	0.0832	0.087	0.082	0.0819	0.0823	0.0818	0.0818	0.0819	0.0817	0.0822
		0.0865	0.0849	0.0844	0.0834	0.0847	0.0826	0.0826	0.0823	0.0835	0.083	0.0843	0.0817
		0.0922	0.0867	0.0889	0.0883	0.0867	0.0868	0.087	0.0879	0.0847	0.086	0.0879	0.0852
		0.0999	0.0984	0.0938	0.1008	0.0974	0.097	0.0984	0.0972	0.0997	0.096	0.1015	0.099
		0.1482	0.1617	0.1873	0.1452	0.1363	0.1332	0.128	0.1364	0.1351	0.1397	0.1696	0.1369
		0.1209	0.1587	0.1572	0.149	0.1376	0.1312	0.1465	0.1507	0.1777	0.1486	0.161	0.1469
		0.1178	0.1284	0.1399	0.1508	0.1369	0.1392	0.1187	0.1383	0.1449	0.141	0.1556	0.1539
		0.1194	0.1571	0.132	0.1528	0.2261	0.1629	0.1568	0.1696	0.1493	0.1498	0.1515	0.1046

Figure A1: Checkerboard schematic from Figure 4.12 including OD values.